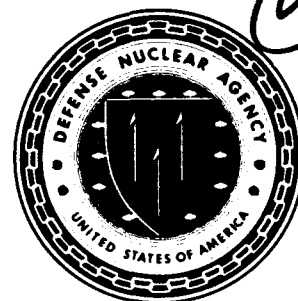


**AD-A243 454**



**Defense Nuclear Agency  
Alexandria, VA 22310-3398**



**DNA-TR-90-216-V1**

# **Evaluation of Laboratory Scale Testing of Tunnels and Tunnel Intersections Volume I**

**Jeremy Isenberg, et al.  
Weidlinger Associates, Inc.  
4410 El Camino Real, Suite 110  
Los Altos, CA 94022-1049**

**November 1991**

**Technical Report**

**DTIC  
ELECTRONIC  
DEC 03 1991  
S B D**

**CONTRACT No. DNA 001-87-C-0290**

**Approved for public release;  
distribution is unlimited.**

**91-16855**



01 10 00 018

Destroy this report when it is no longer needed. Do not return to sender.

PLEASE NOTIFY THE DEFENSE NUCLEAR AGENCY,  
ATTN: CSTI, 6801 TELEGRAPH ROAD, ALEXANDRIA, VA  
22310-3398, IF YOUR ADDRESS IS INCORRECT, IF YOU  
WISH IT DELETED FROM THE DISTRIBUTION LIST, OR  
IF THE ADDRESSEE IS NO LONGER EMPLOYED BY YOUR  
ORGANIZATION.



## DISTRIBUTION LIST UPDATE

This mailer is provided to enable DNA to maintain current distribution lists for reports. We would appreciate your providing the requested information.

- ☐ Add the individual listed to your distribution list.
- ☐ Delete the cited organization/individual.
- ☐ Change of address.

**NOTE:**  
Please return the mailing label from the document so that any additions, changes, corrections or deletions can be made more easily.

NAME: \_\_\_\_\_

ORGANIZATION: \_\_\_\_\_

### OLD ADDRESS

### CURRENT ADDRESS

\_\_\_\_\_  
\_\_\_\_\_  
\_\_\_\_\_

\_\_\_\_\_  
\_\_\_\_\_  
\_\_\_\_\_

TELEPHONE NUMBER: (    ) \_\_\_\_\_

SUBJECT AREA(s) OF INTEREST:

\_\_\_\_\_  
\_\_\_\_\_  
\_\_\_\_\_

\_\_\_\_\_  
\_\_\_\_\_  
\_\_\_\_\_

DNA OR OTHER GOVERNMENT CONTRACT NUMBER: \_\_\_\_\_

CERTIFICATION OF NEED-TO-KNOW BY GOVERNMENT SPONSOR (if other than DNA):

SPONSORING ORGANIZATION: \_\_\_\_\_

CONTRACTING OFFICER OR REPRESENTATIVE: \_\_\_\_\_

SIGNATURE: \_\_\_\_\_

CUT HERE AND RETURN



Director  
Defense Nuclear Agency  
ATTN: TITL  
Washington, DC 20305-1000

Director  
Defense Nuclear Agency  
ATTN: TITL  
Washington, DC 20305-1000

REPORT DOCUMENTATION PAGE			Form Approved OMB No. 0704-0188	
<small>Public reporting burden for this collection of information is estimated to average 1 hour per response, including the time for reviewing instructions, searching existing data sources, gathering and maintaining the data needed, and completing and reviewing the collection of information. Send comments regarding this burden estimate or any other aspect of this collection of information, including suggestions for reducing this burden, to Washington Headquarters Services, Directorate for Information Operations and Reports, 1215 Jefferson Davis Highway, Suite 1204, Arlington, VA 22202-4302, and to the Office of Management and Budget, Paperwork Reduction Project (0704-0188), Washington, DC 20503.</small>				
1. AGENCY USE ONLY (Leave blank)	2. REPORT DATE 911101	3. REPORT TYPE AND DATES COVERED Technical 861002 - 901130		
4. TITLE AND SUBTITLE Evaluation of Laboratory Scale Testing of Tunnels and Tunnel Intersections Volume I		5. FUNDING NUMBERS C-DNA 001-87-C-0290 PE - 62715H PR - RS TA - RH WU - DH018650		
6. AUTHOR(S) Jeremy Isenberg, Felix Wong, Ivan Nelson (Weidlinger); J. L. Merritt (BDM); Richard Goodman, Pierre-Jean Perie (University of California, Berkeley)				
7. PERFORMING ORGANIZATION NAME(S) AND ADDRESS(ES) Weidlinger Associates, Inc. 4410 El Camino Real, Suite 110 Los Altos, CA 94022-1049		8. PERFORMING ORGANIZATION REPORT NUMBER  FR8944		
9. SPONSORING/MONITORING AGENCY NAME(S) AND ADDRESS(ES) Defense Nuclear Agency 6801 Telegraph Road Alexandria, VA 22310-3398 SPSD/Senseny		10. SPONSORING/MONITORING AGENCY REPORT NUMBER  DNA-TR-90-216-V1		
11. SUPPLEMENTARY NOTES  This work was sponsored by the Defense Nuclear Agency under RDT&E RMC Code B4667D RS RH 00045 SPSS 3440A 25904D.				
12a. DISTRIBUTION/AVAILABILITY STATEMENT  Approved for public release; distribution is unlimited.			12b. DISTRIBUTION CODE	
13. ABSTRACT (Maximum 200 words) <p>A major goal of this project is to advise DNA on the future role of small size (laboratory scale) testing in supporting design and target assessment of deep underground structures. The project team reviewed past laboratory size tests and small size structural models loaded in field tests. The testing was sponsored primarily by DNA and conducted by SRI International, TerraTek, Inc. and the University of Illinois in the past 10-15 years. Data from the U.S. Army Engineer Waterways Experiment Station and foreign literature on the subject were also evaluated.</p> <p>The core issue addressed is: has laboratory scale testing, whether in the form of replica-scale testing or material-scale testing, established itself as a legitimate means to study prototype tunnel behavior? The answer based on our review is a qualified no. There are sufficient questions of geometry at SRI and boundary conditions at Terra Tek to cast doubts on the validity of their results as prototype behavior. However, if it is assumed that the effects of geometry and boundary are comparable for different types of tunnel liners, replica scale or material scale testing can be</p>				
14. SUBJECT TERMS Scale Testing Replica Testing Rock Simulants			15. NUMBER OF PAGES 254	
			16. PRICE CODE	
17. SECURITY CLASSIFICATION OF REPORT UNCLASSIFIED	18. SECURITY CLASSIFICATION OF THIS PAGE UNCLASSIFIED	19. SECURITY CLASSIFICATION OF ABSTRACT UNCLASSIFIED	20. LIMITATION OF ABSTRACT SAR	

UNCLASSIFIED

SECURITY CLASSIFICATION OF THIS PAGE

CLASSIFIED BY:

N/A since Unclassified

DECLASSIFY ON:

N/A since Unclassified

19. Abstract (continued)

used to evaluate the relative merit of different reinforcing types in a given medium.

The consensus of the reviewers is that laboratory scale testing is most useful when the tests are conducted within current limits of the machines (viz., size, rate, boundary condition and precision). Furthermore, if laboratory test results are to be used to influence targeting, the tests must simulate failure, which means that the materials used in the laboratory must have the same failure characteristics (including dilatancy and post peak behavior) as prototype materials. Future testing should adhere to this requirement which is by and large ignored in previous work.

SECURITY CLASSIFICATION OF THIS PAGE

UNCLASSIFIED

## SUMMARY

Small size laboratory testing sponsored primarily by DNA and conducted by SRI International, Terra Tek, Inc., and the University of Illinois in the past 8-12 years has been reviewed. The core issue addressed is: has laboratory scale testing, whether in the form of replica-scale testing or material-scale testing, established itself as a legitimate means to study prototype tunnel behavior?

The answer based on our review is a qualified no. There are sufficient questions of geometry at SRI and boundary conditions at Terra Tek to cast some doubt on the validity of their results in a truly quantitative sense. On the other hand, if it is assumed that the questions of geometry and boundary effects are comparable for different types of lining, either concept of testing can be used to evaluate the relative merit of different reinforcing type in a given medium. Since geometry and boundary effects are apt to be more medium dependent, we have less confidence, without further analytical work, to say that SRI and Terra Tek could define relative hardness, for given lining types, in different media (e.g., sandstone versus granite). Furthermore, if laboratory test results are to be used to influence targeting, the tests have to simulate failure, which means that the materials must have the same failure characteristics as prototype materials. This imposes further requirements on simulants, including dilatancy and post peak behavior, which have remained unaddressed.

However, laboratory tests are valuable because they produce high fidelity data; the tests are conducted under controlled conditions so that the results can be understood in terms of the parameters that are varied, one at a time if necessary. The data indicate trends which may not be deduced from field tests; these trends include the effect of lateral confinement, pore water and strain path. It appears that for rocks which can be considered continuous, the phenomena observed in the laboratory are qualitatively similar to those in the field. Laboratory data are also useful in verifying computer codes. Field tests, by contrast, are usually much more specific and less controllable; field test data do not lend themselves readily to generalization. They are usually incomplete, and contain large uncertainties so that they are less useful in code validation.

Given current laboratory capabilities and limitations, we recommend that the role of small size laboratory testing be changed from the dominant emphasis on replicating prototype tunnel behavior, to that of understanding phenomenology and improving the predictive capability of computer models.

<b>Accession For</b>	
NTIS CR&I	<input checked="" type="checkbox"/>
DTIC TAB	<input type="checkbox"/>
Unannounced	<input type="checkbox"/>
Justification	
By	
Distribution/	
<b>Availability Codes</b>	
Dist	Avail and/or Special
A-1	4

## PREFACE

A major goal of this project is to advise DNA on the future role of small size testing in supporting design and target assessment of deep underground structures. In preparing an advisory statement, the project team expended most of its resources on a review of past laboratory size tests and small size structural models loaded in field tests. The major sources of data are SRI International and TerraTek, Inc. We also considered data from the University of Illinois, U.S. Army Engineer Waterways Experiment Station and foreign literature on the subject.

Since there are at least 6 individuals (Isenberg, Wong, Nelson, Merritt, Goodman, Perie) who made major contributions to the project, differences inevitably arise in what to emphasize in reviewing previous data. If our objective were to summarize past results or to write a history of small size testing it would be possible to enforce uniform reporting within the project. Instead, the goal of the review is to ascertain what has been learned from past small size testing and to recommend how extensions of previous work can contribute to future DNA programs. Therefore, the only essential common element of the various reviews is to say at the end of each one what was learned from the testing.

In a review of this type it is inevitable that much emphasis will be given to aspects of the testing that could be improved. This is consistent with our goal of improving future tests relative to past ones. As a result, a somewhat negative overall impression may be given. At the outset, the reviewers wish to state that we do not intend to recommend against all future small size testing. Furthermore, we recognize the difficulties of performing such tests and respect the efforts of those who conducted them. We also understand that many of the projects may have been redirected during the course of the study resulting in a test program that years later may appear incoherent.

# CONVERSION TABLE

Conversion factors for U.S. Customary to metric (SI) units of measurement

MULTIPLY TO GET	BY	TO GET DIVIDE
angstrom	1.000 000 X E -10	meters (m)
atmosphere (normal)	1 013 25 X E +2	kilo pascal (kPa)
bar	1.000 000 X E +2	kilo pascal (kPa)
barn	1.000 000 X E -28	meter <sup>2</sup> (m <sup>2</sup> )
British thermal unit (thermochemical)	1.054 350 X E +3	joule (J)
calorie (thermochemical)	4.184 000	joule (J)
cal (thermochemical) cm <sup>2</sup>	4.184 000 X E -2	mega joule/m <sup>2</sup> (MJ/m <sup>2</sup> )
curie	3 700 000 X E +1	giga becquerel (GBq)
degree (angle)	1.745 329 X E -2	radian (rad)
degree Fahrenheit	$t_c = (t_f + 459.67)/1.8$	degree kelvin (K)
electron volt	1.602 19 X E -19	joule (J)
erg	1.000 000 X E -7	joule (J)
erg/second	1.000 000 X E -7	watt (W)
foot	3 048 000 X E -1	meter (m)
foot-pound-force	1.355 818	joule (J)
gallon (U.S. liquid)	3.785 412 X E -3	meter <sup>3</sup> (m <sup>3</sup> )
inch	2.540 000 X E -2	meter (m)
jerk	1.000 000 X E +9	joule (J)
joule/kilogram (J/kg) (radiation dose absorbed)	1.000 000	Gray (Gy)
kilotons	4.183	terajoules
kip (1000 lbf)	4.448 222 X E +3	newton (N)
kip/inch <sup>2</sup> (ksi)	6 894 757 X E +3	kilo pascal (kPa)
ktop	1.000 000 X E +2	newton-second/m <sup>2</sup> (N-s/m <sup>2</sup> )
micron	1 000 000 X E -6	meter (m)
mil	2.540 000 X E -5	meter (m)
mile (international)	1.609 344 X E +3	meter (m)
ounce	2.934 952 X E -2	kilogram (kg)
pound-force (lbf avoirdupois)	4.448 222	newton (N)
pound-force inch	1.129 848 X E -1	newton-meter (N-m)
pound-force/inch	1.751 268 X E +2	newton/meter (N/m)
pound-force/foot <sup>2</sup>	4.788 026 X E -2	kilo pascal (kPa)
pound-force/inch <sup>2</sup> (psi)	6.894 757	kilo pascal (kPa)
pound-mass (lbm avoirdupois)	4.535 924 X E -1	kilogram (kg)
pound-mass-foot <sup>2</sup> (moment of inertia)	4.214 011 X E -2	kilogram-meter <sup>2</sup> (kg-m <sup>2</sup> )
pound-mass/foot <sup>3</sup>	1.601 946 X E +1	kilogram/meter <sup>3</sup> (kg/m <sup>3</sup> )
rad (radiation dose absorbed)	1.000 000 X E -2	Gray (Gy)
roentgen	2.579 760 X E -4	coulomb/kilogram (C/kg)
shake	1 000 000 X E -8	second (s)
slug	1.459 390 X E +1	kilogram (kg)
torr (mm Hg, 0° C)	1.333 22 X E -1	kilo pascal (kPa)

\*The becquerel (Bq) is the SI unit of radioactivity; 1 Bq = 1 event/s.

\*\*The Gray (Gy) is the SI unit of absorbed radiation.

## TABLE OF CONTENTS

Section	Page
Summary.....	iii
Preface.....	iv
Conversion Table .....	v
List of Illustrations.....	ix
List of Tables .....	xiv
1 Introduction.....	1
2 Replica or Geometric Scaled Tests at SRI International .....	2
2.1 Equipment Design and Validation .....	2
2.1.1 Machine Designed In 1974.....	2
2.1.2 Subsequent Improvement In 1977 .....	3
2.1.3 Need For Larger Machine, 1977 .....	3
2.1.4 Typical Pressure Environment.....	6
2.1.5 Boundary Effects.....	6
2.1.6 Test-To-Test Variation.....	11
2.2 Choice and Mechanical Properties of Simulants.....	11
2.2.1 Need for Simulants .....	11
2.2.2 History of Simulants.....	17
2.2.3 Summary of Simulant Properties.....	18
2.2.4 Comparison of Simulant and Native Rock.....	33
2.2.5 Variability in Simulant Properties .....	49
2.2.6 Strain Rate Effects on Simulant Properties.....	49
2.3 Experiments in Continuous (Unjointed) Specimens .....	56
2.3.1 Tests Prior to 1975.....	62
2.3.2 Tests to Study Liner, Pore Pressure and Strain Path .....	62
2.3.3 Tests in Support of MIGHTY EPIC Structures .....	74
2.3.4 Tests in Support of DIABLO HAWK .....	82
2.3.5 Synthesis of Data.....	86
2.3.6 Observations on Tests of Continuous Specimens.....	89
2.4 Joint Properties .....	90
2.5 Experiments in Jointed Specimens .....	100
2.5.1 Early Lab Tests.....	100
2.5.2 Tests in Support of DIABLO HAWK .....	100
2.5.3 Synthesis of Data and Comments .....	107

## TABLE OF CONTENTS (Continued)

Section	Page
3 Add-On Experiments In Field Tests .....	115
3.1 DINING CAR .....	115
3.1.1 Review of Test Parameters.....	115
3.1.2 Results on Direct Contact Tunnels .....	115
3.1.3 Backpacker Liner Tunnels.....	119
3.1.4 Evaluation of Replica Testing By Comparing Laboratory and Small Field Scale Specimens.....	125
3.2 MIGHTY EPIC.....	125
3.2.1 Mini Built-Up Backpacker Structures.....	128
3.2.2 Direct Contact Mini-Structures .....	128
3.2.3 Mini-Structures in 6B Simulant .....	128
3.2.4 Assessment of Replica-Scaling in MIGHTY EPIC .....	135
3.3 DIABLO HAWK - Jointed Specimens .....	135
3.3.1 Jointed Rock.....	135
3.3.2 Parametric Specimens .....	136
3.3.3 Comparison Between Lab and Field Jointed-Rock Results.....	140
3.3.4 PILE DRIVER Scaled Specimens.....	140
3.3.5 Assessment of Replica Scaling .....	147
3.4 DIABLO HAWK - Continuous Rock.....	147
3.4.1 Mini-Structures.....	147
3.4.2 MIGHTY EPIC Results.....	148
3.4.3 Mini-Structure Response.....	148
3.4.4 Assessment of Replica-Scaling .....	148
4 Review of Terra Tek Material Scaling Experiments.....	149
4.1 Design of Testing Apparatus.....	149
4.2 Mechanical Properties of Simulant .....	151
4.3 Data for Tunnels in Continuous (Unjointed) Specimens .....	156
4.3.1 Straight Tunnel Section.....	156
4.3.2 Test of Tunnel Intersections in Two Grouts .....	156
4.3.3 Reliability of Experimental Results, Continuous Specimens.....	166
4.4 Data for Tunnels in Jointed Specimens .....	171
4.4.1 Quasistatic Tests.....	173
4.4.2 Dynamic Tests.....	173

## TABLE OF CONTENTS (Continued)

Section	Page
5 The UI Program Involving Strength-Scaled Materials and Systematically Jointed Specimens .....	178
5.1 The Test Program .....	178
5.2 Brief Comparison of Results.....	191
5.3 Observations on Response of Jointed-Specimens.....	205
6 Summary and Recommendations .....	206
6.1 Summary Observations on SRI Program.....	206
6.1.1 Significant Strengths.....	206
6.1.2 Some Concerns.....	206
6.2 Summary Observations on Terra Tek Program.....	207
6.2.1 Significant Strengths.....	207
6.2.2 Some Concerns .....	207
6.3 Summary Observations on UI Program.....	208
6.3.1 Significant Strengths.....	208
6.3.2 Some Concerns.....	208
6.4 Some General, Retrospective Concerns .....	209
6.5 Recommendation for Future Lab Testing.....	209
6.5.1 Fundamental Issues.....	210
6.5.2 Outstanding Fundamental Questions In Laboratory Testing.....	215
6.5.3 Recommended Test Matrix.....	220
7 List of References.....	230
Appendix	
A Bibliography.....	235

## LIST OF ILLUSTRATIONS

Figure		Page
1	Trace Set Showing Wave Propagation Effect Arising From Reverberation Loading Technique .....	4
2	Pressure Data From a Uniaxial Strain Test in the Small Testing Machine, DUX-74, Showing Improvement of Lateral Pressure Pulses .....	5
3	Pressure Data from Uniaxial Strain Test LDUX-10 .....	7
4	The Response of Tunnels with Various Diameters to Static Uniaxial Strain Loading .....	8
5	Vertical pressure to produce specified crown-invert tunnel closure versus specimen-to-tunnel diameter ratio .....	9
6	Vertical pressure to produce specified crown-invert tunnel closure versus specimen-to-tunnel diameter ratio - 16A rock simulant .....	10
7	Experimental and Theoretical Closure Versus Applied Pressure for Static, Isotropic Loading of 6B Rock .....	12
8	Vertical Tunnel Closure Versus Applied Vertical Pressure-Comparison of Data Obtained by SRI and WES for Static Uniaxial Strain Loading of SRI RMG 2C2, A 6061-T0 Liner, $a/h = 4.0$ .....	13
9	Vertical Tunnel Closure Versus Vertical Pressure for Uniaxial Strain Loading of Saturated SRI RGM 2C2, 6061-T0 Aluminum Liner, $a/h = 11.5$ .....	14
10	Comparison of Tunnel Closures in WES Test and Special SRI Test, SUX-90, In Which Lateral Boundaries of Rock are Allowed to Move Out 0.1% (Reached at $P_v = 4.7$ ksi) .....	15
11	Mohr Failure Envelope .....	21
12	Uniaxial Strain Condition Stress-Strain Relationship .....	22
13	Confining Pressure Versus Axial Pressure for Uniaxial Strain Tests ( $K_0$ Consolidation Test) .....	23
14	Composite of Confining Versus Axial Pressure Relationships for Uniaxial Strain and Triaxial Failure Conditions .....	23
15	Stress-Strain Curves for Moisturized 6B Rock Simulant .....	26
16	Horizontal Pressure Versus Vertical Pressure for Uniaxial Strain for Saturated 6B Rock Simulant .....	27
17	Stress-Strain Curve Under Uniaxial Strain Loading for Saturated 6B Rock Simulant .....	28
18	Mohr Diagrams for Moisturized 6B Rock at Different Test Ages .....	29
19	Stress-Strain Curves for Dry 6B Rock Simulant .....	30
20	Horizontal Pressure Versus Vertical Pressure for Uniaxial Strain for Dry 6B Rock Simulant .....	31
21	Mohr Diagram for Dry 6B Rock .....	32
22	Uniaxial Strain - 56th Day .....	35
23	Hydrostatic/Triaxial Compression, Pore Pressure 10 Bars .....	36
24	Hydrostatic Compression Test Summary .....	37
25	HF4: Crush Strength as a Function of Time for Batches B1-B7 .....	38
26	HF4 Hydrostatic Test Results .....	39
27	Deviatoric Stress-Strain Curves for Triaxial Test 21 Through 24 .....	40
28	HF4 Failure Surface .....	41
29	Volumetric Stress-Strain for Triaxial Tests 21 Through 24 .....	42
30	HF4 Response at 28 and 72 Days Normalized by Crush Strength .....	43
31	Straight Tunnel Closure (LSUX-52 - LSUX-57) .....	44

## LIST OF ILLUSTRATIONS (Continued)

Figure		Page
32	Straight Tunnel Closure Versus Normalized Load (LSUX-52 - LSUX-57) .....	46
33	Comparison of Pressure-Volume and Strength Properties Between 2C3 Grout and Ash Fall Tuff .....	47
34	Comparison of Pressure-Volume and Strength Properties Between 2C4 Grout and Ash Fall Tuff .....	48
35	Unconfined Crush Strength of Rock-Matching Grout RMG2C4.....	50
36	Splitting Tensile Strength of Rock Matching Grout RMG 2C4 .....	51
37	Time Histories of Applied Loads .....	52
38	Strain Rates Versus Strength .....	53
39	Strain Rate Summary for Unconfined Compression Tests .....	54
40	Triaxial Compression Test Summary, Confining Pressure 0.5 kbar .....	55
41	Variation of Concrete Strengths with Strain Rate .....	59
42	Rate Dependence (Malvern) $f_c = 15.3$ ksi, Static, Limestone Aggregate .....	60
43	Variation of Strength with Strain Rate at Room Temperature and Pressure Except Where Noted. Numbers at the Left of Each Line Indicate the Slope of That Line.....	61
44	Comparison of Unlined and Lined Tunnel Response at Increasing Load Levels Under Uniaxial Strain Conditions.....	66
45	Experimental and Theoretical Closure Versus Applied Pressure for Static, Isotropic Loading of 6B Rock .....	67
46	Vertical Tunnel Closure Versus Vertical Pressure for Uniaxial Strain Loading of Saturated 6B Rock .....	69
47	Response of a Steel-Lined Tunnel in Saturated Rock to Static, Uniaxial Strain Loading - $a/h = 50$ , $P_{Vmax} = 12,500$ psi, $\Delta D_V/D = 0.1135$ .....	70
48	Vertical Tunnel Closure Versus Vertical Pressure for Uniaxial Strain Loading of Dry 6B Rock.....	71
49	Response of a Steel-Lined Tunnel in Dry Rock to Static, Uniaxial Strain Loading -- $a/h = 50$ , $P_{Vmax} = 23,500$ psi, $\Delta D_V/D = 0.175$ .....	72
50	Comparison of Static and Dynamic Response of a Steel-Lined Tunnel to Isotropic Loading -- $a/h = 50$ .....	73
51	Comparison of Tunnel Closures in SRI RMG 2C2 for Uniaxial Strain and Isotropic Loading -- A 6061-T0 liner, $a/h = 11.5$ .....	76
52	Comparison of Tunnel Closures in SRI RMG 2C2 for Uniaxial Strain and Isotropic Loading -- A 6061-T0 Liner, $a/h = 6.5$ .....	77
53	Comparison of Tunnel Closures in SRI RMG 2C2 for Uniaxial Strain and Isotropic Loading -- A 6061 T0 Liner, $a/h = 4.0$ .....	78
54	Comparison of Tunnel Closures in SRI RMG 2C2 for Static Isotropic and Uniaxial Strain Loading.....	79
55	Comparison of Tunnel Closures in SRI Test and Special SRI Test, SUX-90, in which Lateral Boundaries of Rock are Allowed to Move Out 0.1% (Reached at $P_V = 4.7$ ksi) .....	80
56	Tunnel Closure at Crown-Invert and Springline Diameters Versus Vertical Pressure for Overconfined, Underconfined and Uniaxial Strain Loading of SRI RMG 2C2, 6061-T0 Aluminum, $a/h=11.5$ .....	81

## LIST OF ILLUSTRATIONS (Continued)

Figure	Page
57	Tunnel Closure Versus Applied Pressure for Isotropic Loading of SRI RMG 2C2. Liner: 6061-T0 Aluminum, $a/h = 11.5$ ..... 84
58	Vertical Tunnel Closure Versus Applied Vertical Pressure for Uniaxial Strain Loading of SRI RMG 2C2. Liner: 6061-T0 Aluminum, $a/h = 11.5$ ..... 85
59	Model 2 Parameters..... 87
60	Vertical Tunnel Closure Versus Vertical Pressure for Uniaxial Strain Loading of Saturated SRI RMG 2C2. Liner: 6061-T0 Aluminum, $a/h = 11.5$ ..... 91
61	Ratio of In-Situ Strength to Core Strength Versus Ratio of Tunnel Diameter to Joint Spacing..... 92
62	Static Tests on Intact, Single-Joint and Double-Joint Rock Specimens to Determine Rock Joint Effects..... 93
63	Failure Envelope for 16A Simulant in Direct Shear..... 94
64	Failure Envelope for Granite Simulant in Direct Shear..... 96
65	Mohr Envelopes for Intact and Jointed 16A Simulant Models from Triaxial Compression Tests (12.7 mm Joint Spacings) ..... 98
66	Engineering Classifications for Intact Rocks ..... 99
67	Variation of Reduction Factor with Rock Quality..... 101
68	Comparison of Tests in Intact and Jointed Media..... 103
69	Vertical Tunnel Closure Versus Vertical Pressure for Uniaxial Strain Loading of Jointed 16A Rock Specimens..... 104
70	Sectioned Specimen from Static Uniaxial Strain Test LSUX-13 ( $P_V = 17$ ksi, $P_H = 7.4$ ksi, $\Delta D_V/D_V = 10.2\%$ , $\Delta D_H/D_H = 0.25\%$ )..... 108
71	Enlargement of Tunnel Region in LSUX-13 Specimen..... 109
72	Sectioned Specimen from Static Uniaxial Strain Test LSUX-14 ( $P_V = 17$ ksi, $P_H = 4.6$ ksi, $\Delta D_V/D_V = 8.90\%$ , $\Delta D_H/D_H = -5.10\%$ ) ..... 110
73	Enlargement of Tunnel Region in LSUX-14 Specimen..... 111
74	Lined Tunnel Experiment -- $P_V = 20,000$ psi, $P_H = 5,000$ psi..... 112
75	Lined Tunnel Specimen Tested in DINING CAR, Showing Classical Shear Cracks ..... 113
76	Experimental Layout in DINING CAR Crosscuts..... 116
77	Scale Model Tunnel in Simulated Intact Geology..... 117
78	Comparison of 5/8" Lab (Static, Isotropic 6B, Saturated but Drained) and 6" DINING CAR Data..... 118
79	Comparisons of Liner Buckling in Large and Small Field Structures and in Laboratory Structures -- $a/h = 50$ Direct Contact Liner..... 120
80	Significant Features of behavior around failing opening..... 121
81	Comparison of 5/8" Lab (Static, Uniaxial 6B, Saturated but Drained) and 6" DINING CAR Data..... 122
82	Comparison of 5/8" Lab (Static, Isotropic 6B, Saturated but Drained) and 5/8" DINING CAR Data..... 123
83	Comparisons of Fracture Patterns in Large and Small Field Structures and in Laboratory Structures -- $a/h = 25$ Liner with Backpacking ..... 124

## LIST OF ILLUSTRATIONS (Continued)

Figure	Page
84	Comparison of 5/8" Lab (Static, Isotropic 6B, Saturated but Drained) and 5/8" DINING CAR Data..... 126
85	Comparison of 5/8" Lab (Static, Isotropic 6B, Saturated but Drained) and 5/8" DINING CAR Data..... 127
86	Comparison of 6" Built-Up (Field) and 4' Built-Up (Field)..... 129
87	Experimental and Theoretical Closure Versus Applied Pressure for Static, Isotropic Loading of 6B Rock..... 130
88	Peak Oval-Plus-Hoop Mode Deformation Versus Normalized Incident Load for Side-On Aluminum Ministtructures ..... 131
89	Peak Oval-Plus-Hoop Mode Deformation Versus Incident Load for Side-On Steel Ministtructures ..... 132
90	Peak Oval-Plus-Hoop Mode Deformation Versus Normalized Incident Load for Side-On Steel Ministtructures ..... 133
91	Rock Opening Diameter Changes Versus Load-To-Strength Ratio $p/p_5$ for Ministtructures in 6B Rock..... 134
92	Experimental and Theoretical Closure Versus Applied Pressure for Static Isotropic Loading of 6B Rock in the Laboratory ..... 134
93	Jointing Arrangement for Models Assembled from 16A Rock Simulant..... 138
94	Vertical Tunnel Closure Versus Vertical Pressure for Uniaxial Strain Loading of Jointed 16A Rock Specimens..... 141
95	Joint Profiled Around Pile Driver Structures (a), (b) and (c) and for Laboratory Scale Model (d)..... 142
96	Scale Model of Pile Driver Structures..... 143
97	Liner Buckling and Fractures in Pile Driver Structure BL10..... 145
98	Response of Pile Driver Ministtructure Model ..... 146
99	Terra Tek's Polyaxial Cube Test Facility for Loading 1 m <sup>3</sup> Blocks of Intact or Jointed Rock..... 150
100	Unconfined Compression Tests of Batch #2 of Scaled Tuff Simulant Grout ..... 154
101	Comparison of Failure Surfaces for SRI and TTI Grouts ..... 157
102	Stress Strain for Unconfined Compression, SRI and Terra Tek Grouts.. 158
103	Stress Difference Versus Axial and Radial Strain for Triaxial Compression, SRI and TTI Grouts..... 158
104	Vertical Closure in 2 In. Tunnel Intersections in SRI and Terra Tek Grouts..... 161
105	Vertical Closure in 4.5 In. Tunnel Intersections in SRI and Terra Tek Grouts..... 162
106	Comparison of Vertical Closure at Center of Tunnel Intersections in SRI and Terra Tek Grouts ..... 163
107	Springline Closure in 2 In. Tunnel Intersections in SRI and Terra Tek Grouts..... 164
108	Springline Closure in 4.5 In. Tunnel Intersections in SRI and Terra Tek Grouts..... 165
109	Variations of Applied Stress with Time During Proportional Loading Test #1 ..... 167
110	Stress Path for Quasi-Static Test #2 ..... 168
111	Stress Path for Dynamic Test #2..... 169
112	Variation of Applied Axial Load with Time for Dynamic Test #2..... 170

## LIST OF ILLUSTRATIONS (Continued)

Figure	Page
113	Unconfined Compression Test for Final, Selected Grout, Utelite Mix JN10B..... 172
114	Quasi-Static Tests on Jointed Specimens ..... 174
115	Dynamic Tests on Jointed Specimens, Vertical Deformation..... 176
116	Dynamic Tests on Jointed Specimens, Horizontal Deformation ..... 177
117	Dimensions of the Specimen and Test Arrangement..... 179
118	Summary of Specimen Geometry..... 180
119	Rock Bolt Configuration Relative to the Joint Pattern..... 181
120	Typical Unconfined Stress-Strain Curves for a Cylinder to Determine Modulus and Poisson's Ratio ..... 184
121	Joint Shear Test Device ..... 184
122	Friction Coefficient of Teflon to Teflon Friction Reducing System With and Without Lubrication ..... 185
123	Deformations in Test JR3 from the Photographic Analysis..... 186
124	Deformations in Test JR5 from the Photographic Analysis..... 187
125	Dial Gage Setup for Measuring Tunnel Deformations..... 188
126	Deformation of the Tunnel Opening and Surface Above the Crown for Specimen JR1..... 189
127	Deformation of the Loaded Surface with Surface Pressure for Specimen JR1 After the Original Test of the Specimen..... 190
128	Sequence of Rock Bolt Breakage in Test JR7..... 192
129	Damage to Specimen JR4..... 193
130	Damage for Specimen JR5..... 194
131	Deformation of the Tunnel Opening and Surface Above the Crown in Test JR4..... 195
132	Comparison of Tests JR2 and JR 3..... 196
133	Comparison of Tests JR2 and JR4 ..... 197
134	Comparison of Tests JR3 and JR4 ..... 198
135	Comparison of Tests JR3 and JR5 ..... 199
136	Comparison of Tests JR3 and JR6 ..... 200
137	Comparison of Tests JR5 and JR7 ..... 201
138	Comparison of Tests JR6 and JR7 ..... 202
139	Comparison of Tests JR7 and JR8 ..... 203
140	Comparison of Tests JR6 and JR8 ..... 204
141	Key Technical Issues for Deep Basing ..... 212
142	Experiment Layout in DINING CAR Crosscuts..... 213
143	Boxes Enclosing Issues from Figure 141 Where Laboratory Testing Applies..... 214
144	Recommended Text Matrix and Related Actions/Programs..... 221
145	Schematic Configurations for Tests of Rock Bolts ..... 228

## LIST OF TABLES

Table	Page
1 Comparison of SRI and WES test procedures.....	16
2 Recipe & Mechanical Parameters of Several Simulants .....	19
3 Properties of 6A.....	20
4 Rock Simulant Constitutive Parameters .....	24
5 2C4 Grout Test Matrix .....	34
6 Tunnel and Material Strengths for LSUX-52 - LSUX-57 .....	45
7 Properties of Rock-Matching Grout RGM 2C4, Low Density Rock-Matching Grout LD 2C4, and Nevada Test Site Tuff.....	57
8 Dynamic Tests on Unlined Tunnels in an Intact Medium .....	63
9 Dynamic Tests on Lined Tunnels in an Intact Medium .....	63
10 Summary of Dynamic, Unlined Tunnel Tests in an Intact Medium.....	64
11 Summary of Dynamic, Lined Tunnel Tests in an Intact Medium.....	65
12 Tests in SRI RMG 2C2 (Tuff Simulation).....	75
13 SRI RMG 2C2 Test Matrix .....	83
14 Laboratory Experiments/Material Properties.....	88
15 Unconfined Compression Strength, $\sigma_u$ , for Various Joint Configurations..	97
16 Summary of Dynamic, Unlined Tunnel Tests in Jointed Media .....	102
17 Jointed Model Test Matrix .....	106
18 Planned Test Matrix.....	137
19 Hoop and Oval Mode, Tunnel Deformations in Jointed Rock.....	139
20 Comparison of Properties of Natural Tuff, Tuff Simulant and Scaled Simulant .....	152
21 Young's Modulus, Poisson's Ratio and Unconfined Comparative Strengths of Batch #2 Tuff Simulant Grout.....	153
22 Comparison of Material Properties of Terra Tek and SRI Grouts.....	155
23 Summary of Maximum Closures in Tunnel Intersections in SRI and Terra Tek Grouts.....	160
24 Summary of Test Results .....	182
25 Persons, Other Than Members of Project Team, Contacted Individually or by Groups .....	211
26 Fundamental Questions Outstanding in Laboratory Testing .....	216

## SECTION 1

### INTRODUCTION

A review of small size testing sponsored primarily by DNA has been conducted in order to evaluate the contributions of such testing to the DNA Underground Technology Program (UTP) and to recommend a role for future small size tests. The main contributors to the program whose work is reviewed below are SRI International (SRI), Terra Tek, Inc. (TT), and the University of Illinois (UI). During the 12 years of work considered below, SRI has applied the principles of replica-scale testing. Here, geometrically scaled models of prototype tunnels are manufactured from rock simulants with selected properties that resemble those of the prototype rock. The models are subjected to prototype load magnitudes. A practical consequence of this approach is that the model tunnels tested in the laboratory are typically small, on the order of one inch. Replica-scaling is part of the databases and resources on the behavior of deep underground tunnels in rocks available to the defense community. Our review addresses: (a) what has been done in the lab, (b) what have we learned from these tests, (c) how can we apply this data to prototype situations, and (d) what should we do from this point on? The core of these questions is the basic issue: has replica-scale testing (as practiced at SRI) established itself as a legitimate means to study prototype tunnel behavior?

During about eight years of work considered below, Terra Tek has applied the principles of material scaling. In this approach, material properties and loads, as well as geometry, are all related to the prototype by the same scale factor. One of the main motives of adopting this approach is that, by making the model materials much weaker than the prototype rock, specimens with model tunnels from 2 to 6 inches can practically be tested in a laboratory. Our review addresses: (a) how several of the most important test series were conducted by Terra Tek, (b) what was learned from those tests, (c) the relationship of tests using material scaling to parallel tests using geometric scaling and (d) what should be the future role of material scaling?

Work at the University of Illinois also has used material scaling. In the context of model testing for defense applications of rock tunnels, UI basically initiated this concept. Models using continuum (Heuer) and jointed specimens (Rosenblad) were performed much earlier using somewhat different loading techniques. Additionally the materials used were even more generic than those used in the current series. As a result, no effort was expended in trying to compare these much earlier results. Furthermore, the systematic jointing and rock bolting used in the current UI series precludes comparison in any realistic way the UI and SRI tests of jointed specimens. Nevertheless, we pose a similar core question to that raised above in reference to replica testing: has material scaled testing (as practised by TT and UI) established itself as a legitimate means to study prototype tunnel behavior.

Later in the project the scope of the work was enlarged to include review of the (then) recently completed testing of tunnel intersections performed at SRI and TT. Results of this review are given in an addendum, and included as Appendix E of the report.

Professors Richard Goodman of the University of California at Berkeley and Michael Pender of University of NSW and their students have undertaken a comprehensive survey of the open literature in non-DOD and foreign publications on laboratory testing of underground openings. Although their survey produces no direct impact on the evaluation of the SRI, TT and UI test programs, it is a very good summary of the state-of-the-art in small size testing in non-DOD quarters. Results of their survey are documented as Appendix F.

## SECTION 2

### REPLICA OR GEOMETRIC SCALED TESTS AT SRI INTERNATIONAL

This section presents some of the important findings of the SRI lab test program. We begin with a discussion of the simulants used in the lab (Section 2.2), and attempt to relate them to prototype rocks which the simulants are designed to simulate. For ease of discussion, the simulants and the test data obtained are divided into two groups: continuous specimens (Section 2.3) and jointed specimens (Sections 2.4 and 2.5). By continuous rocks, we refer to rocks such as tuff which are macroscopically continuous even though they contain fissures, cracks and local weakness. Jointed rocks refer to rocks, such as granite, which can have joints or other significant "planes" of weakness.

Since the lab data depend on the testing equipment and procedures from which they are obtained, an understanding of the design and operation of the testing apparatus at SRI is important in evaluating the data. SRI has described the design, calibration and checkout, and operation of the apparatus. We have included the more significant aspects of machine design and performance in Section 2.1.

#### 2.1 EQUIPMENT DESIGN AND VALIDATION.

The main issues to be discussed are the basis for the 4" specimen size (5/8" tunnel size) and the repeatability of dynamic loading and stress environment applied to the tunnel.

Basically two types of testing machines have been used at SRI: a smaller machine which can accommodate 4" diameter x 4" height specimens, and a larger machine which can test 12" diameter specimens with a height which is adjustable between 12" and 18". (Twelve inch height was used in the earlier tests and 18" was used in later tests involving intersections and straight tunnels located within a single specimen.) The former was designed and used for the first series of dynamic tests (circa 1974), the first dynamic tests of its kind. The tunnel structures tested are mostly 5/8" diameter, and a companion test machine of similar size was used for the static tests. The larger machine was built to accommodate scale tunnels in jointed simulants (circa 1977), and the same machine was used for both dynamic and static tests. Simple tunnels typically have a 2" diameter. This machine is currently used for testing of intersecting tunnels of 1" diameter. Hence, 5/8" tunnel usually refers to the older machine and tests, and 2" or 1" tunnel usually refers to the newer and larger machine.

The earliest attempt at replica-scale testing, reported in [DNA 3610F] concentrates on dynamic tests. Static tests were performed mainly to support the evaluation of the dynamic test results. The specimen size is 4" diameter x 4" height, and the tunnel size is 5/8" diameter.

##### 2.1.1 Machine Designed In 1974.

[DNA 3610F], Appendix C, lists requirements of the dynamic test machine, which are worth re-evaluating at this time. They are:

- (1) 0.5 to 1.5 kbar peak pressure
- (2) scaled pulse shape typical of stress ranges of interest from large nuclear explosions
- (3) divergent flow at large distances from a point source
- (4) friction-free boundaries
- (5) structure in a semi-infinite half-space
- (6) overburden or lithostatic stress to 200 bars
- (7) representative material.

SRI addressed these requirements by using the following approach:

- (1) The dynamic waveforms to match are scaled pulses from profiles measured in Dido Queen and Husky Ace, which have a (scaled) rise time of 100  $\mu$ sec and a decay constant of 4x rise time.
- (2) The minimum scale size was dictated by need for a convenient tunnel size suitable for high speed photography (1/2") and for possible strain gage mounting. Hence, a 5/8" diameter was chosen.
- (3) Specimen size was determined through a trade-off between two constraints: boundary conditions and wave propagation effects.

Wave propagation effects are negligible because the transit time across the tunnel opening is short compared with the rise time of the pulse and hence loading is quasi-static. The only other requirement for dynamic loading is the ability to apply a realistic time history.

The boundary (top and side) influence effect is estimated by the elastic solution for the stress around a cavity. A wave propagation analysis provides an estimate on the overstressing effect from reflection at the boundary. This led to a specimen of 4" diameter by 4" long. For this combination of specimen and tunnel, the distance from the center of the tunnel to the nearest boundary is 4.8 times the tunnel radius. According to elastic analysis, the stress at 4.8 radii is effectively that at infinity. The wave propagation analysis indicated an overstress of about 30% at the downstream boundary for a rise time of 120  $\mu$ sec and three round-trip passages of the loading wave through the specimen. The midsection of the specimen is not significantly overstressed. These findings are confirmed by calibration tests (Fig.1).

The report also mentions that the generated peak gas pressure has a variation of  $\pm 10\%$  from the mean value, which is also taken to be the 90% confidence limits. Strain transducers vary  $\pm 3\%$  in the elastic region of material response and  $\pm 10\%$  after yielding.

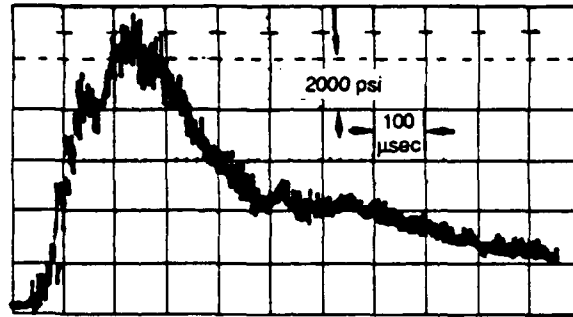
#### 2.1.2 Subsequent Improvement ([DNA 4425F-1], July 1977).

It was later found that the oscillation in the pressure pulse can be reduced by (1) constricting the holes through the specimen receiver plate and (2) placing lead shot in the copper can under the specimen to dampen the impact-rebound sequence. Figure 2 shows the improvement in the pressure environment for test DUX-74 as compared to data in Fig.1.

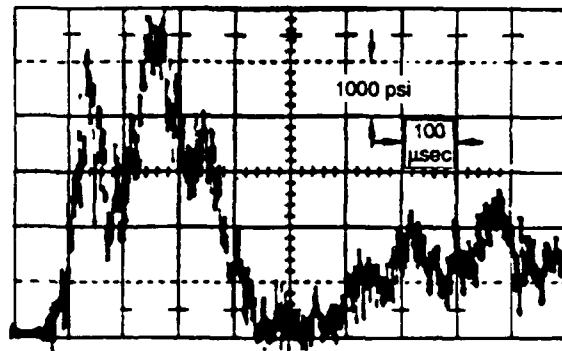
#### 2.1.3 Need For Larger Machine ([DNA 4425F-1], July 1977).

Under DNA sponsorship, SRI constructed a larger machine (for 12" diameter specimen vs. 4" specimen) because the small size limits the kind and amount of instrumentation that can be used to obtain data. Also, the small-scale structures that line the tunnel must be fairly simple because of the size limitation. SRI also argued that a large scale testing machine was needed to reduce size effects in the rock specimen. It afforded the following advantages:

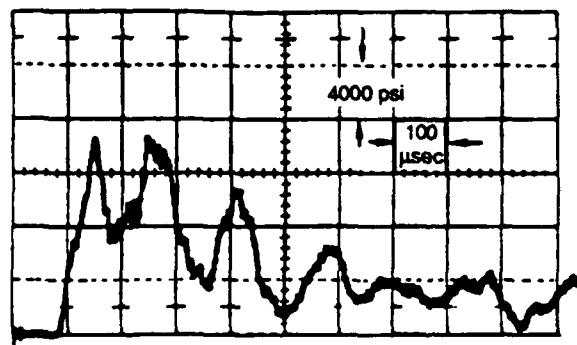
- 1) The influence of the specimen boundaries on the deformation of the rock in the vicinity of the tunnel could be observed.
- 2) Any grain-size effects are reduced.



(a) Primary Loading Pressure  
2000 psi/div.



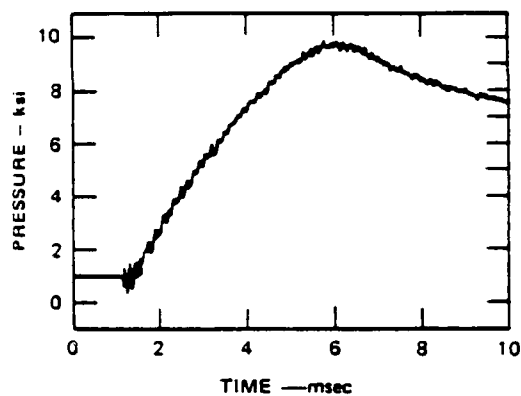
(b) Constraining Pressure (Liquid)  
1000 psi/div.



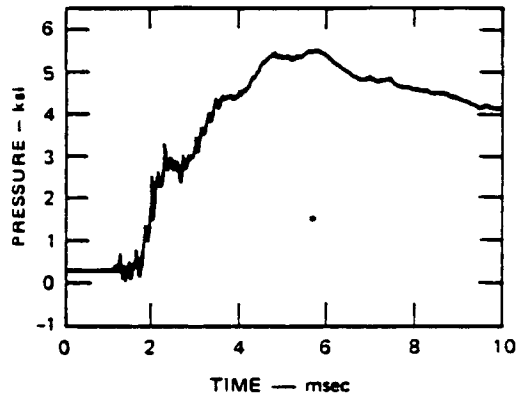
(c) Reflected Stress  
4000 psi/div.

All Sweeps: 100  $\mu$ sec/div.

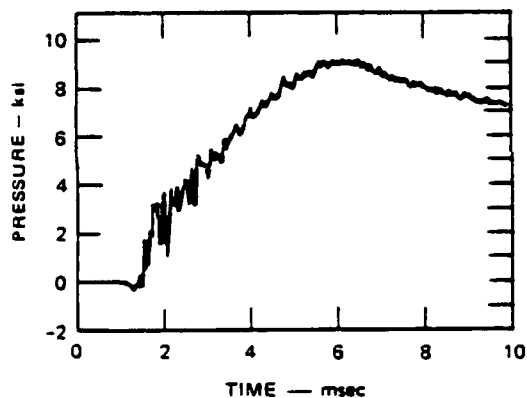
Figure 1. Trace set showing wave propagation effect arising from reverberation loading technique.



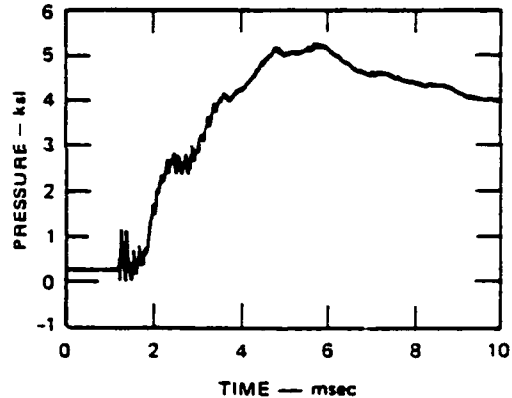
(a) P1-GAS PRESSURE ABOVE SPECIMEN



(c) P2-OIL PRESSURE IN LATERAL CHAMBER (NEAR CENTER)



(b) P4-OIL PRESSURE BELOW SPECIMEN



(d) P3-OIL PRESSURE IN LATERAL CHAMBER (SLIGHTLY LOWER)

Figure 2. Pressure data from a uniaxial strain test in the small testing machine, DUX-74, showing improvement of lateral pressure pulses.

3) Testing with the larger rock specimens, joints and bedding planes surrounding an underground structure could be modeled. Accurate simulation of the deformation of a structure in jointed rock requires that the joint spacing in the specimen be small compared to the tunnel size but large compared to the rock grain size.

#### 2.1.4 Typical Pressure Environment ([DNA 4425F-1], July 1977).

Pressure records obtained in a uniaxial strain test, LDUX-10, are shown in Fig.3. A comparison of the vertical pressures above and below the specimen (Fig.3a and Fig.3b) shows that they are near identical. This indicates that the loading of the specimen is uniform and there is no evidence of wave propagation effects along the axis of the specimen. Figures 3c and 3d show two of the records of the pressure pulse in the lateral chamber, and are also near identical. There is an oscillation superimposed on the desired lateral confining pressure, which is subsequently reduced by constricting the holes through the specimen receiver plate.

#### 2.1.5 Boundary Effects ([DNA 4023F], 1976, [DNA 5208F], 1979).

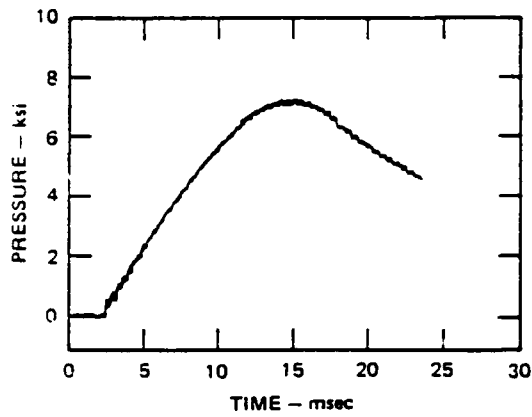
Two-dimensional elastic (uniaxial strain) analysis of a circular hole in infinite medium shows that at 4-radii distance from the hole, the stress states are very close to the free-field stresses. This is one of the factors contributing to the decision to use a 5/8" hole in 4" diameter specimen.

SRI performed static tests with different tunnel diameters (5/16", 7/16" and 5/8") to confirm the adequacy of this criterion when plastic deformation is involved [DNA4023F]. The results are shown in Fig.4, which indicates that the effect of hole size (and, hence, the proximity of the boundary of the specimen) is at most 15% on the load required to produce a specific closure. All three tests use a steel liner with a/h (ratio of tunnel diameter to liner thickness) of 25. The simulant used is HARM (HUSKY ACE rock-matching) grout and is the same material used to fill the DAC crosscuts in the DINING CAR Event. The material is chosen for its small grain size; it has an unconfined compressive strength of about 1 ksi and an internal friction angle of 5 deg as noted in DNA 5208F. From the accompanied photograph of the specimen after the tests shown in Fig.4, it is obvious that the specimen did not undergo uniaxial deformation. Furthermore, this low strength, low friction grout has no relation to any prototype rock. The test result has limited value.

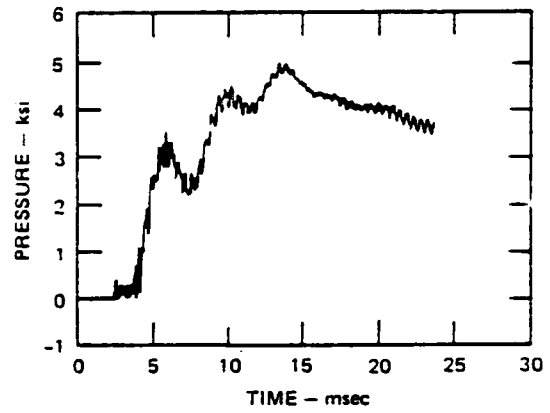
Additional information on this series of tests as well as on other tests performed to address boundary effects is given in [DNA5208F]. The data in Fig.4 are presented in a different format in Fig.5, which shows that closure does not depend on tunnel size in 2C2. As is noted in DNA 5208F, the entire specimen of 2C2 grout becomes inelastic at low stress levels. Since the inelastic region is not limited to the immediate vicinity of the opening, but extends throughout the specimen to its surface, the deformation of the opening is deemed to be influenced by boundary effects.

A parallel series in which a strong rock simulant, called 16A, is used, produces the results shown in Fig.6. The data show that greater pressure must be applied to specimens containing larger tunnels to obtain a specified crown-invert tunnel closure. It is concluded that for the stronger simulant, a plastic zone around the tunnel grows outward toward the specimen boundary. Plastic zones around larger tunnels interacted with the specimen boundary sooner than those around smaller tunnels.

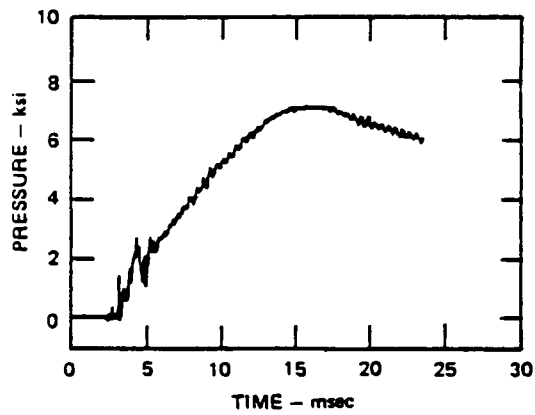
We have performed computer analysis of the effects of specimen size on tunnel response. Results of the analysis, given in Appendix C, support the conventional practice of using a simulant block which is 6 times the radius of the tunnel opening.



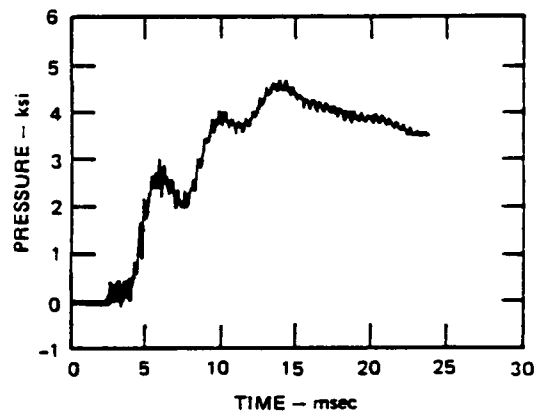
(a) P1-GAS PRESSURE ABOVE SPECIMEN



(c) P3-OIL PRESSURE IN LATERAL CHAMBER (UPPER)

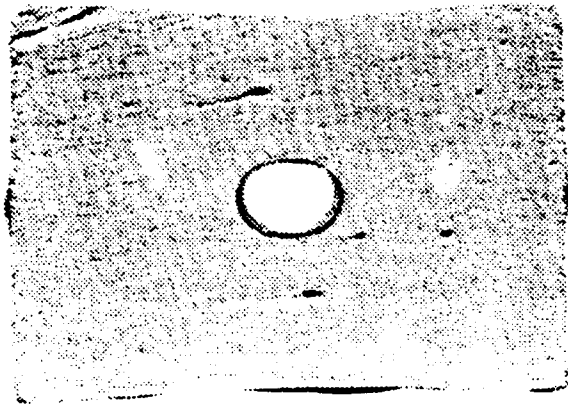


(b) P6-OIL PRESSURE BELOW SPECIMEN



(d) P4-OIL PRESSURE IN LATERAL CHAMBER (CENTER)

Figure 3. Pressure data from uniaxial strain test LDUX-10.



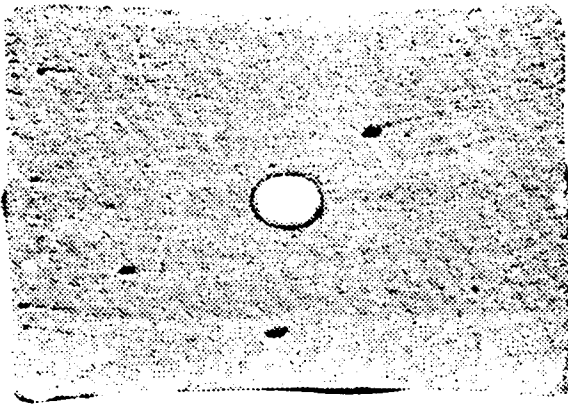
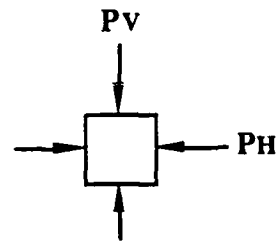
(a)  $D = 5/8"$  (SUX-45)

$P_{VMAX} = 4250$  psi

$P_{HMAX} = 1880$  psi

$\Delta D_V/D = 21\%$

$\Delta D_H/D = -14\%$



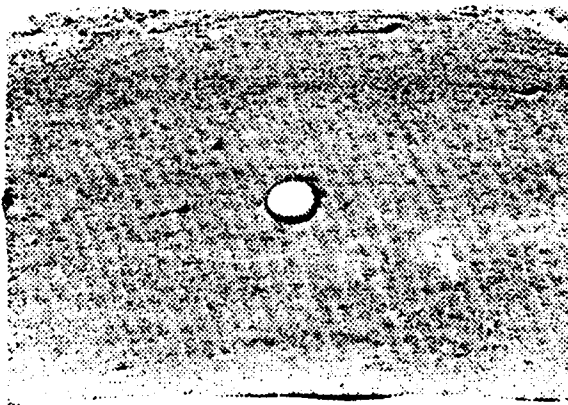
(b)  $D = 7/16"$  (SUX-46)

$P_{VMAX} = 4000$  psi

$P_{HMAX} = 1690$  psi

$\Delta D_V/D = 21\%$

$\Delta D_H/D = -12\%$



(c)  $D = 5/16"$  (SUX-42)

$P_{VMAX} = 3500$  psi

$P_{HMAX} = 1420$  psi

$\Delta D_V/D = 16\%$

$\Delta D_H/D = -12\%$

Figure 4. The response of tunnels with various diameters to static uniaxial strain loading.

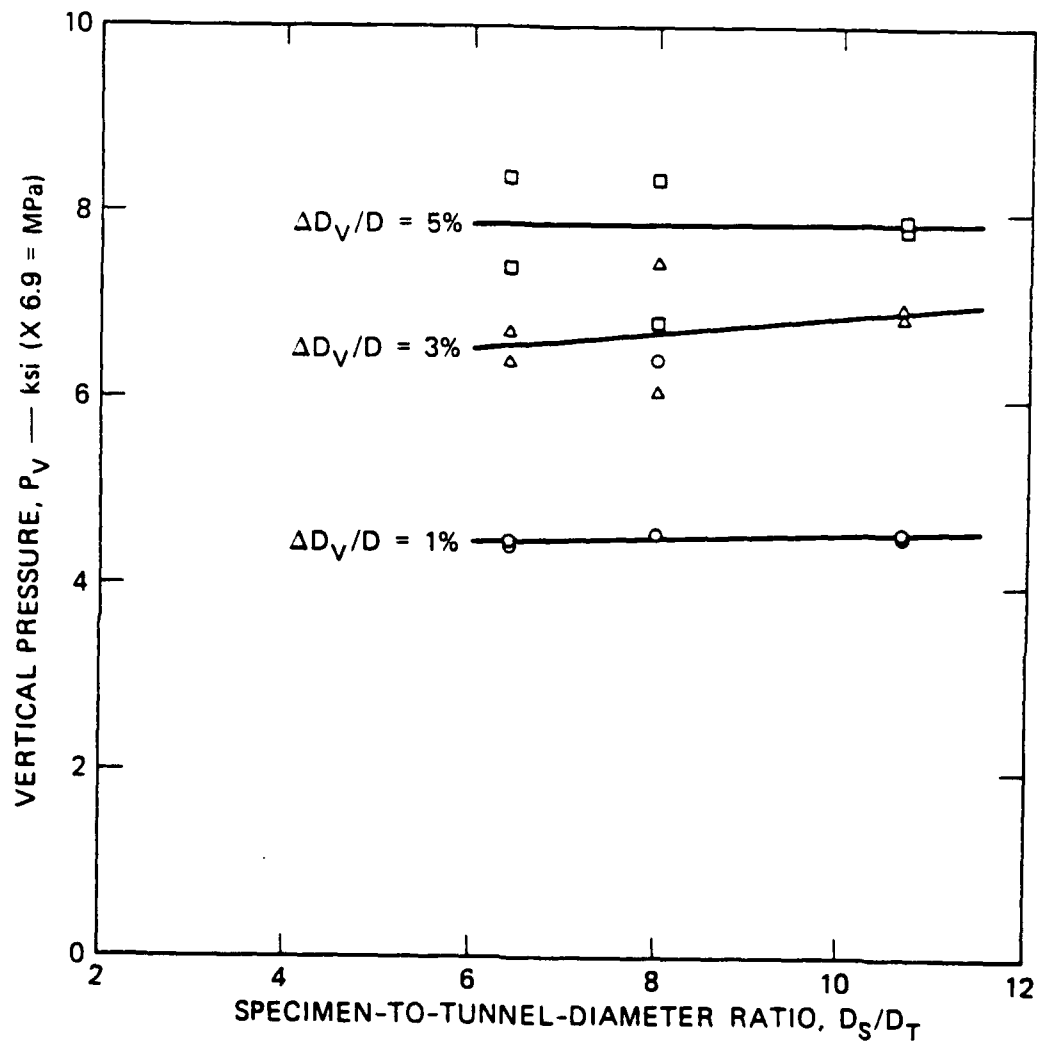


Figure 5. Vertical pressure to produce specified crown-invert tunnel closure versus specimen-to-tunnel diameter ratio—2C2.

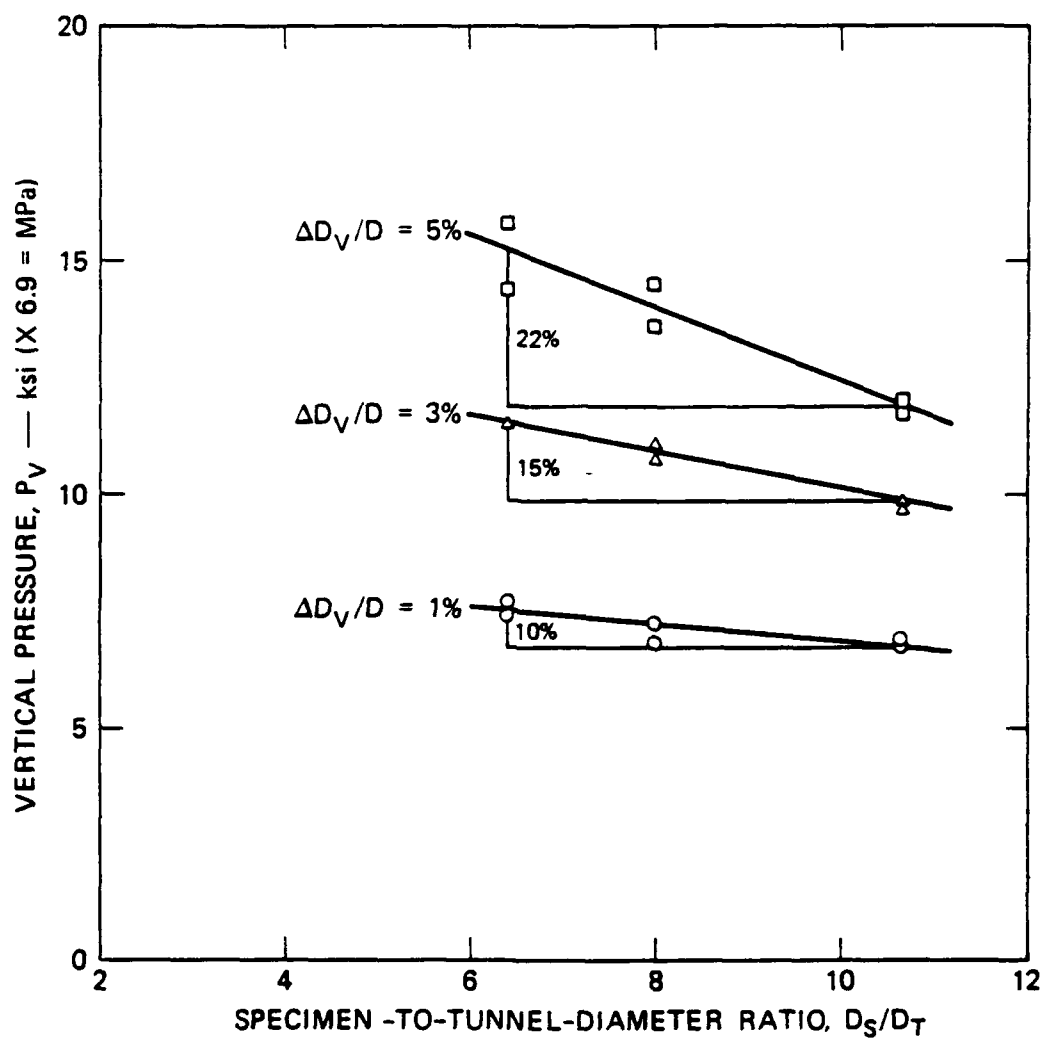


Figure 6. Vertical pressure to produce specified crown-invert tunnel closure versus specimen-to-tunnel diameter ratio—16A rock simulant.

### 2.1.6 Test-To-Test Variation ([DNA 4023F], 1976).

The same figure (Fig.4) contains results from replicas of tests for tunnel diameters of 5/8" and 7/16",  $a/d=25$ . By comparing these replicate results, the test-to-test variability is assessed to be within  $\pm 8\%$ .

Replicate results are also obtained for tunnel diameter 5/8",  $a/d=50$ , as part of a larger test series (Fig.7, open and dark circles). In these tests, the simulant is saturated 6B grout, but the pore water is allowed to drain. Variability measured by the range in pressure for a specific closure is about 10% (e.g., an uncertainty band of 2 ksi for a loading level of 20 ksi).

Test SUX-90 was performed to investigate the difference in tunnel closure reported by SRI and WES for the uniaxial strain loading of 2C2 specimen with a liner of  $a/h=4$ . It appears that this test is the only one conducted to date for such purpose. The discrepancy in test results is shown in Fig.8; SRI considered the discrepancy to be greater than can be accounted for by experimental error.

Several possible causes for the discrepancy are identified as:

(1) Difference in scale. The WES result is from a 30" diameter rock specimen with 4" openings (inclusive of liner), 7 times larger than the 5/8" openings used at SRI.

A single comparison at SRI between a test with a 12" diameter 2C2 rock and a 4" diameter rock showed loading pressures to be 25% smaller in larger rock (Fig.9). These tests have a 6061-T0 aluminum monocoque liner with  $a/h=11.5$ ; diameter of opening is 2" (see [DNA 4380F], February 1978). Since the only differences in these tests is in rock size and test time relative to size, this suggests that the effect of scale alone may be dominant.

(2) Differences in simulated rock properties. Curing could be different at large and small sizes. WES tunnel was cast in place while the SRI specimen was bored into place.

(3) Differences in loading method. At SRI, lateral loading was applied with a hydraulic pressure PH which was increased with increasing vertical pressure PV to maintain zero hoop strain at the rock specimen surface. At WES, lateral loading was applied by mechanical confinement with 7" thick steel rings. The effect of compliant lateral boundary is investigated by another SRI test, SUX-90, which shows that the boundary constraint has significant effect on tunnel closure (see Fig.10).

(4) Differences in test procedure. There are other differences related to test procedure which are summarized in Table 1. Information on WES testing is not complete.

## 2.2 CHOICE AND MECHANICAL PROPERTIES OF SIMULANTS.

### 2.2.1 Need for Simulants.

As stated by SRI investigators, rock simulants are used because they should have less specimen-to-specimen scatter than real rocks, and because they allow the experimenter to select grain size as well as the various constitutive parameters ([DNA 5208F]). We quote:

"We decided to use a simulated rock to reduce the problem of statistical variation between samples. In selection of a rock simulant, scaling of geometric features cannot easily be extended to the microstructure. We considered it enough for the grain size of the aggregate used to be small relative to structure size. The grout was specifically designed to simulate the general characteristics

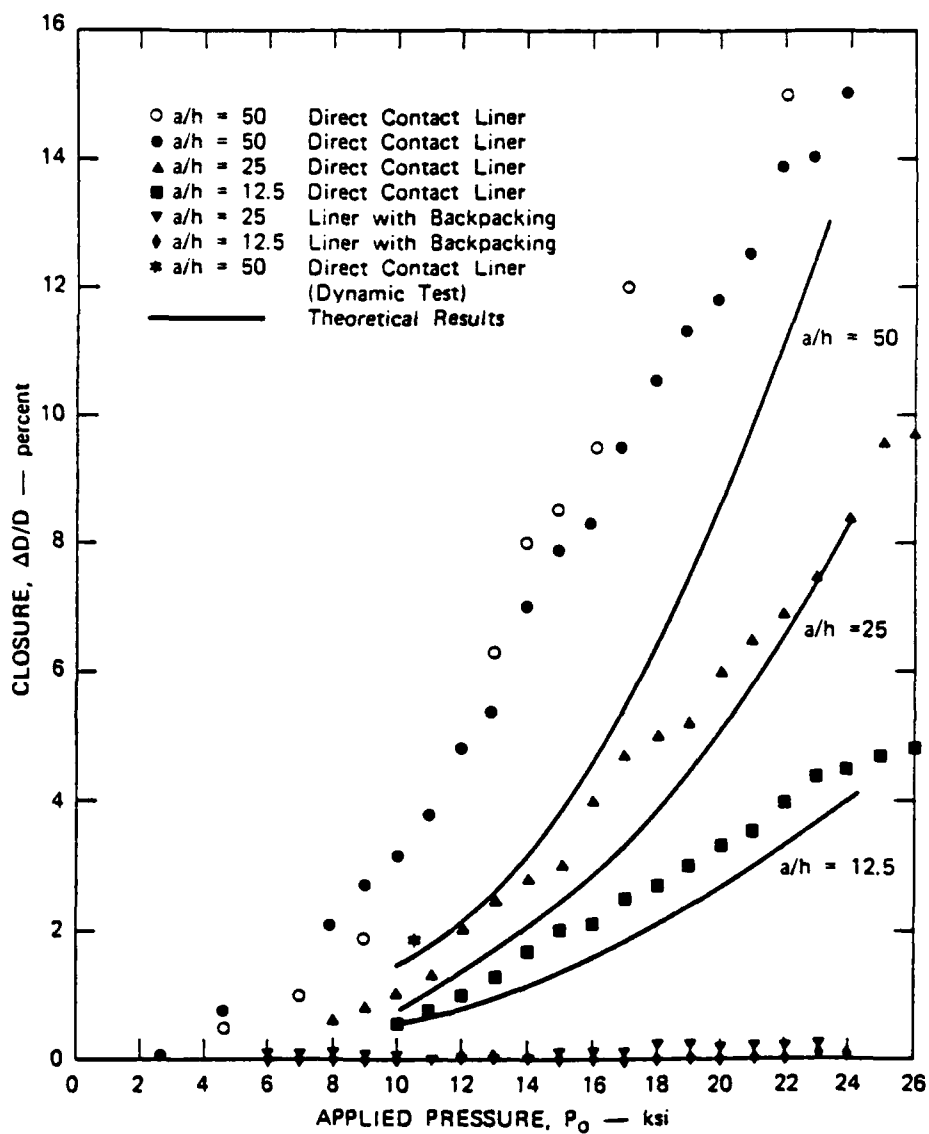


Figure 7. Experimental and theoretical closure versus applied pressure for static, isotropic loading of 6B rock.

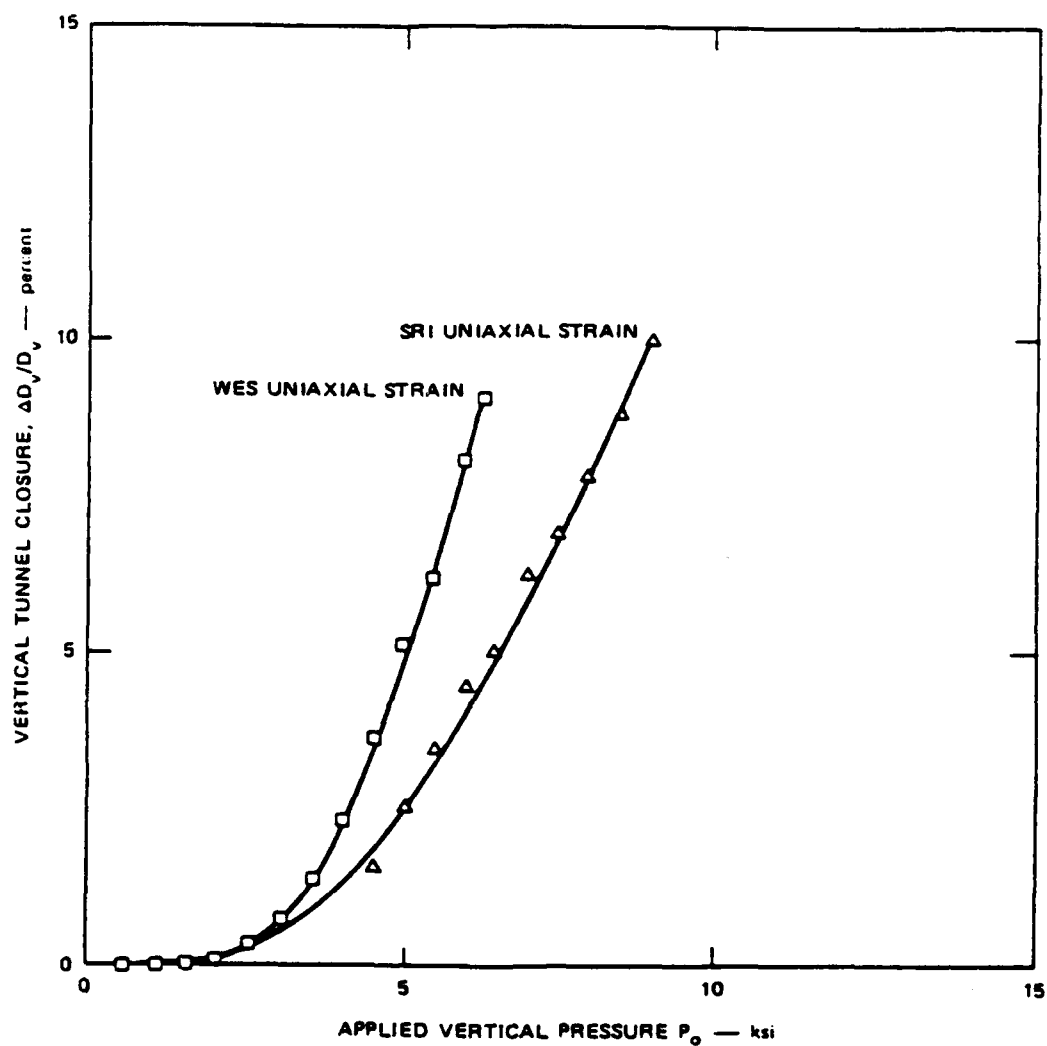


Figure 8. Vertical tunnel closure versus applied vertical pressure-- comparison of data obtained by SRI and WES for static uniaxial strain loading of SRI RMG 2C2, A 6061-T0 liner,  $a/h = 4.0$ .

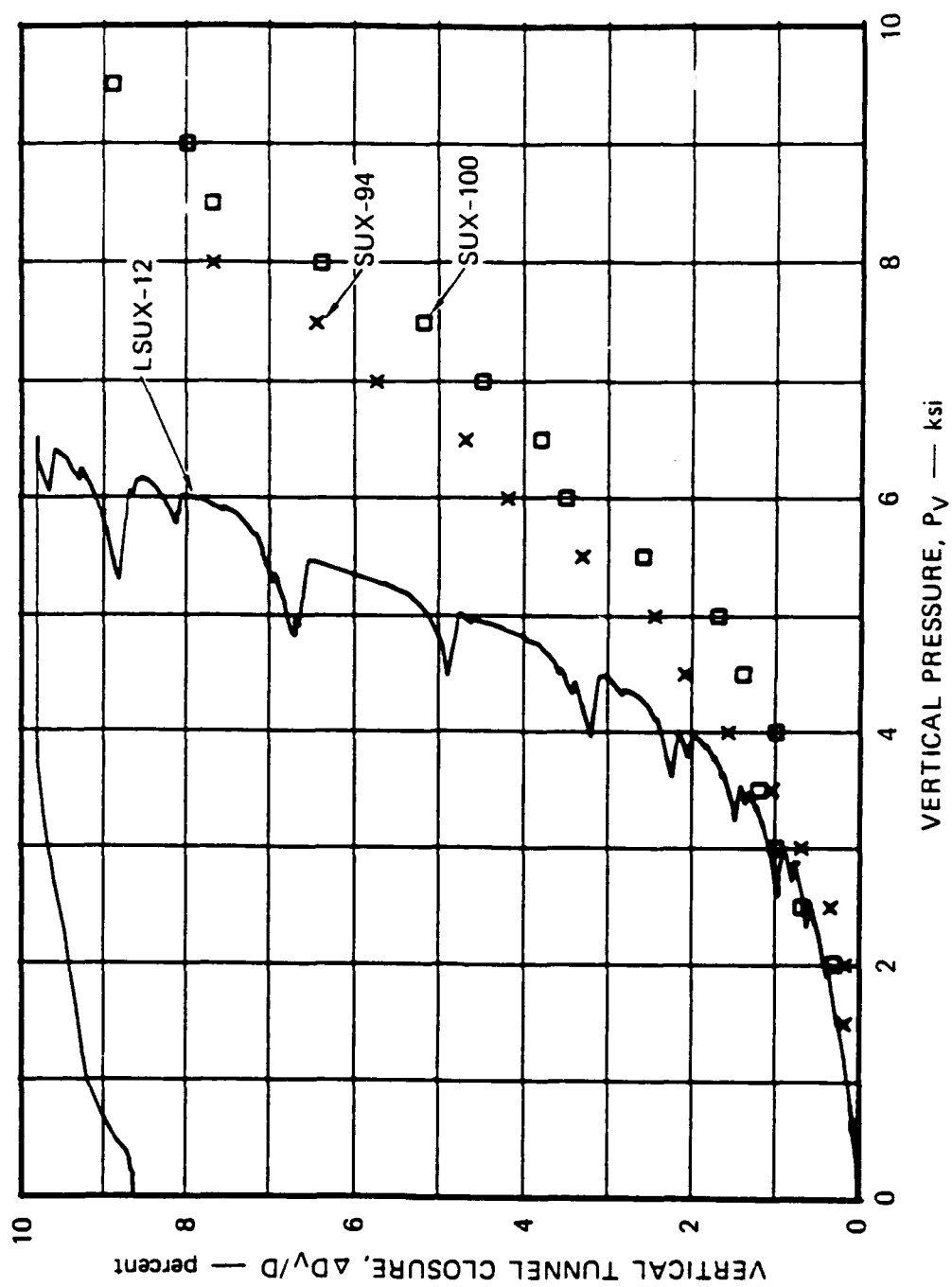


Figure 9. Vertical tunnel closure versus vertical pressure for uniaxial strain loading of saturated SRI RGM 2C2, 6061-T0 aluminum liner,  $a/h = 11.5$ .

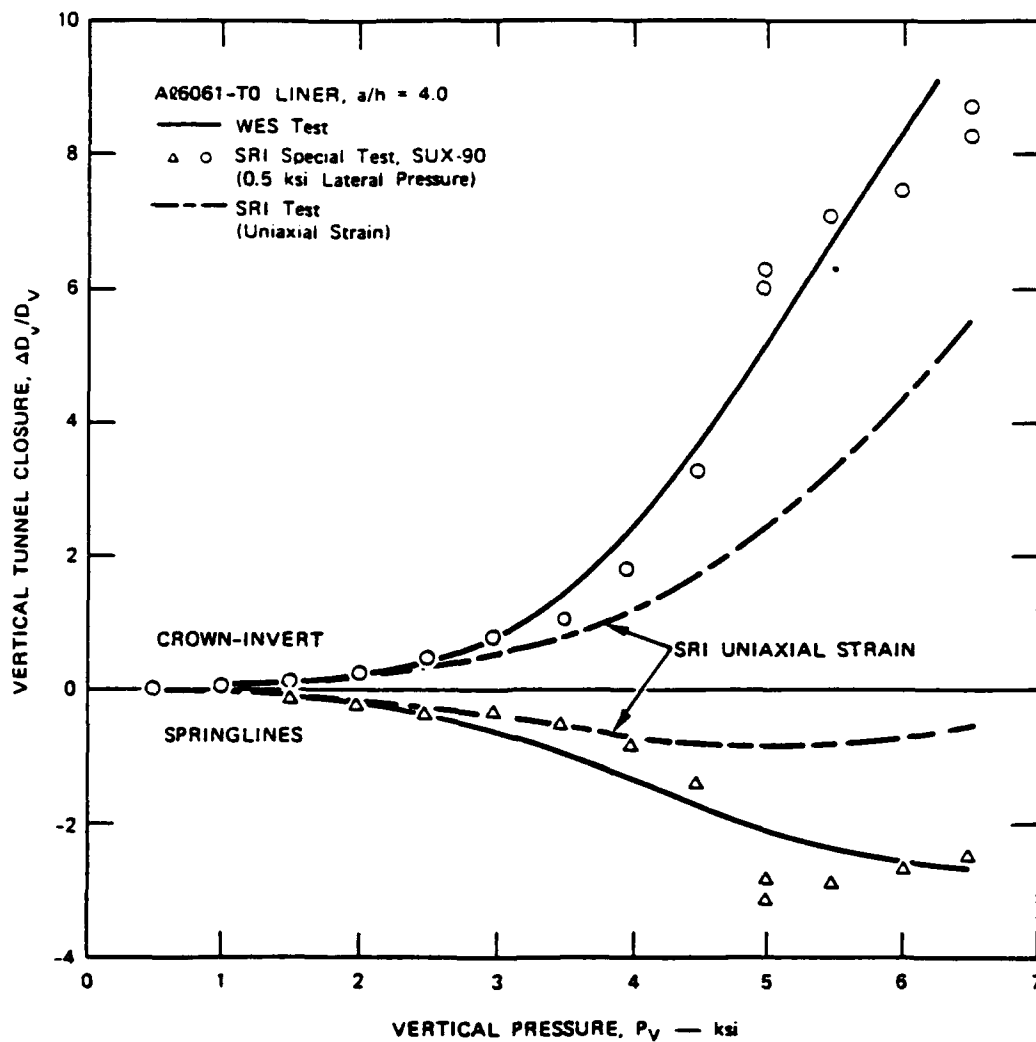


Figure 10. Comparison of tunnel closures in WES test and special SRI test, SUX-90, in which lateral boundaries of rock are allowed to move out 0.1% (reached at  $P_v = 4.7$  ksi).

Table 1. Comparison of SRI and WES test procedures\*.

Procedure	SRI	WES
1. Source of ingredient materials for 2C2 simulant	WES stores at NTS <sup>†</sup>	Local Vicksburg supply
2. Rock specimen size <sup>‡</sup>	4-inch dia. x 4-inch tall	30-inch dia. x ?
3. Specimen fabrication <sup>‡</sup>	Cast in 15-inch length, cut and grind into three 4-inch specimens	Cast in machine and cured in polyethylene bag
4. Tunnel fabrication <sup>‡</sup>	Drill, then counterbore at ends for end fittings	Liner cast in place
5. Liner installation	Insert liner, fill back about 30 mils on radius with pourstone	
6. Method of rock saturation	Keep rock submerged in water between all stages of preparation and assembly. Time to insert into sealed unit for test is about 3 min	?
7. Method of porewater drainage	Allow leakage into tunnel at ends and at weep holes near each end	?
8. Vertical Load	Oil pressure across thin diaphragm	Ram and 10-inch thick steel platten
9. Lateral load <sup>‡</sup>	Oil pressure to maintain zero sum of strains from two circumferential gages on copper can. Can is set into intimate contact with rock by initial 500 psi seating pressure. Individual strains are about 50 m strain at 5% closure	Reaction force through watertight polyethylene bag to steel confining rings
10. Transition between rock lateral pressure and tunnel ambient pressure	O-ring seals in end fittings	?
11. Test time	1 to 1½ hours	?

\*Standard laboratory procedures, such as methods for measuring pressures and displacements, are not listed.

<sup>†</sup>For special comparison tests with WES, specimens were cored by WES from block made of same raw materials as for WES models.

<sup>‡</sup>These procedures have a known direction of influence, tending to cause more deformation (lower critical pressures) in the WES tests than in SRI tests.

of native rocks of interest. Grout properties can be varied over a range wide enough to examine the effects of uncertainties in native rock characteristics." (DNA 3610F)

### 2.2.2 History of Simulants.

It is helpful to look back at the history of simulant evolution, and gain some insight on how past events took place. The following is excerpted from a summary written by Dr. J.L. Merritt of BDM. The complete summary is included as Appendix D of the report.

#### Simulant For Stemming

The original motive for developing simulants was to contain the explosion. Hence, materials with very low shear strength were used since they could literally flow into the cracks, either naturally formed or created by the explosion, in the medium. The low shear strength materials are recently referred to as superlean grout.

#### Simulant For Laboratory Scale Programs

Containment experiments were soon conducted in the lab (SRI). The properties of the simulant were selected to match the important constitutive properties for the conditions expected near the explosion. The material used for these early tests was designated 2C2 tuff simulant. As more data on tuff became available at various induced stress levels of interest, the simulant was improved to become 2C4 tuff simulant.

When the first dynamic tests were performed, the emphasis had shifted to hard rock. Consequently, the simulant used is called 6A, and was taken from blocks of such grouts left over from the Air Force Hard Rock Silo program (circa 1968-1970).

#### Simulant Used In Field Tests

For stemming purposes, the principal criterion for designing a rock matching grout was the matching of the acoustic impedance to that of the natural material. However, in the DINING CAR experiment, it was discovered that a grout (HUSKY ACE Rock Matching, HARM, grout) with an acoustic impedance match was not sufficient. The low strength of the grout led to failure of some of the structures. Consequently, a number of tests were made of various materials with emphasis on matching the hydrostat and the failure envelope, resulting in a material called ME-8-11 for MIGHTY EPIC. This material has an elastic modulus of 1.E6 psi, unconfined compressive strength of 2.3 ksi, and a friction angle of 11 degrees.

Analytical evaluations of the response of the structures in MIGHTY EPIC were made to assess the presence of the ME-8-11 around the structures, and the effect was found to be small. As a result, ME-8-11 was concluded to have reproduced the important parameters of natural tuff, and it was also used to surround the structures in MIGHTY OAK. ME-8-11 has never been used in the lab as a tunnel specimen.

#### Simulants Used In Deep Basing And Targeting

Early siting studies by the Air Force Deep Basing program indicated that sandstone would be a likely medium. Consequently, SRI and WES developed simulant 6B to represent the properties of generic sandstone. At the same time, there was interest in granitic media and the 16A simulant was developed. The angle of friction for 16A was probably lower than that of most intact granitic rocks.

### Simulants For Recent Lab Tests

SRI has developed the high friction (HF) simulants for studies of tunnel intersections. These series of tests also apply to some of the sites where targets of interest may be located.

#### 2.2.3 Summary Of Simulant Properties.

Properties of many simulants which have been used in lab testing are summarized in Table 2. The mix recipe and physical properties are listed together with the references from which the data are extracted. In the following we present the important stress-strain data and notes which are also available from the references. Other simulants are tested but not used widely in structural tests; e.g., 2A, 2B, 2C, 2C1, 2C3, SLG, HSSL-1A, DSRMG-2 ([DNA 3935F]), LD2C4 ([DNA 6121F]), and GS3 ([DNA 5601F]), and data on these simulants are, therefore, not reproduced here.

#### Simulant 6A For Hard Rock (DNA 3610FL 1975)

Grout 6A (6A4 refers to a large block of 6A material labeled No.4) is a grout material left over from the Hard Rock Silo Program, which is judged by WES to be the best approximation to the specifications. It is used in the first series of dynamic tests involving jointed specimens.

General properties of 6A4 provided by WES are given in Table 3. Triaxial test data are given in Fig.11, where the failure envelope indicates the friction angle  $\phi=30$  degrees. Figure 12 summarizes the preliminary stress-strain data obtained from WES for two uniaxial strain tests on the 6A4 material. Figures 13 and 14 summarize the  $K_0$  consolidation data from the two uniaxial-strain tests ( $K_0$  is the ratio of lateral to axial stress needed to maintain zero lateral strain. For elastic conditions,  $K_0=v/(1-v)$  where  $v$  = Poisson's ratio. This provides a relatively unambiguous measure of Poisson's ratio whereas strain measurements and lateral displacement measurements are necessarily limited and at times misleading.). The variation in test data from one sample to the other demonstrates the variability of material properties within the 6A4 block. Although this simulant appears to have properties that correlate well with native rock, it was subsequently abandoned for reasons that are unclear.

#### Simulant 6B And 16A For Medium Rock. And 2C2 For Soft Rock (DNA 5208F, 1976, from WES)

Simulants 6B and 16A have strengths representative of medium strength rock, whereas 2C2 has material properties similar to ash-fall tuff found at the Nevada Test Site. The primary difference between the two medium-strength rock simulants and the ash-fall tuff simulant is the lower angle of internal friction for ash-fall tuff (see Table 4).

The major difference between the 6B and 16A rock simulants is not in their constitutive parameters but in the size of the largest sand particles used in the simulant. Both are made from commercial sand, but larger grains are present in the 6B formulation. All grains passing through a No.6 sieve are used in the 6B formulation (hence the designation 6), while only those passing through a No.16 sieve are used in the 16A formulation (hence the designation 16).

The B in 6B designates that it is the second formulation studied by WES. The A formulation, 6A, is stronger and used earlier in the program. All three simulants are used in the intact specimens, but only the 16A simulant is used in the study of jointed specimens.

Table 2. Recipe and mechanical parameters of several simulants.

Physical	6A(WES)	6B(WES)	16A(WES)	SRIRMG 2C'2 (Wet-Dry)	TT 2C4	SRI HF4	TUFF	OTHERS 2A 2B 2C 2C1 2C3 SLG HSSL-1A DSRMG2 LD21C4 GS3
Unconf. Strength	8370 psi	3600	3740	3100-3680	3970.	4000	3530	
$\sigma_u$								
Tensile Strength	470 psi				530.		1920.	
$\sigma_t$								
Angle Frict. $\phi$	30°							
Young's Mod E	3.3E6 psi	20-36	29.	2.5-15		30		
Young's at 0.5 $\sigma_u$	2.5E6 psi				2.64E6	3.5E6	1.67E6	
Shear Mod $\mu$	-	0.8-1.6E6	1.25E6	0.47E6	1.E6		0.63E6	
Seismic Vel c	12,500 fps				10,800 fps		9,680 fps	
Density, $\rho$	2.2-2.3 (g/cc)		.23	2.05	.28		1.87	
Poisson Ratio $\nu$	0.165	.25		.2-.23			.32	
Press Coeff. $N_\phi^*$		2-3.8	2.88	1.09				
Density %				43%	39	2-10	34	
Porosity %		B-1, B-2, B-3-7			7-21			
Figs.	B-1, B-2, B-4							
Refs.	DNA3610F	B-1, B-2, DNA5208F DNA4023F	DNA3935F DNA4425F DNA6121F TT81-56	DNA3935F DNA4425F DNA6121F TT81-56	DNA3935F DNA4425F DNA6121F TT81-56	SRIPR 9-11 PYU-3771	SRIPR 9-11 PYU-3771	DNA3935F DNA6121F DNA5601F
Mix (% by Wt)	6A	6B	16A	2C2	TT 2C4	SRI HF4		
Pc, Type I-II	20.8	10.25	18.61	31.14	32.691	17.875		
Limestone Sand	28.25	81.04	61.37					
Granite Sand	38.5		6.62					
Monterey Sand				20.86	21.896	#10 18.688 #16 23.0 #30 17.188 #60 10.125		
Barite								
Bentonite	.05			19.89	20.848			
CFR2				2.73	2.837			
Water	12	8.71	13.40	0.076	21.65	13.125		
* $N_\phi = (1 + \sin \phi) / (1 - \sin \phi)$								

Table 3. Properties of 6A.

<u>Physical Properties</u>	<u>Values Supplied by WES</u>
Unconfined compressive strength, $\sigma_u$	8370 psi
Angle of internal friction, $\phi$	30°
Young's modulus, E (initial)	$3.3 \times 10^6$ psi
Young's modulus, E ( $0.5 \sigma_u$ )	$2.5 \times 10^6$ psi
Seismic velocity, C	12,500 fps
Density, $\rho$	2.2-2.3
Poisson ratio, $\nu$	0.165
Tensile strength, $\sigma_{\text{tensile}}$	470 psi

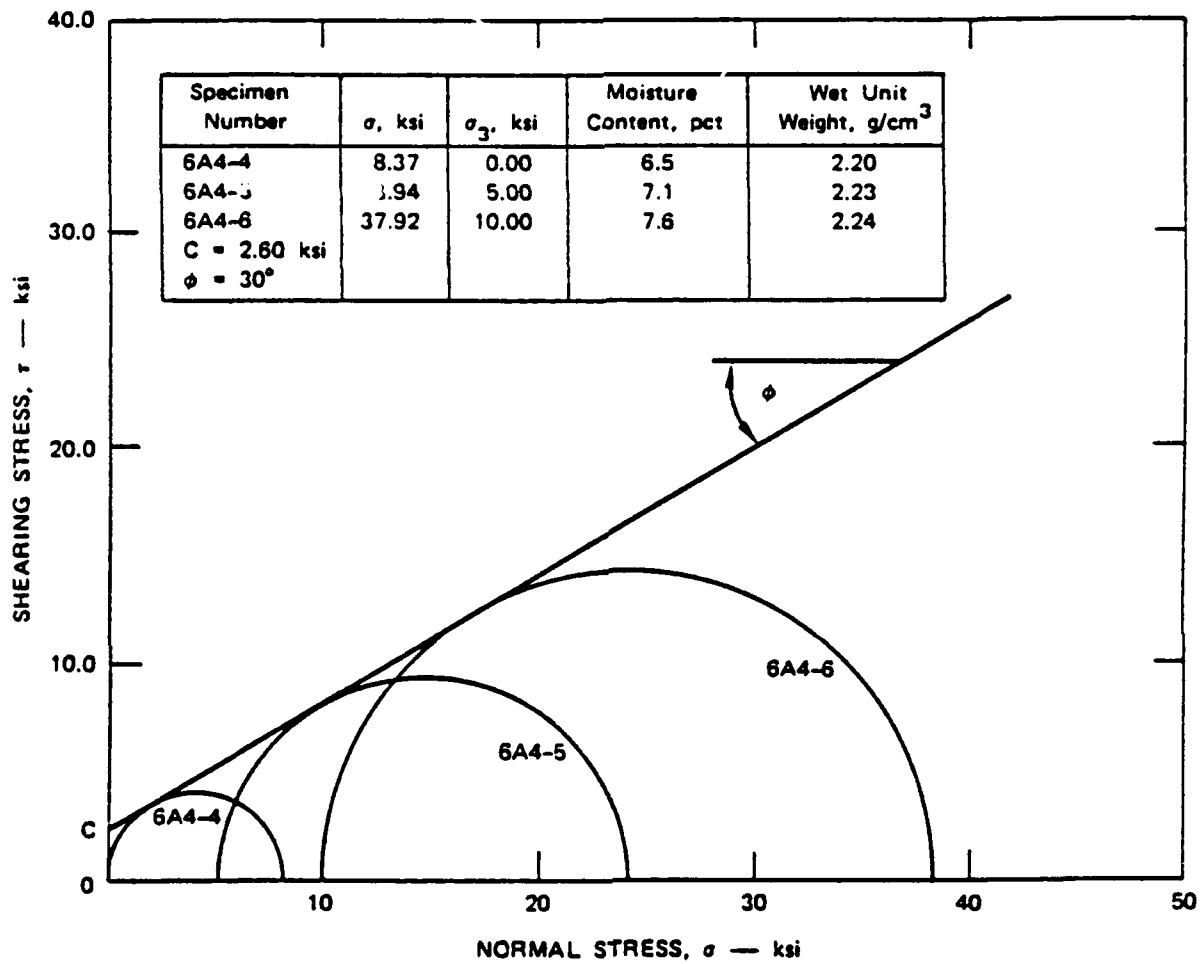


Figure 11. Mohr failure envelope. (R. L. Stowe, Waterways Experiment Station)

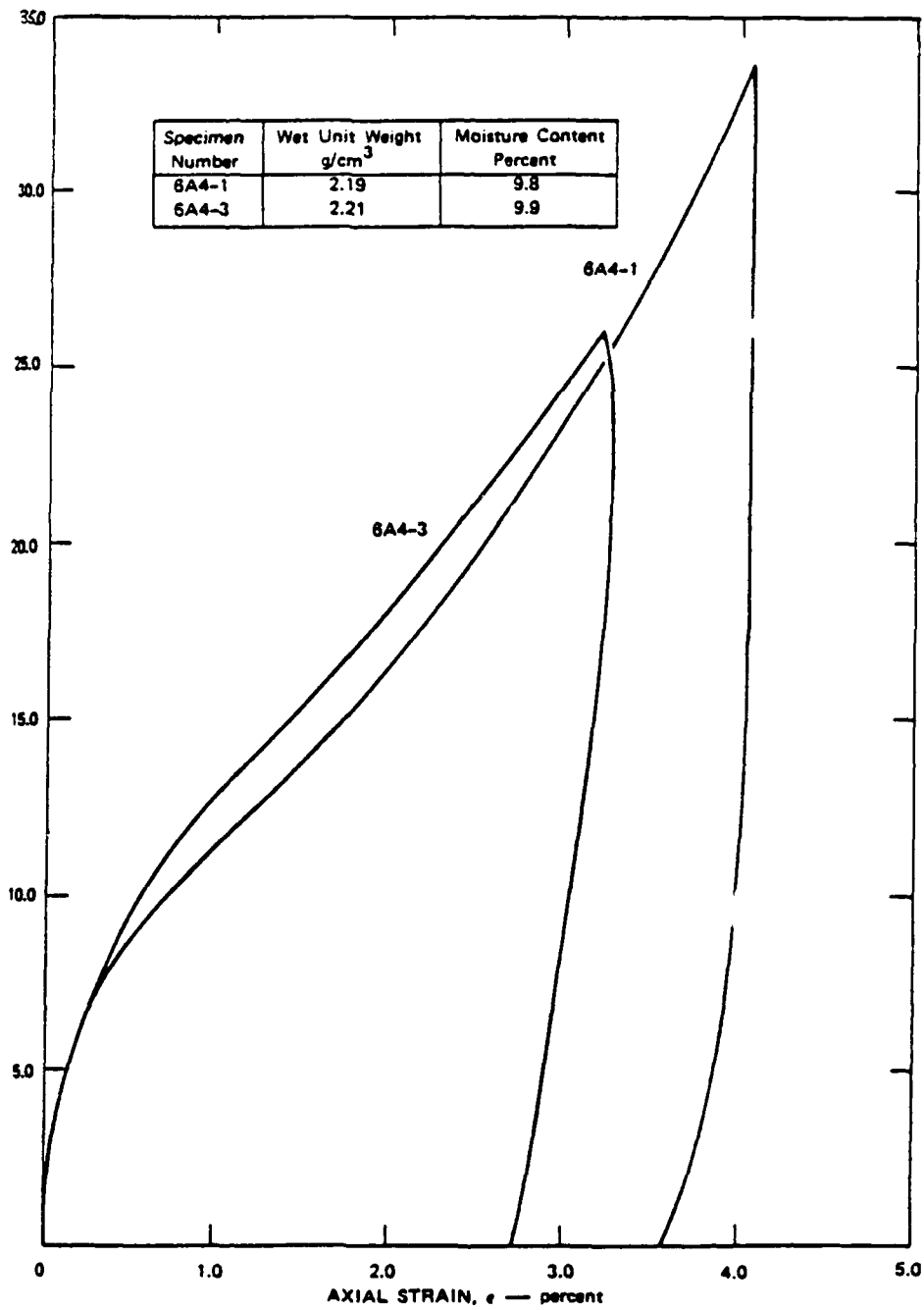


Figure 12. Uniaxial strain condition stress-strain relationship.  
(R. L. Stowe, Waterways Experiment Station)

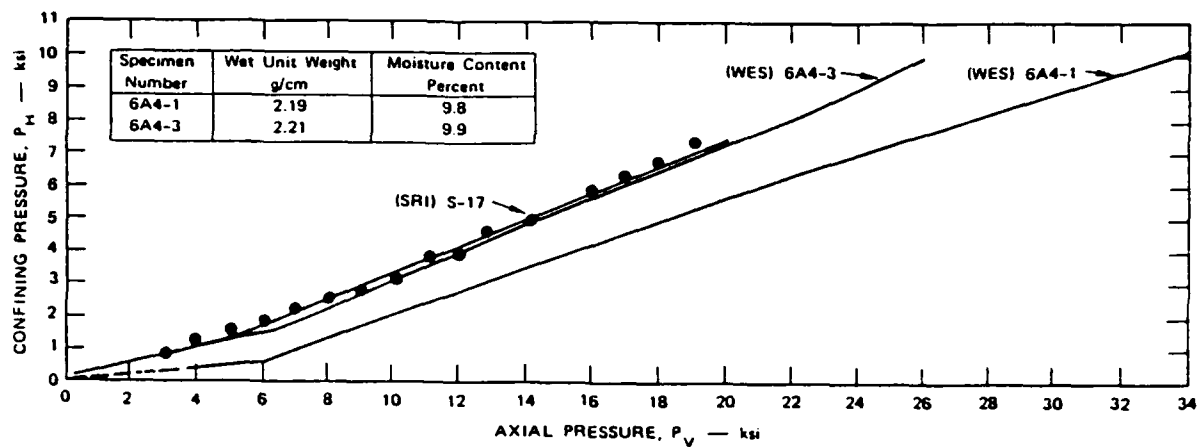


Figure 13. Confining pressure versus axial pressure for uniaxial strain tests ( $K_0$  consolidation test). (R. L. Stowe, WES)

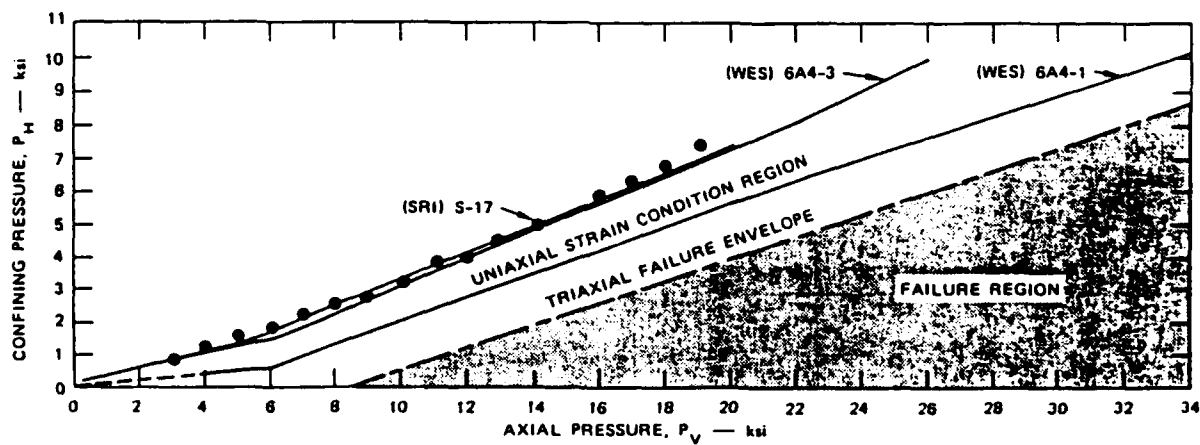


Figure 14. Composite of confining versus axial pressure relationships for uniaxial strain and triaxial failure conditions. (R. L. Stowe, Waterways Experiment Station)

Table 4. Rock simulant constitutive parameters.

Parameter	6B	16A	SRI RMG 2C2
Water saturation (%)	0	100	100
Shear modulus* $\mu$ ( $10^6$ psi) (GPa)	0.80→ 1.6 5.5 →11.0	1.25 8.6	0.47 3.2
Poisson's ratio, $\nu$	0.25	0.23	0.23
Compressive strength,* $\sigma_u$ (ksi) (MPa)	3.60 24.8	3.74 25.8	3.68 25.3
Friction angle* $\phi$ (deg.)	20→36	29.	2.5
Pressure coefficient, $N_\phi =$ ( $1+\sin\phi$ )/( $1-\sin\phi$ )	2.0→3.8	2.88	1.09

\* Modulus and friction decrease with increasing stress. Range given for 6B corresponds to stress range in tunnel tests, for later comparison with theory.

### Properties of Saturated 6B Rock

Material property tests on 6B rock simulant were performed by WES and by SRI ([DNA 4023F], 1976) on samples of the rock in the fully water-saturated condition. Stress-strain curves for unconfined rock are shown in Figure 15. The offset between the SRI and WES is caused by the strain required to seat the specimen. The unconfined strength and average modulus from the curves are in good agreement. Both curves indicate an unconfined strength of 4000-4500 psi and an average elastic modulus slightly over  $2E6$  psi.

Figure 16 shows a plot of horizontal pressure versus vertical pressure for uniaxial strain, and Fig.17 is a plot of axial stress versus axial strain from WES uniaxial-strain tests on two specimens of the 6B rock.

Mohr failure envelopes for the saturated rock at various test ages are shown in Fig.18. The rock was kept moist during aging, and as the test age increases, the moisture content and degree of saturation increase. This causes the amount of pore water pressure that develops during the test to increase in undrained tests. The angle of internal friction for the effective Mohr failure envelope would be between 30 and 40 degrees for low stress levels, but the friction angle is considerably reduced at high stress levels (10 ksi).

### Properties of Dry 6B Rock

Material property tests were also performed on samples of the rock in the dry (20% saturation) condition. Figure 19 shows the stress-strain curve provided by WES for unconfined rock. The elastic modulus and unconfined compressive strength are slightly lower than the values for the saturated rock. The curve indicates an unconfined strength of 3000-4000 psi and an average elastic modulus of about  $2E6$  psi.

Figure 20 shows a plot of horizontal pressure vs. vertical pressure for uniaxial strain. These data are very close to those for the saturated rock. Figure 21 shows a Mohr failure envelope obtained by WES for dry 6B rock. Since no pore water pressure is present, the friction angle remains high (36 degrees) for normal stresses up to 2 kbar.

These data do not address uncertainties in properties or sample-to-sample variation. Also they are obtained from static testing and do not provide information on the effect of loading(strain) rates.

### Simulants 2C2 And 2C4 For Tuff (ITT 81-56)

As mentioned previously, 2C2 and 2C4 were used extensively as models for tests involving stemming for underground nuclear tests and, hence, are investigated quite thoroughly.

The data given in the following on 2C type simulants are obtained from tests conducted during the period from August 1980 to April 1981. (Tests on 2C2 simulant are described in [DNA 4425F], 1977 and [DNA 3935F], 1976. Tests on 2C4 simulant are described in [DNA TR-81-56], 1981 and [DNA 6121F], 1982). Ninety-seven (97) tests were run on 2" diameter by 2.5" cylindrical samples of the grout simulant in seven categories: uniaxial strain, strain rate, hydrostatic compression, triaxial compression, permeability, special drainage, and physical property. Our review is focused on uniaxial, triaxial, and strain-rate test data. We wish to know how consistent the mechanical properties of 2C4 are from sample to sample, and if the properties are sensitive to loading rates. Strain rates range from  $10^{-4}$  to  $10^{-1}$ /sec, and the confining pressure ranges from .069 kb (1ksi) to 4 kb. It is reported that the axial and lateral strains are measured to within .025% accuracy, the stress difference to  $\pm 20$  bars, and the strain rates to  $\pm 10\%$ .

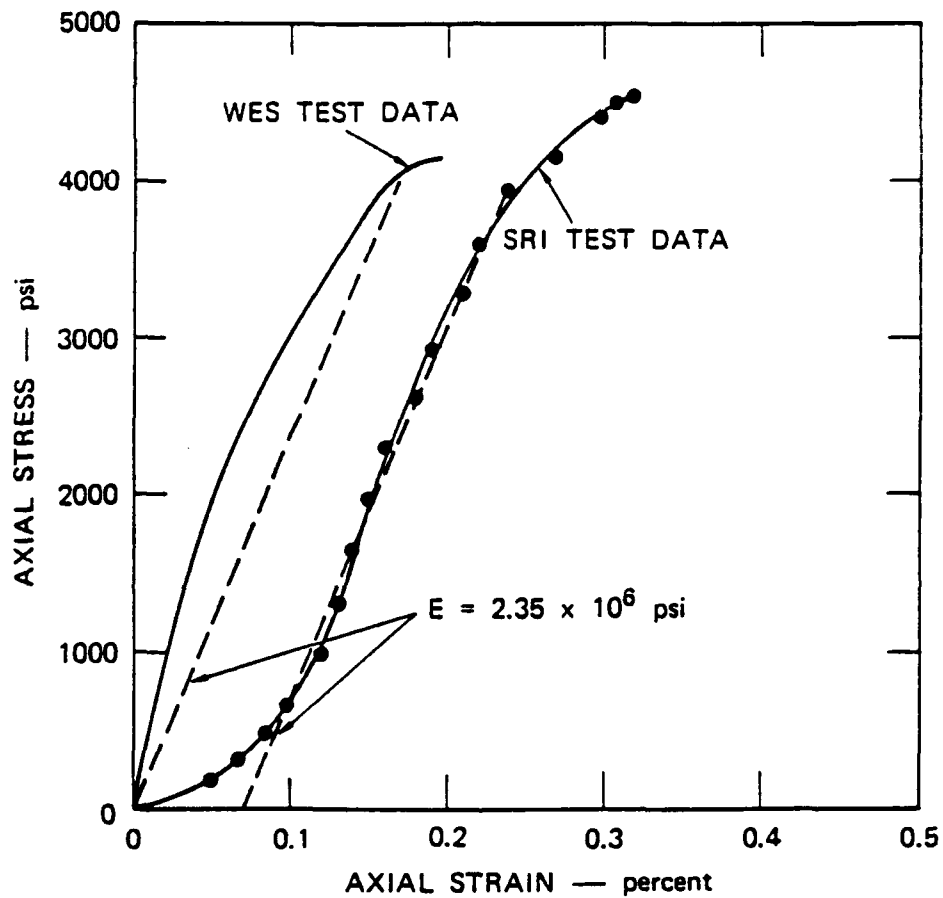


Figure 15. Stress-strain curves for moisturized 6B rock simulant.

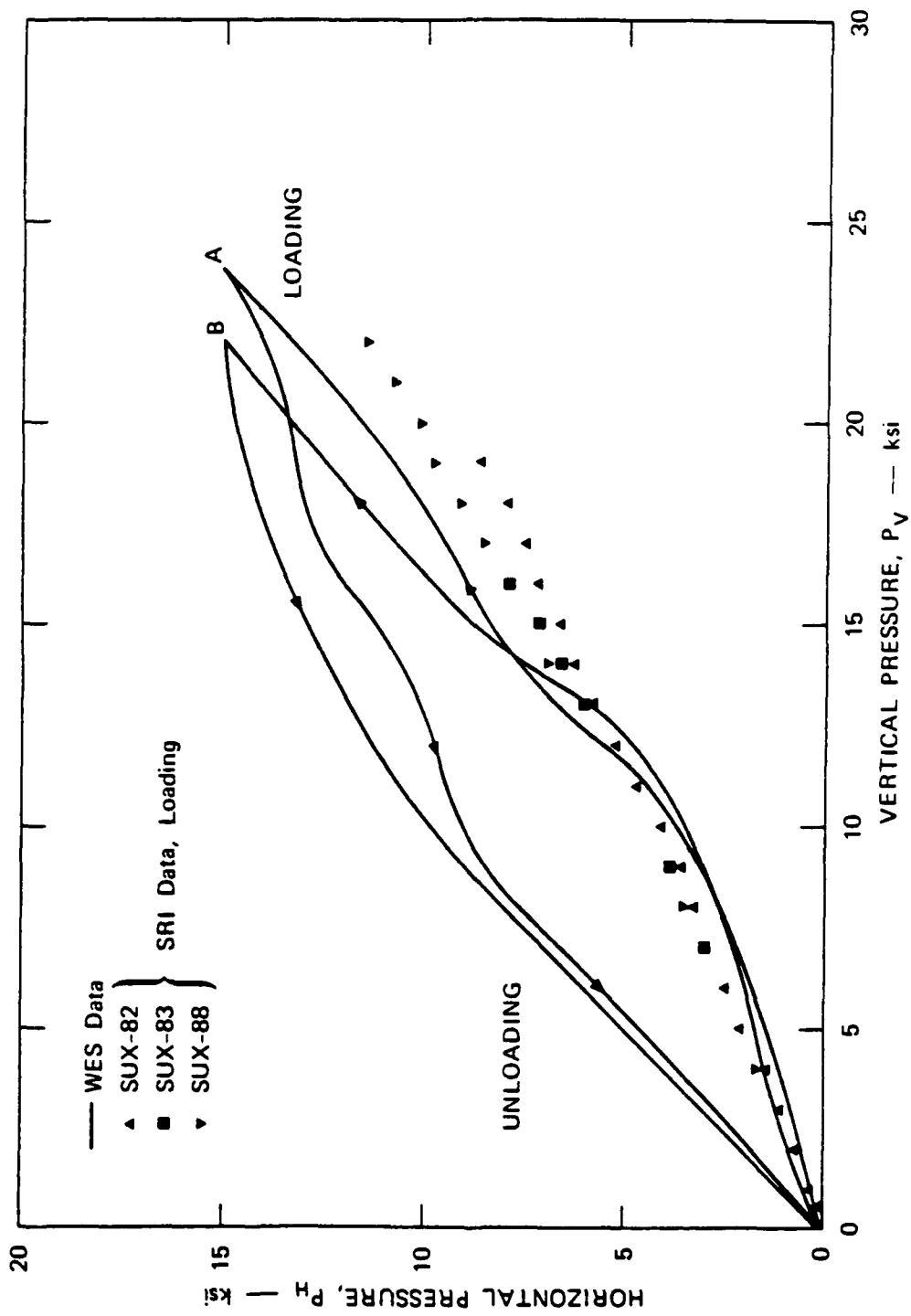


Figure 16. Horizontal pressure versus vertical pressure for uniaxial strain for saturated 6B rock simulant.

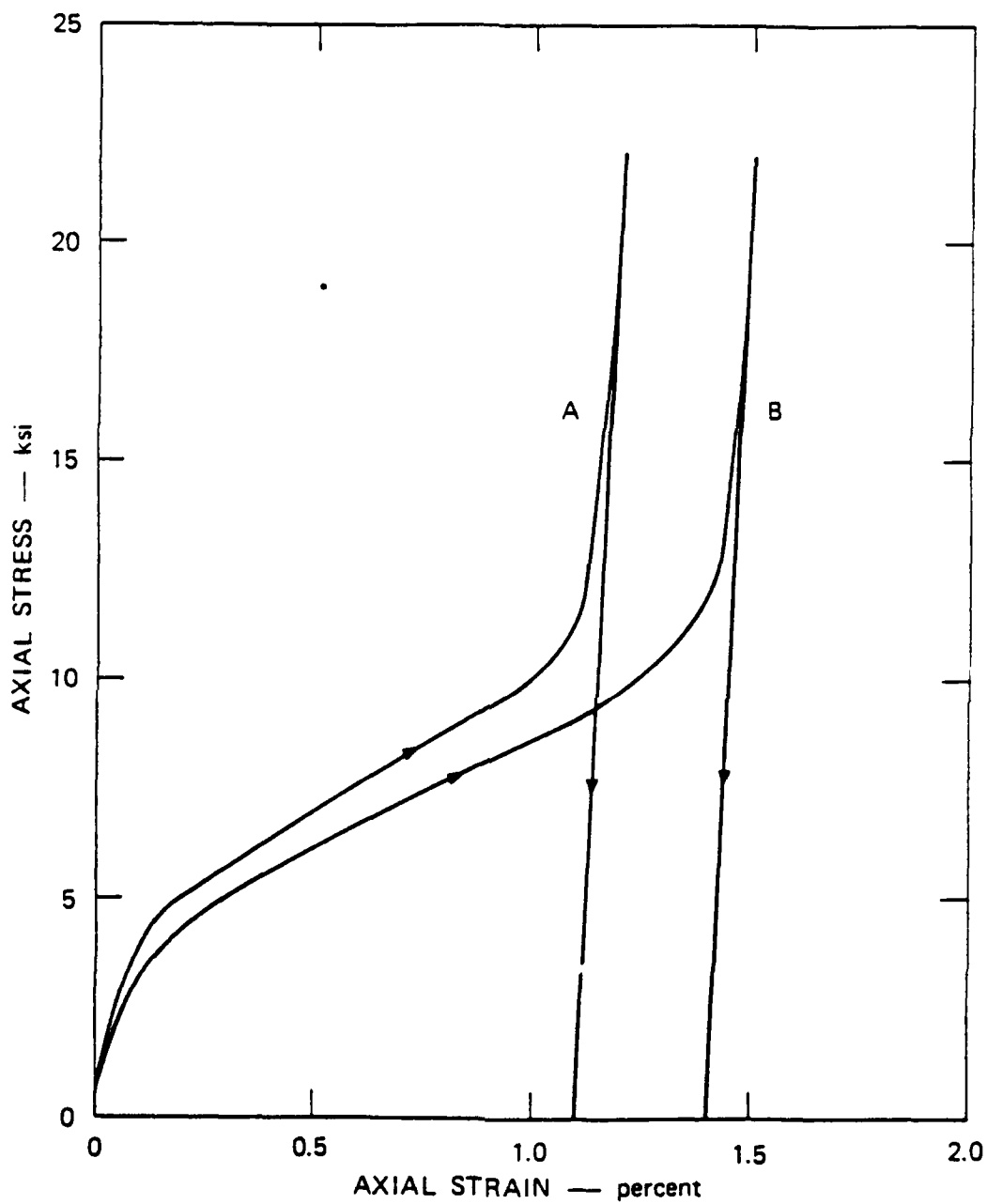


Figure 17. Stress-strain curve under uniaxial strain loading for saturated 6B rock simulant.

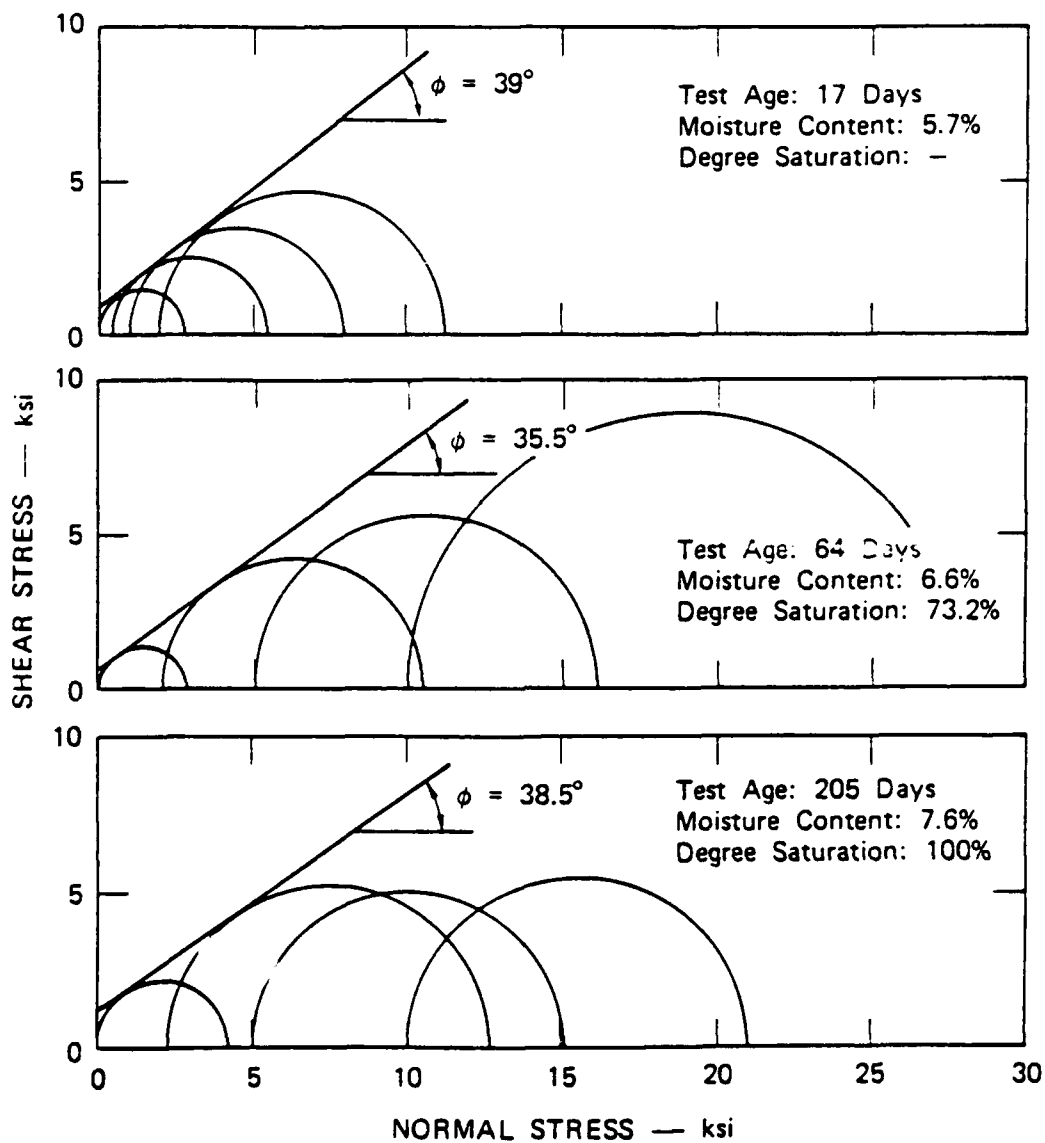


Figure 18. Mohr diagrams for moisturized 6B rock at different test ages.  
(R. L. Stowe, Waterways Experiment Station)

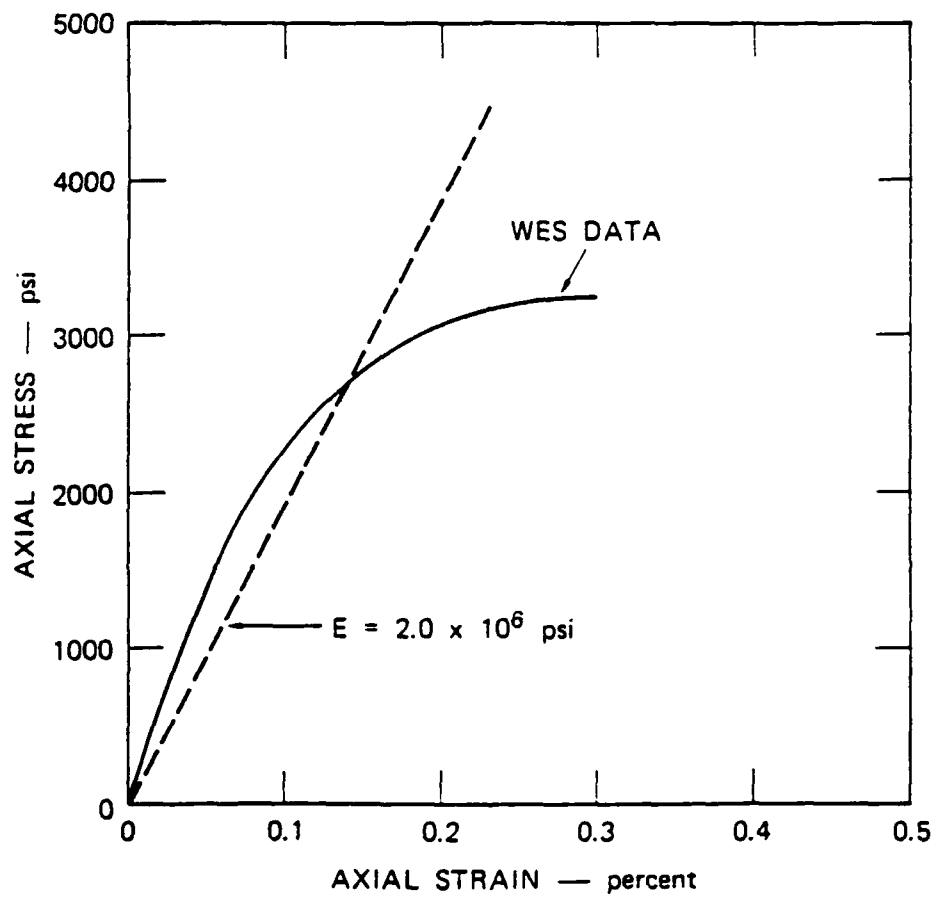


Figure 19. Stress-strain curves for dry 6B rock simulant.

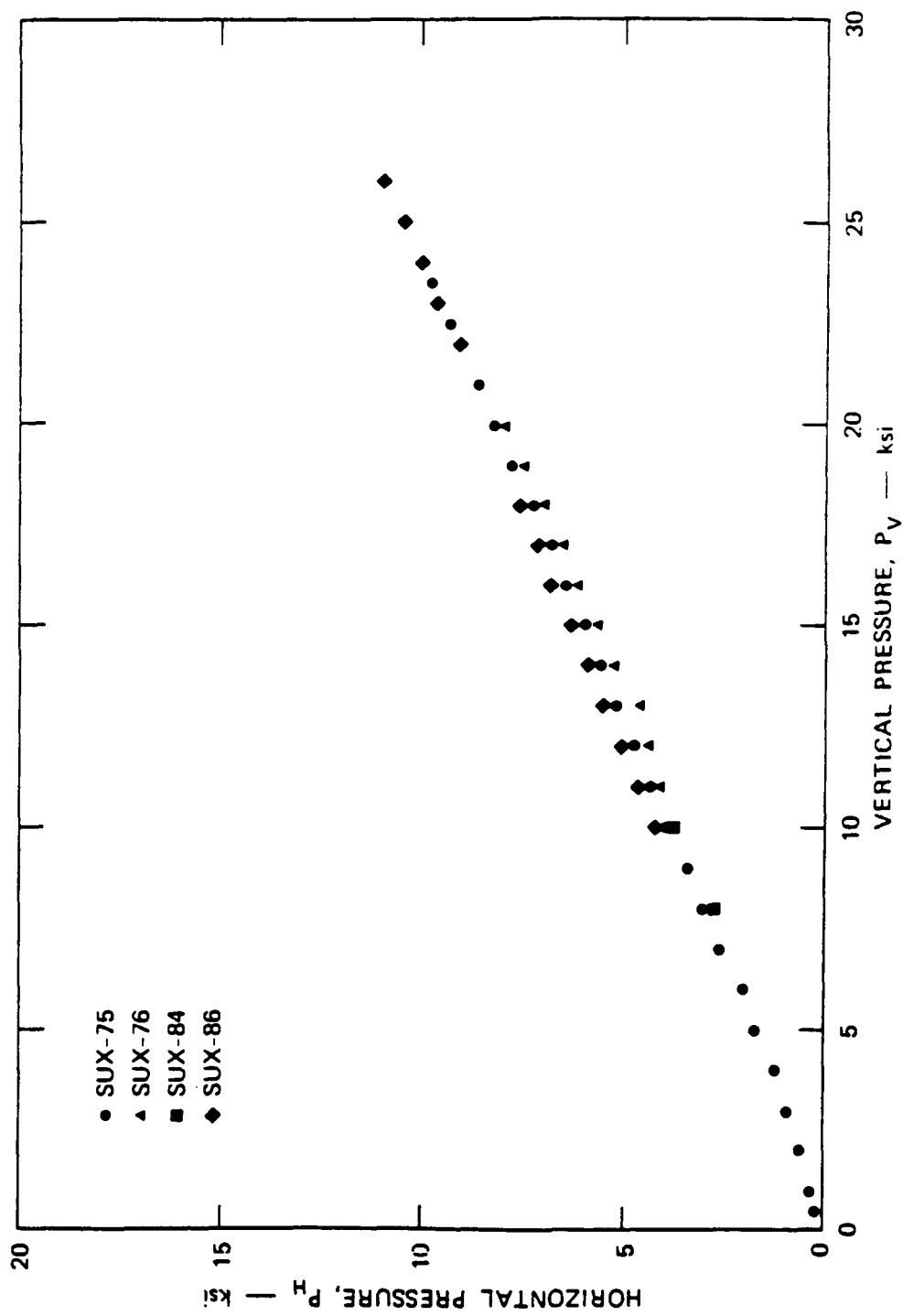


Figure 20. Horizontal pressure versus vertical pressure for uniaxial strain for dry 6B rock simulant.

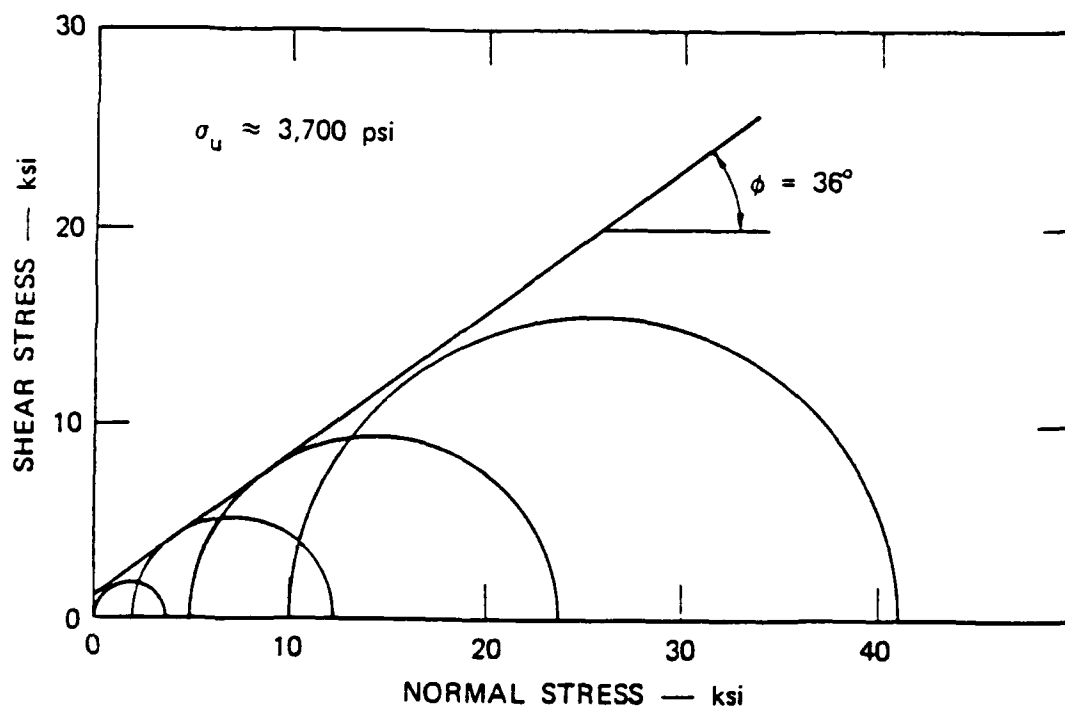


Figure 21. Mohr diagram for dry 6B rock.

The number of tests are summarized in Table 5. Interpretation of the results is complicated by the long drainage times required due to the low permeability of the sample materials. The main results from uniaxial, hydrostatic compression, and triaxial tests are given in Figs. 22 through 24. The report concludes that the drained strength of 2C4 grout at 4 kbars confining stress has an approximate lower bound of 0.3 kbars (the measured strength of the drained uncycled samples) and an approximate upper bound of 0.42 kbars (the measured strength of the drained cycled samples; repeated loading may have stiffened the material but also affected the pore water pressure).

Results on strain rate are discussed in Section 2.2.6.

#### Simulant HF4

HF4 grout is a high friction, high strength rock simulant (SRI monthly progress reports, PYU-3771, September 1987, November 1987, June 1988 [Simons, 1988]). HF4 is favored because of its high repeatability of material properties. Figure 25 plots the data from seven batches. The coefficient of variation (ratio of standard deviation to the mean) is 9.2%.

Hydrostatic and triaxial test results are shown in Figs. 26 and 27, from 2" and 4" cylinder specimens. The failure surface for the material is shown in Fig. 28. The friction angle varies from 30 degrees initially to 13 degrees at 8 ksi confinement. The pressure-volumetric strain response is shown in Fig. 29. After yielding in shear, dilatation of up to about 5% is observed.

Other factors affecting variability are found to be (1) aging (averaged 85-89% of nominal), (2) settling of solids in the sample (bottom sample is 6% stronger than top sample), and (3) age of sample. The effect of the latter is shown in Fig. 30 which compares the HF4 test data at 28 and 72 days.

More recent and more material data including effect of divergent wave strain paths are given in SRI's latest progress reports ([Simons], 1988).

Six straight tunnel closure curves taken from the intersection tunnel experiments using HF4 are compared in Fig. 31. The values for tunnel strength (load at 5% closure) are compared in Table 6 (col.1). To ascertain the contribution to the variability due to variability in material strength (col.2 of Table 6), the tunnel closure curves are repeated with the load normalized by the measured unconfined compressive strength for each experiment (col.3, Table 6). The results are shown in Figure 32, which indicates that the variability in tunnel strength may be due to factors other than compressive strength of HF4.

#### 2.2.4 Comparison Of Simulant and Native Rock.

According to the principles of geometric scaling followed by SRI, the mechanical properties of the simulant should be the same as those of the prototype for all stress/strain paths. Few direct comparisons were found. An example of comparisons between rock matching grouts and the natural rock they are intended to simulate is shown in Figures 33 and 34. Figure 33, from [DNA 4149F], 1976, compares the response of 3 batches of rock matching grout RMG 2C3 with that of Ash-Fall Tuff. The stress paths match fairly well, with maximum deviation in strength from that of tuff being about 7%, see Fig. 33b. The stress strain curves, however, show that all samples of simulant are stiffer than the natural material.

The opposite situation occurs when the uniaxial strain response of rock matching grout RMG 2C4 is compared with that of Nevada Test Site (NTS) Tuff (Fig. 34). Here, the stress strain curves for the two materials, Fig. 34a, agree very well up to a mean normal stress of 0.6 kbar, and

Table 5. 2C4 grout test matrix.

Showing the number of tests conducted of each test type or the number of tests conducted at each condition, whichever applies.

# Uniaxial Strain Tests Curing Time Effects Study

Test Type	7	14	16	18	21	28	56
Cast → Room Temperature	2	2					
Cast → Refrigerated	3	3	3	3	3	3	**

## Uniaxial Strain (Undrained and Cycled)

Cast → Room Temperature	2	2	2	2	2	2	2
Cast → Refrigerated	3	3	3	3	3	3	**

## Strain Rate Study

Test Type	Strain Rate (in./in./sec)						
	10 <sup>-5</sup>	10 <sup>-4</sup>	10 <sup>-3</sup>	10 <sup>-2</sup>	10 <sup>-1</sup>	10 <sup>-1</sup>	10 <sup>-1</sup>
Unconfined Compression	2	2	2	2	2	2	2
Uniaxial Strain (Undrained)	3	*	*	3			
Triaxial Compression (Undrained; σ <sub>3</sub> = 0.5 kb)	1	*	*	1			

- \* Conducted in other studies
- \*\* Arrows indicate the sequence of testing

# Hydrostatic Compression Tests T0 σ<sub>3</sub> = 4 KBARS

## Test Conditions

- Pore Pressure Controlled

Pp 10 bars	2	**
Pp 500 bars	2	
Unjacketed Cp = Pp	2	
Undrained	2	

## Triaxial Compression Tests

Test Conditions	Conf. Pressure (kb)						
	0	0.069	1/4	1/2	1	2	4
Pp = 10 bars		1	1	1	1	1	2
Pp = 500 bars				1	1	1	2
Undrained I	1		1	1	1	1	1
Undrained but previously stressed to s <sub>3</sub> = 4 kb					1	1	1
Unjacketed Cp = Pp							2

- Pp = 10 bars
- Pp = 500 bars
- Undrained I
- Undrained but previously stressed to s<sub>3</sub> = 4 kb
- Unjacketed Cp = Pp
- After uniaxial strain tests

Undrained	2	2	2	2	2	2	2
Drained	1	1	1	1	1	1	1

Uniaxial Strain  
 DNA 2C4 Grout  
 56th Day Undrained  
 AVE Samples 1 - 24, 1 - 2 Room Temp Cure  
 ----- AVE Samples 1 - 10A, 1 - 10B, 2 - 19  
 Refrigerated

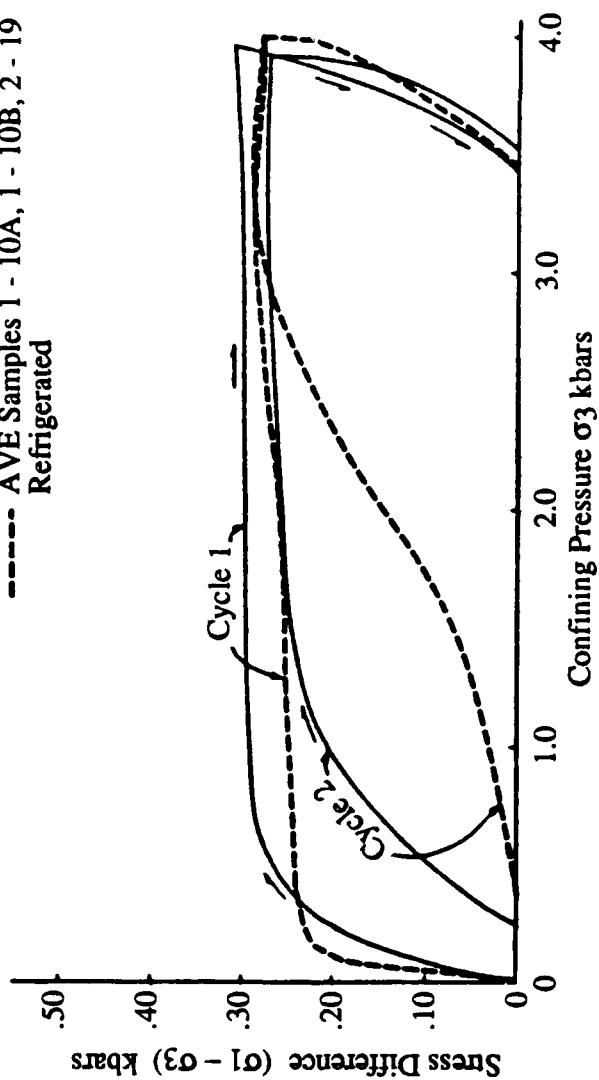


Figure 22. Uniaxial strain - 56th day.

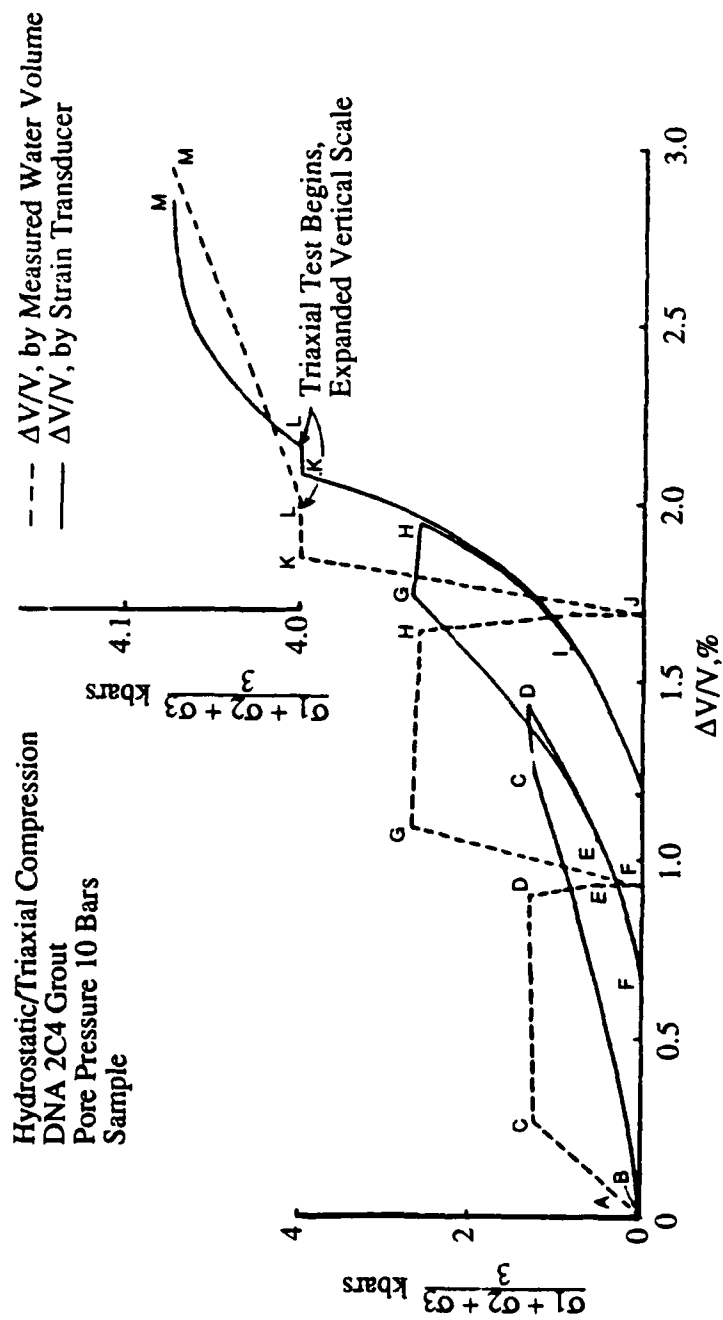


Figure 23. Hydrostatic/triaxial compression, pore pressure 10 bars.

# Hydrostatic Compression Tests, Summary DNA 2C4 Grout

- Unjacketed (2 Tests Averaged)
- ◇ Undrained (2 Tests Averaged)
- Drained - 10 bars (2 Tests Averaged)
- ◆ Drained - 500 bars (1 Test)
- ▽ LAP18 Lustre Sand, Porosity 37% (TR78-78)
- Water
- A Calculated Drain Compressibility for Grout.

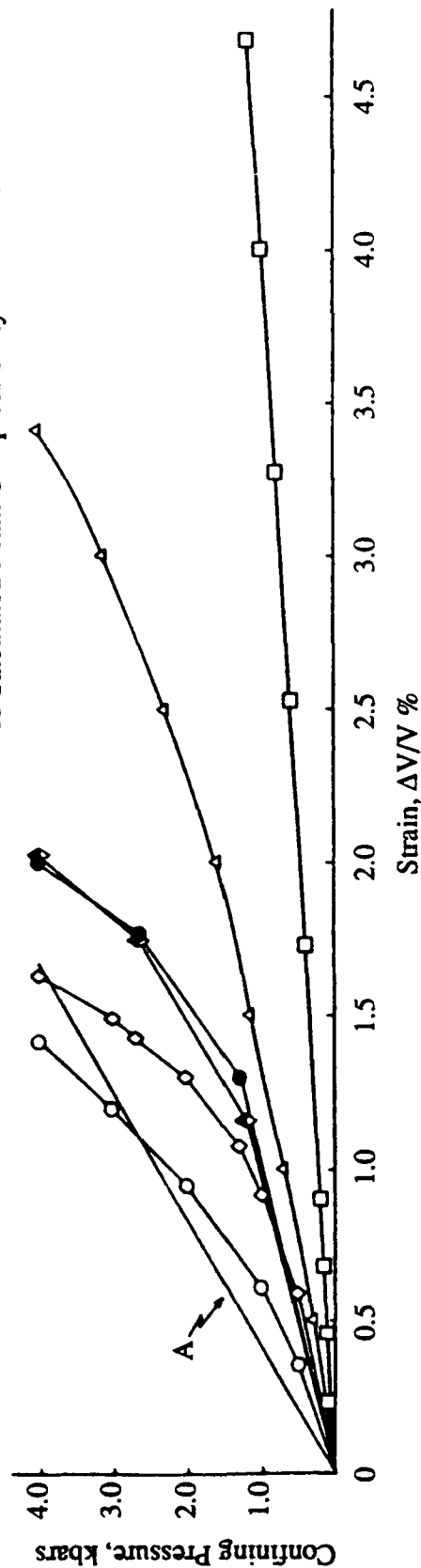


Figure 24. Hydrostatic compression test summary.

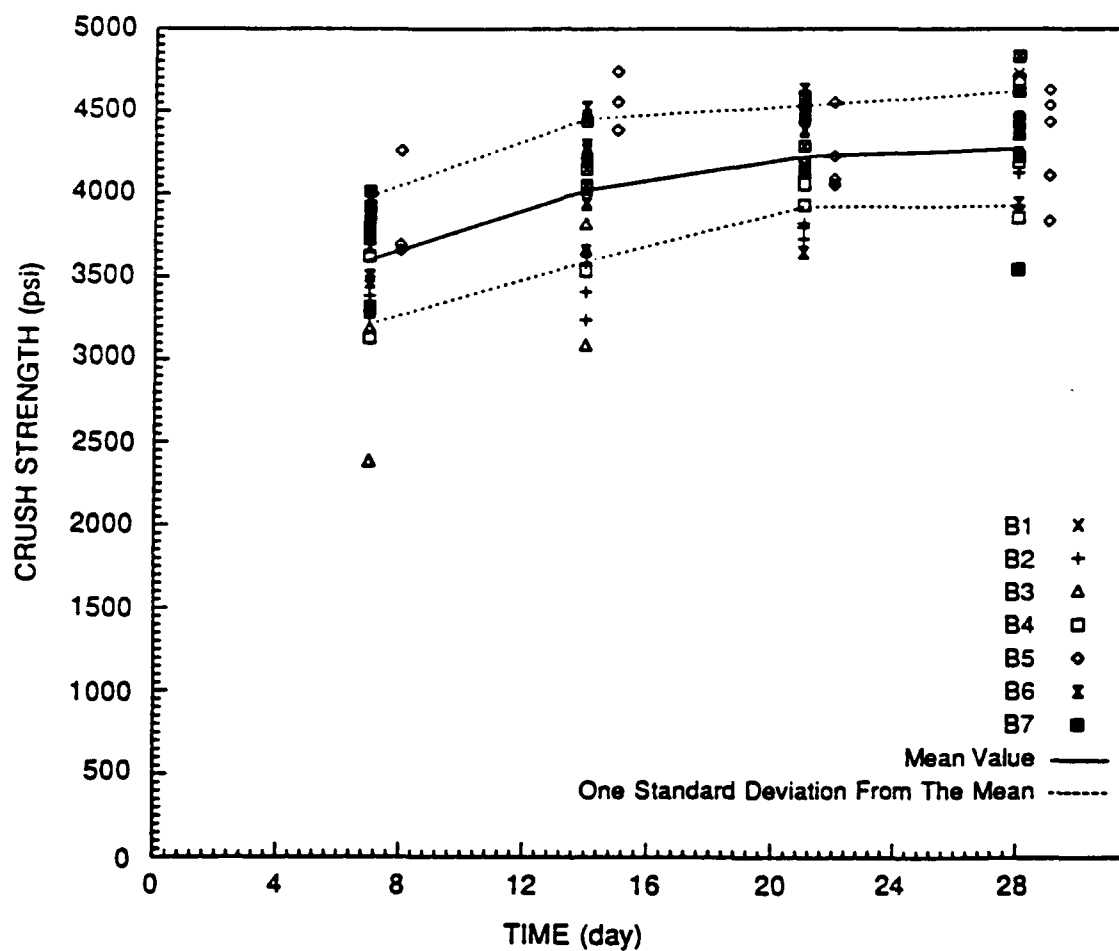
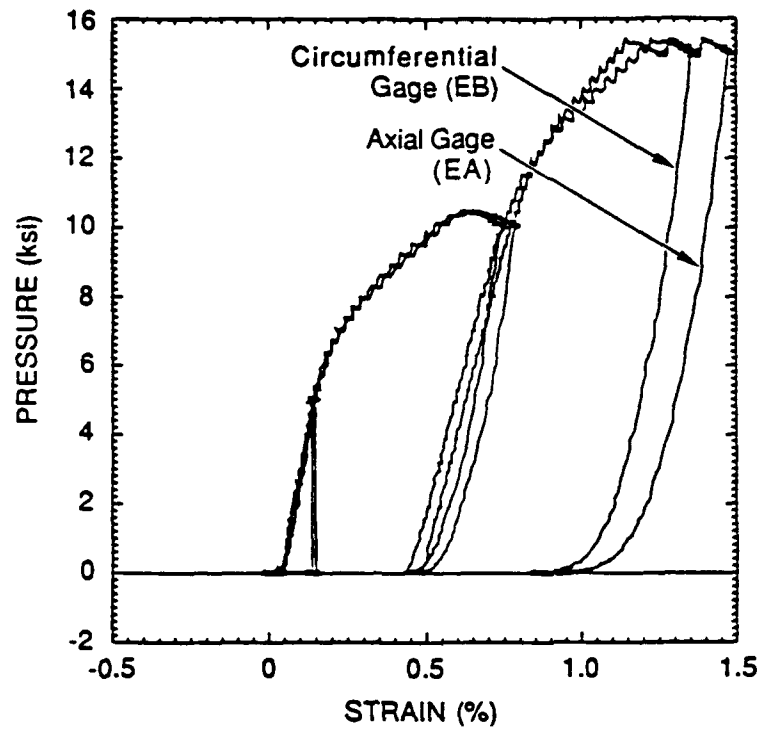
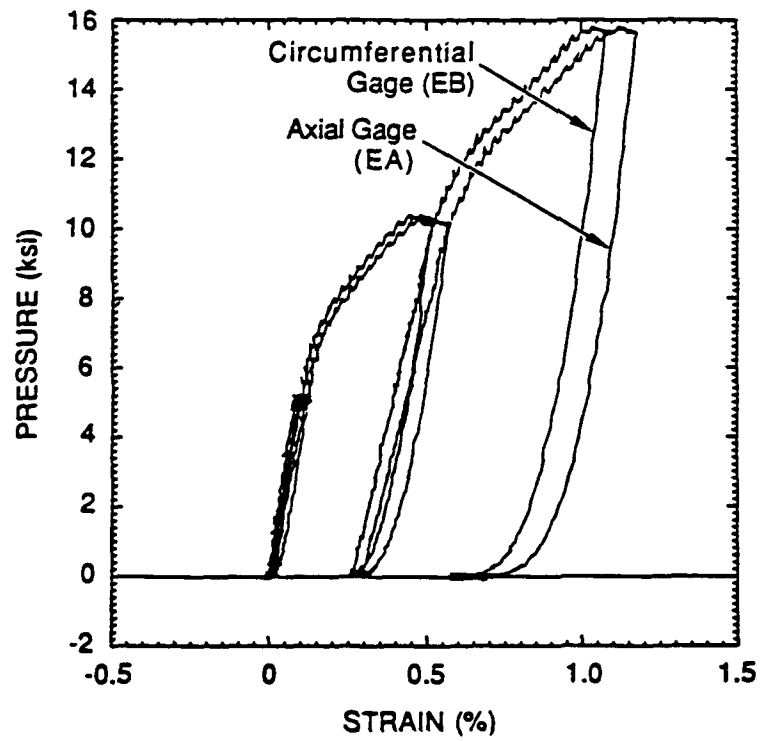


Figure 25. HF4: crush strength as a function of time for batches B1 - B7.



(a) Test 19



(b) Test 20

Figure 26. HF4 hydrostatic test results.

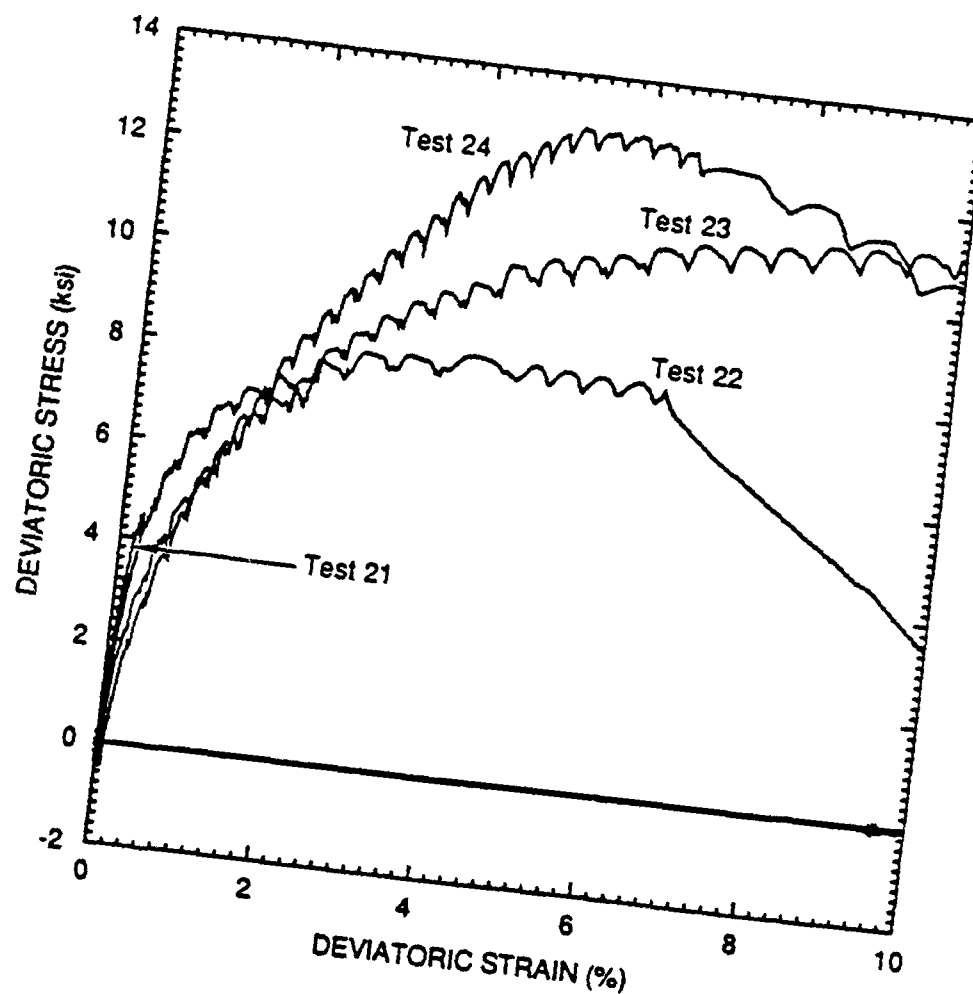
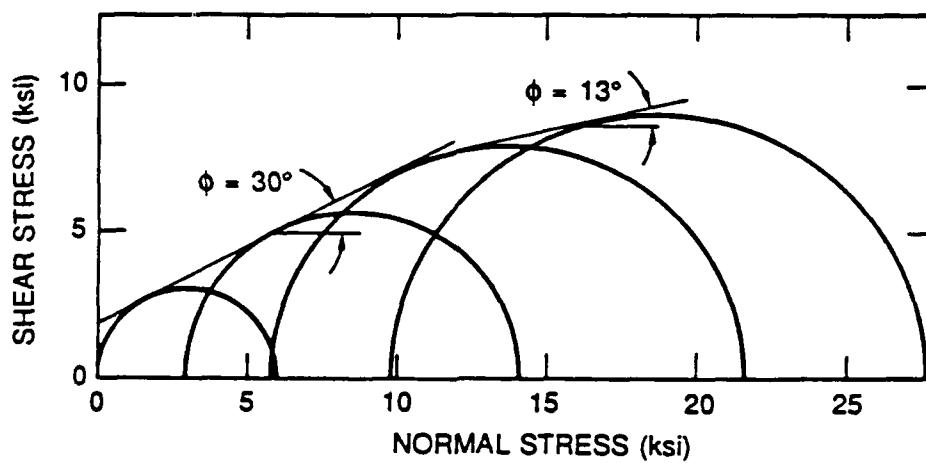
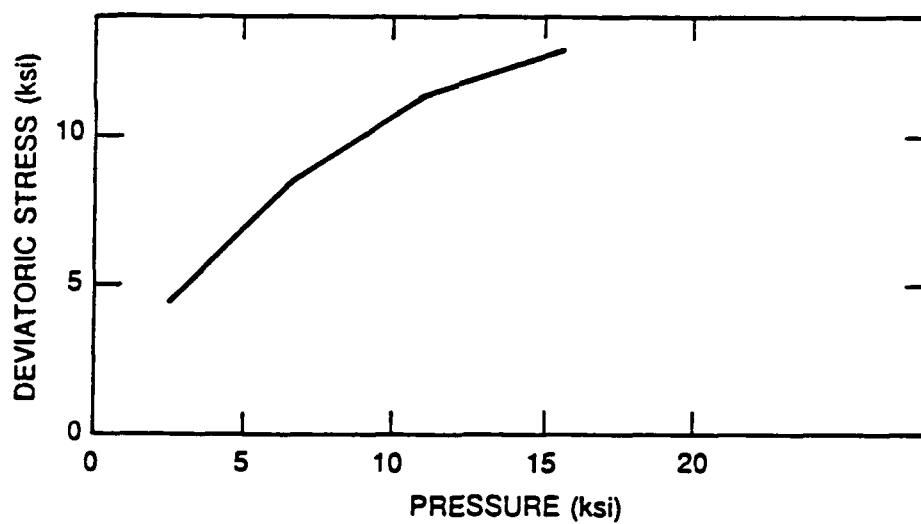


Figure 27. Deviatoric stress-strain curves for triaxial test 21 through 24.



(a) Mohr's circle envelope.



(b) Deviatoric stress versus pressure.

Figure 28. HF4 failure surface.

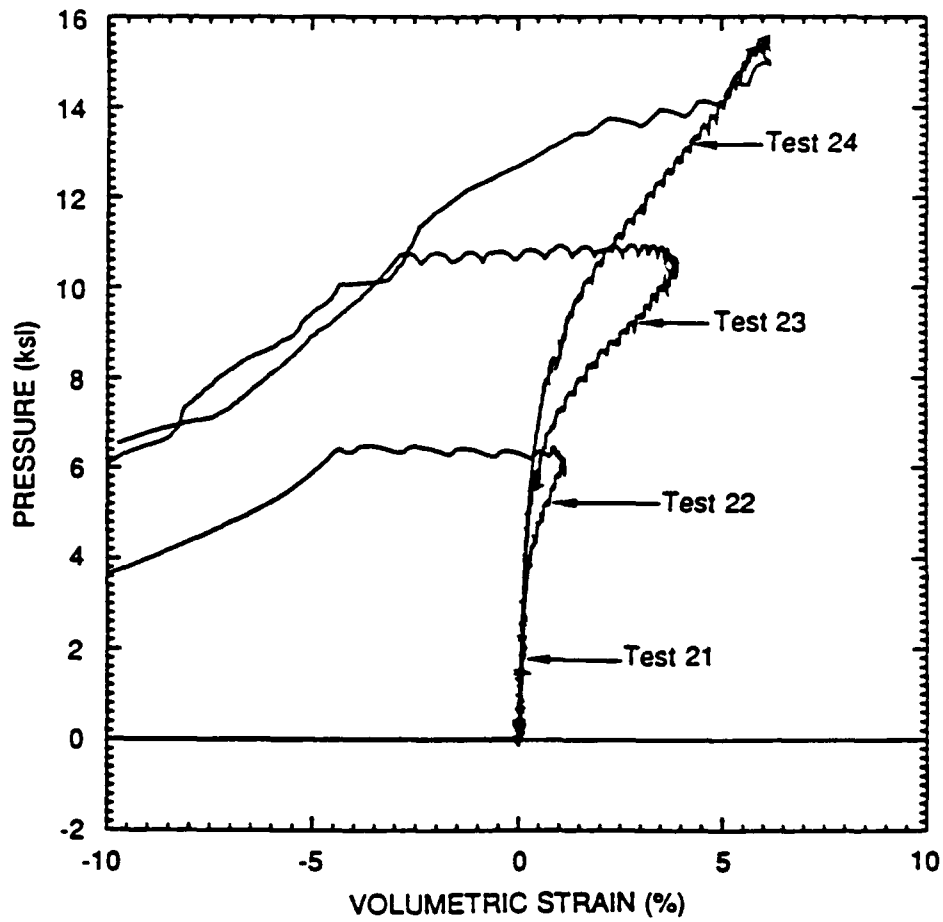
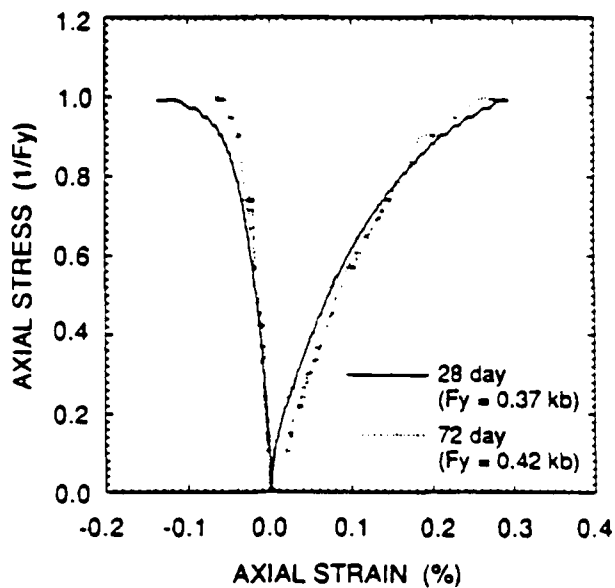
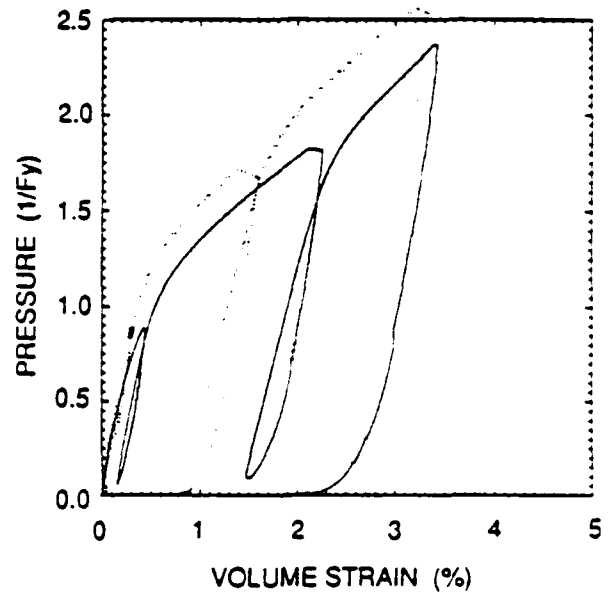


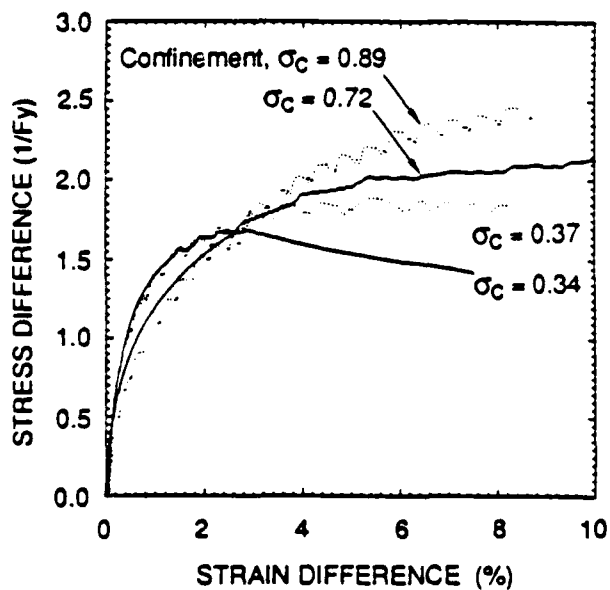
Figure 29. Volumetric stress-strain for triaxial tests 21 through 24.



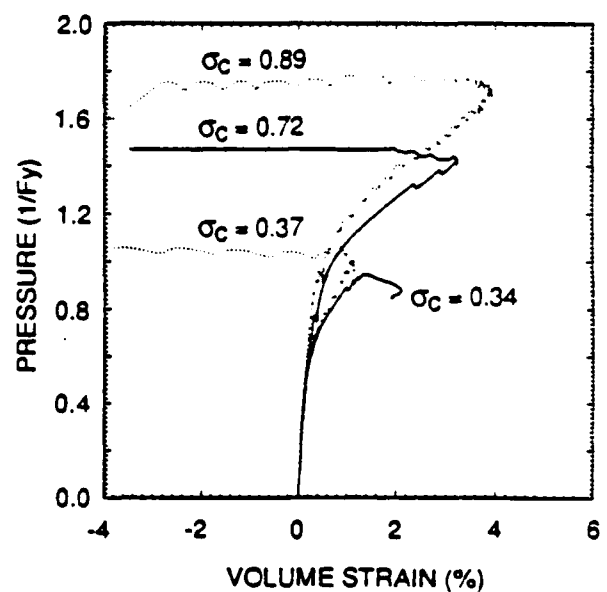
(a) Unconfined compression.



(b) Hydrostatic test



(c) Shear response for triaxial compression.



(d) Volumetric response for triaxial compression.

Figure 30. HF4 response at 28 and 72 days normalized by crush strength.

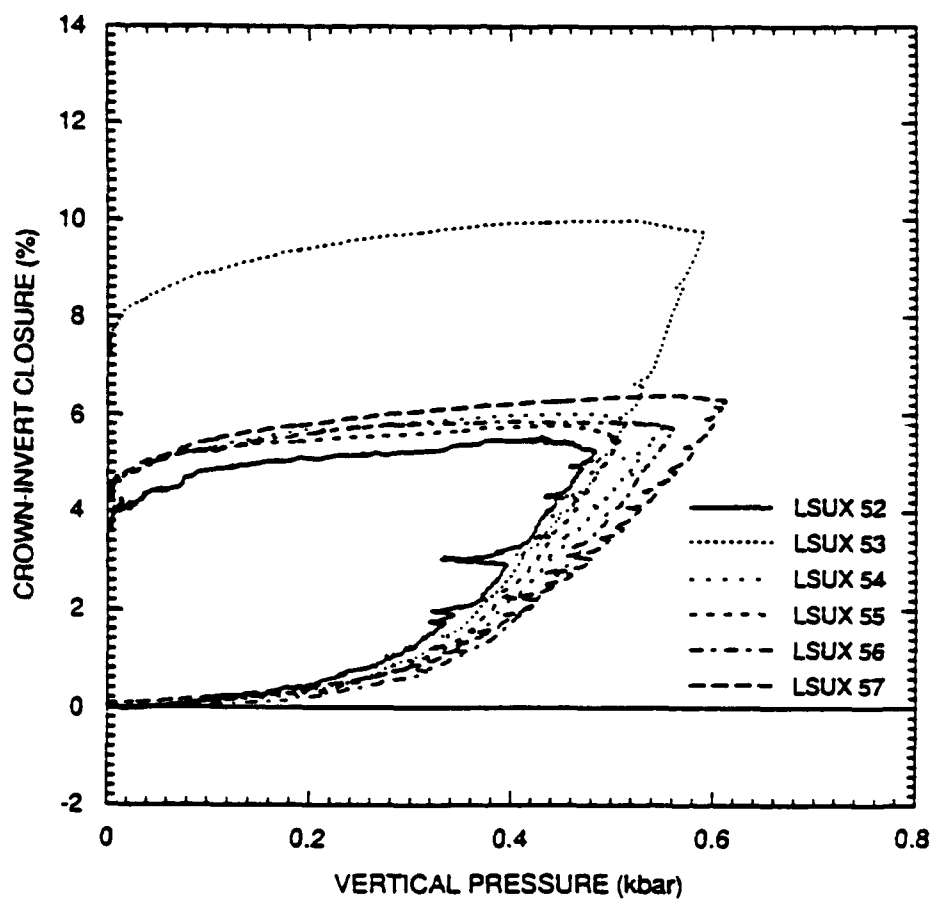


Figure 31. Straight tunnel closure (LSUX-52 - LSUX-57).

Table 6. Tunnel and material strengths for LSUX-52 - LSUX-57.

Test No.	Tunnel Strength (TS)		Material Strength ( $f'_c$ )		Ratio (TS/ $f'_c$ )
	(kbar)		(kbar)		
LSUX-52	0.472		0.280		1.66
LSUX-53	0.490		0.265		1.85
LSUX-54	0.524		0.271		1.93
LSUX-55	0.499		0.301		1.66
LSUX-56	0.538		0.308		1.75
LSUX-57	0.578		0.341		1.70
Average	0.517		0.294		1.76
Deviation	0.038 (7.4%)		0.028 (9.6%)		0.11 (6.3%)

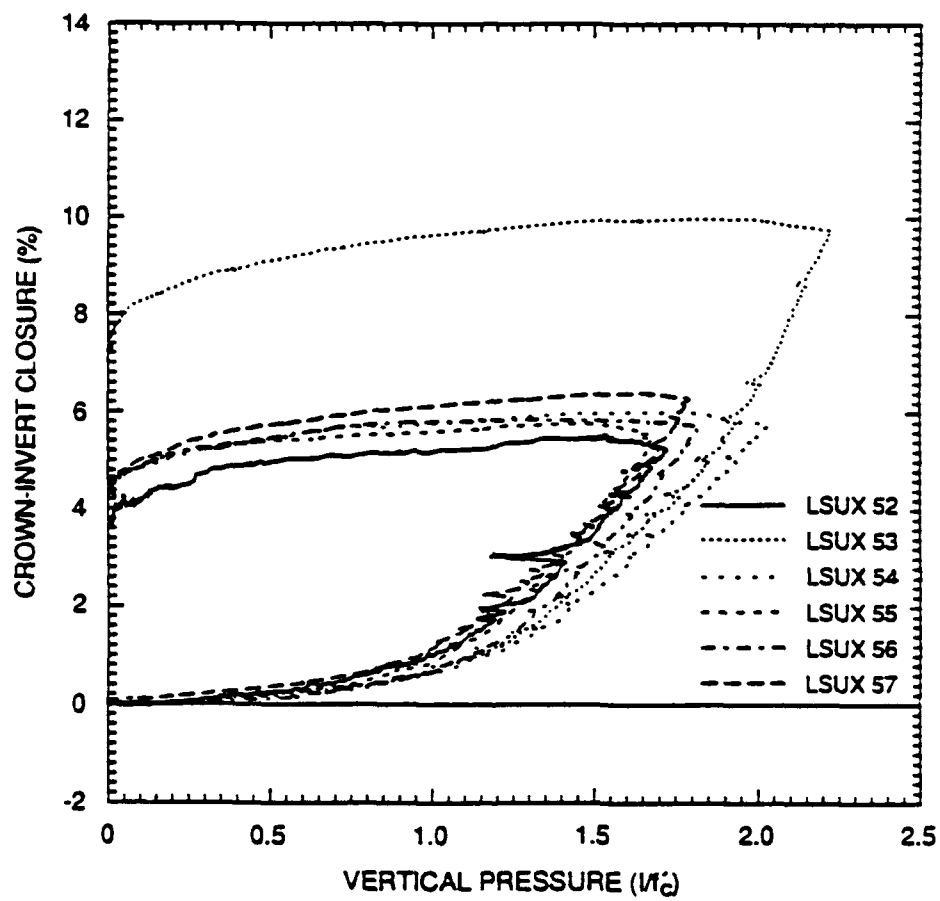


Figure 32. Straight tunnel closure versus normalized load (LSUX-52 - LSUX-57).

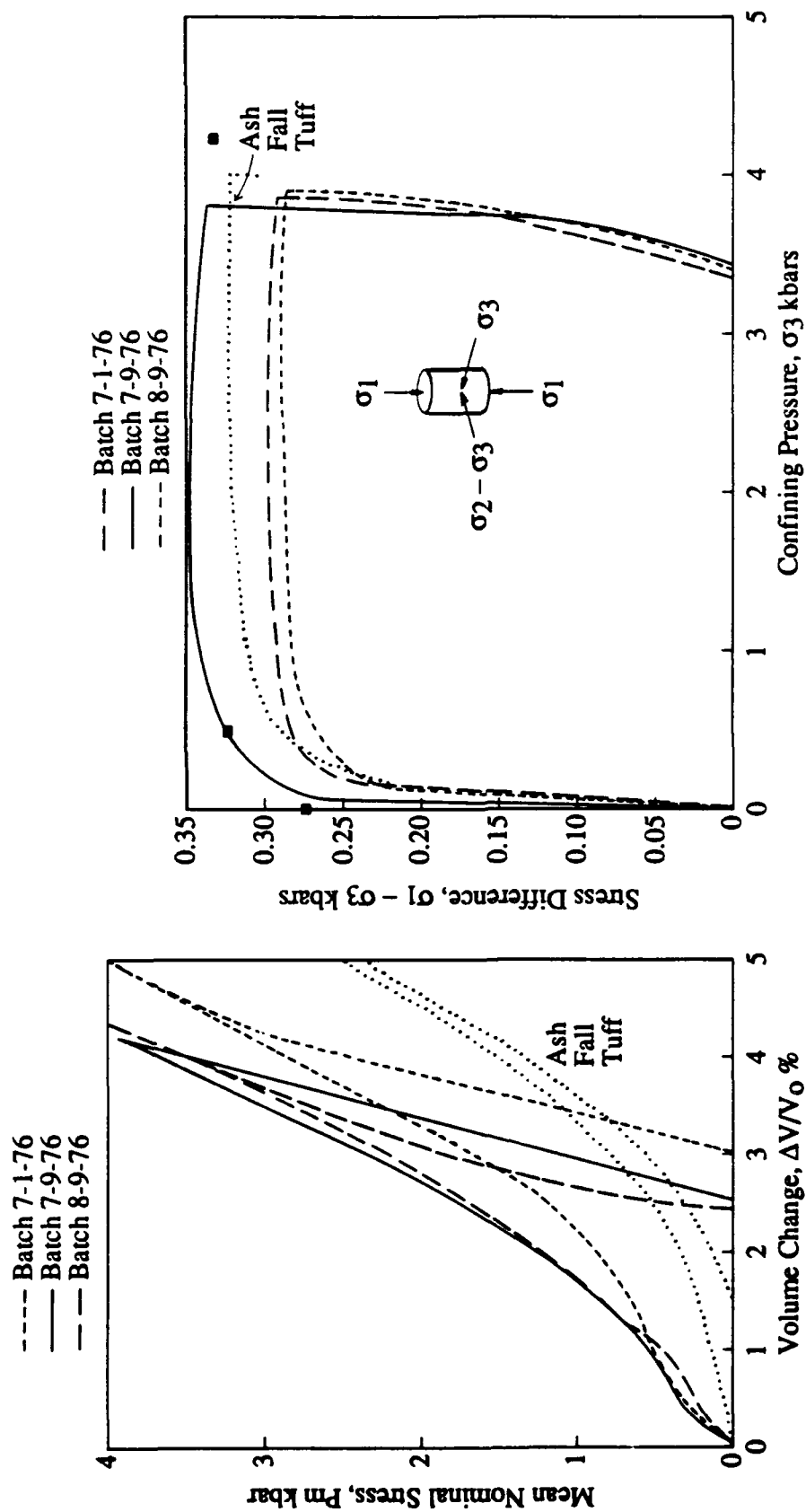


Figure 33. Comparison of pressure-volume and strength properties between 2C3 Grout and Ash Fall Tuff.  
(DNA 4149G)

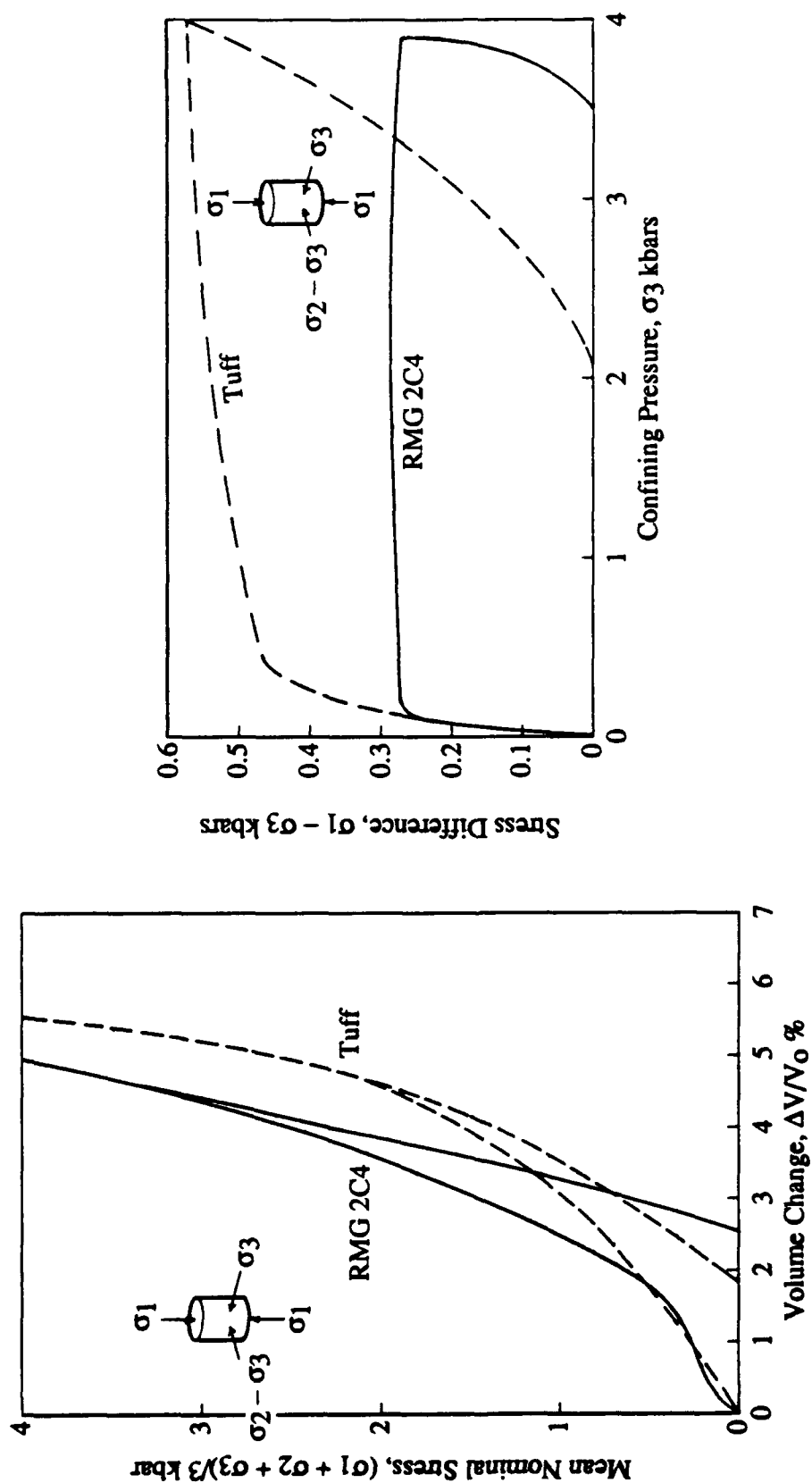


Figure 34. Comparison of pressure-volume and strength properties between 2C4 Grout and Ash Fall Tuff. (DNA 4149F)

reasonably well at higher stresses. However, the stress paths, Fig.34b, agree only to confining pressures of 0.1 kbar. At higher confining pressures, the strength of the natural tuff is twice that of RMG 2C4.

#### 2.2.5 Variability In Simulant Properties.

As for other Portland Cement based materials, the simulants show variabilities in their properties which are similar to concrete. Much data on sample to sample variability, variability with age and other factors are available but they have not been systematically collected as was done for the more recent HF4 (see previous discussion). An example of the "older" data is Fig.35 which shows the variability in the unconfined crush strength of 2C4, and Fig.36 for the splitting tensile strength.

#### 2.2.6 Strain Rates Effect On Simulants Properties.

One question which arises in evaluating dynamic tests is whether the similitude is preserved with respect to rate of loading between model and prototype. Another is whether, at the high rates required for strain rate similitude, rate-dependence alters properties of the model material such that similitude with respect to strength and stiffness between model and prototype is destroyed. In order to address these questions, we first consider what are the strain rates found at field scale and what are the corresponding rates to be used in laboratory scale testing.

##### Strain Rates In Lab (IDNA 3610FL 1975)

The dynamic loading machine at SRI uses controlled release of explosive gases from vented canisters. To provide independent control of vertical and lateral pressures, loading is applied by two separate explosive canisters. The device is capable of a peak load of 2 kbars. However, there is no interaction between the vertical and lateral load. They are "programmed" before the experiment to follow specific waveforms independently.

Typical pressure pulses from the vertical and lateral loading chambers are shown in Fig.37. The rise time is 100-200  $\mu$  sec, and the decay time constant is 300-400  $\mu$ sec; the total pulse duration is about 1000  $\mu$ sec. For a 5/8" tunnel model and a 10' prototype tunnel, these times would scale (by a factor of 200) to 20-40 msec, 60-80 msec, and 200 msec, respectively. For a 30' prototype tunnel, these numbers should be increased by another factor of 3.

Consider a typical strain at the peak loading of 2%. The loading strain rate for the dynamic lab specimen is then:  $0.02/200 \mu\text{sec} = 100 \text{ in/in/sec}$ .

##### Strain Rate In Field

Using the same reference strain of 2% and a rise time of 40 msec for the field pulse, the loading strain rate for the field is:  $0.02/40 \text{ msec} = 0.5 \text{ in/in/sec}$ . Hence, the lab strain rate is about 200 times the field rate, as the scale factor dictates, which as shown below, implies an increase in strength and stiffness for the lab tests in many cases.

##### Rate Sensitivity Of Simulant Materials

Few data exist on the sensitivity of the simulant properties to strain rate. Figure 38 from TT 81-56 plots the strength of 2C4 grout vs strain rates in the range E-5 to E-1 in/in/sec. Figure 39 gives the strain rate summary for unconfined compression tests, and Fig.40 gives the data for

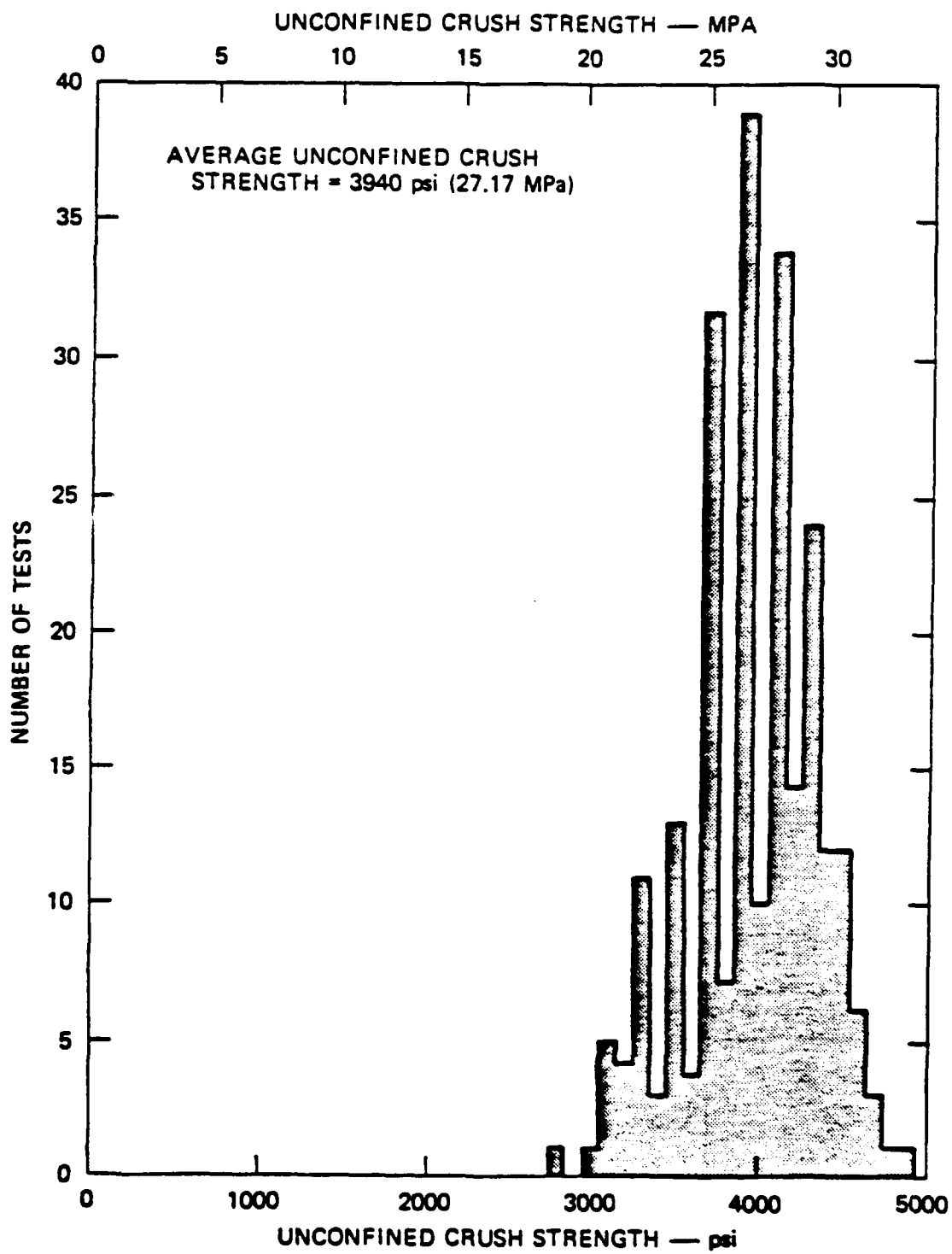


Figure 35. Unconfined crush strength of Rock-Matching Grout RMG2C4.

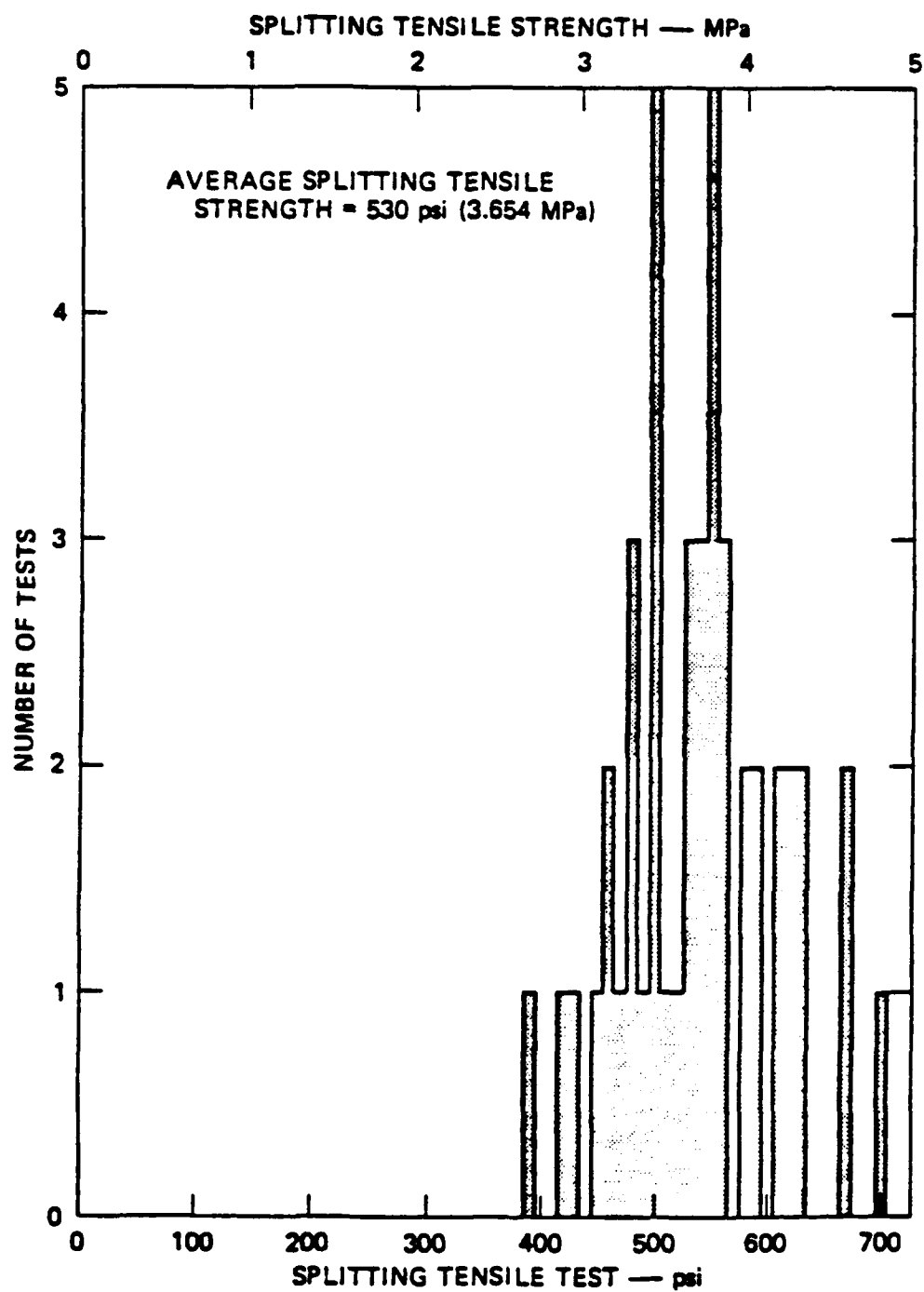
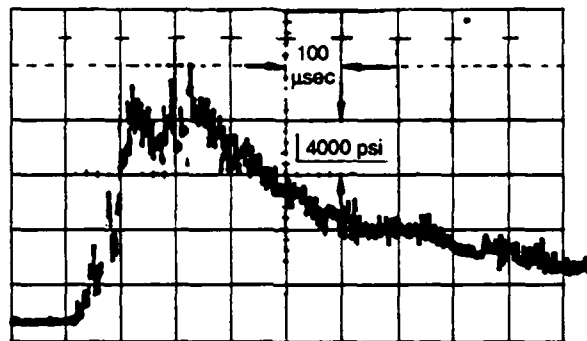
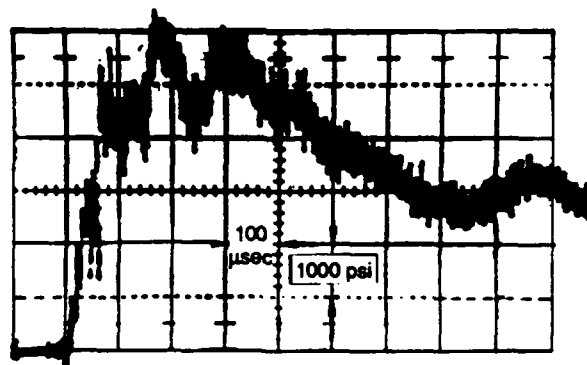


Figure 36. Splitting tensile strength of Rock-Matching Grout RMG 2C4.



(a) Upper Chamber Pulse



(b) Side Chamber Pulse

Figure 37. Time histories of applied loads.



Strain Rate Summary  
DNA 2C4 Grout  
Unconfined Compression Tests

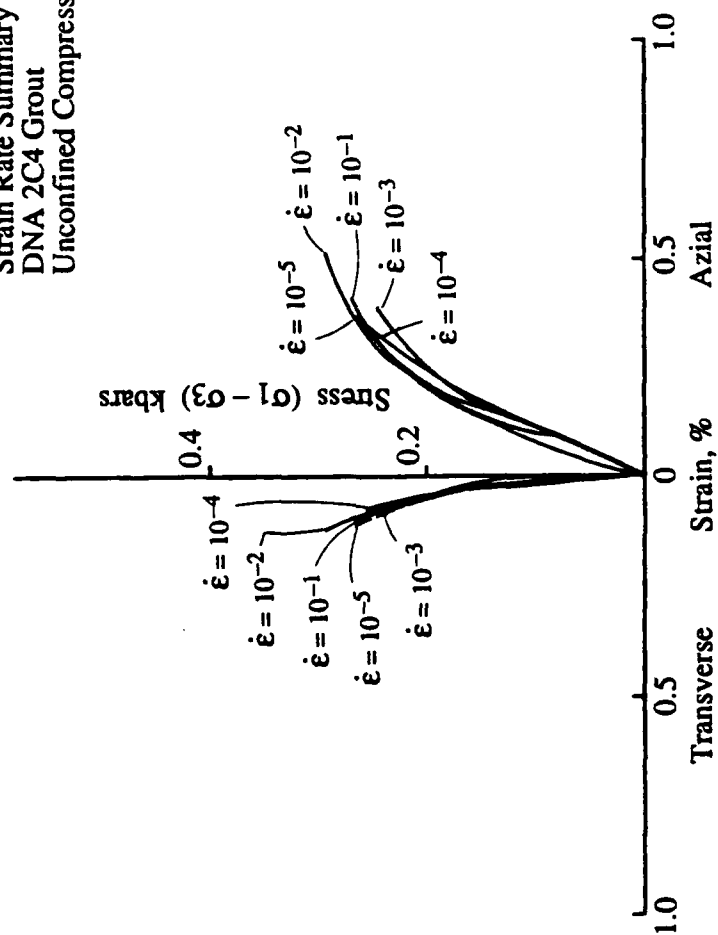


Figure 39. Strain rate summary for unconfined compression tests.

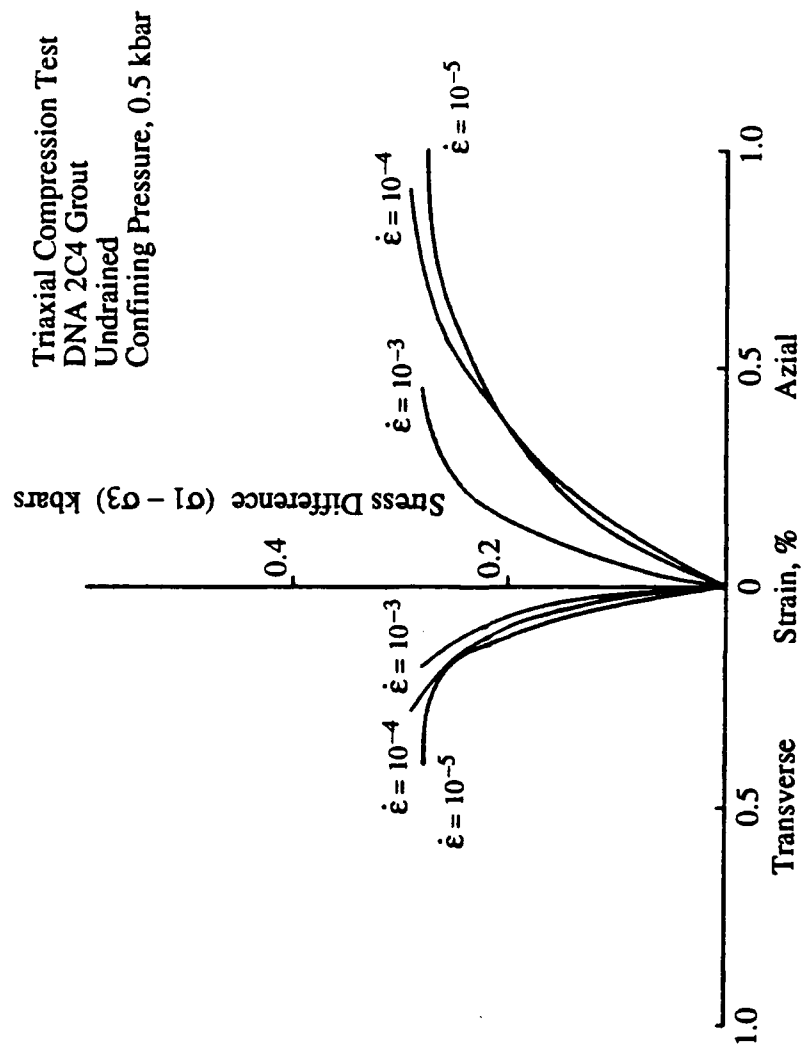


Figure 40. Triaxial compression test summary, confining pressure 0.5 kbar.

triaxial compression. There is apparently no rate effect for the rates considered. The stress difference is fairly constant at 0.25 kbars.

The results indicating that 2C4 is rate independent over the range of rates considered is valuable if these are the rates that apply to tests on tunnels. Materials such as these grouts which are based on portland cement exhibit significant rate effects at rates above .1-1.0 in/in/sec (see split Hopkinson bar data by Malvern, and data by Surendah Shah discussed presently). Furthermore, static/dynamic tunnel tests run at SRI apparently exhibit rate effects, but those tests may have much higher strain rates.

However, from one other source ([DNA 6121F]), we note there are some strain rate data on 2C4 which are purportedly taken from Terra Tek test programs. These are reproduced here as Table 7. With reference to Table 7, we see that at a strain rate of 0.15/sec, which is comparable to the highest rate tested in TT 81-56, 2C4 shows a 34% increase in compressive strength over the static value and a 70% increase in the tensile strength. This discrepancy in data needs to be resolved.

Since all simulants are Portland cement based materials, an estimate of their rate sensitivity can be gleaned from the vast amount of published data on concrete. A rule of thumb is to enhance the static properties by 20% for use in dynamic analysis. Figure 41 gives an example of the data on strain rate effect on the compressive and tensile strength of concrete ([Suaris and Shah]). For the strain rates encountered in the lab (100 in/in/sec), the dynamic/static ratio exceeds a factor of 2 for compressive strength and a factor of 6 for tensile strength. For the field strain rate of 0.5 in/in/sec, the dynamic multiplicative factor is about 1.3 for the compressive strength and 1.7 for tensile strength. Hence, there is significant difference in the effect of strain rate in the lab and in the field. Figure 42 gives the enhancement factor for high strength concretes at very high strain rates obtained with the split Hopkinson bar ([Malvern]).

#### Rate Sensitivity Of Rock

Rocks exhibit strain rate sensitivity, but the sensitivity is different for different rock types and is pressure dependent. Figure 43 summarizes the effect of strain rate on compressive strength (stress difference at failure in triaxial tests) for 14 rock types. Aside from the two marbles, quartzite and solenhofen limestone, the strain rate sensitivity is approximately the same for all other rocks shown.

Data from medium strength concrete (Watstein, Fig.41) and high strength concrete (Malvern, Fig.42) are superimposed as curves (x) and (y), respectively, in the rock data figure. The strain rate effect for medium strength concrete is comparable to that of rocks.

### **2.3 EXPERIMENTS IN CONTINUOUS (UNJOINTED) SPECIMENS.**

Tests conducted prior to 1975 on continuous specimens with straight tunnels are useful primarily to evaluate the performance of the test apparatus. Initially, the apparatus was capable of subjecting small specimens of 4" by 4" (5/8" tunnel openings) to both static and dynamic loading. Subsequently, larger apparatus of similar design were built to test 12" by 12-18" specimens (1"-2" tunnel openings), also statically or dynamically.

Later tests considered the effect of varying parameters. A series involving parameters in opposition such as wet vs. dry, static vs. dynamic, was conducted. Several test series were conducted to support field tests; notably DINING CAR, MIGHTY EPIC and DIABLO HAWK, in an effort to establish relationship between lab specimen response and larger size field specimen response.

**Table 7. Properties of rock-matching grout RGM 2C4, low density rock-matching grout LD 2C4, and Nevada test site tuff.**

**(a) Physical Properties**

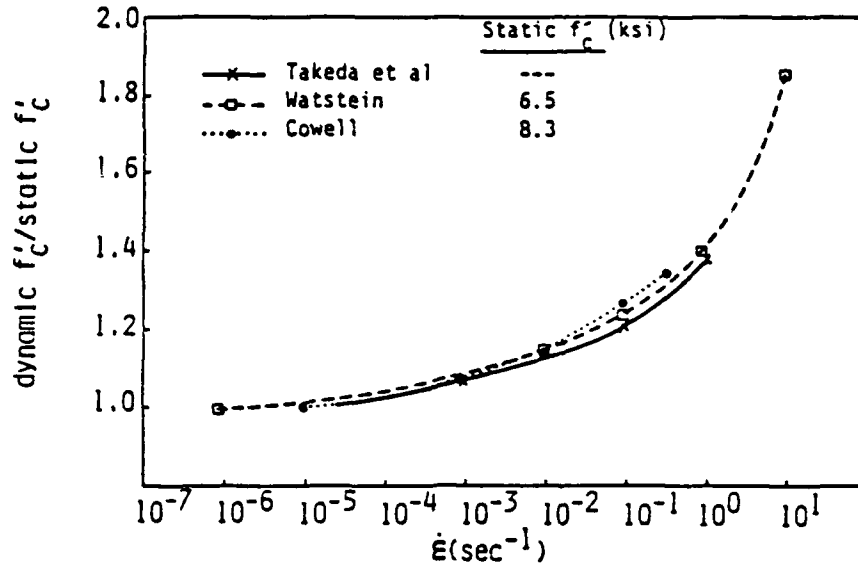
Physical Property	RMG 2C4	LD* 2C4	Tuff
Density (g/cm <sup>3</sup> )			
Aged	2.15	1.90	1.87
Dry	1.75	1.57	1.54
Grain	2.87	2.68	2.34
Water by Wet Weight (%)	18.6	17.4	17.9
Porosity (%)	39	43	34
Saturation (%)	100	86	97.6
Air Voids (%)	0	13.4	0.8
Longitudinal Velocity (km/sec)	3.29	3.13	2.95
Shear Velocity (km/sec)	1.82	1.78	1.53
Modulus in Compression (psi)	$2.64 \times 10^6$	$2.20 \times 10^6$	$1.67 \times 10^6$
Shear Modulus (psi)	$1.03 \times 10^6$	$8.74 \times 10^5$	$0.63 \times 10^6$
Bulk Modulus (psi)	$2.00 \times 10^6$	$1.53 \times 10^6$	$1.55 \times 10^6$
Poisson's Ratio	0.28	0.26	0.32
Permeability (μd)	3.0	—	—

\* Standing for Low Density

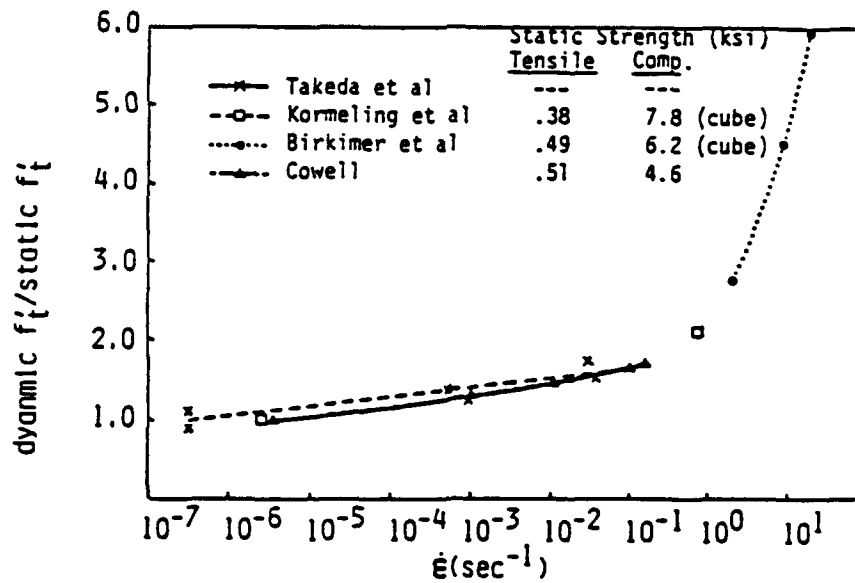
Table 7. Properties of rock-matching grout RGM 2C4, low density rock-matching grout LD 2C4, and Nevada test site tuff (continued).

(b) Mechanical Properties

Material	Average Strain Rate (sec <sup>-1</sup> )	Compressive Strength (psi)	Tensile Strength (psi)
RMG 2C4	Static	3970	530
RMG 2C4	0.15	5330	900
LD 2C4	Static	3200	460
LD 2C4	0.15	5000	780
Tuff	Static	3530	1920

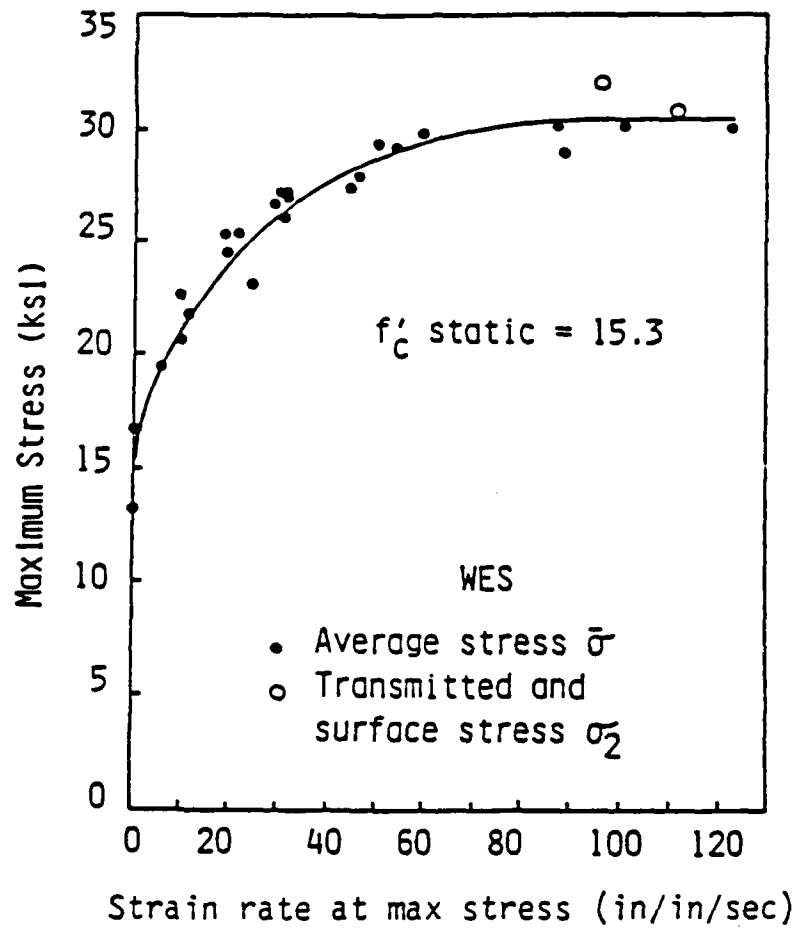


Effect of strain rate on the compressive strength of concrete,  $f'_c$



Effect of strain rate on the tensile strength of concrete,  $f'_t$

Figure 41. Variation of concrete strengths with strain rate.  
(Suaris and Shah, 1982)



Split Hopkinson bar data of Malvern,  $f'_c = 15.3$  ksi

Figure 42. Rate dependence, (Malvern)  $f_c = 15.3$  ksi, static, limestone aggregate.

- |                                  |                           |
|----------------------------------|---------------------------|
| (a) 250, QUARTZITE, 8 KB, 900°   | (h) 18, DIORITE, 0.7 KB   |
| (b) 5, MARBLE, 5 KB              | (i) 18, TUFF              |
| (c) 18, SOLENHOFEN, 1%           | (j) 5, SOLENHOFEN, 0.7 KB |
| (d) 15, SANDSTONE, 0.7 KB        | (k) 14, GRANITE           |
| (e) 42, MARBLE, 5 KB, 500°       | (l) 13, BASALT            |
| (f) 10, WESTERLY GRANITE, 1.5 KB | (m) 17, WESTERLY GRANITE  |
| (g) 11, DIABASE, 1.5 KB          | (n) 15, TONALITE          |

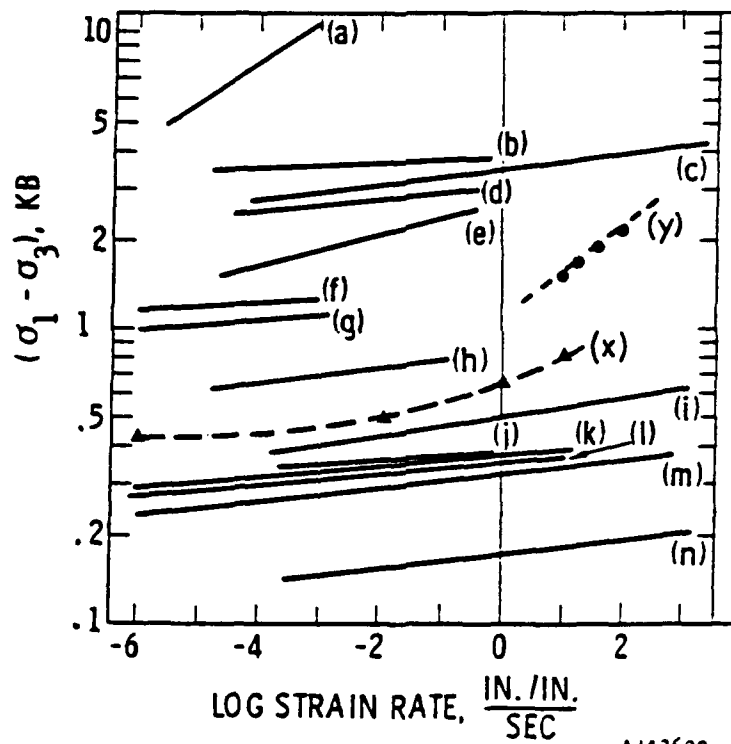


Figure 43. Variation of strength with strain rate at room temperature and pressure except where noted. Numbers at the left of each line indicate the slope of that line. (Brace and Jones, 1971)

Most recently, the tests of continuous rock simulants involve intersecting tunnels.

### 2.3.1 Tests Prior To 1975.

#### Effect of Lateral Pressure ([DNA 3610F], 1975)

The earliest tests were dynamic tests performed with a stiff simulant (6A) to examine the effect of lateral confining pressure on tunnel and rock response. Unlined and lined tunnels were tested with increasing load levels under uniaxial conditions (Tables 8 and 9, lateral pressure is applied to maintain zero lateral strain). Predictably, as the load level increases, damage to tunnel increases (Table 10). Liners were found to retard the damage process since they confine the rock and thereby increase the strength (Table 11).

At a sufficiently high load level, the rock-simulant surrounding the tunnel fractures. When that happens, blocks move along the fracture surfaces and deform into the tunnel (whether lined or unlined) directly (Fig.44). The loading on the liner changes from a smoothly varying pressure around its circumference to local bending at the edges of the blocks and tunnel damage increases rapidly with load. Formation of such wedge-shaped pieces or blocks, if they are large rather than localized, can disrupt the continuum assumptions of the model scaling. Furthermore, fractures formed adjacent to the tunnel intersect the surface of the overall specimen, thus violating the assumptions of an infinite medium.

### 2.3.2 Tests To Study Liner, Pore Pressure and Strain Path([DNA 4023F], 1976).

These tests were conducted with rock simulant 6B (medium strength) with an improved test apparatus. Preliminary tests were also performed to check the validity of the experiments, but these will not be reviewed here.

#### Effect of Liner Thickness

Six static isotropic (lateral and vertical stresses on cylindrical specimen are equal) loading experiments were performed on models in water-saturated simulant under drained conditions. Three contact liners with different a/h ratios were used to study the effect of liner thickness. The results are given in Fig.45. Note the test results give tunnel closures which are larger than theoretical predictions. The reason is attributed to buckling of the liner which is not modeled in the prediction.

#### Effect of Pore Water

Pore water has two effects: it reduces the friction angle of the simulants and it carries part of the load. The first effect weakens the rock and leads to more tunnel deformation. The second effect relieves the solid matrix by carrying part of the load. Barring buckling of the liner due to fluid migration, the opening appears stronger. In static lab testing on saturated but drained specimens, there is no pore water pressure built-up and the only effect of pore water is a reduced friction angle. In dynamic lab tests on saturated but drained specimens, simulant properties such as permeability, and loading rate determine how much pore pressure can be built up and, hence, offset the reduced friction.

Reduced Friction - Five static uniaxial-strain loading experiments were performed on specimens with direct-contact liners in dry 6B simulant; the results can be compared with their counterpart wet (saturated but drained) specimens. The general behavior of wet specimens (Figs.46 and 47) is similar to dry specimens (Figs.48 and 49), but openings in dry specimens are

Table 8. Dynamic tests on unlined tunnels in an intact medium.  
(DNA 3610F, 1975)

AMR No.	P <sub>V</sub> (psi)	P <sub>H</sub> (psi)
6	8,500	1,500
3	8,500	1,100
1	8,500	0
7	11,000	5,000
8	12,000	3,700
9	16,000	4,500
24	20,000	5,000
14	19,000	4,500

Table 9. Dynamic tests on lined tunnels in an intact medium.  
(DNA 3610F, Oct. 1975)

AMR No.	P <sub>V</sub> (psi)	P <sub>H</sub> (psi)
16	8,500	0
12	12,000	3,700
18	16,000	4,500
13	20,000	5,000

Table 10. Summary of dynamic, unlined tunnel tests in an intact medium.  
(DNA 3610F, Oct. 1975)

$P_V$ (psi)	$P_H$ (psi)	$\frac{P_H}{K_0 P_V}$	$\Delta D_V/D_i$ (%)	$\Delta D_H/D_i$ (%)	$\epsilon_{lat}$ (%)	Comments
8,500	1,500	1.0	-1	0	0	Negligible springline flaking, no visible shear cracks
8,500	1,100	0.8	-2	11	0.5	Light springline flaking, shear cracks observed
8,500	0	0	-100	--	--	Specimen was fractured to rubble
11,000	5,000	2.0	-1	1	0	Very light springline flaking, no visible shear cracks
12,000	3,700	1.0	-6	18	0.5	Moderate springline flaking, shear cracks observed
16,000	4,500	1.0	-8	24	1.1	Heavy springline flaking, extensive shear cracks
20,000	5,000	0.9	-43	2	5	Very severe springline flaking, obvious slippage along shear cracks
19,000	4,500	0.8	~-60	--	--	Severely damaged specimen, could not be removed from fixture intact

Table 11. Summary of dynamic, lined tunnel tests in an intact medium.

$P_V$ (psi)	$P_H$ (psi)	$\frac{P_H}{K_0 P_V}$	$\Delta D_V/D_I$ (%)	$\Delta D_H/D_I$ (%)	$\epsilon_{lat}$ (%)	Comments
8,500	0	0	-2	1	0.4	No apparent liner damage, one shear crack visible
12,000	3,700	1.0	-4	1	0.8	No apparent liner damage, one shear crack barely visible
16,000	4,500	1.0	-8	4	2.7	Slight ovaling of liner, no visible shear cracks
20,000	5,000	0.9	-15	6	2.3	Ovaling and severe local bending of liner, exten- sive shear cracks

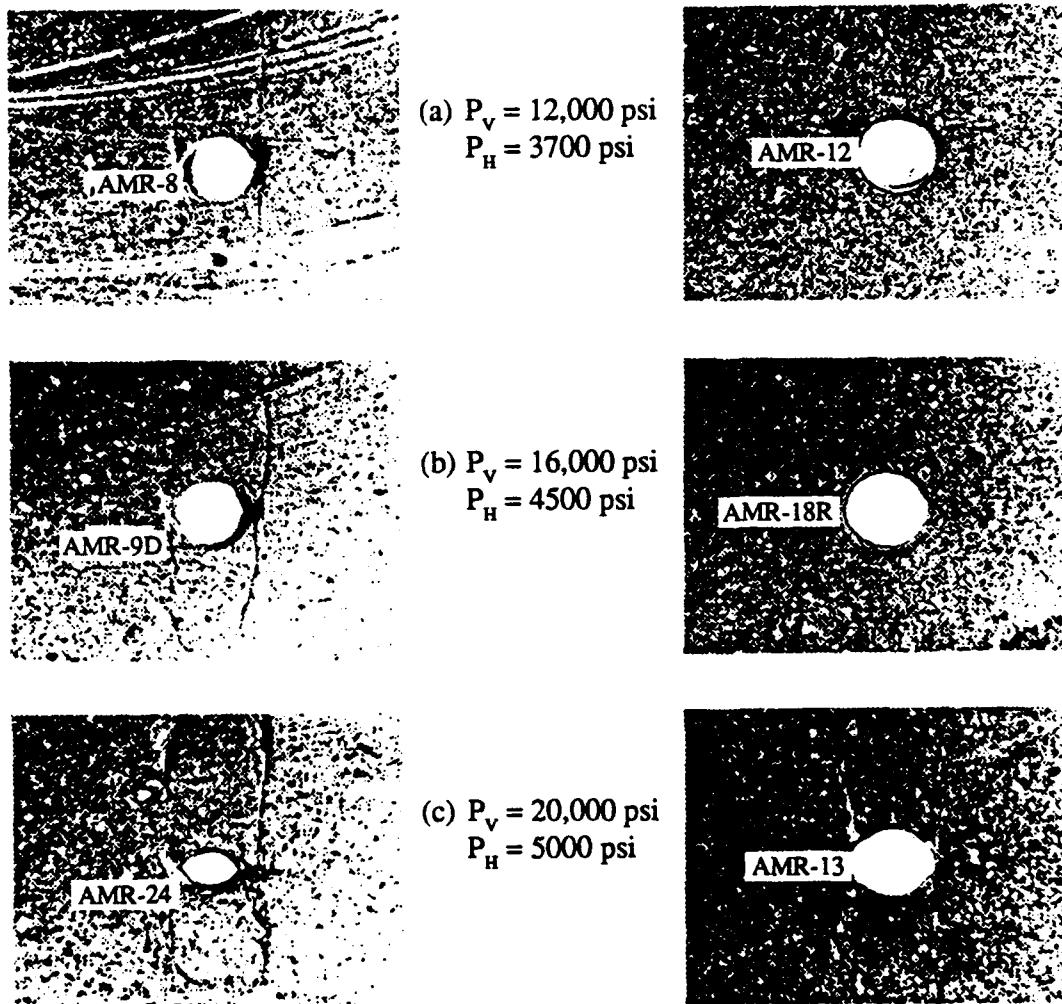


Figure 44. Comparison of unlined and lined tunnel response at increasing load levels under uniaxial strain conditions.

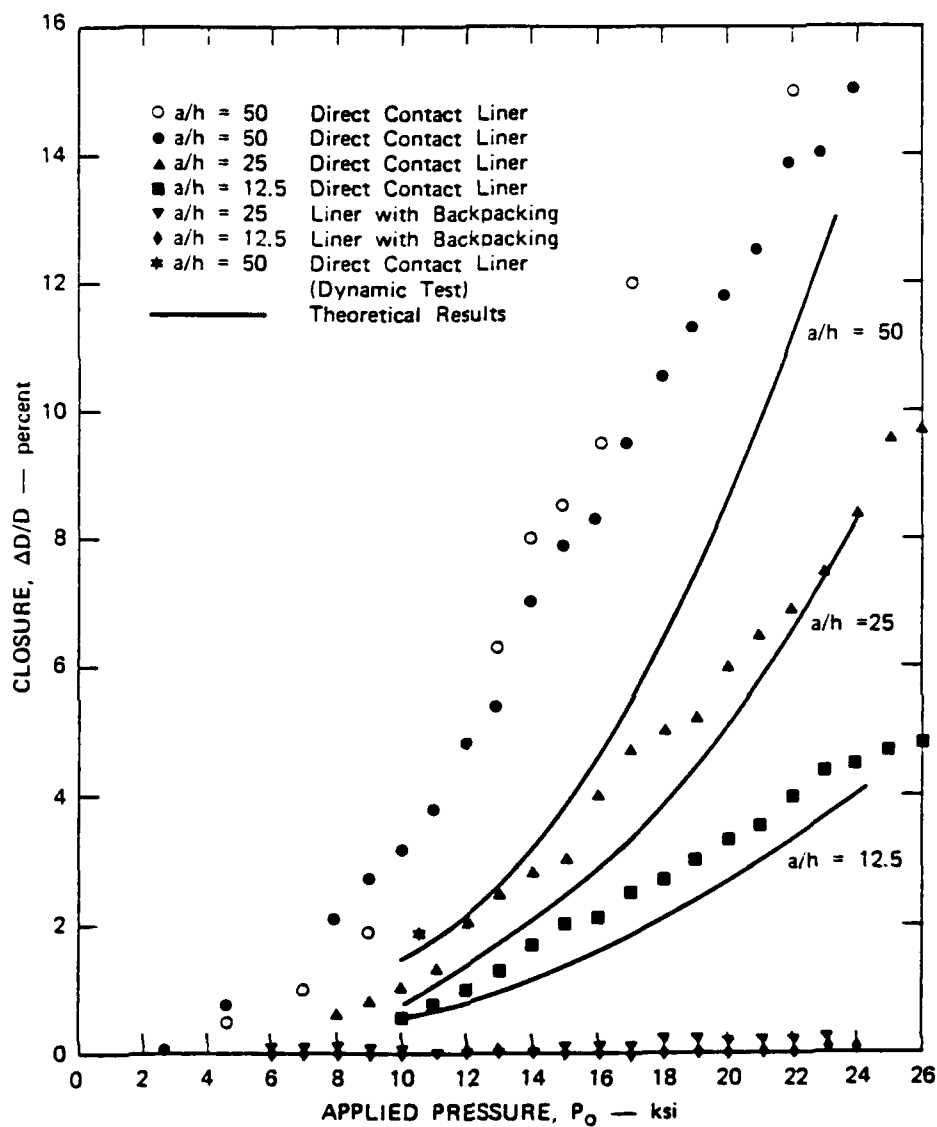


Figure 45. Experimental and theoretical closure versus applied pressure for static, isotropic loading of 6B rock.

less compliant than those in saturated drained specimens. These results confirm the notion that dry rock maintains a larger friction angle at high load than wet rock.

**Reduced Load** - An isotropic loading test was performed on the  $a/h=50$  direct contact liner in saturated drained 6B simulant. Under dynamic loading porewater pressure developed. This test is compared with its static counterpart described previously to assess the effect of pore pressure (see Fig.45). An increase of approximately 40% in load is required to achieve the same closure (2%) if the load is applied dynamically. Comparing this result with other tests where no pore pressure developed, it appears that the load-carrying aspect of pore-pressure overcomes the lubricating (reduced friction) effect of water. Figure 50 shows that wrinkling of the steel liner occurs under both static and dynamic load. The observation that the wrinkling is precipitated at much lower load in the specimen loaded dynamically is attributed to the build up of pore pressure at the rock-liner interface.

Three complications in the experiment should be kept in mind in evaluating these results. First, strain rate sensitivity of the simulant may mask the effect of pore water pressure by making the opening stronger. Second, in the present case, the liner buckled due to water pressure migrating from the rock to the liner area during test, which should be looked for in field tests on direct contact liners. Third, the pre-programmed dynamic lateral stress overconfines the specimen. Despite these complications, the finding establishes that the load carrying aspect of saturated, undrained conditions is more significant, and probably much more significant than the reduced friction effect.

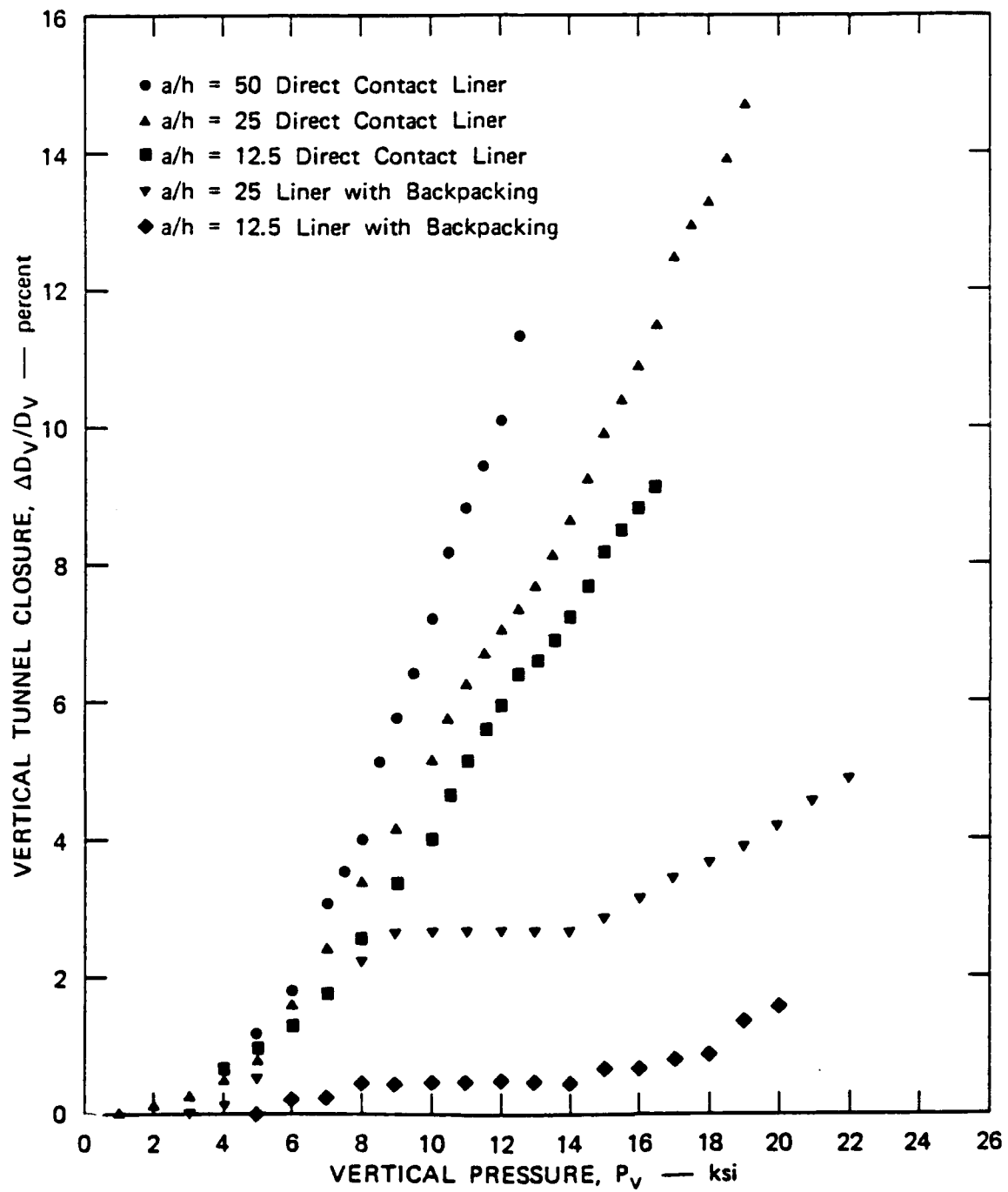
Further discussion on this subject is given in Section 2.3.4.

#### Effect of Strain Path

Five static, drained uniaxial-strain loading experiments were performed on the direct contact liners in saturated rock. The results are shown in Figs.46 and 47. The relationship between closure and liner thickness is the same as for isotropic loading, but the strengthening effect of increasing liner thickness is diminished. The reason is related to the tendency for an isotropically loaded liner to resist deformation through hoop compression, the most efficient means of resistance for a thin-walled shell. Thus, under isotropic loading the liner carries a significant part of the total load. For uniaxial strain loading, the liner resists deformation through a combination of hoop compression and bending, which is less efficient means of resistance. Consequently, the liner can carry a smaller part of the load, with the major part carried by the rock. Since the rock carries most of the load, the type (thickness) of the liner used has little effect on the response of the system.

The data demonstrate that the benefit of increasing liner thickness that is realized in isotropic loading is substantially reduced when the loading is non-isotropic. If the test matrix had been completed with isotropic tests on dry 6B specimens, and similar conclusions obtained for dry isotropic versus dry uniaxial-strain conditions, the conclusion would have been even more powerful. More data of this nature on 2C2 (a much weaker grout) are given in DNA 4425F-2 and DNA 4380F, and they are discussed in Sections 2.3.3 and 2.3.4.

This finding emphasizes the approximations inherent in the Hendron-Aiyer method when applied to field scale tests where loading is not isotropic. The assumption of isotropic loading in the analysis credits the liner with too much strength. This is compensated by exaggerating the strength reduction factor used to convert strength of the rock from intact properties to rock mass properties. The exaggerated strength reduction must be greater for contact liners and less for backpacked liners.



MP-3743-54

Figure 46. Vertical tunnel closure versus vertical pressure for uniaxial strain loading of saturated 6B rock.

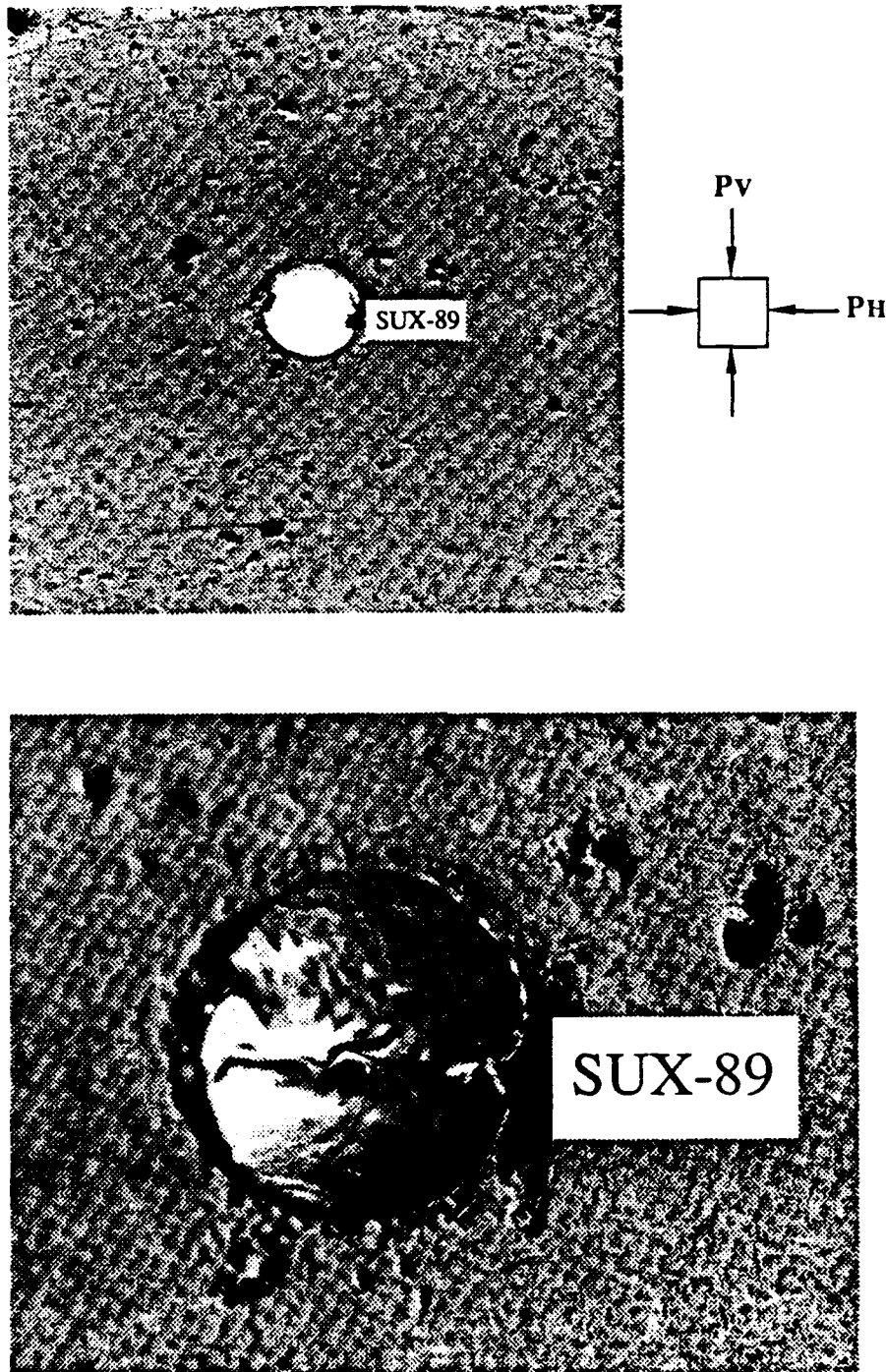


Figure 47. Response of a steel-lined tunnel in saturated rock to static, uniaxial strain loading-- $a/h = 50$ ,  $P_{Vmax} = 12,500$  psi,  $\Delta D_V/D = 0.1135$ .

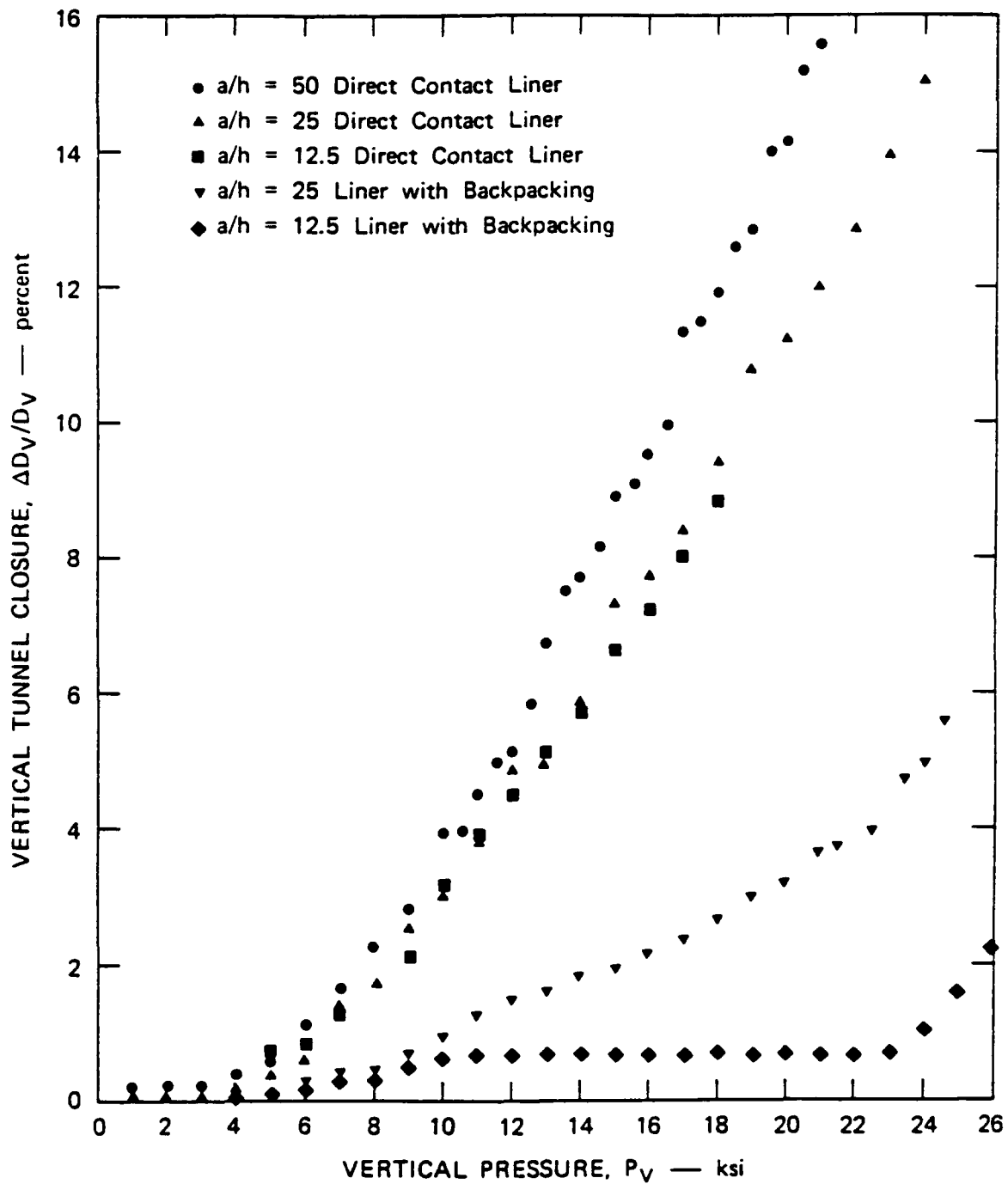


Figure 48. Vertical tunnel closure versus vertical pressure for uniaxial strain loading of dry 6B rock.

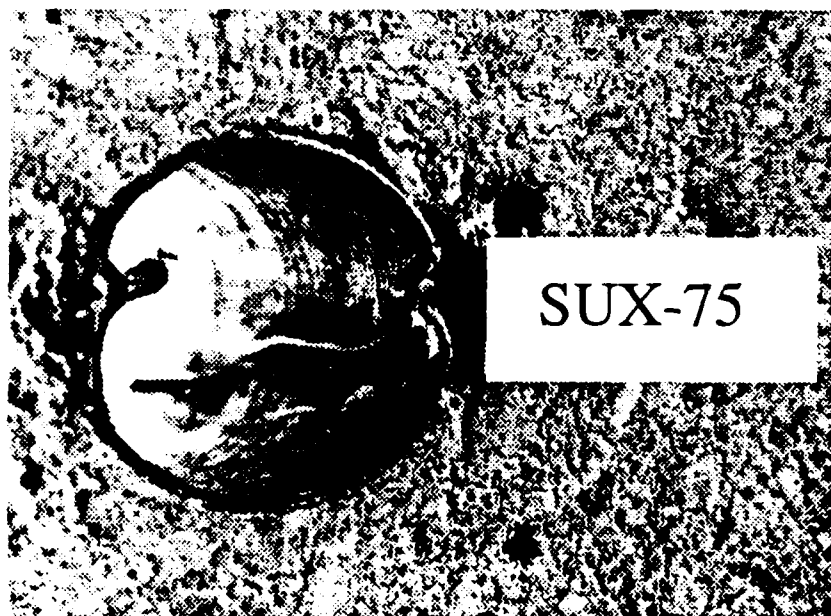
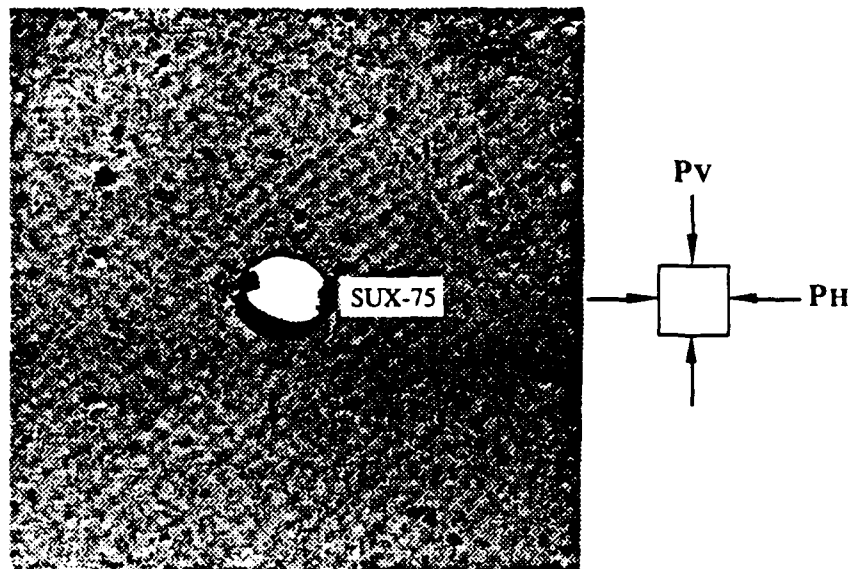


Figure 49. Response of a steel-lined tunnel in dry rock to static, uniaxial strain loading-- $a/h = 50$ ,  $P_{Vmax} = 23,500$  psi,  $\Delta D_V/D = 0.175$ .



(a) Static Response at  $P_o = 22,000$  psi



(b) Dynamic Response at  $P_o = 10,500$  psi

Figure 50. Comparison of static and dynamic response of a steel-lined tunnel to isotropic loading-- $a/h = 50$ .

### 2.3.3 Tests In Support Of MIGHTY EPIC Structures ([DNA4425F-2], 1979).

The tests were conducted on 4" diameter specimens of 2C2 (water-saturated SRI RMG 2C2) containing reinforced tunnels which model 5 different direct-contact structures fielded in MIGHTY EPIC. Uniaxial and symmetric loading were simulated statically and dynamically (Table 12). However, by and large, the most useful information is derived from the static tests.

Results of the tests on AL6061-TO liners (Figs.51, 52 and 53) indicate that :

- (1) tunnel closures measured under static isotropic loading are less than those for static uniaxial strain loading (see composite figure, Fig.54), and the difference increases as the strength (thickness) of the liner increases, and,
- (2) tunnel closures obtained under dynamic loading are considerably smaller than those for static loading.

These results are consistent with those obtained previously for 6B. The wet static tests were performed under drained conditions (with zero porewater pressure) while the dynamic tests generate porewater pressure.

Comparison with the results on 6B grout presented in the previous section indicates that the effect of dynamic loading on 2C2 is much greater. In particular, for wet 6B grout, isotropic tests with steel liner of  $a/h=50$  show that static closure is about 1.4 times dynamic closure. This observation is based on one dynamic data point, which is the only dynamic data available for this material. For wet 2C2 grout, isotropic tests with aluminum liner of  $a/h=4$  to 11.5, static closure is 5 times dynamic closure; the same set of tests under uniaxial strain condition gives static closures which are 10 times dynamic closures. Unlike the 6B tests, this observation is based on more than 15 dynamic data points.

There are obvious differences in the 6B and 2C2 tests which make a direct comparison of the test results difficult. In particular, there are differences in grout material (2C2 versus 6B) and liner material (steel versus aluminum). Nevertheless, the effects due to dynamic loading exhibited in the 6B and 2C2 data sets are firmly established. More dynamic data on dry, 6B grout would have completed these two excellent test matrixes.

Much more data on dry and wet 2C2 specimens are obtained in [DNA 4380F] and will be discussed in Section 2.3.5.

#### Effect of Lateral Confinement

A special test was performed to investigate the effect of under- or overconfinement on the lateral surface of the specimen with reference to the uniaxial strain condition. The results are given in Fig.55. The implication is that closures much larger than expected (based on lab uniaxial strain tests) could be obtained if the specimens are underconfined relative to uniaxial strain.

More data on effect of lateral confinement are reported in [DNA 5208F]. Four-inch specimens of SRI RMG 2C2 with 5/8" steel tunnels are used. The lateral confining pressure is reduced to 90%, 80% and increased to 120% of the uniaxial strain lateral confining pressure in separate tests. Figure 56 plots tunnel closure as a function of vertical pressure for these experiments, and the solid line gives the uniaxial-strain results for comparison. The results show that vertical loads needed to produce a specified crown-invert closure approximately echo the small deviations from the lateral confining pressure required to enforce uniaxial strain. Springline closure, however, is especially sensitive to underconfinement.

Table 12. Tests in SRI RMG 2C2 (tuff simulation).

Model Type	Strength		a/h	Static Loading		Dynamic Loading	
	P <sub>i</sub> (psi)	Design P <sub>o</sub> (kbar)		Isotropic Stress	Uniaxial Strain	Isotropic Stress	Uniaxial Strain
Al 6061-T0	3300	0.6	4	SI-77 SI-97 SI-80a	SUX-78 SUX-96 SUX-79a SUX-90b SUX/SI-102 <sup>c</sup>	DI-64	DUX-72
Al 6061-T0	2100	0.5	6.5	SI-91 SI-101	SUX-93 SUX-99	DI-63 DI-69	DUX-74
Al 6061-T0	1200	0.4	11.5	SI-92	SUX-94 SUX-100	DI-65	DUX-73
Monocoque steel	2100	0.5	18	--	SUX-95	--	DUX-75
Stiffened steel	2100	0.5	18	--	SUX-98	--	DUX-76

<sup>a</sup>Cycling loading.

<sup>b</sup>Underconfined.

<sup>c</sup>Followed by isotropic loading.

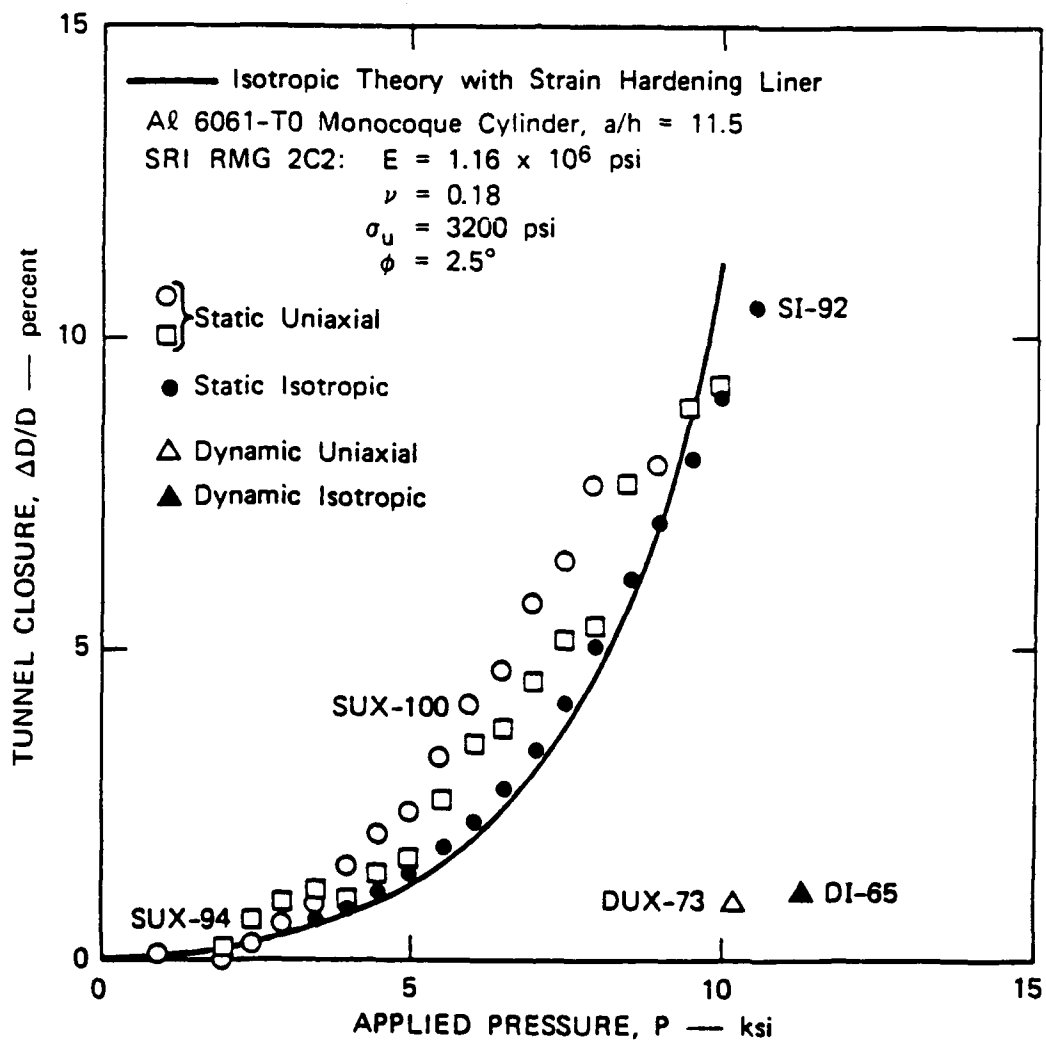


Figure 51. Comparison of tunnel closures in SRI RMG 2C2 for uniaxial strain and isotropic loading -- A 6061-T0 liner,  $a/h = 11.5$ .

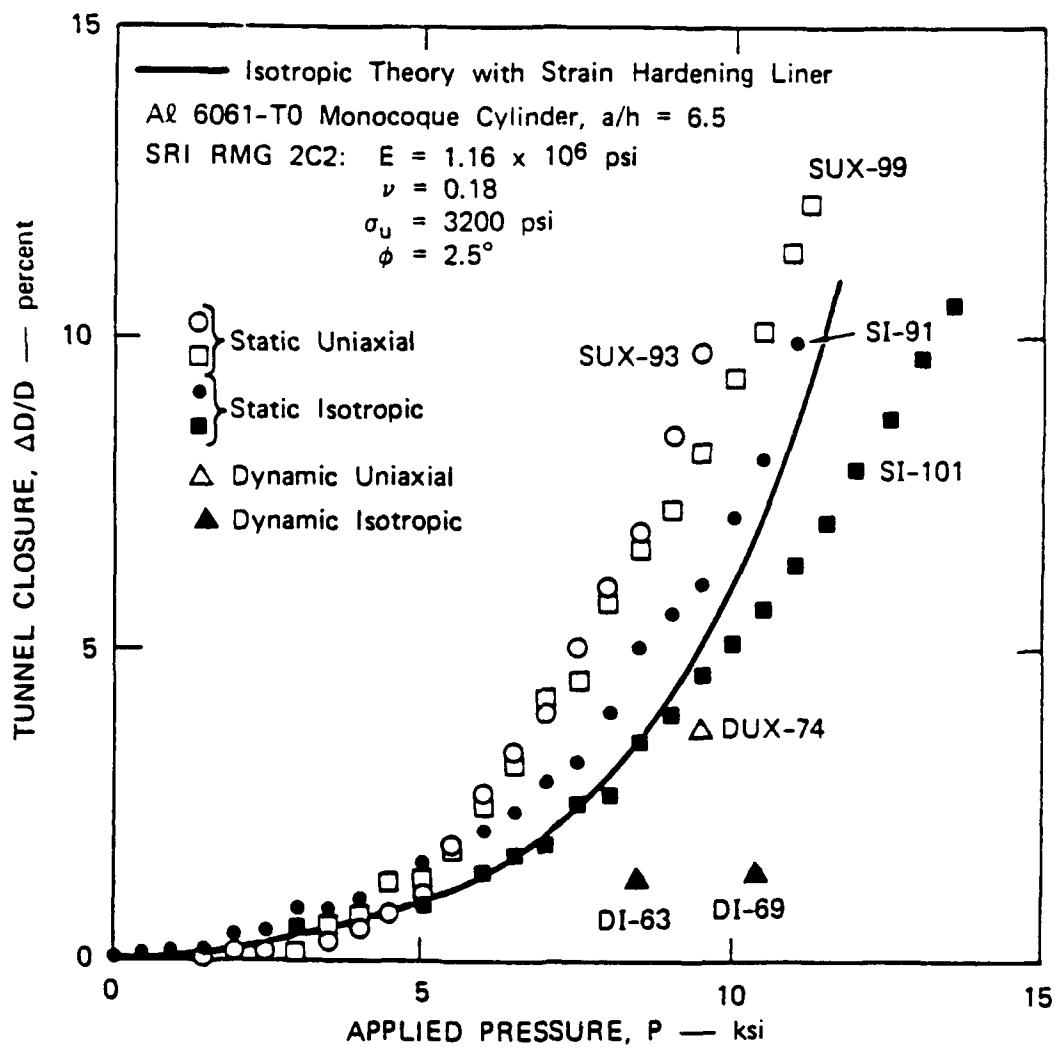


Figure 52. Comparison of tunnel closures in SRI RMG 2C2 for uniaxial strain and isotropic loading -- A 6061-T0 liner,  $a/h = 6.5$ .

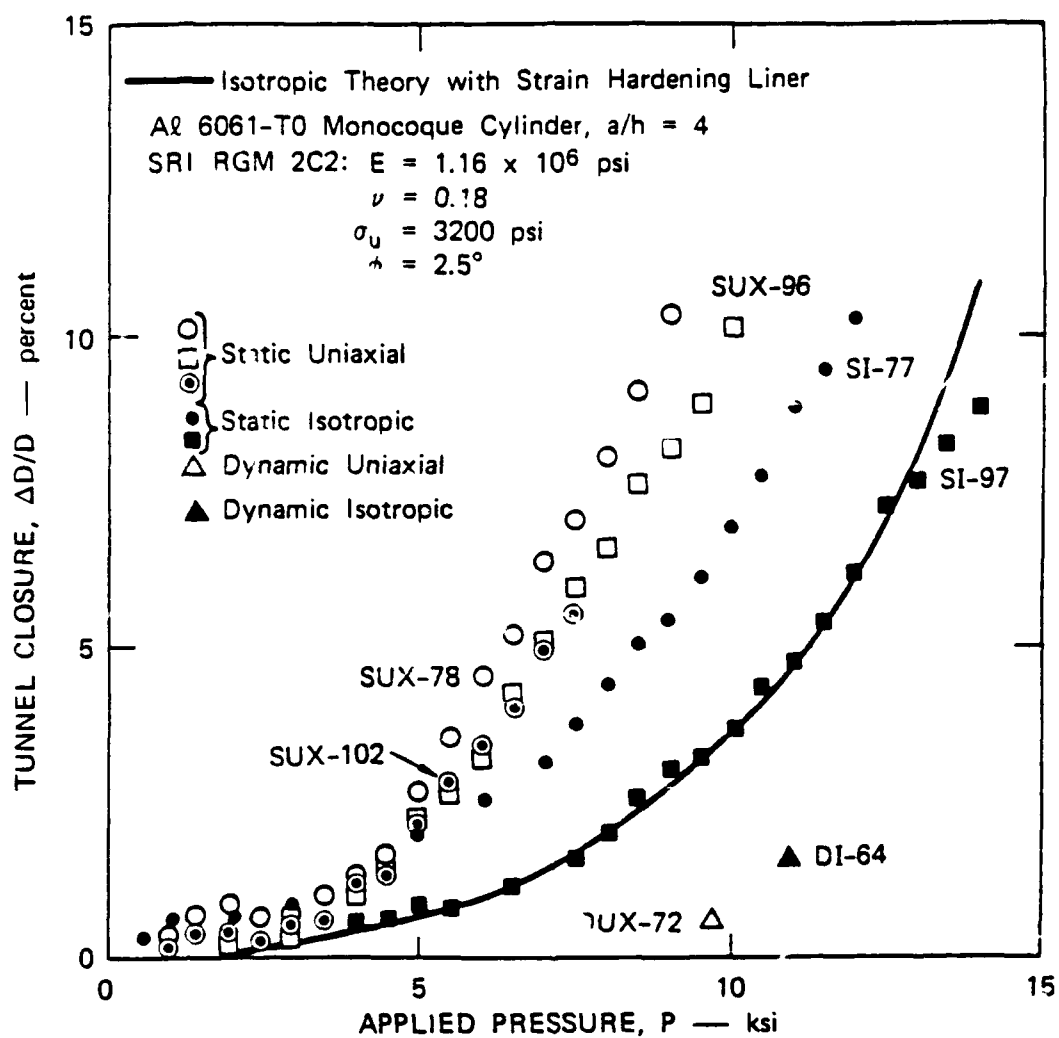


Figure 53. Comparison of tunnel closures in SRI RGM 2C2 for uniaxial strain and isotropic loading -- Al 6061 T0 liner,  $a/h = 4.0$ .

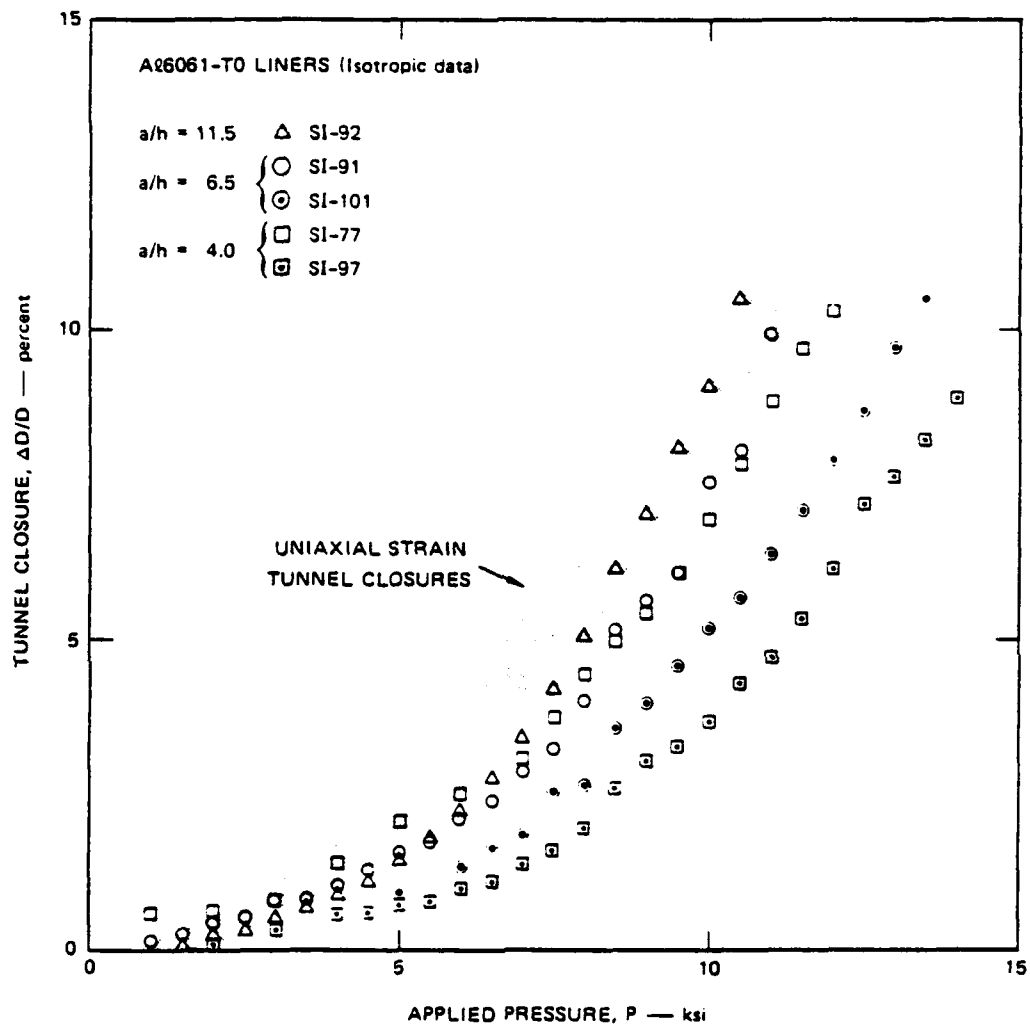


Figure 54. Comparison of tunnel closures in SRI RMG 2C2 for static isotropic and uniaxial strain loading.

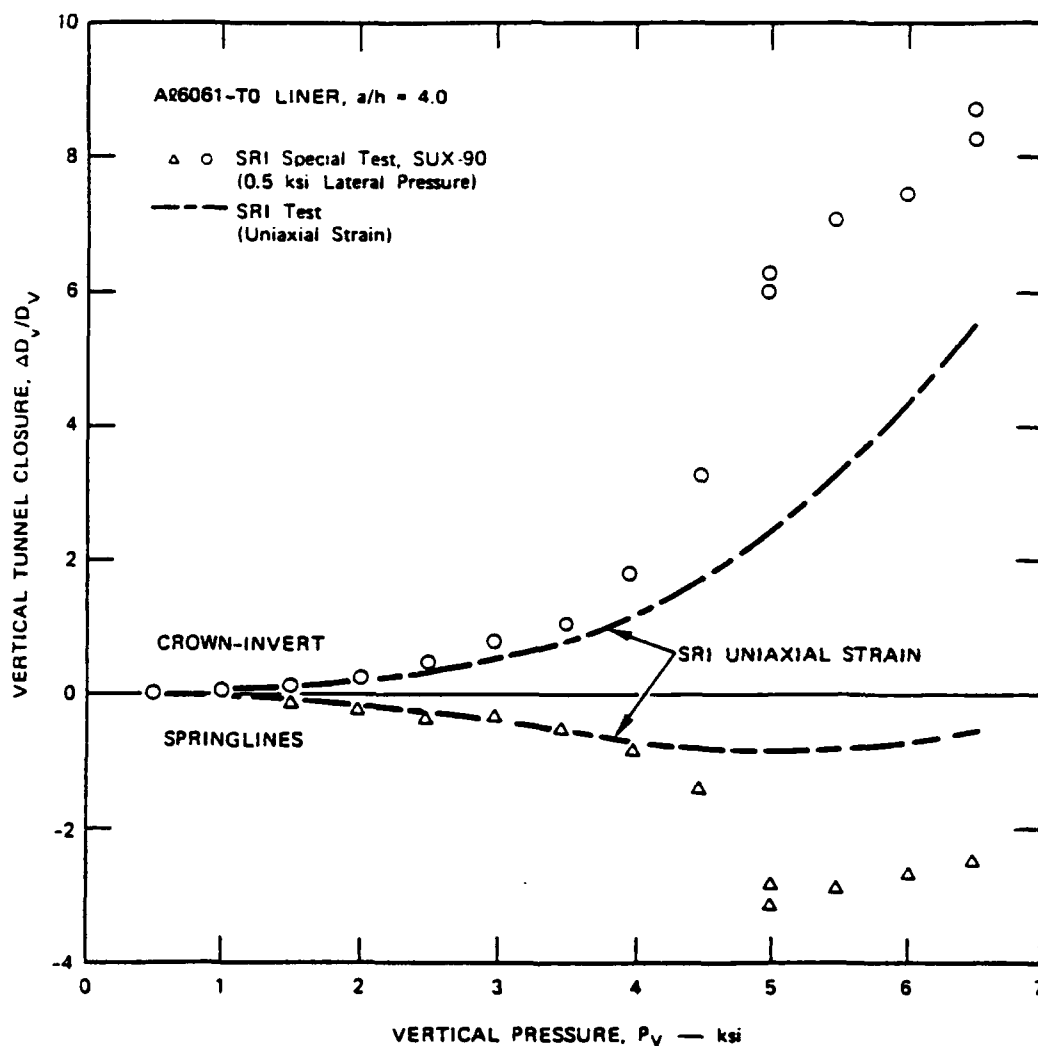


Figure 55. Comparison of tunnel closures in SRI test and special SRI test, SUX-90, in which lateral boundaries of rock are allowed to move out 0.1% (reached at  $P_V = 4.7$  ksi).

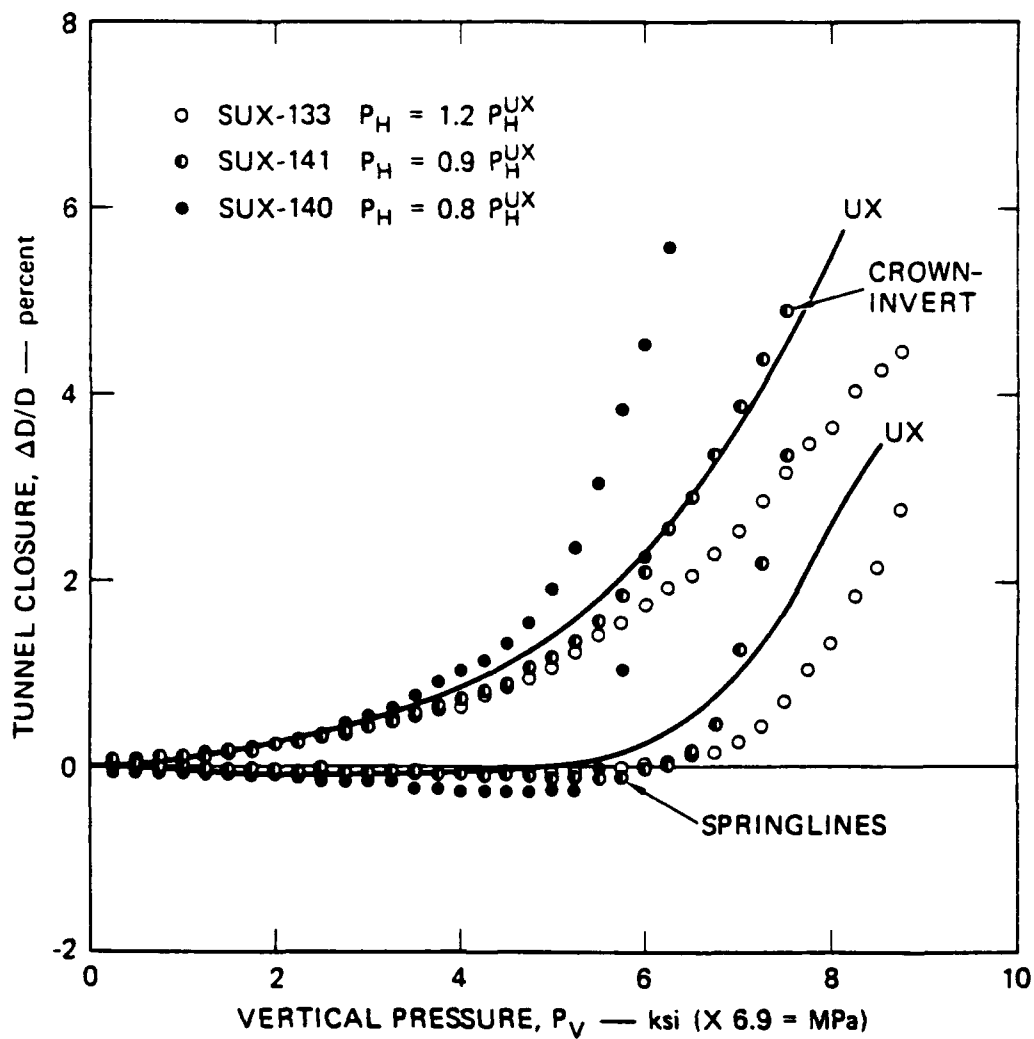


Figure 56. Tunnel closure at crown-invert and springline diameters versus vertical pressure for overconfined, underconfined and uniaxial strain loading of SRI RMG 2C2. 6061-TO aluminum liner,  $a/h = 11.5$

These results clearly demonstrate the impact of lateral confinement, and foreshadow recent computational results that spherical divergence of the free field ground shock, even though slight, can significantly reduce tunnel hardness significantly as measured by crown-invert closure.

#### 2.3.4 Tests In Support Of DIABLO HAWK ([DNA 4380F], 1978).

The tests address dynamic effects, including strain rate and porewater pressure. A single liner thickness ( $a/h=11.5$ ) is used throughout, and both dry and saturated specimens are tested. It is unclear why SRI did not use  $a/h=12.5$  and steel so as to make the results directly comparable with previous series\*. By comparing tunnel closures in static and dynamic tests on dry specimens, the effect of strain rate on rock skeleton behavior can be examined. By comparing tunnel closures in saturated specimens with those in dry specimens for both static and dynamic tests, respectively, the effect of porewater pressure can be examined. Both isotropic and uniaxial strain loadings are used, and the static, saturated tests are drained as before.

The test matrix is given in Table 13. The specimens were 4"x4" cylinders of SRI RMG 2C2, with 5/8" diameter tunnels lined with 6061-T0 aluminum monocoque cylinders ( $a/h=11.5$ ). The results are given in Figs.57 and 58. Note tunnel closure data from the dry specimens, both static and dynamic, lie between the static and dynamic data for saturated specimens. This is true for both isotropic and uniaxial loading conditions.

##### Wet vs dry

The completed matrix of tests on 2C2 grout with isotropic vs uniaxial, wet vs dry and static vs dynamic, produces very useful results and lead to definite conclusions on the role of pore water (better than what could be concluded from the 6B series discussed previously). Comparison of static wet with static dry data given in Figs.57 and 58, indicates that saturated specimens are weaker than dry specimens; the effect of lubrication due to presence of pore water is quantified. Furthermore, the effect is approximately the same for isotropic and uniaxial-strain loading conditions.

Comparison of dynamic wet with dynamic dry data given in the same figures shows that saturated specimens are (much) stronger than dry specimens under dynamic loading. In other words, the effect of porewater pressure (plus strain rate effect) overpowers the effect of friction reduction in the wet material. Despite the large scatter in the dynamic data, the pore pressure effect appears more prominent in uniaxial loading than in isotropic loading.

##### Strain rate

To achieve 5% closure in a dynamic test requires about 20% more pressure in a static test, due to strain rate effects only. This is the first example known to the present authors for which the effect of strain rate is isolated for these types of test.

When porewater pressure is included in addition to strain rate (by comparing saturated static and dynamic tests), the difference in loading pressures increases to about 70%. The present authors surmise that, at the response level of 5% closure in isotropic loading, the strain rate effect is 20% and the porewater pressure effect is 50%, if the effects are additive.

---

\* The reason may be that a larger tunnel deformation requires weaker liners and, hence, reduced liner thickness. However, thin steel liners tend to buckle. With aluminum liners, stiffness is reduced without reducing thickness.

Table 13. SRI RMG 2C2 test matrix.

<u>Specimen</u>	<u>Load Type</u>		
	<u>Static</u>		<u>Dynamic</u>
	<u>Isotropic</u>	<u>Uniaxial Strain</u>	<u>Uniaxial Strain</u>
Dry	SI-115	SUX-103 SUX-114	DI-94, DI-95 DI-96, DI-97 DI-98
			DUX-77, DUX-78 DUX-81, DUX-83
Saturated	SI-92	SUX-94	DI-65, DI-99 DI-100, DI-101
			DUX-73, DUX-79 DUX-80, DUX-82

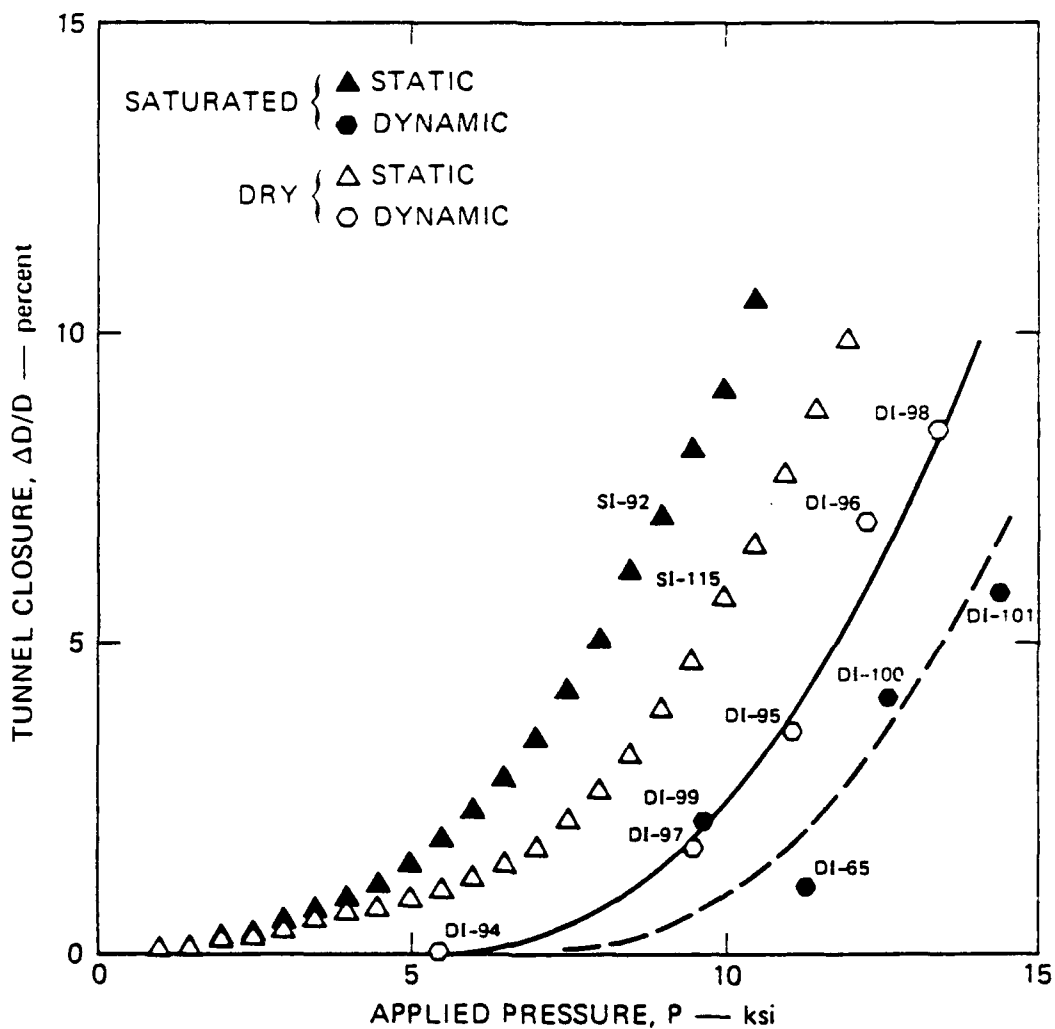


Figure 57. Tunnel closure versus applied pressure for isotropic loading of SRI RMG 2C2. Liner: 6061-T0 aluminum,  $a/h = 11.5$ .

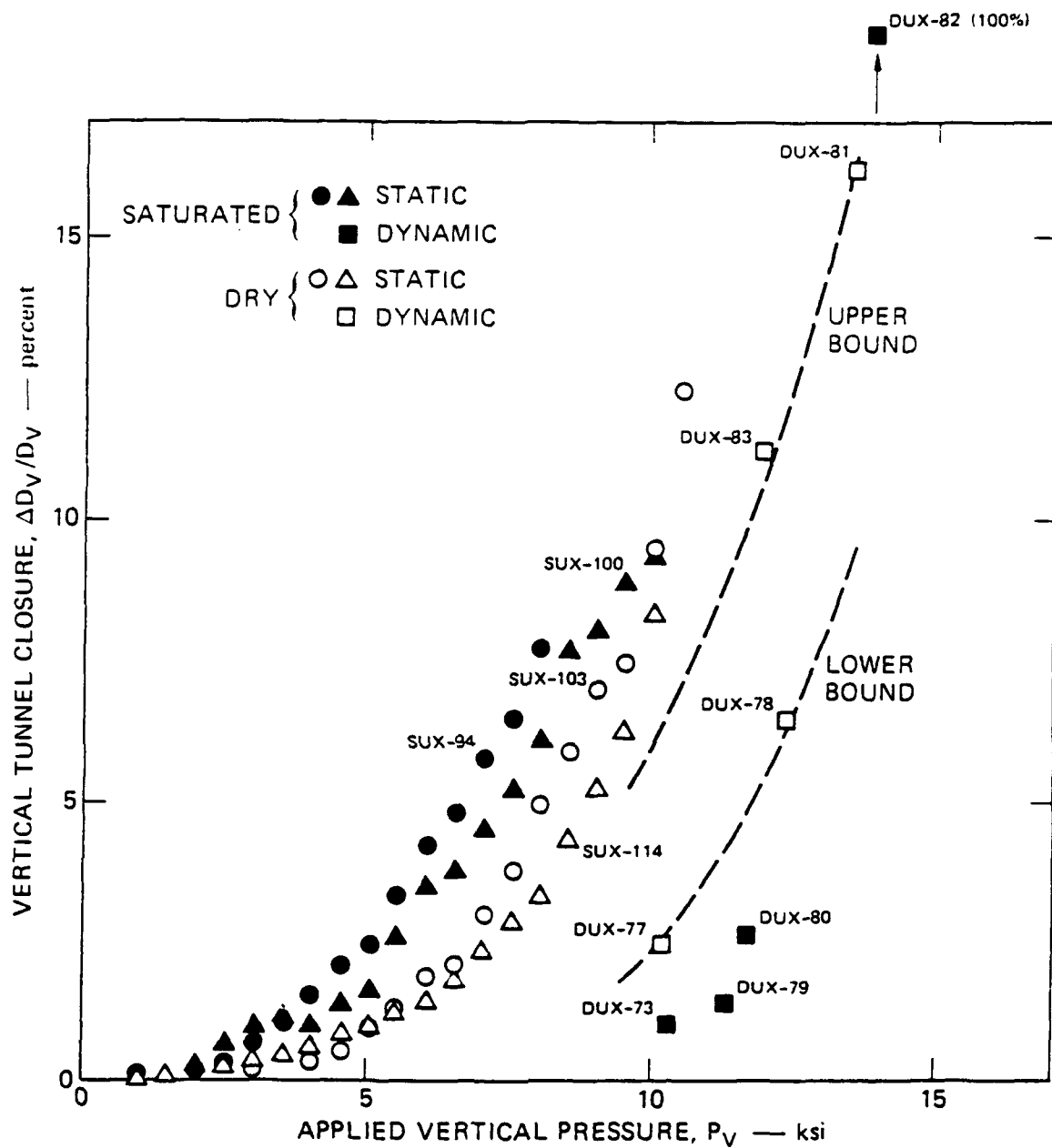


Figure 58. Vertical tunnel closure versus applied vertical pressure for uniaxial strain loading of SRI RMG 2C2. Liner: 6061-T0 aluminum,  $a/h = 11.5$ .

Dashed lines represent upper and lower bounds to tunnel closure under dynamic uniaxial strain loading for dry SRI RMG 2C2.

Whereas in static tests uniaxial strain can reliably be imposed with confidence, in dynamic tests the required confining pressure must be assumed and pre-programmed. Since the strain rate and porewater pressure effects are unknown before the test, the required lateral pressure history cannot be predicted accurately. This makes comparison of dynamic and static tests in uniaxial strain tests somewhat questionable; isotropic loading, in contrast, can be applied with confidence in both static and dynamic tests. Using the upper and lower bounds at 5% closure, Fig.58 shows that the higher strain rate can require a 10 to 40% increase in pressure, compared with 20% in isotropic loading. Despite these uncertainties, these two figures contain tantalizing hints of the effect of strain rate and porewater pressure effects, at least for 2C2 grout.

### 2.3.5 Synthesis Of Data.

The test data identify certain important trends in tunnel response; the effects of boundary proximity, lateral confinement, liner thickness, strain path, pore water, dynamic loading and strain rates have been demonstrated. The most notable observations are perhaps that (1) tunnel response is very sensitive to lateral confinement, and foreshadows the importance of divergent wave condition and (2) the beneficial effect of increasing liner thickness is most prominent in isotropic loading and much less prominent in uniaxial strain loading condition. Significant effects of water on tunnel response are observed but the reasons are mixed. Static test data on dry and wet specimens establish that tunnels in saturated but drained specimens sustain larger deformation; this effect is attributed to a reduction in strength or cohesion of the material, or buckling of the liner due to water migration. Under undrained condition, pore pressure reduces the effective stress in the rock matrix and hence the shear strength of the material. Dynamic test data on dry and wet specimens establish that tunnels in saturated specimens are much stiffer; the phenomenon is attributed to strain rate effect and the stiffening of the rock matrix by pore water pressure. Results on boundary proximity are mixed, but the effects of boundary are shown to be sensitive to properties of the simulant.

Because test series were performed at different times for various program objectives, several simulants were used. It is useful to synthesize the data groups and present them in a unified format. SRI personnel processed portion of their data base with this in mind, and a sample result is given in Fig.59 (from [Simons], 1988). The tunnel is lightly lined, with no enforced composite action (i.e., liner is not tied to grout by studs or bolts), and the loading condition is uniaxial strain. The crown-invert closure vs. load relationship is expressed as:

$$c(\%) = p/a_1 + (p-a_2)/(a_3 * f_c'), \quad p \text{ and } f_c' \text{ in ksi} \quad (2-1)$$

where  $f_c'$  is the unconfined compressive strength and the parameters  $a_1$ ,  $a_2$  and  $a_3$  are determined by fitting data from lab tests listed in Table 14. At present,  $a_1$  depends on the Young's modulus of the simulant,  $a_2$  depends on the strength of the simulant, and  $a_3$  the lateral (elasto-plastic) loading coefficient  $N(\phi)$  where

$$N(\phi) = [1 + \sin(\phi)]/[1 - \sin(\phi)]$$

and  $\phi$  is the friction angle. More details are given in a forthcoming SRI report. Hence, the closure of a lightly lined, with no enforced composite action (i.e., liner is not tied to grout by studs or bolts), tunnel in a simulant under uniaxial strain loading in the geometry used by SRI can be predicted based on the Young's modulus, unconfined compressive strength and friction angle of the simulant. However, Equation 2-1 is not a panacea and should be used with care as noted in the next subsection.

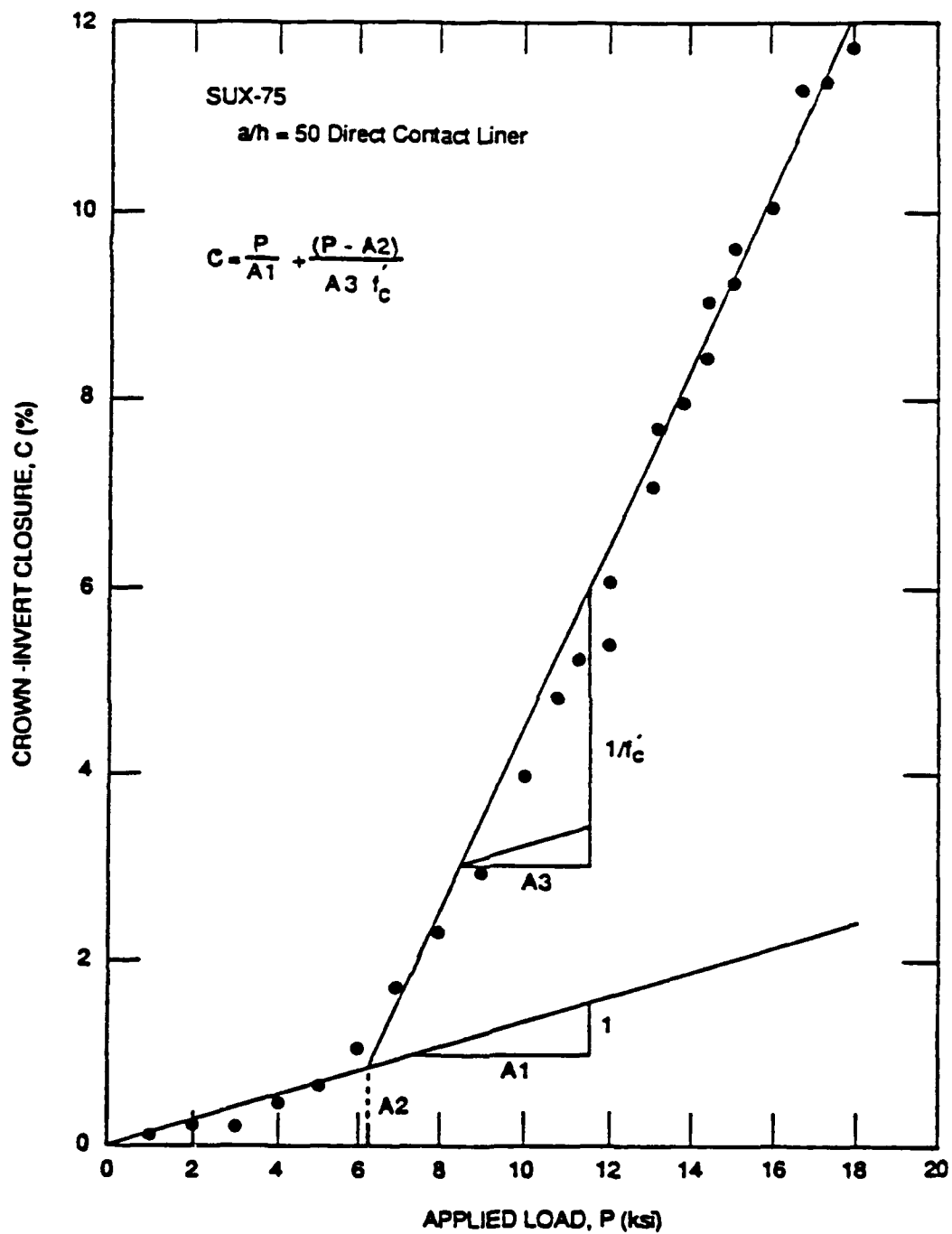


Figure 59. Model 2 parameters.

Table 14. Laboratory experiments/material properties.

### Laboratory Experiments

Material	Symbol	Expt. No.	Liner (R/h)	A1 (ksi/%)	A2 (ksi)	A3 (1/%)
HARM	x	SUX:42-46	12.5	1.33	2.05	.131
2A	+	SUX:105	Unlined	1.12	3.38	.070
2C2	Δ	SUX:128-135	11.5	1.16	6.00	.102
2C2 (dry)	□	SUX:103,114	11.5	5.32	5.15	.197
2C2 (wet)	◇	SUX:94,100	11.5	4.27	5.76	.150
2C4	⌘	LSUX-26	Unlined	4.55	6.74	.086
P-Tunnel tuff	■	LSUX-29	Unlined	2.42	3.92	.093
16A	▽	—	Backpacked	11.8	7.10	.226
6B (dry)	◆	SUX-75	50	10.0	6.50	.290
6B (wet)	⬢	SUX-89	50	6.67	5.20	.196
HF3 (low)	⌘	LSUX-48	Unlined	4.54	3.92	.079
HF3 (high)	⬢	LSUX-49	Unlined	6.67	6.09	.096
HF4	▣	LSUX:52-57	Unlined	5.88	5.51	.115
HF5	▲	LSUX:35,44,46,47	Unlined	7.14	8.52	.124

### Material Properties

Material	E (ksi)	$f'_c$ (ksi)	$\theta$ (degrees)
HARM	0.70	1.00	5
2A	1.00	1.50	4.3
2C2	1.15	4.35	5
2C2 (dry)	1.15	3.68	15
2C2 (wet)	1.15	3.68	2.5
2C4	1.30	5.5	20
P-Tunnel tuff	1.00	2.28	15
16A	3.08	3.68	29
6B (dry)	3.0	4.30	36
6B (wet)	2.35	4.25	35
HF3 (low)	1.3	2.90	26
HF3 (high)	1.3	4.30	30
HF4	2.4	4.35	31
HF5	1.7	4.93	30

### 2.3.6 Observations On Tests Of Continuous Specimens.

The responses of continuum models are, in general, consistent. For example, all closure versus pressure curves have similar shapes: there is a straight portion at low pressures when the tunnel-simulant system remain elastic; at a critical pressure, the slope increases and reaches a transition phase, while at still higher pressures, an incrementally linear relationship is again found.

How to use the data quantitatively remains uncertain. The effects of liner thickness, loading path, pore water and dynamic loading appear as variations on closure-pressure curves and percentages of pressure differences at 5% closure. However, these results cannot be interpreted directly in terms of prototype response for two reasons.

First, they are not deterministic numbers since variations from test to test exist. For example, quantitative results can be repeated within 10-20%. It is not correct to say that the effect of liner thickness in uniaxial strain loading condition is 10% as Fig.58 shows, because this is within the test-to-test variation of unlined tunnels. It is correct to say, however, that the effect of liner thickness in uniaxial strain is small compared with its effect in isotropic loading, which is a qualitative and relative valuation.

Second, and more important, the relationship between the various simulants and a prototype rock has not been established. The SRI researchers and the present reviewers recognize that it is difficult and probably futile to attempt to establish such a relationship. Properties of simulants have inherent random uncertainties, and natural rocks have much larger variations. Hence, if the properties of laboratory specimens are compared with those in native rocks, assuming that the necessary relationship is at hand, the resulting uncertainty bands would be large enough to obscure the trends demonstrated in the laboratory specimens. A glimpse of that is given by Eq.2-1, where  $a_1$ ,  $a_2$  and  $a_3$  have standard deviations of 38%, 14% and 38%, respectively. These numbers are for lab materials (simulants) and for the geometry adopted for the tests.

If the lab data cannot be used directly and quantitatively, how can they be used? Laboratory testing of the type described above are valuable for exploring the influence of various environmental parameters such as moisture and stress state. It appears to the present reviewers that, for rocks which can be considered continuous, the phenomena observed in the lab are qualitatively similar to those in the field. Grain-size is a complicating factor, but as long as the rock medium responds mechanically as a continuum, grain-size does not affect the phenomenon but only the quantitative deformation. Confidence that the phenomena are similar begins to erode when slabbing, spalling or "block motion" caused by cracks initiated at the tunnel perimeter (Fig.44) begin.

Lab data can also serve as a quantitative reference for certain effects. For example, the sensitivity of closure to small variations in lateral confinement that has been observed at laboratory scale suggests that computational models should consider even slight spherical divergence. More work needs to be done, first analytically to address the effects of geometry and then experimentally.

As a general conclusion, however, the present reviewers consider that the SRI laboratory testing alone has not addressed geometric or replica scaling in a definitive manner. The testing of tunnels of several sizes to validate the choice of the specimen size (Figs 5 and 6) is not very useful because of the simulant used and the nearness of the boundary to the tunnel. A much better approach would be to test replica tunnels in the small machine (4" specimen diameter) and the large machine (12" specimen diameter), respectively. The tunnel to specimen diameter ratio of 1:6 can be preserved while the replica scale is increased 5/8": 2" or 1:3. If the same simulant is used in

both cases, the effect of scale, including grain-size, could be examined within existing lab testing capabilities.

Such an effort is reported in [DNA 4380F]. In checking out the larger machine, a 2" diameter tunnel of 6061-T0 aluminum liner in a 12" diameter specimen of saturated SRI RMG 2C2, with  $a/h=11.5$ , was tested and the results were compared with two earlier tests using 5/8" diameter tunnels in 4" specimens, with the same  $a/h$  ratio. Loading was static and the specimens were saturated. The load versus closure relations are compared in Fig.60. Initially, the responses of large and small specimens agree, but for vertical pressures greater than 3.5 ksi, or 1.5% closure, closure of the large specimen is greater than in the small specimens. At 5% closure, the large tunnel supports 70% as much load as the smaller tunnels. To put the difference more dramatically, at a pressure of 6 ksi, the large tunnel is close to failure (closure of 10% and increasing quickly) while the small tunnels have closure of only 4%. The report suggests the difference may be due to differences in porewater pressure. Such different results are significant and affect the credibility of laboratory size experiments and the esteem in which they are held. It is unclear to the present reviewers why SRI has not pursued the subject further.

## 2.4 JOINT PROPERTIES ([DNA 3610F]).

Measurements of residual friction angle were performed by testing rock wafers on an inclined plane with no external pressure applied to the surface of the wafers. Slip between the wafers, which were ground smooth on both surfaces and which contained no material between the layers, started when the plane reached an angle of 21-23 degrees (this is the residual friction angle) with respect to the horizontal. It is assumed that this condition exists in some types of natural in-situ joints.

The authors considered evaluating statistically the equivalent unconfined strength for jointed rock mass,  $\sigma_u$ , for the jointed rock to compare with predicted values from intact rock measurements in order to evaluate empirical parameters, such as those proposed by Hendron. Since they had only enough rock simulant to fabricate six specimens, only one specimen ( $D/S=5$ ,  $\theta=0$ ; wafers horizontal) was tested in unconfined compression. The indicated ratio of equivalent rock mass strength to intact rock strength,  $\sigma_u'/\sigma_u$ , was 0.72 to 0.75 for that sample (see Fig.61) as compared with a value of 0.5 given by the Hendron curve. We recall, however, that the Hendron curve represents the nominal fit to a large scatter of test data and is derived through several major assumptions.

Useful insight into the role of joints on unconfined compressive strength may also be gained by testing specimens without tunnels but having various joint-spacing and orientation angle with respect to the principal directions of loading. The result may not be used directly with Hendron's reduction factor, which implies a tunnel and must be used with the Hendron-Aiyer method of evaluating tunnel hardness. Three types of static experiments of jointed rock simulant, performed by WES in support of DIABLO HAWK ([POR 6998], 1981), are shown in Fig.62. They include direct shear tests, the unconfined compression tests and uniaxial and triaxial tests. The 16A rock simulant used in mini-models of DIABLO HAWK and the granite simulant used in PILE DRIVER were tested. Samples were constructed of 12.7 mm or 25.4 mm thick plates or square rods assembled into 50.8 by 50.8 by 101.6 mm blocks.

The properties of 16A simulant are illustrated in Fig.63. It is apparently a material of moderate strength ( $f_c = 3.68$  ksi) and is suitable for some kinds of rock. Figure 63 shows that the friction angle for joints is about  $\phi=33^\circ$  which is slightly higher than the value of  $\phi=29^\circ$  given for intact rock. The fact that these two angles of friction are so close in value suggests that sliding on joint planes or failure of the continuum may be equally likely. This, in turn, may explain why joint

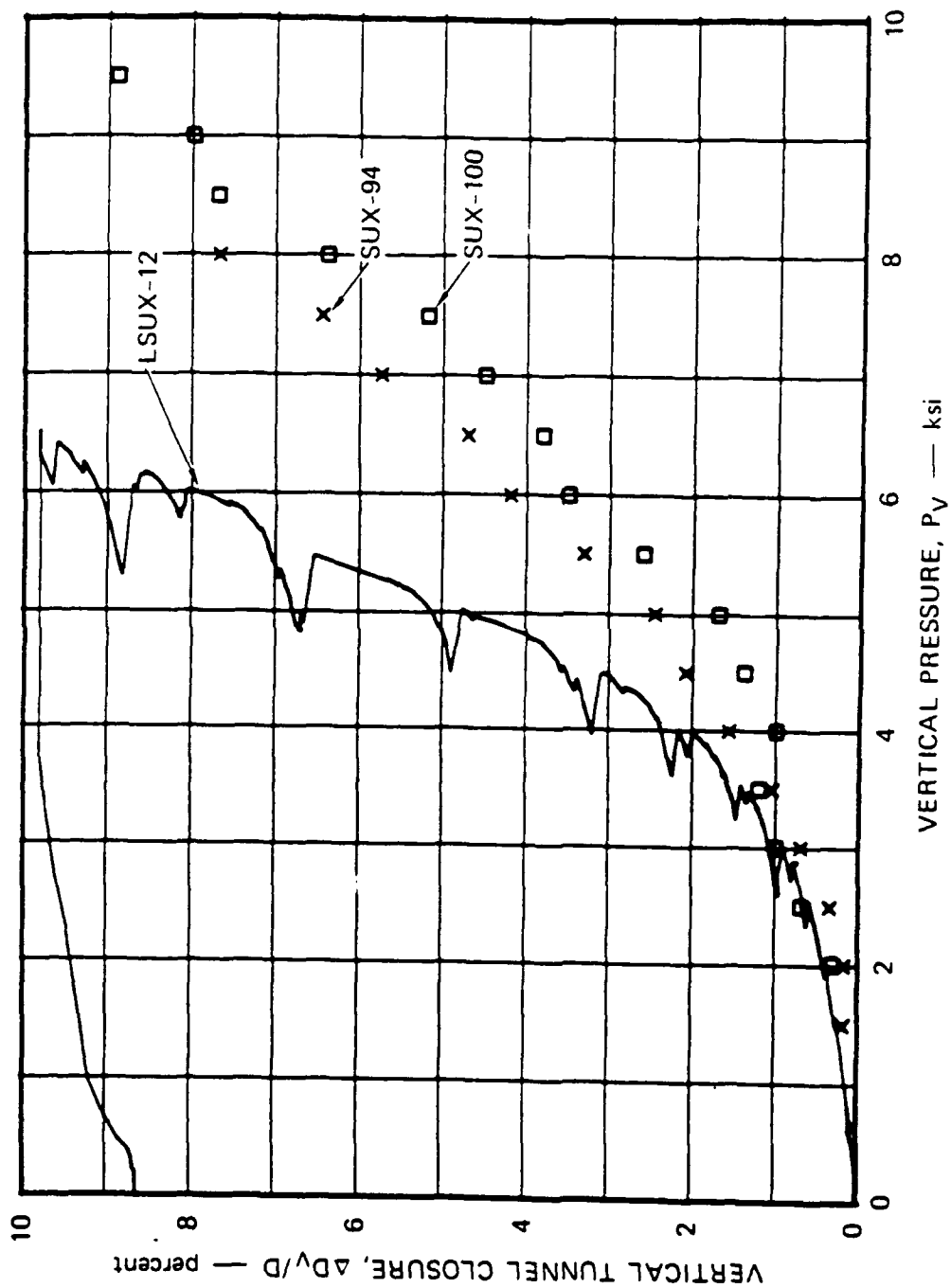


Figure 60. Vertical tunnel closure versus vertical pressure for uniaxial strain loading of saturated SRI RMG 2C2. Liner: 6061-T0 aluminum,  $a/h = 11.5$ .

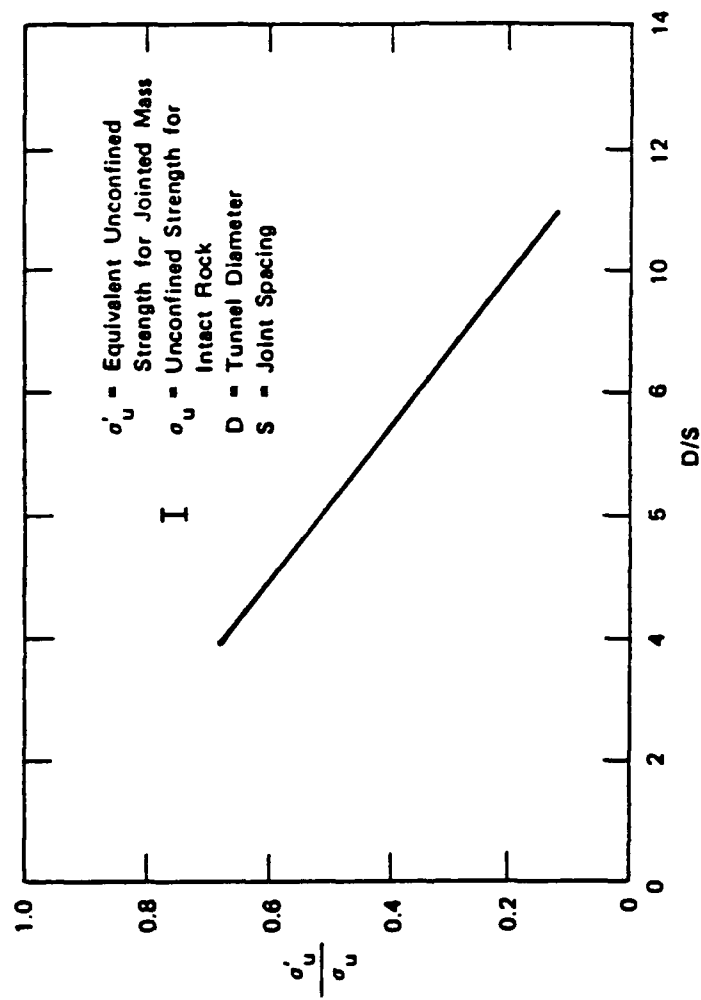
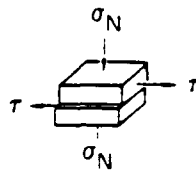
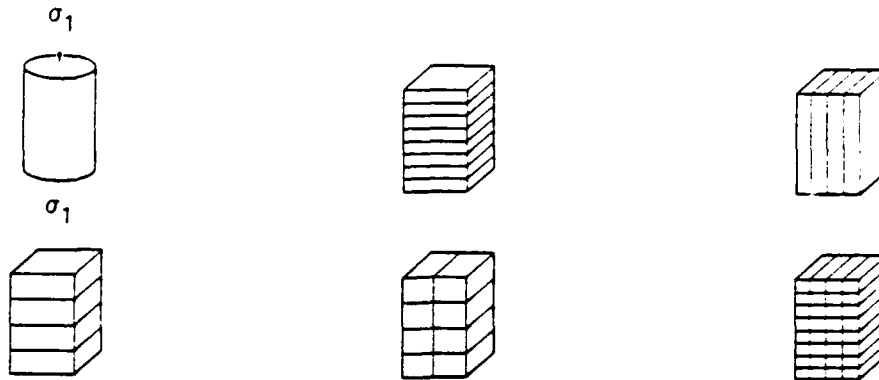


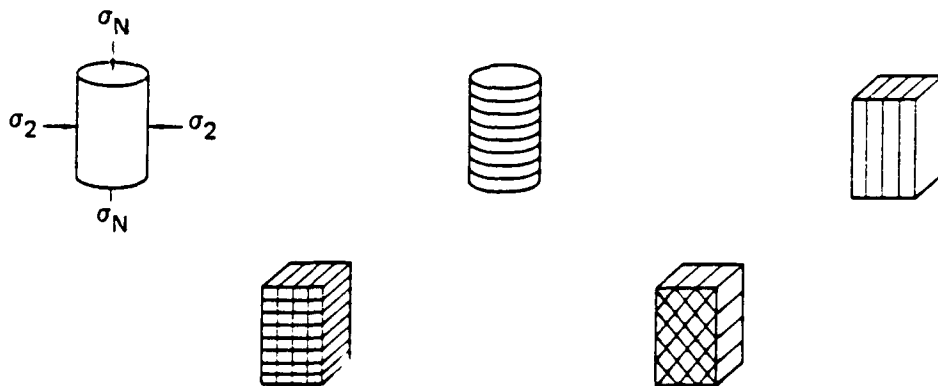
Figure 61. Ratio of in-situ strength to core strength versus ratio of tunnel diameter to joint spacing.



(a) DIRECT SHEAR TEST



(b) UNCONFINED COMPRESSION TESTS



(c) UNIAXIAL AND TRIAXIAL TESTS

Figure 62. Static tests on intact, single-joint and double-joint rock specimens to determine rock joint effects.

(Cylindrical specimens are 101.6 mm long and 50.88 mm in diameter. Rectangular specimens are 101.6 mm long and have a 50.8-mm-square cross section. Square rod and plate thicknesses are either 12.7 mm or 25.4 mm.)

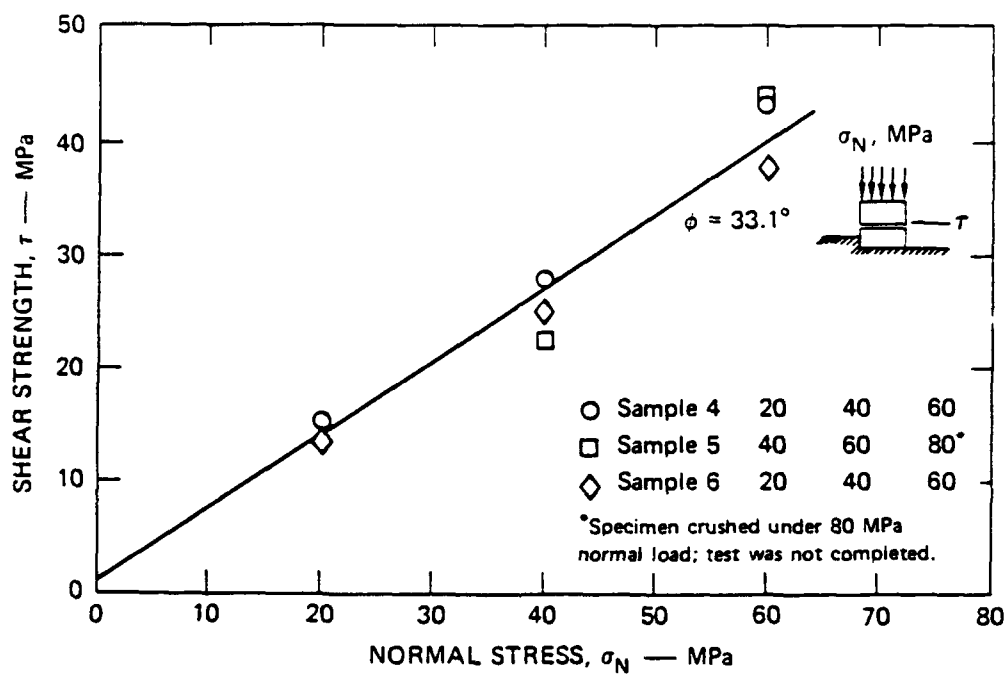


Figure 63. Failure envelope for 16A simulant in direct shear.

slip does not seem to dominate the failure mode in a large number of cases involving jointed specimens in the SRI tests. Figure 64 shows that the angle of friction for sliding on joints in the granite simulant is about  $\phi=30^\circ$ . The angle of friction for the intact granite simulant is not reported. However, if we assume it to be the same as the value of  $\phi=57^\circ$  reported by the Omaha District Corps of Engineers for intact samples of PILE DRIVER granite, the joints in the granite simulant significantly weakens the strength of the simulant mass.

Unconfined compressive strengths are given in Table 15, which shows that strength strongly depends on joint configuration. Joints with slip planes parallel to the loading direction reduce strength to only 40% of that with joint planes perpendicular to the loading direction; the latter are apparently 30% stronger than continuous specimens. Since it is counterintuitive that jointed specimens are stronger than unjointed ones, it is tempting to assume that 30% represents the variability of specimen properties and testing technique. Indeed, variations in specimen ages makes comparisons doubtful. Other counterintuitive findings also appear in the table. For example, comparison of row 2 with row 4 shows that as the joint spacing decreases by a factor of 2, the strength decreases by 4% (36.1 to 34.6); row 5 and row 6; row 2 and row 6, etc. These findings conflict with other data reported by SRI and discussed in Section 2.5.1, which show that closure is unaffected by the presence of horizontal joints.

Mohr envelopes obtained from triaxial tests for five different joint configurations are presented in Fig.65. For confining stresses above 12 MPa, shear strength is lowest for the  $\pm 45^\circ$  diagonal joints, higher for the 0 and  $90^\circ$  joints, higher yet for the vertical joints, and highest for the horizontal joints. As expected, the strength of the intact specimen is higher than all the jointed specimens. This is consistent with results recently obtained using computational models of tunnels surrounded by joints, which show that strength depends on orientation of the joints with respect to the principal directions of loading. The results also suggest that, in order for jointed specimens to show any significant difference from unjointed ones, the confinement needs to be higher than 12 MPa.

The present examples of specimens with throughgoing joints in specimens do not represent jointed rock masses because they are without kinematic constraints at the boundary. The present reviewers recommend that future tests of this type consider how ground shock loading deforms jointed rock masses and whether there needs to be included in tests of this type a volume of the jointed rock mass surrounding whose deformation is somewhat constrained by variations in the joint pattern. The best size of specimen and boundary conditions would depend on the regularity of the joints, joint properties, intact rock properties, the distribution of the length and spacing of the joints, and their relationship to the tunnel diameter.

### Relation To Prototype Rocks

Intact rocks are characterized by the graph of modulus versus strength plot shown in Figure 66 based on a combination of five strength categories and three modulus ratios. Categories into which common rocks fall are shown on the plot. These include granite, flow (basalt, andesite, dacite, rhyolite) and sedimentary (limestone and dolomite, sandstone) rocks. The granites all fall into a single category of hard rock with medium modulus ratio. Limestone and dolomite range from medium to high strength with medium to high modulus ratio. The flow rocks range widely in strength, from low to very high, but all have medium modulus ratio. Sandstone ranges most widely of all, from virtually no strength to high strength, with medium or low modulus ratio.

The intact 6B model rock properties are indicated in Fig.66 ( $E=2 \times 10^6$  psi,  $\sigma_u=4300$  psi). This point lies near the low strength extreme of the intact flow rock properties. However,

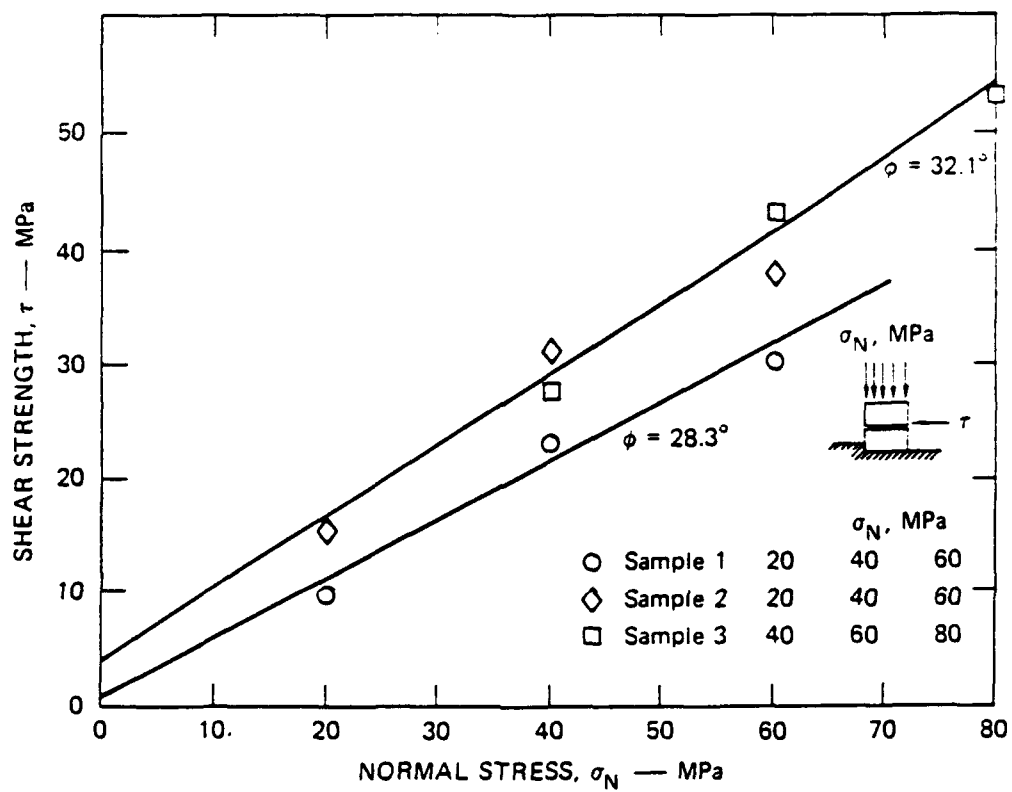

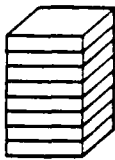
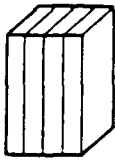
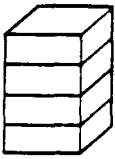
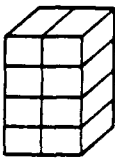
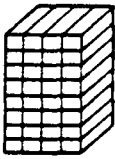


Figure 64. Failure envelope for granite simulant in direct shear.

Table 15. Unconfined compression strength,  $\sigma_u$ , for various joint configurations.

SPECIMEN CONFIGURATION	ROCK SIMULANT	AGE (days)	COMPRESSION STRENGTH $\sigma_u$ (MPa)	YOUNG'S MODULUS (MPa $\times 10^4$ )
	16A	—	26.1	2.12
	16A	420	34.6	0.86
	16A	605	20.7	1.01
	16A	418	36.1	1.00
	16A	450	28.8	0.70
	GRANITE (GS)	40	100.9	1.65
	16A	120	21.6	0.52
	GRANITE (GS)	40	90.7	1.65

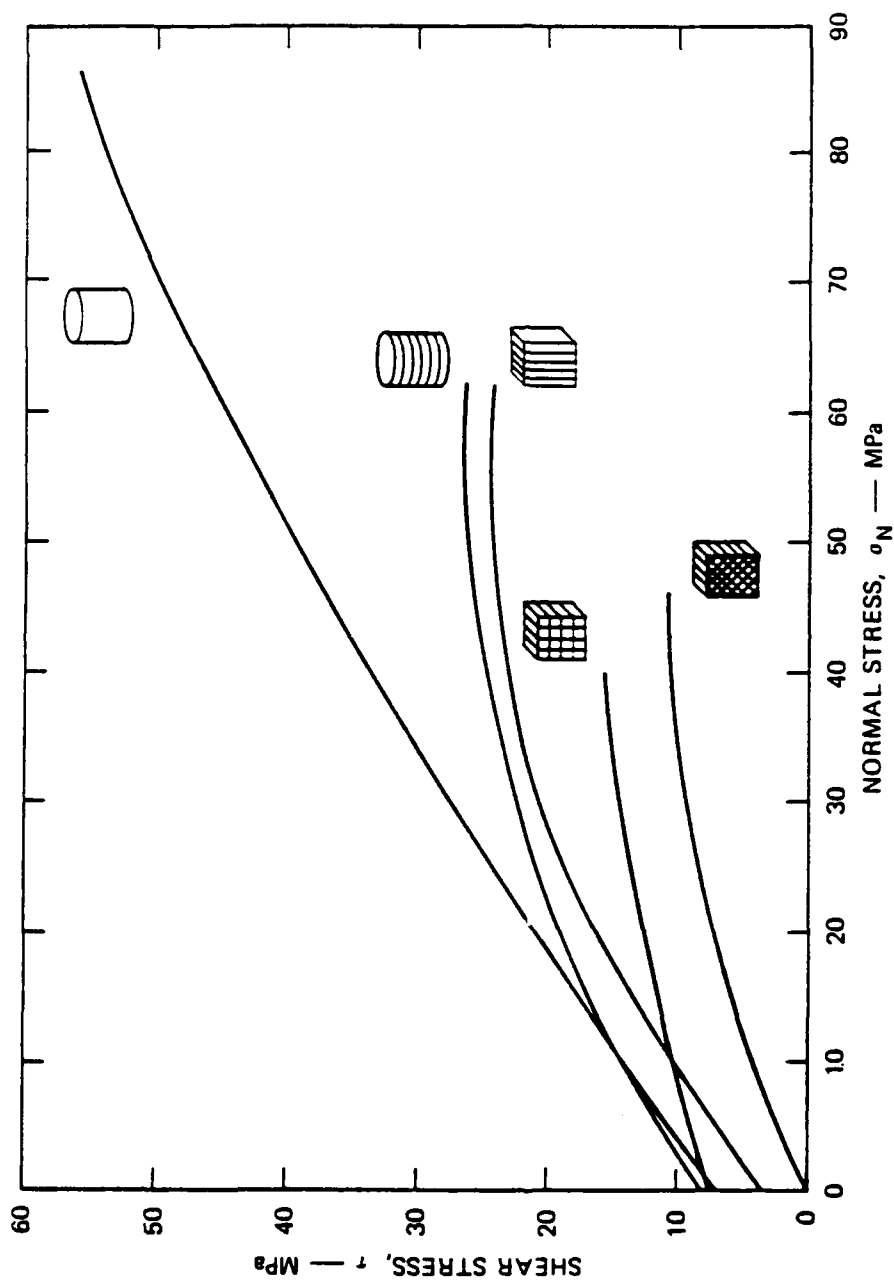


Figure 65. Mohr envelopes for intact and jointed 16A simulant models from triaxial compression tests (12.7 mm joint spacings).

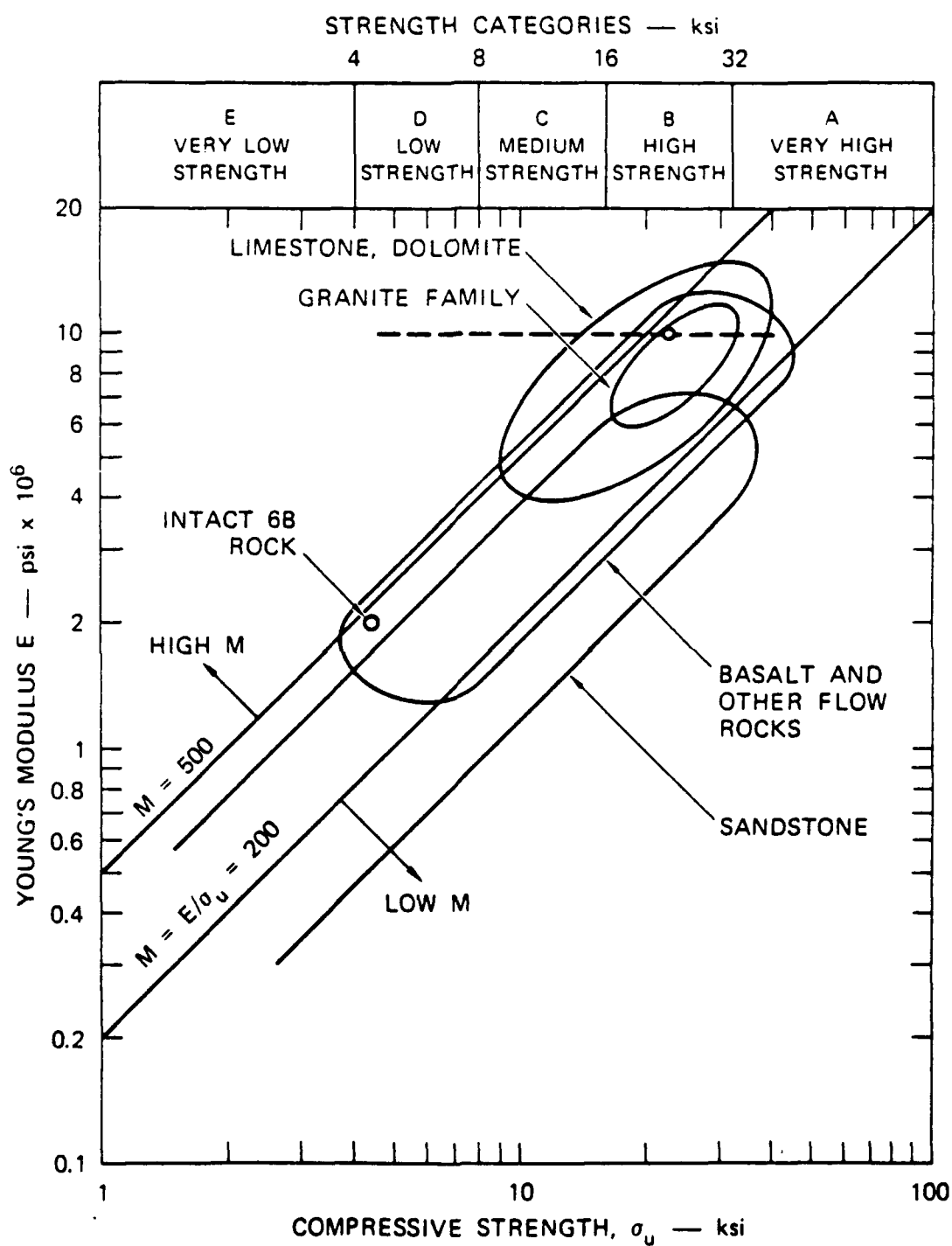


Figure 66. Engineering classification for intact rocks.

interpreted as a model of in-situ jointed rock, it models rocks near the high strength extremes indicated by the dash line in the figure. This is because the effective modulus of jointed rock is about 1/5 of intact rock (see data in Fig.67).

## 2.5 EXPERIMENTS IN JOINTED SPECIMENS.

SRI conducted experiments on jointed specimens in several test series. The laboratory-size models contained parallel joint planes; intersecting joints delineating cubical blocks were used only in field tests (DIABLO HAWK). The tests aimed to study the effects of joints on tunnel hardness and, indirectly, to evaluate the approach to strength reduction proposed by Hendron to account for joint-related size effects in PILE DRIVER and HARD HAT.

### 2.5.1 Early Lab Tests ([DNA 3610F], 1975).

The earliest jointed rock experiments were dynamic tests of unlined tunnels in horizontally layered rock simulant. Tests with two tunnel diameter-to-joint-spacing ratios were performed using the first dynamic testing machine:  $D/S=5$  and  $D/S=10$ . The tunnel diameter was 5/8", and the specimen diameter was 4". The simulant used is relatively strong 6A, and lateral loading is applied to approximate uniaxial strain conditions.

The four tests which make up the series are listed in Table 16, together with the results of the tests in terms of the vertical and horizontal closures. Note that the vertical diametral distance is shortened but the horizontal diametral distance is lengthened. Note also the rectangular nature of opening and the vertical block displacement shown in Fig.68.

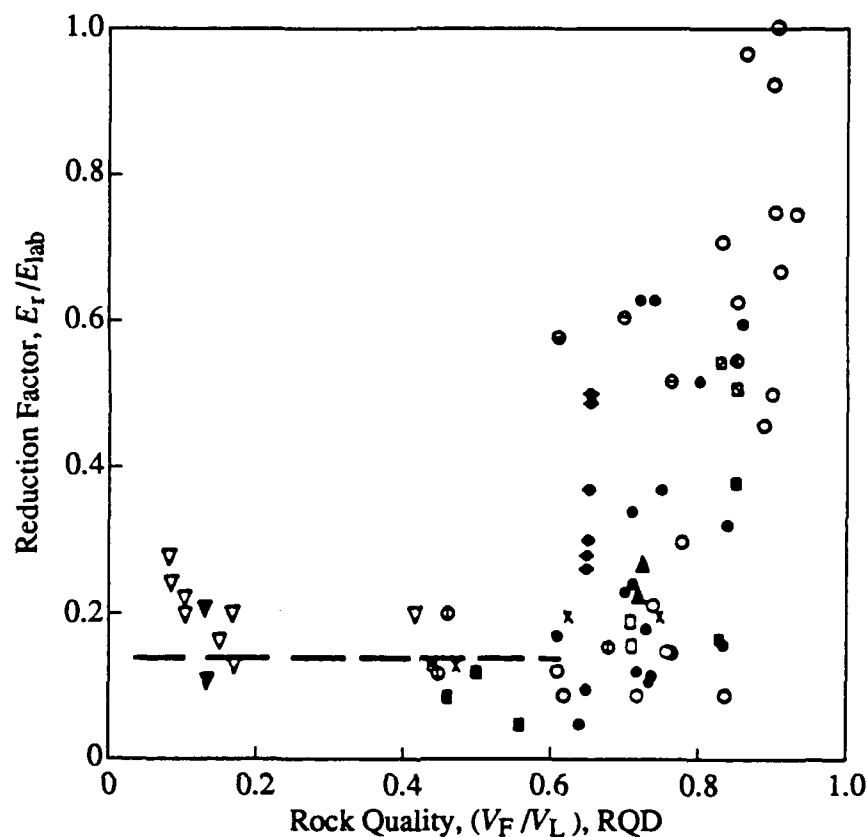
Based on a comparison of the closures for the two  $D/S$  ratios and those for their intact rock counterparts, it is concluded that jointed specimens are more severely damaged than the intact specimens. The specimen with  $D/S=10$  experiences more damage than the one with  $D/S=5$ ; tunnel hardness decreases as the number of joints per diameter increases. This trend, which is qualitatively consistent with the Hendron reduction factor, reflects the damage mode which involves shear or shear/flexure of plates of rock over and underlying the opening. However, in later static tests, horizontal joints were found to have no effect on tunnel closure; that is, specimens with horizontal joints respond as intact specimens (see below).

### 2.5.2 Tests In Support Of DIABLO HAWK ([DNA 4380F], 1978).

Three static uniaxial strain loading tests were performed on 12" diameter specimens that contained reinforced 2" diameter tunnels. One specimen was an intact 2C2 model while the other two specimens were jointed 16A rock simulant models with different joint orientations. The ratio  $D/S=6$ . The reinforcing structure is a 1015 steel liner with  $a/h=12.5$ .

Results from tests on the jointed specimens showed that joint orientation influenced greatly the tunnel deformation. There are qualitative and quantitative differences between the  $0^\circ$  and  $45^\circ$  specimens. The vertical closure is much less for  $0^\circ$  than for  $45^\circ$ , and the springlines of  $0^\circ$  moved inward slightly while those for  $45^\circ$  moved outward considerably.

Figure 69 shows vertical tunnel closure as a function of vertical pressure for both tests. For comparison the closure data from a uniaxial strain loading test on a 4" diameter specimen of intact 16A rock is also plotted. The jointed rock data indicate a sharp increase at very low pressure, due to closing of the initial gaps between the plates. Vertical closure then increases smoothly with pressure; the closure is greater for  $45^\circ$  case than the  $0^\circ$  case, which is about the same as the closure of the intact specimen.



- Dworshak Dam, pressure chamber test (F), buried gauges 17
- Dworshak Dam, pressure chamber test (F), surface gauges 17
- Dworshak Dam, pressure chamber test (E), buried gauges 17
- Dworshak Dam, pressure chamber test (E), surface gauges 17
- Dworshak Dam, jacking tests, surface gauges 17
- Dworshak Dam, jacking tests, buried gauges 17
- Latiyan Dam, Iran 19
- ▲ Kariba Dam, slightly weathered gneiss 19
- ▼ Kariba Dam, heavily jointed quartzite 19
- × Nevada test site, dacite porphyry 20
- Morrow Point Dam 21, 22
- Ananaigawa Dam 23
- Agri River, Italy 24
- Koshiybu Dam, jacking tests
- Koshiybu Dam, pressure chamber tests
- El Noville, Mexico 25
- ▽ Onodera 26
- Vajont Dam, Italy, upper slope, pressure chamber test 27, 28

Figure 67. Variation of reduction factor with rock quality.

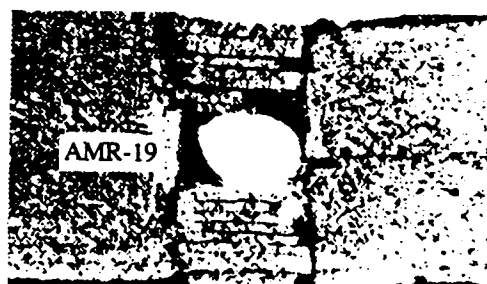
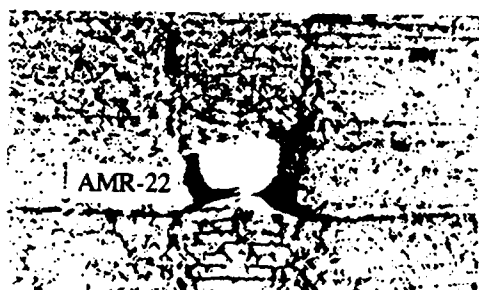
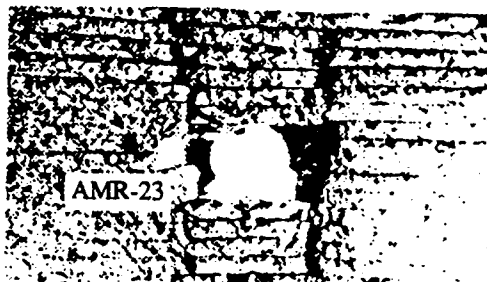
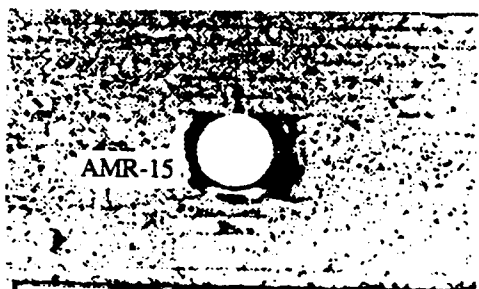
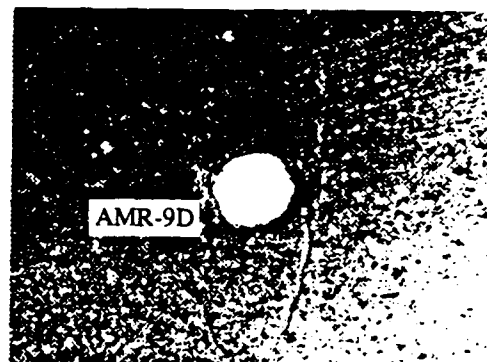
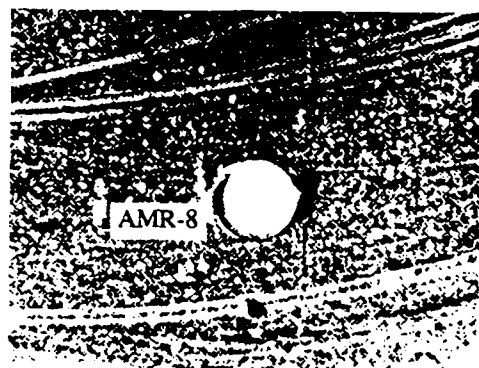
Table 16. Summary of dynamic, unlined tunnel tests in jointed media.

1/8 - inch joint spacing,  $D/S = 5$

$P_V$ (psi)	$P_H$ (psi)	$\frac{P_H}{K_0 P_V}$	$\Delta D_V/D_i$ (%)	$\Delta D_H/D_i$ (%)	$\epsilon_{lat}$ (%)	Comments
12,000	3,700	1.0	-8	16	--	Severe flaking along sides of tunnel, no visible shear cracks
	(Intact		-6	18)		
16,000	4,500	1.0	-9	81	--	Severe flaking along sides of tunnel, extensive shear cracks
	(Intact		-8	24)		

1/16 - inch joint spacing,  $D/S = 10$

$P_V$ (psi)	$P_H$ (psi)	$\frac{P_H}{K_0 P_V}$	$\Delta D_V/D_i$ (%)	$\Delta D_H/D_i$ (%)	$\epsilon_{lat}$ (%)	Comments
12,000	3,700	1.0	~30	~30	--	Severe side flaking and partial collapse of roof, extensive shear cracks
16,000	4,500	1.0	~40	--	--	Specimen collapsed during handling, extensive shear cracks and flaking



(a)  $P_V = 12,000$  psi  
 $P_H = 3700$  psi

(b)  $P_V = 16,000$  psi  
 $P_H = 4500$  psi

Figure 68. Comparison of tests in intact and joined media.

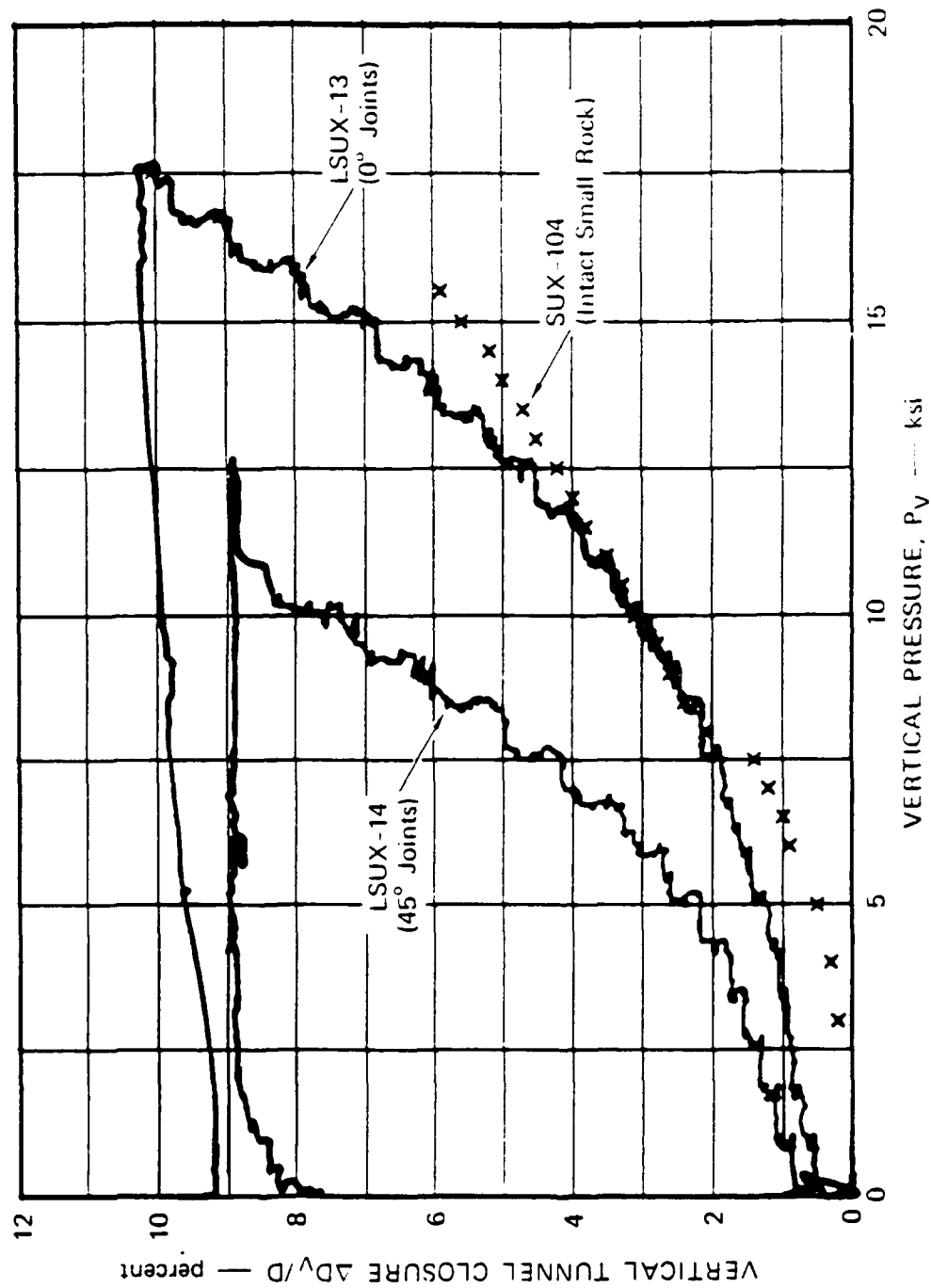


Figure 69. Vertical tunnel closure versus vertical pressure for uniaxial strain loading of jointed 16A rock specimens.

Data from a test on an intact 4-inch-diameter specimen, SUX-104, is plotted for comparison. 1015 steel liner  $a/h = 12.5$ .

Ten tests on jointed specimens are reported in [DNA 5208F, 1979] to study the effects of joint orientation and repeated loading (see Table 17). These are static uniaxial strain tests on 12" specimens that contain a single set of parallel equally spaced joints such as those reported in [DNA 4380F, 1978]. The results on the effect of load-joint orientation support those shown in Fig.69. More discussion is given below.

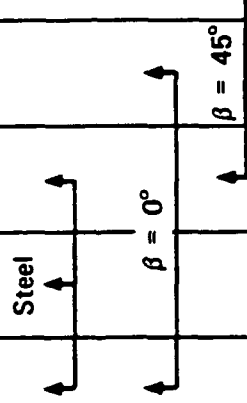


**Monotonic Loading. Jointed Rock Masses** - As a prelude to tests on cyclic loading, monotonic uniaxial strain loading of jointed rock specimens was performed in which joints at three different angles to the major principal stress were considered (0, 30 and 45 deg); an intact specimen was considered for reference. The 0 deg and 45 deg cases of monotonic loading provide a valuable standard against which to interpret the later cyclic load tests because the only change was the loading program. The relationships between vertical closure and applied load show an initial phase during which the closure is dominated by compliance of the joints; closure increases rapidly until the space between the joints is eliminated. The vertical stiffnesses of the 0 deg and 30 deg specimens are about halfway between those of the unjointed and 45 deg jointed specimens. These data are echoed in the springline closure data, which show that the jointed specimens undergo ovaling (springline diameter increase) whereas the springline diameter of the intact specimen initially increases but eventually decreases. Together, these data suggest that jointing decreases lateral confinement; they also suggest that, as the joints become more nearly perpendicular to the springline, the lateral confinement decreases. Apparently joint compliance works to allow the springline diameter to increase by shielding the springline from lateral stress. The lesson for field scale response is that the angle of a predominant joint plane significantly influences the amount of ovaling because it influences the springline confinement. Joint planes which make a significant angle with the horizontal diameter have the same qualitative effect on ovaling as divergent geometry.

This type of effect illustrates one of the chief advantages of lab scale testing when it is used to vary parameters (in this case, the angle of inclination of the joints) in a systematic manner. Because only one parameter was varied at a time, we are able to trace the effect (increase in springline diameter) directly to its cause (reduced lateral stiffness). This would not be possible to do at field scale because the orientation of the joints to the tunnel and the loading conditions are not as readily controlled; the effect would almost certainly be masked.

**Repeated Loading. Monolithic and Jointed Rock Masses** - [DNA 5208F] contains results of model lined tunnels subjected to repeated loads. The goal of the experiments is to investigate whether repeat loading up to the previous maximum resulted in significant additional closure. This knowledge pertains to the issue of whether multiple attacks can cause a target to collapse by incremental closure. There are many factors to be considered in such a question, including how energy is coupled during second and subsequent attacks and how ground shock attenuates in previously shocked rock masses. The study in [DNA 5208F] is restricted to the rock-liner interaction aspects of the problem. Analysis based on Hendron-Aiyer and on finite element was used to develop insight into the mechanism of hysteresis in load-closure curves for both hydrostatic and uniaxial strain loading. Both analytical models assume that the rock is characterized by elastic, ideally plastic properties, which is appropriate for 6B, 16A and 2C2 grouts used in the experiments. No additional information is presented in the report that indicates how accurately these grouts may simulate the properties for rock masses and stress levels of interest, such as limestones at confinements below the brittle-ductile transition.

The responses of both intact and jointed specimens are reported. The intact specimens were tested under previous programs. Jointed specimens were tested under the present program. The basic finding from both types of analysis and from experiments on both intact and jointed specimens is that the relation between closure vs peak stress for monotonic loading is a backbone for the relation under repeated loading and unloading-reloading. Closure increases beyond the

Table 17. Jointed model test matrix.

Test Number: LSUX-	13	24	14	17	21	20	19	25	22	23
Loading Type	Mono	Mono	Mono	Repeat	Repeat	Mono	Mono	Mono	Mono	Mono
Load-Joint Orientation $\beta$ (DEG)	0	30	45	0	45	0	30	45	30	30
Tunnel-Joint Orientation $\gamma$ (DEG)	90	90	90	90	90	90	90	90	60	69.3
Reinforcement Type	Steel	Steel	Steel	Steel	Steel	Foam	Foam	Foam	Steel	Steel
Response Comparisons:										
	Joint Orientation									
										
	Repeat vs. Mono									
Steel vs. Foam										
	Tunnel Orientation									
										

previous maximum at load levels slightly less than the previous maximum. The agreement between analysis and laboratory measurements is impressive, despite the fact that the analytical models seem to indicate slightly more damage during second and subsequent cycles than was observed in the experiments.

The authors of [DNA 5208] present analysis which shows that, during hydrostatic loading into the plastic regime, stresses are locked in which precipitate yielding at a lower load level on reloading than on first loading. This effect is probably more reliably captured in specimens made of 16A simulant than 2C2 simulant. This is because, as results presented in [DNA 5208F] show, the zone of inelasticity is more completely confined in the region of the opening in the stronger 16A simulant; in contrast, the fact that inelasticity extends throughout the specimen of 2C2 simulant probably prevents stresses from being locked in. The test data on 16A simulant indicate that, in principle, it is possible to increase closure, perhaps even to collapse, by repeated loading which does not exceed the previous maximum load. However, the results of this study indicate that the extra closure caused by repeated loading is too small to be exploited in a practical attack scenario.

The test series covers a wide range of parameters -- three different grouts, wet and dry specimens, intact and jointed specimens with joints at two different angles relative to the principal directions of loading, uniaxial strain and hydrostatic loading, and direct contact and backpacked liners. The results are all consistent with each other and with the analyses insofar as the basic findings described above are concerned. Since a wide range of conditions are encompassed by the experiments, it seems probable that the results are representative of field scale behavior in at least some rock masses.

The influence of cyclic and monotonic uniaxial strain loading for tunnels in 16A jointed specimens can be evaluated for joint angle of 0 and 45 deg relative to the load direction. The cyclic loading results exhibit the same influence of joint angle as do the monotonic loading results cited above. This is apparently because the lateral confinement for the 45 deg case is less than that for the 0 deg case. The hysteresis loops grow with the number of reloading cycles, probably due to slip at the rock-liner interface.

### 2.5.3 Synthesis Of Data And Comments.

A qualitative lesson can be learned by looking at closeup photographs of the tunnels as shown in Figs.70 through 73. Several cracks formed near the crown and invert and they appeared to be caused by bending (of the simulant plates). This should be contrasted to the intact case where classical spiral shear cracks emanate from the springline or vicinity due to shear flow (Figs.74 and 75). In both cases, the cracks change the load distribution on the tunnel but apparently in different ways.

Although the joint pattern in prototype jointed rocks is less regular, the present reviewers agree that cracking in continuous material between joints similar to that observed in the lab is likely to occur near the tunnel. The cracks, initiated in shear or flexure, create smaller additional planes of sliding, increase the ratio of D/S and influence the load distribution on the tunnel.

Initially, the tests on jointed specimens appeared promising. Tests in 6A simulant with horizontal joints and D/S=10 indicated more damage than for D/S=5, which agrees with current understanding of PILE DRIVER and HARD HAT. The damage mode was apparently shear cracking through the layers of rock between joints. Damage apparently propagated to top and possibly to the bottom boundaries of the specimen, and hence may have been influenced by specimen size. However, these results were not confirmed by tests of a lined tunnel with D/S=6 and a/h=12.5 in 16A simulant with horizontal joints. Thus, one test indicates that horizontal joint spacing affects strength and another indicates that it does not. Of course, there may be an explanation which is able to reconcile this apparent conflict; for example, the liner may play a

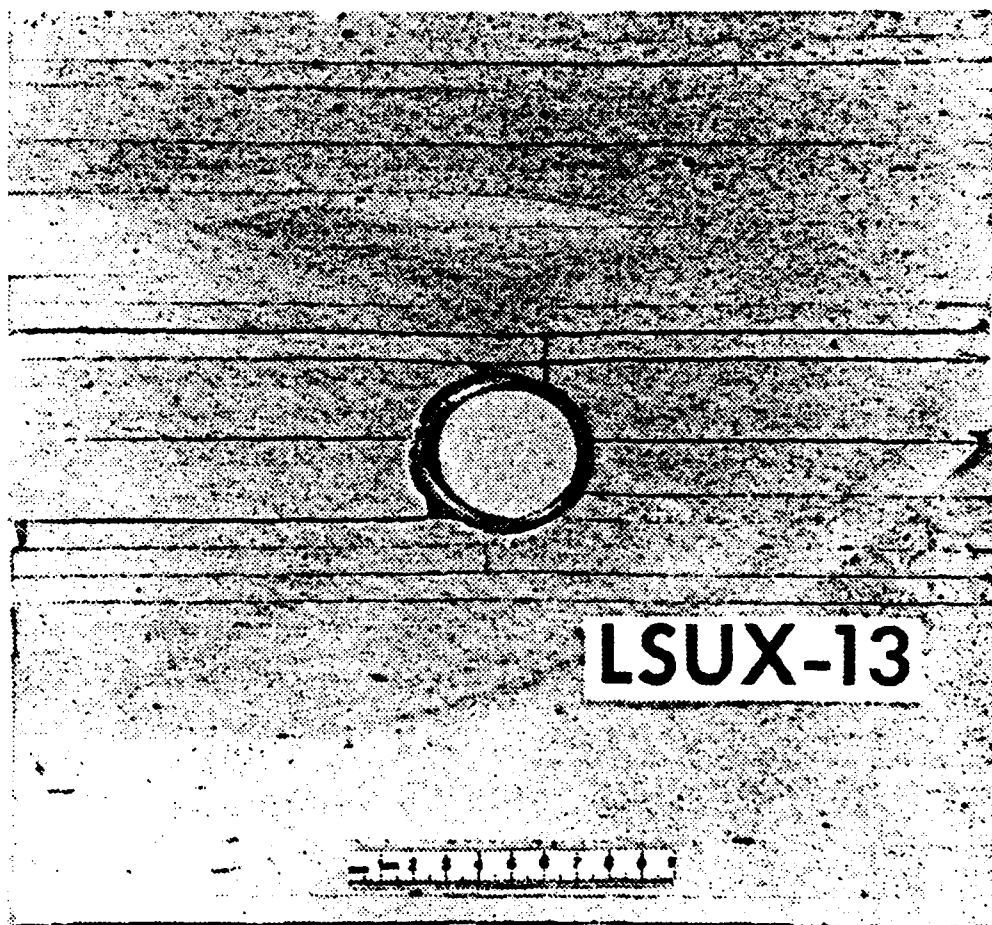


Figure 70. Sectioned specimen from static uniaxial strain test LSUX-13  
( $P_V = 17$  ksi,  $P_H = 7.4$  ksi,  $\Delta D_V/D_V = 10.2\%$ ,  $\Delta D_H/D_H = 0.25\%$ ).

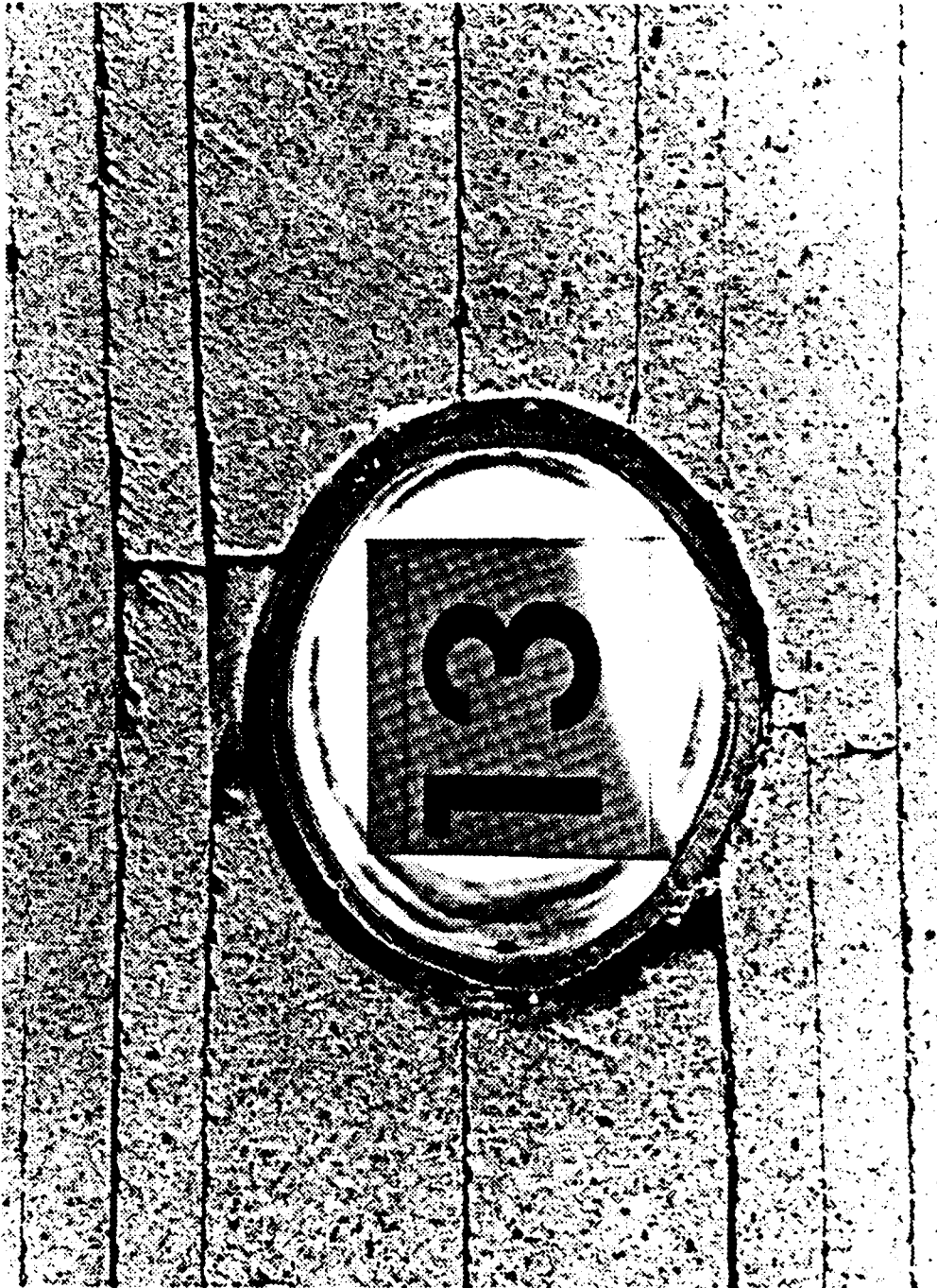


Figure 71. Enlargement of tunnel region in LSUX-13 specimen.



Figure 72. Sectioned specimen from static uniaxial strain test LSUX-14  
( $P_V = 17$  ksi,  $P_H = 4.6$  ksi,  $\Delta D_V/D_V = 8.90\%$ ,  $\Delta D_H/D_H = -5.10\%$ ).

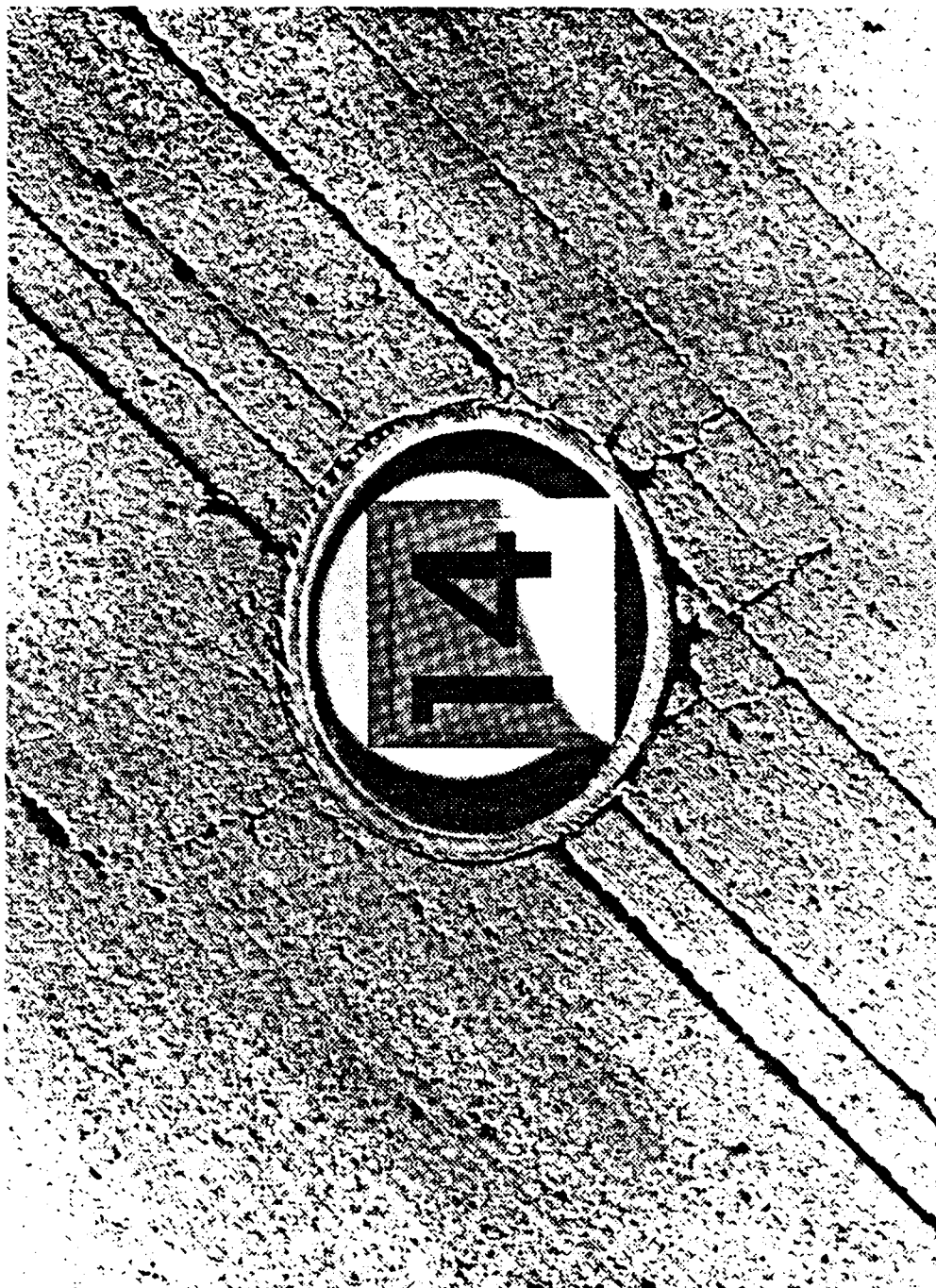


Figure 73. Enlargement of tunnel region in LSUX-14 specimen.

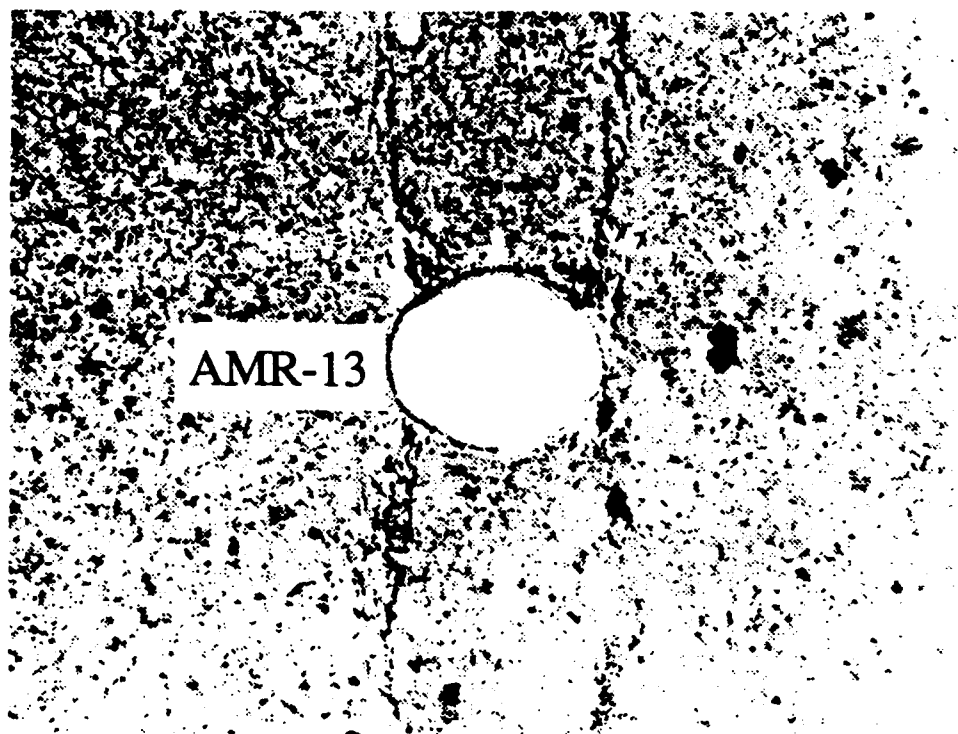


Figure 74. Lined tunnel experiment— $P_V = 20,000$  psi,  $P_H = 5,000$  psi.

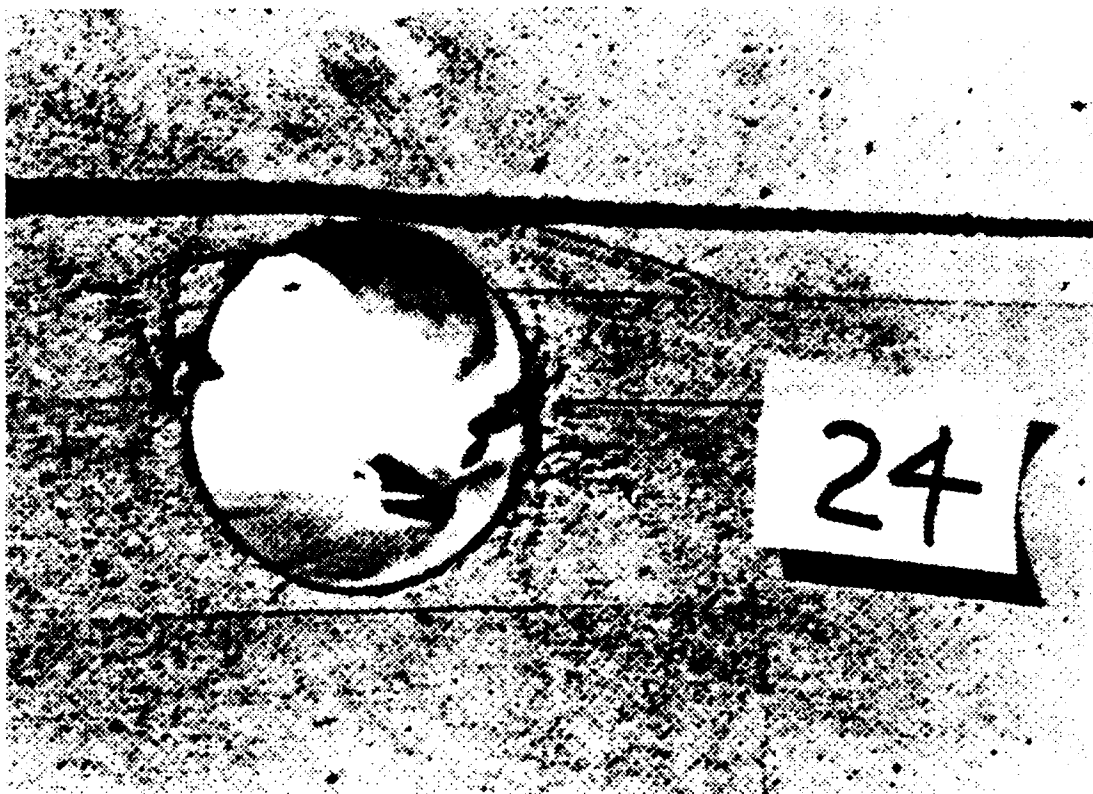


Figure 75. Lined tunnel specimen tested in DINING CAR, showing classical shear cracks.

significant role in mitigating the effect of horizontal joints. What can be said, however, is that tests were performed and no definite conclusions can be drawn as to whether horizontal joints do or do not affect tunnel strength.

A second finding is that tunnels in specimens with joints at 45 degrees to the principal directions of loading are weaker than tunnels in specimens with (horizontal) joints parallel and perpendicular to the principal loading direction. If it were not for the unresolved conflict among data on horizontal joints discussed in the preceding paragraph, it would be tempting to regard this finding as foreshadowing recent analytical findings reported by Itasca Consulting Group that show the sensitivity of tunnel strength to joint orientation under dynamic loading.

## SECTION 3

### ADD-ON EXPERIMENTS IN FIELD TESTS

Add-on experiments involve experiments using a larger specimen than can be tested with existing laboratory equipment. A contained test at NTS is selected in which there is a convenient test bed for the specimen. Often, there has been a parallel program of laboratory size testing, which presents the opportunity of investigating directly the implications of replica scaling.

#### 3.1 DINING CAR.

##### 3.1.1 Review Of Test Parameters ([DNA 4023F], April 1976, [POR 6887], 1976).

The DINING CAR add-on experiments provide an opportunity to test a larger size of the SRI lab-scale structures at two pressure levels (see Fig.76). Each unit block shown in the figure consists of a 6" tunnel embedded in 3' diameter cylinder of the simulant 6B, and a corresponding 5/8" tunnel scaled-replica of it, to provide direct comparison with 5/8" lab specimens. Hence, the 6" tunnel corresponds to a 1:20 scale with reference to a 10' full size tunnel, and the 5/8" tunnel presents a 1:200 scale as before. Whereas the 5/8" tunnel tested in the lab has the tunnel axis transverse to the axis of the simulant cylinder, the field version has the tunnel axis coinciding with the axis of the simulant cylinder (Fig.77). The tunnel in each unit block is designed to replicate the lab tests; this includes unlined tunnels, various (steel) liner thickness, and backpacked liners.

The NTS tuff is estimated to have an unconfined compressive strength of 1-2 ksi and a friction angle of about  $5^{\circ}$  (these are SRI numbers; we believe that strength of 2-3 ksi and friction angle of  $10-20^{\circ}$  are more representative of the tunnel beds where structures experiments were located). The test bed is used mainly as a loading device to subject models to (assumed) isotropic loading. The space between the models and the edge of the excavation was filled with rock-matching grout (HUSKY ACE Rock Matching grout) which, on account of low shear stress, is assumed to transmit only the hydrostatic component of stress from the surrounding tuff to the models; the load acting on the models is assumed to be symmetric with respect to their geometric axes.

The validity of the assumed stress state is important. Passive measurements from Brinnell gages, the only pressure measurements available, are unreliable. They give non-uniform measurements around the circumference of the simulant block, which makes interpretation difficult. We do not know if the non-uniformity is caused by the performance of the gage, but judging by the deformed shapes of the structures, the loading is asymmetric.

##### 3.1.2 Results On Direct Contact Tunnels.

#### 6" Specimens

Results of the test, in terms of % closures of the tunnel liner, are presented in Fig.78 for the 6" tunnels. For each cross-cut, three sets of data are given as shaded areas and denoted by the three symbols which correspond, respectively, to a/h ratio of 50, 25, 12.5. Because the pressures at the two cross-cuts are not measured precisely, the data are given for two intervals of pressure. Two measured values of closure are reported for each tunnel, the maximum % closure and the average % closure.

The corresponding lab data are plotted as points in the same figure for comparison. The lab data are obtained from static, isotropic tests of drained, saturated specimens (5/8" in size). The

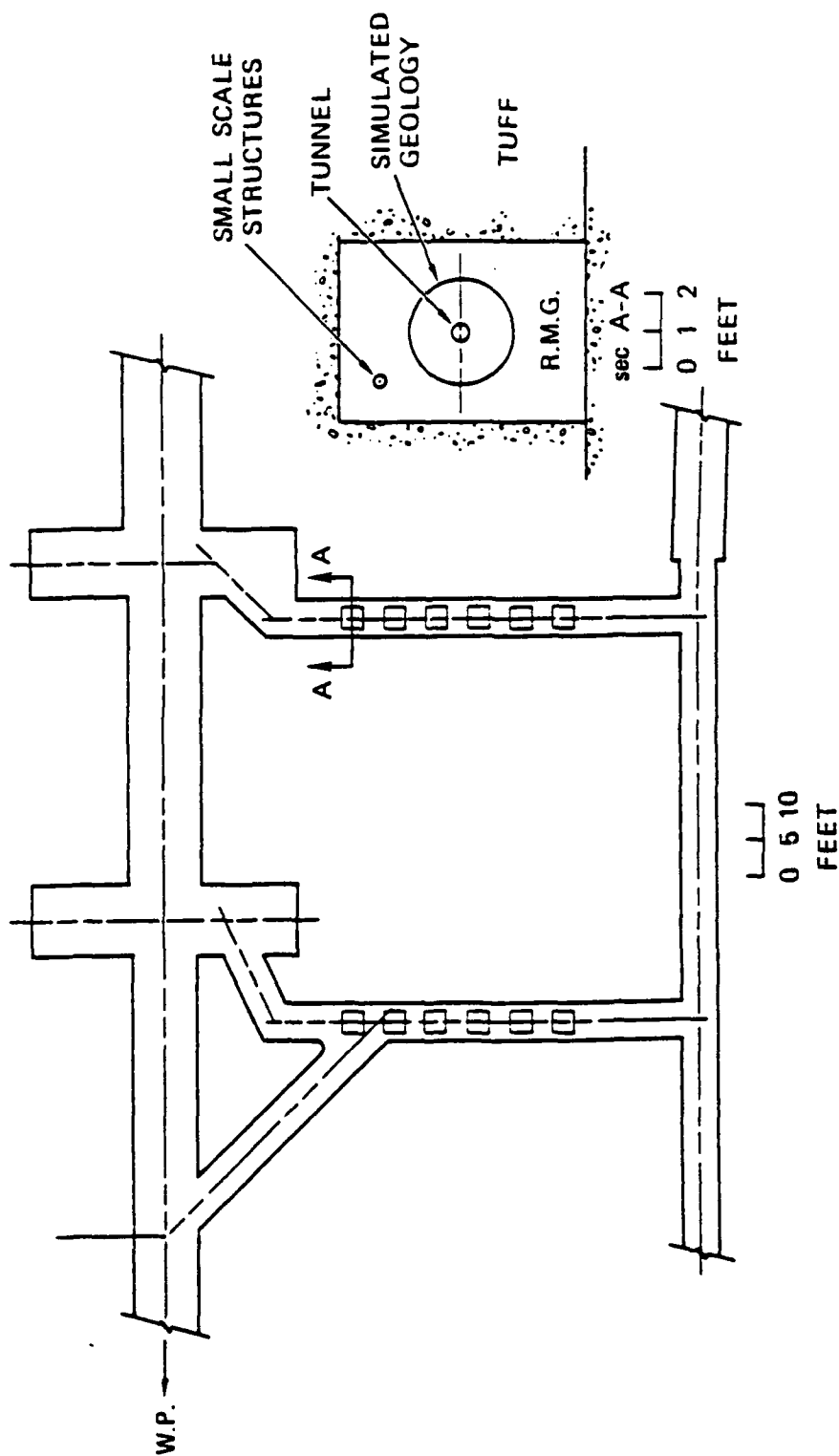


Figure 76. Experimental layout in DINING CAR crosscuts.

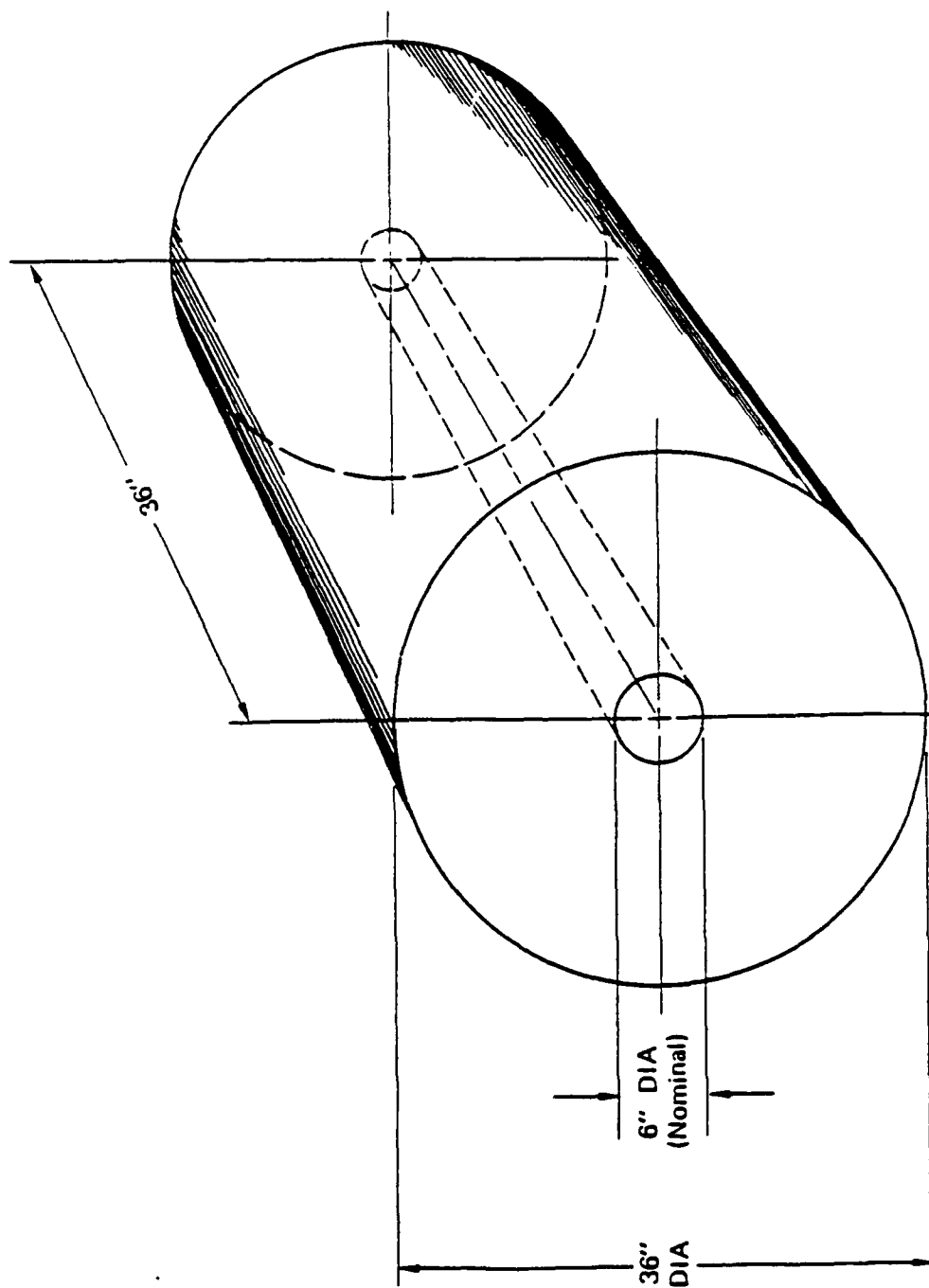


Figure 77. Scale model tunnel in simulated intact geology.

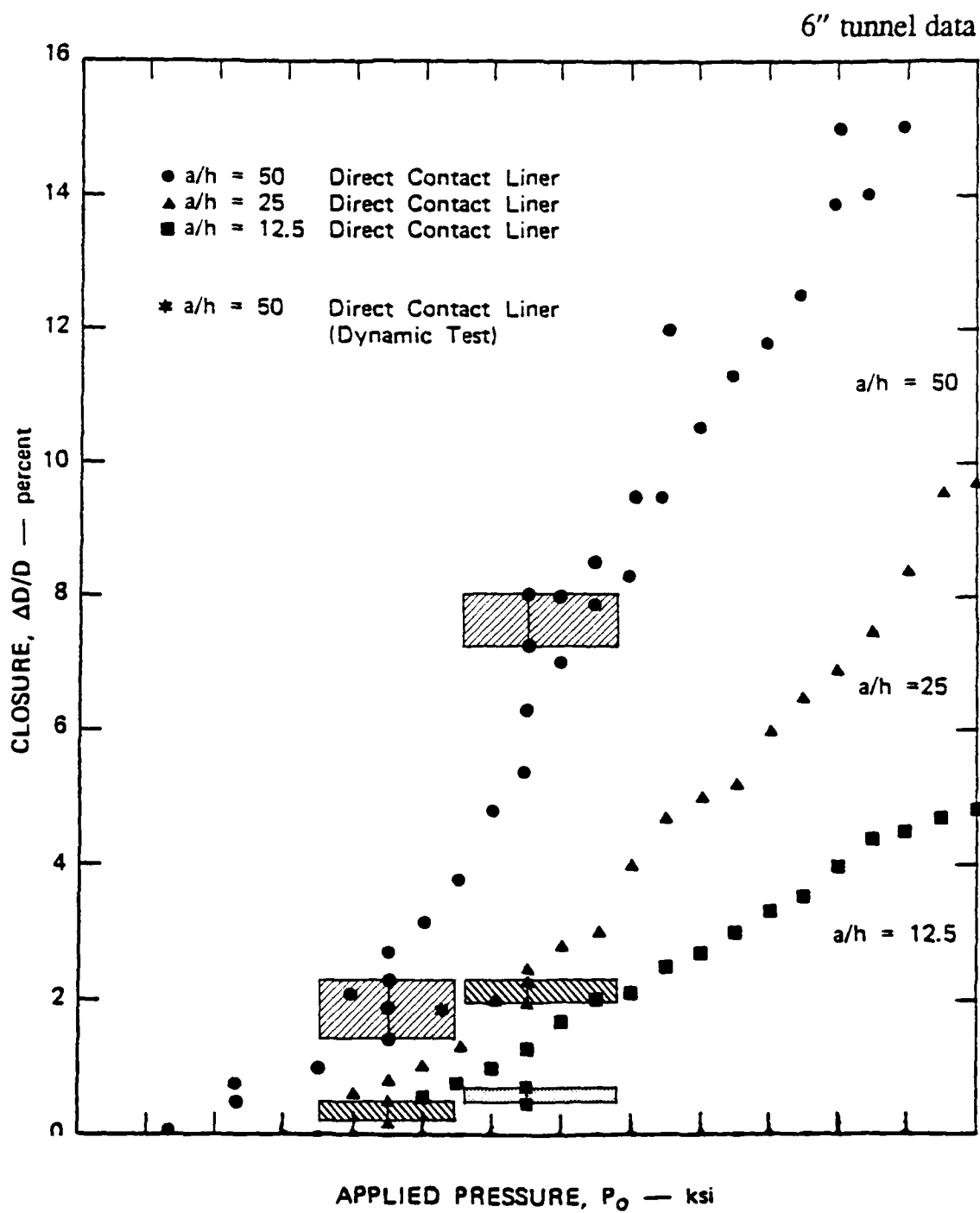


Figure 78. Comparison of 5/8" lab (static, isotropic 6B, saturated but drained) and 6" DINING CAR data.

agreement between field data and lab data is good considering the uncertainty in the loading environment in the field. The comparison is better for  $a/h=50$  (larger closures), than for tunnels with thicker liners (smaller closures). The lone data point obtained dynamically at laboratory scale (denoted by an asterisk) falls a little below its static lab counterpart in the figure. Based on this comparison, replica scaling (5/8" lab vs 6" field, or 1:10) appears to be valid from a quantitative viewpoint.

A qualitative comparison of the damage modes is shown in Fig.79. Focusing on Figs.79b and 79c, we see that the buckling modes of the liner are similar. However, the failure modes of the same rock simulant in the field and in the lab are clearly different. The crack pattern in the field specimen shows the classic failed wedges at the springline, with spiral fractures propagating from the wedge. This pattern has been observed in laboratory scale specimens comprised of rock simulant, and is characterized by Heuer and Hendron as the typical failure mode of an unlined tunnel in soft rock which can be idealized as a continuum (e.g., see Fig.80 which is taken from [Heuer and Hendron, 1971]).

This observation is one example which suggests that the grain size of simulant relative to the diameter of the tunnel may be a significant factor. Another potential source of different response is that the field specimen is loaded end-on whereas the laboratory specimen is loaded side on; ideally, this should make no difference if the load is isotropic, as was intended. To ascertain if symmetric loading condition prevailed in the test, we repeat the comparison using lab data from static uniaxial-strain tests (of saturated specimens allowed to drained). The comparison is shown in Fig.81; note the field data are the same, and only the lab data points are now more "bunched" together close to the unlined tunnel case. The correlation is poor, from which we might conclude that the loading condition in the field is closer to symmetric. It is tentatively concluded that the Brinell measurements were affected by placement orientation.

#### 5/8" Specimens

When the results of testing 5/8" tunnels in the lab and in the field are compared, the correlation is also poor (Fig.82). The field 5/8" response for  $a/h=50$  is close to the lab 5/8" response for  $a/h=25$ .

This disagreement is puzzling because (1) the specimens are apparently identical to each other, and (2) correlation between the field 6" specimens and the lab 5/8" specimens appears satisfactory in spite of differences in dynamic effects and loading conditions. Also, as shown in Fig.79, the damage modes of the linings are similar for the 6" and 5/8" specimens.

### 3.1.3 Backpacker Liner Tunnels.

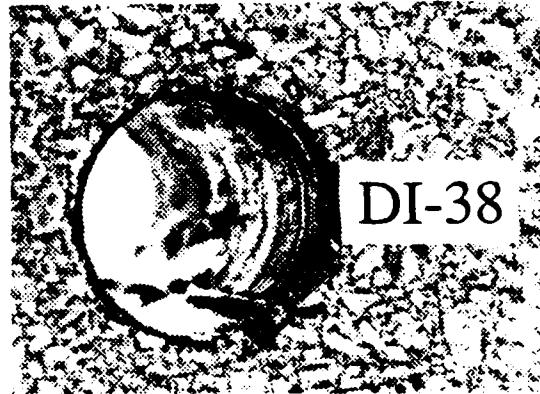
#### 6" Specimens

Lab and field results for the backpacker liners are not readily comparable because in both the laboratory (5/8" tunnels) and the field (6" tunnels), the liner deformations were negligible even in the presence of substantial rock closure and crushing of the backpacking. The deformation modes obtained in the lab and in the field are compared in Figs.83a and 83c. Although both specimens show little or no damage, the crack patterns differ significantly, as is also observed in the direct contact liner case. The field specimen displays the classical spiral crack pattern whereas the lab specimen does not show any noticeable pattern.

#### 5/8" Specimens

In contrast to the 6" tunnels, the 5/8" lab-size tunnels tested in the field sustained light damage. However, the level of damage is definitely higher in the field specimens than is observed

Dynamic  
Lab



(a) Laboratory Experiment—Small Structure  
(5/8) inch diameter tunnel)

Static  
Lab



(b) Field Experiment—Small Structure  
(5/8 inch diameter tunnel)



(c) Field Experiment—Large Structure  
(6 inch diameter tunnel)

Figure 79. Comparisons of liner buckling in large and small field structures and in laboratory structures— $a/h$  = direct contact liner.

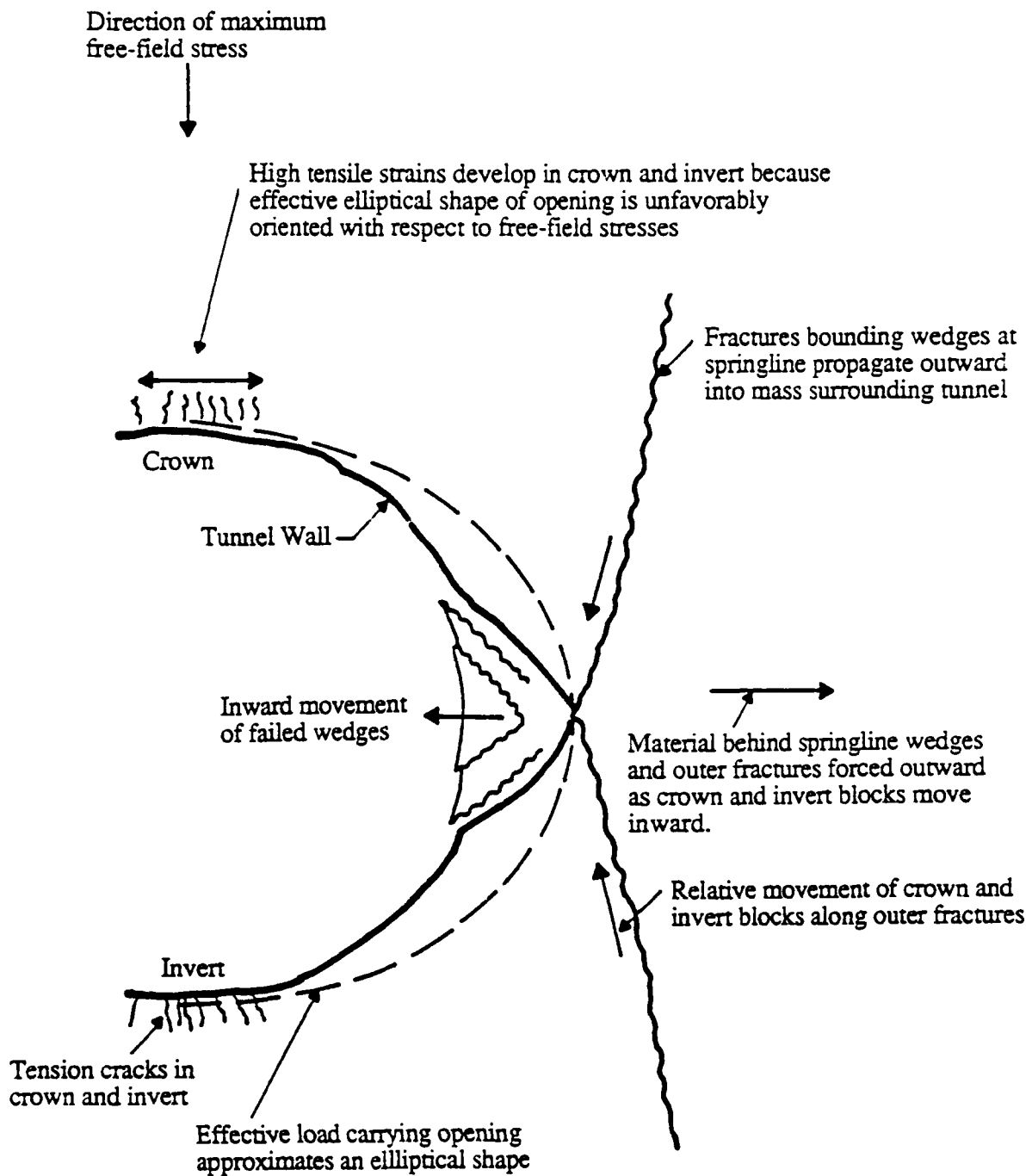


Figure 80. Significant features of behavior around failing opening.  
(Heuer and Hendron, 1971)

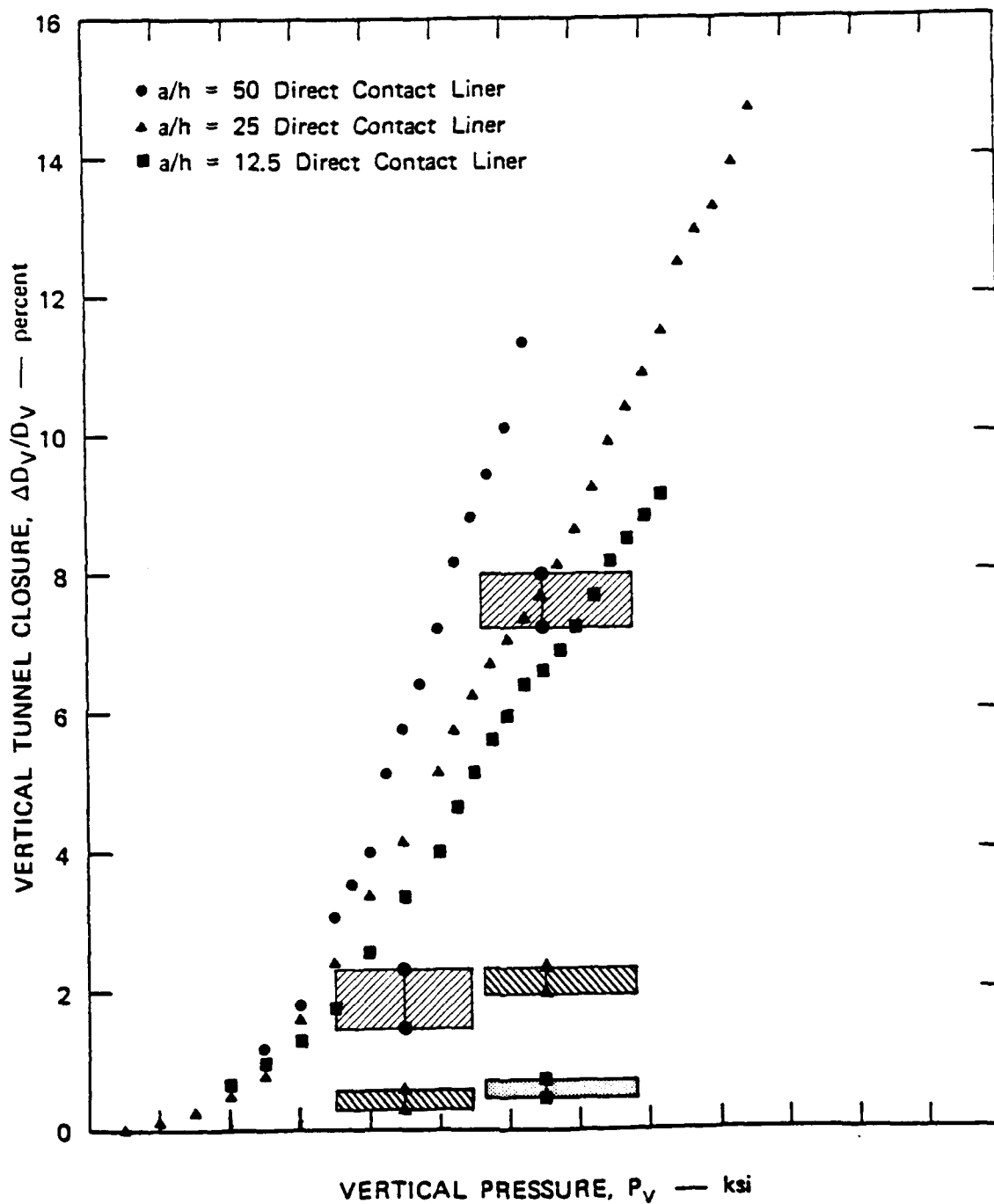


Figure 81. Comparison of 5/8" lab (static, uniaxial 6B, saturated but drained) and 6" DINING CAR data. (DNA 4023F)

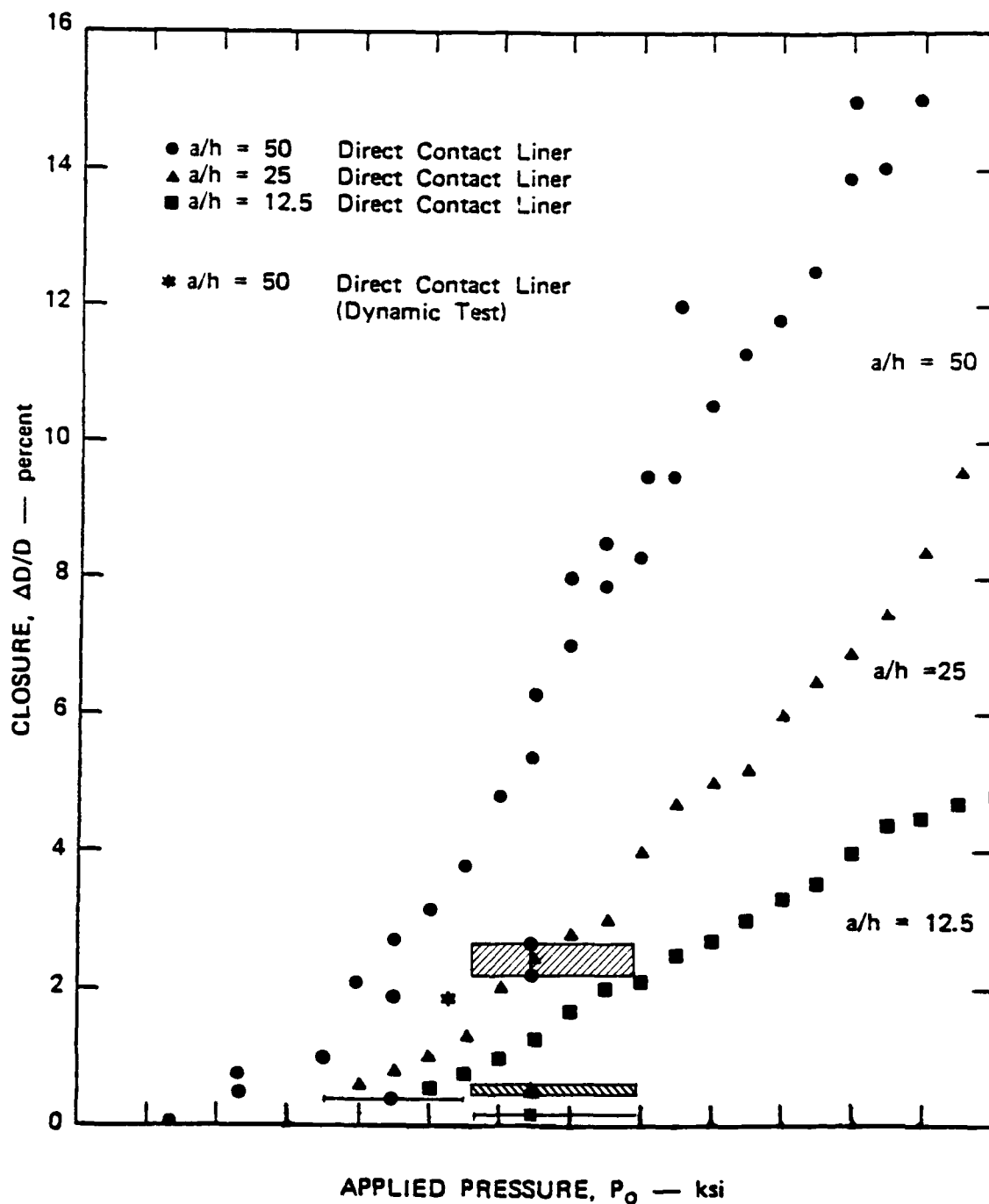
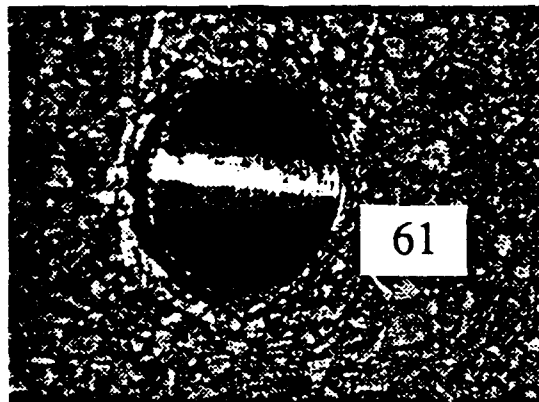


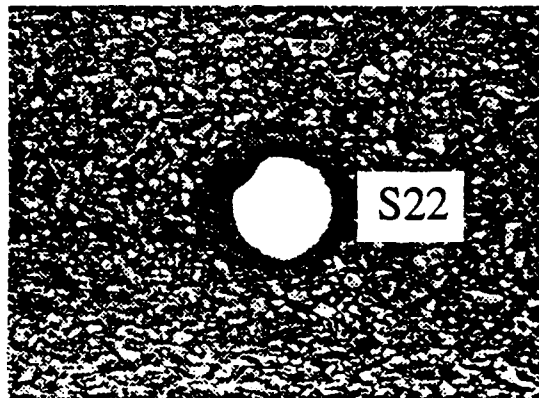
Figure 82. Comparison of 5/8" lab (static, isotropic 6B, saturated but drained) and 5/8" DINING CAR data. (DNA 4023F)

Static  
Lab

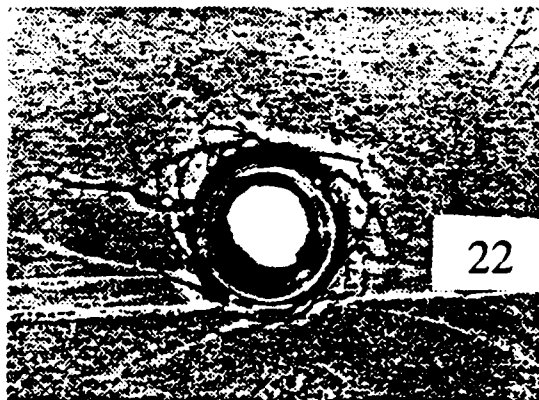


(a) Laboratory Experiment—Small Structure  
(5/8 inch diameter tunnel)

Static  
Lab



(b) Field Experiment—Small Structure  
(5/8 inch) diameter tunnel)



(c) Field Experiment—Large Structure  
(6 inch diameter tunnel)

Figure 83. Comparisons of fracture patterns in large and small field structure and in laboratory structures— $a/h = 25$  liner with backpacking (DINING CAR POR).

in the lab, and this trend is exactly the opposite to that for the direct contact liner case described previously. The field data are compared with lab results obtained under static, isotropic loading condition in Fig. 84. Note that the 2.08% maximum closure for  $a/h=25$  is caused by a small bulge in the liner was attributed to porewater pressure. The 2.24% maximum closure for  $a/h=12.5$  is due to eccentricity of liner caused by grout having extruded behind backpacking. Hence, the causes of approximately the same maximum closure for two liner thicknesses are different.

Figure 85 compares the field data with lab uniaxial strain data on 5/8" back-packed tunnels.

#### 3.1.4 Evaluation Of Replica Testing By Comparing Laboratory And Small Field Scale Specimens.

The field-scale (6") and lab-scale (5/8") specimens appear to have the same failure mode (buckling of liner, crushing of backpacked materials) and show the same trend of increasing damage (closure) with higher loading and thinner liners. They have about the same amount of damage (tunnel closure).

However, there are sizable quantitative differences as measured by closure of the field and lab specimens (between the field 6" and lab 5/8" specimens and, in particular, between the field 5/8" and the lab 5/8" specimens). Closure levels for the field specimens are in general low and not too much should be made of the field data. However, a broad summary of the differences may put the field pressure at 20%-60% higher than the lab pressure for a required closure in the range of 1-5%. In general, the difference grows with increasing liner thickness and pressure. The presence of uncertainties in the field loading condition (peak stress, loading path), dynamic (rate-sensitive) effects on material, the effect of grain-size (to tunnel diameter), role of pore water pressure in the field, field specimen geometry and inconsistent results from the lab-scale (5/8") specimens tested in the field does not permit a more definitive and quantitative statement.

The present reviewers consider the results to be inconclusive in demonstrating that scaling holds among 5/8" specimens tested in the lab and in the field and 6" specimens tested in the field. There are signs of agreement but also evidences of fundamental differences. Whereas the 6 inch specimen failed by propagation of spiral cracks in otherwise intact rock, the 5/8 inch specimen failed by more ductile and pervasive crushing of the rock around the tunnel. Different loads are applied to the tunnel lining in the later stages of loading due to the different modes of failure of the rock adjacent to the lining.

The disagreement between the field 5/8" and lab 5/8" specimens is significant since they are on paper nearly identical; without this comparison, a more positive assessment of replica-testing, based only on a comparison of the 6" field and lab test data, would have been justified in spite of qualitative differences. In view of poor correlation in this case, it is necessary to examine the differences between the field and lab further. These include grain size, load path, load transmitted to the structure, pore water pressure, lab specimen geometry and dynamic effect. They need to be evaluated before the results can support replica scaling.

#### 3.2 MIGHTY EPIC ([POR 6950], 1977).

The present review of MIGHTY EPIC is restricted to the response of the mini-structures and comparison with lab specimens. A total of 53 mini-structures (6" diameter) were tested, of which 8 were of the built-up (composite) type designed as 1/10 scale replica of the 4 ft built-up structures also tested in the event. The remaining 45 of the 53 mini-structures were fielded directly in tuff. However, no direct comparison with the lab data is given; an indirect correlation is provided by a finite element analysis.

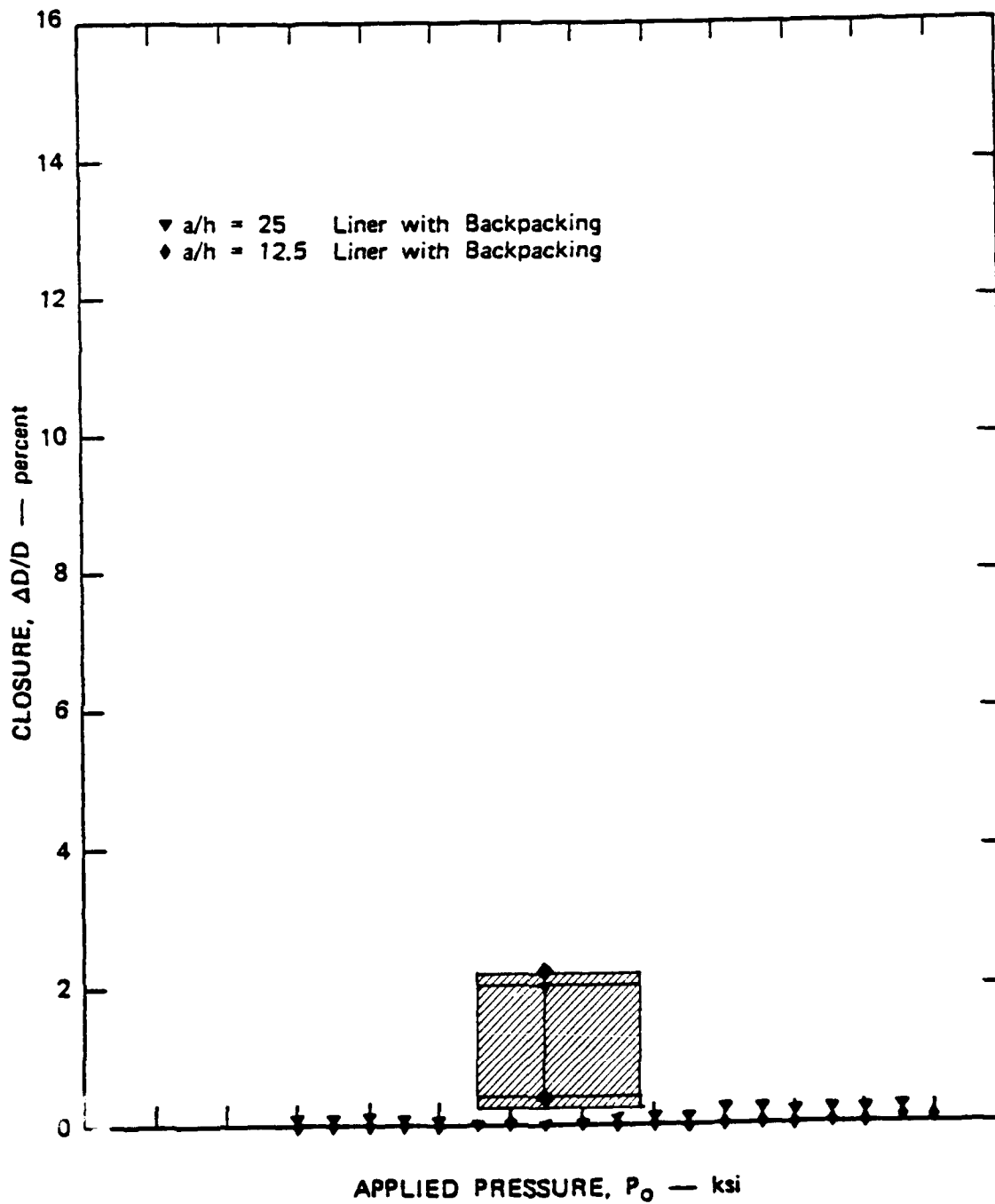


Figure 84. Comparison of 5/8" lab (static, isotropic 6B, saturated but drained) and 5/8" DINING CAR data. (DNA 4023F)

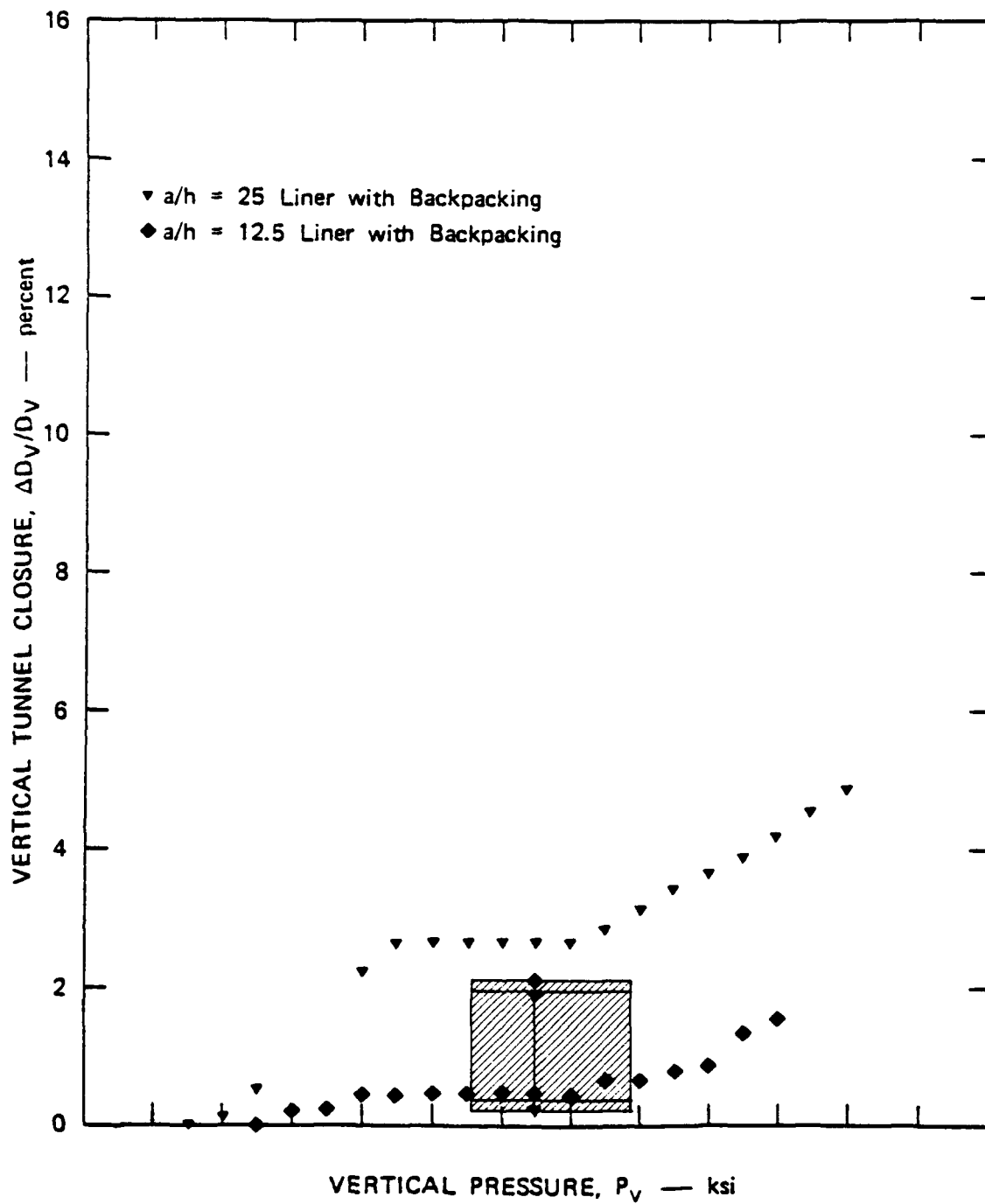


Figure 85. Comparison of 5/8" lab (static, isotropic 6B, saturated but drained) and 5/8" DINING CAR data. (DNA 4023F)

### 3.2.1 Mini Built-Up Backpacked Structures.

The eight mini built-up backpacked structures (6" diameter) were supposedly replicas of the 4' diameter large size models. However, the response does not compare well (see Figs.86a and 86b) even though the two sets of curves in the figures have similar shapes, since the ordinate scale in Fig.86b is 2x that of Fig.86a. Hence, built-up mini's are about twice as strong as the larger built-ups. The blame is laid on the backpack foam used with the mini-structures. The strength of the mini-structure backpack foam in several specimens is 1/3 to 1/4 that of specification in some, and higher (by 30%) than specification in others.

This is a major disappointment. The two sets of built-up structures, with a scale ratio of 4':6", would have provided definitive information on the effect of scaling.

### 3.2.2 Direct Contact Mini-Structures.

The majority of mini-structures of aluminum and steel are designed to obtain duplicate data points from this single test inexpensively. Thirty aluminum models were fielded (15 for side-on loading and 15 for end-on loading), and they were selected from five strengths (wall thicknesses). Fifteen steel models in five wall thicknesses were fielded in the side-on loading configuration only.

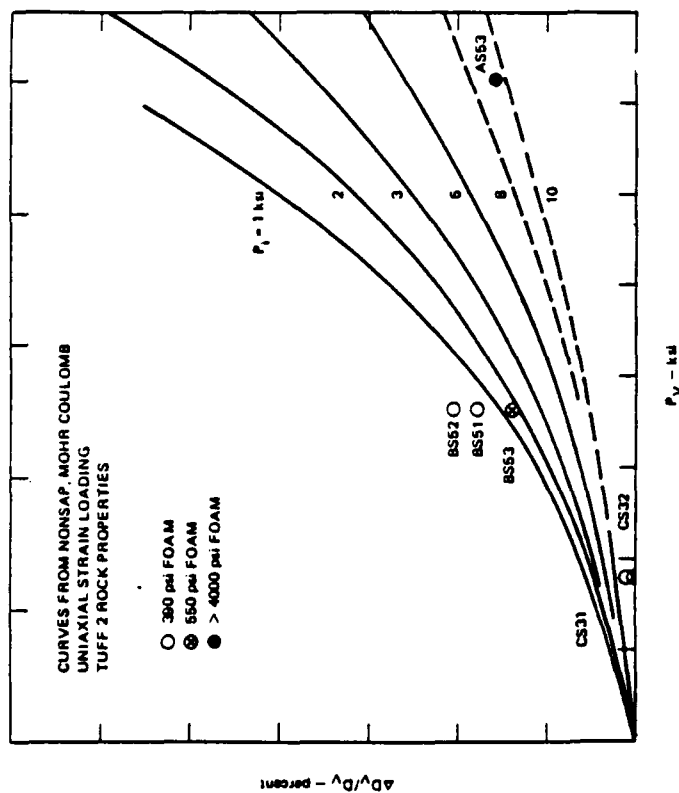
This large array of test data is useful in indicating the general trend of the response and the scatter of the data (e.g., from responses of identical mini-structures fielded in the same drift). Figure 87 summarizes the data for aluminum mini-structures, and an analytic result from NONSAP elastic-plastic calculations is superimposed for reference. The agreement is good. The same data points are replotted in Fig.88 with the incident load normalized by the theoretical load to produce 5% closure for each structure. (When the normalized load is used, all five theoretical curves collapse into a single curve, which makes for easier comparison with test data points). Again, the agreement in trend is clearly shown; the scatter increases with increasing closure.

The calculations do not take into account porewater pressure or strain rate on tuff. In the lab, the combined effect of these factors is to increase the critical loading pressures (pressure at 5% closure) by factors of 1.5 to 2 above those for static drained tests. Water content was high in MIGHTY EPIC. It appears from these facts that the good agreement shown in Fig.88 may be fortuitous and would become poorer when pore-water pressure and strain-rate effects are included. In comparing results of analysis with test data, the effect of assuming different material parameter values should be considered. There is large uncertainty in the Tuff core data, and the analytic model assumed for Tuff 2 is just one of the many possible representations. This step has not been taken.

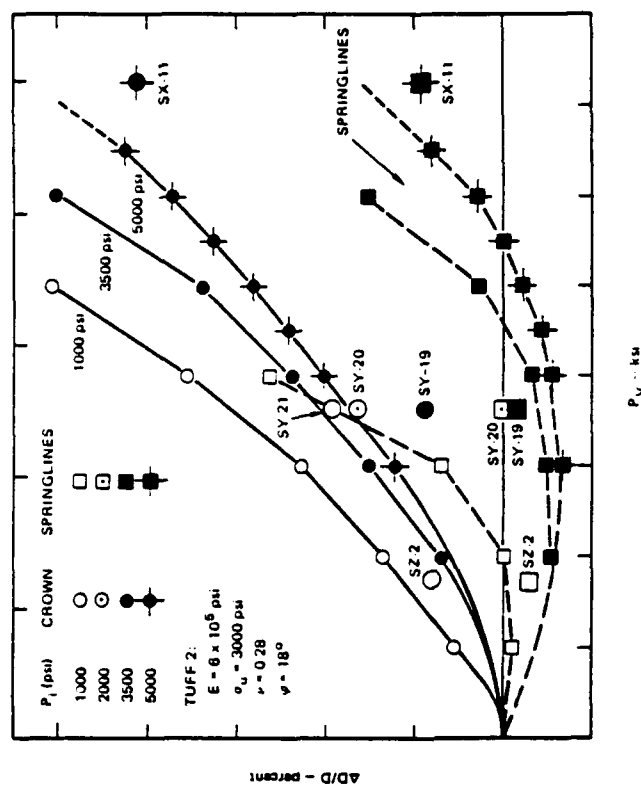
Deformation data from the steel mini-structures are summarized in Figs.89 and 90. Both the trend and scatter are similar to the aluminum data. However, the experimental points in the normalized load plot fall below the theoretical curve, and a nearly constant 2% offset is noted in the figure. This offset is attributed to elastic springback of the models which is more severe for the thinner-walled models made of stronger cold drawn 1015 steel material than for the thicker models made of aluminum 6061-T0. It is concluded that high strength steel is not an ideal material for the model recovery procedure used in the test.

### 3.2.3 Mini-Structures In 6B Simulant.

An additional 5 mini-structures (2 backpacked and 3 direct contact liners) enclosed by cylindrical blocks of 6B simulant were inserted to see if correlation between DINING CAR and the lab can be reproduced. Based on the comparison shown in Fig.91, the correlation is again favorable. Figure 92 is a companion figure and shows a comparison of the same analytical



(a) Peak oval-plus-hoop deformation versus incident load for side-on built-up ministructures.



(b) Comparison of calculated and measured rock closures for built-up structures. (Small symbols are calculated and large symbols are measured closures.)

Figure 86. Comparison of 6" built-up (field) and 4' built-up (field). (DNA POR 6950)  
(Each subdivision of ordinate in right figure is 2 times that of the left.)

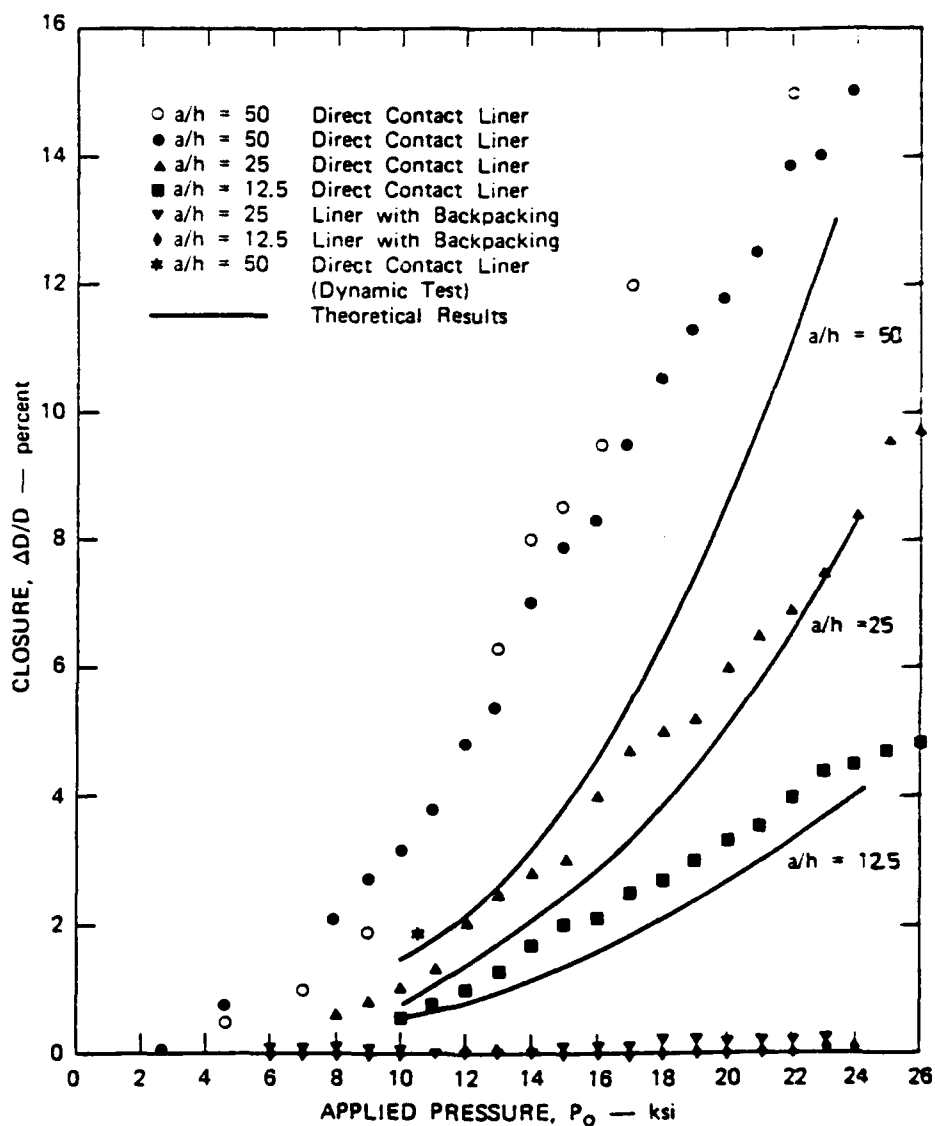


Figure 87. Experimental and theoretical closure versus applied pressure for static, isotropic loading of 6B rock.

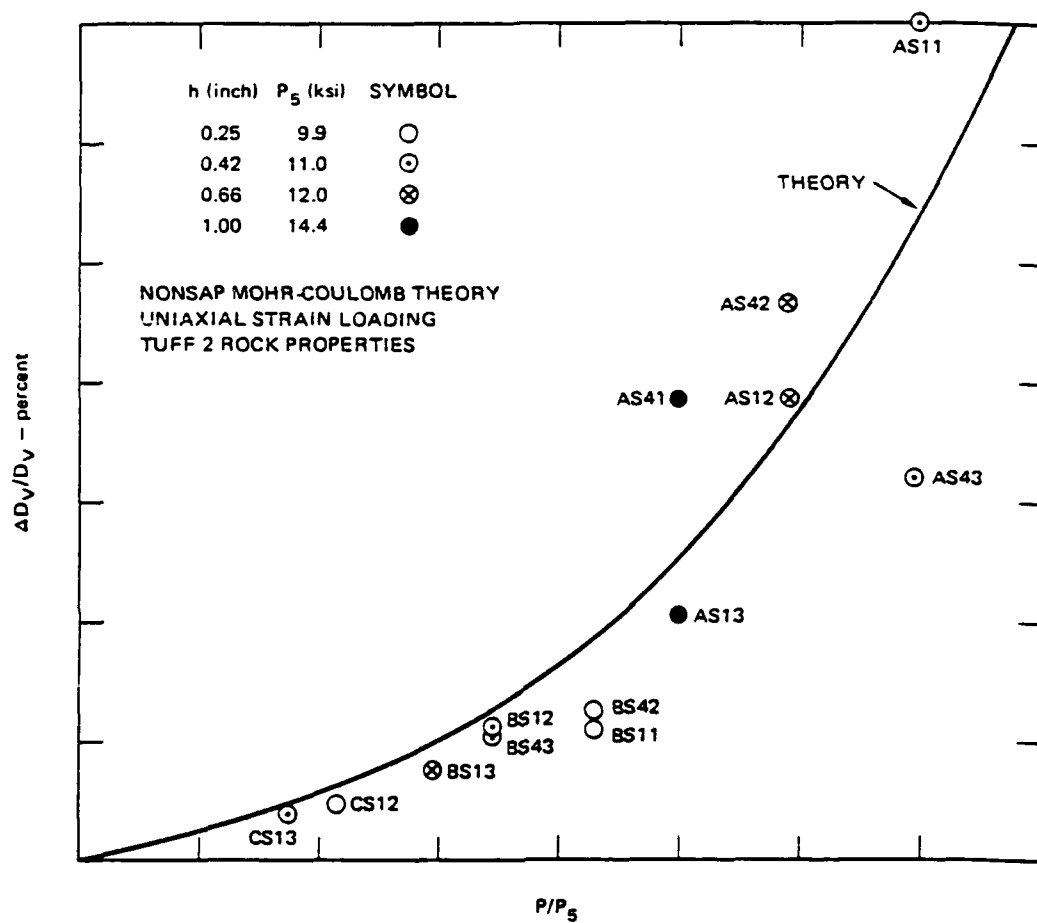


Figure 88. Peak oval-plus-hoop mode deformation versus normalized incident load for side-on aluminum ministructures.

( $P_5$  is load to produce  $\Delta D_v/D_v = 5\%$  for each structure.)

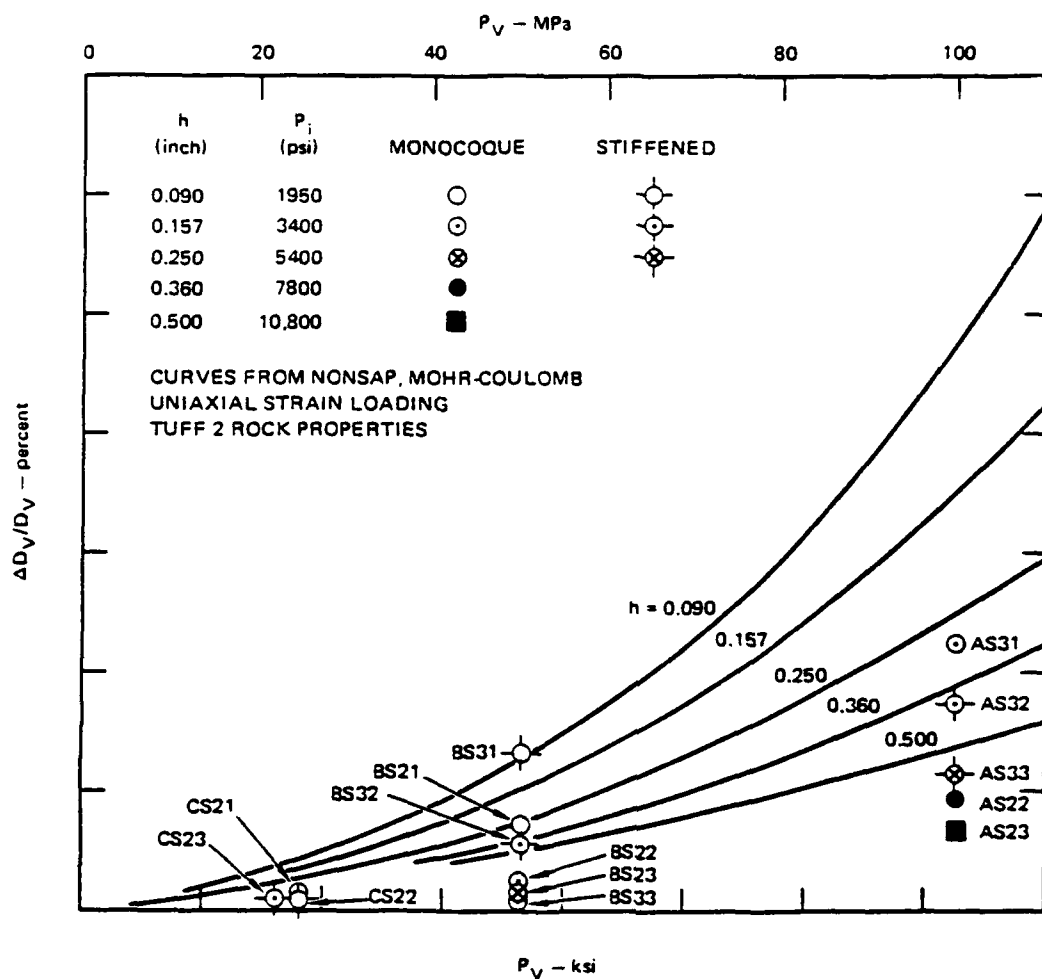


Figure 89. Peak oval-plus-hoop mode deformation versus incident load for side-on steel ministructures.

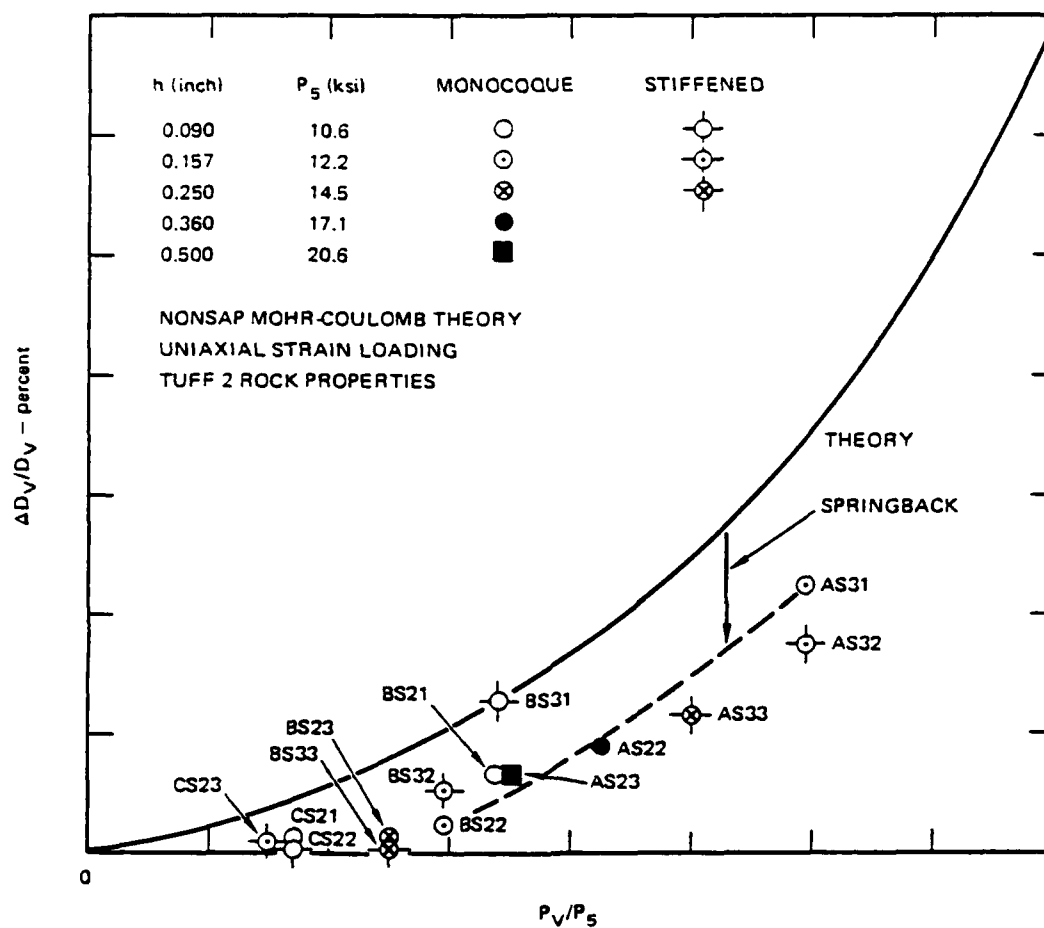


Figure 90. Peak oval-plus-hoop mode deformation versus normalized incident load for side-on steel ministructures.

(P<sub>5</sub> is load that produces  $\Delta D_V/D_V = 5\%$  for each structure.)

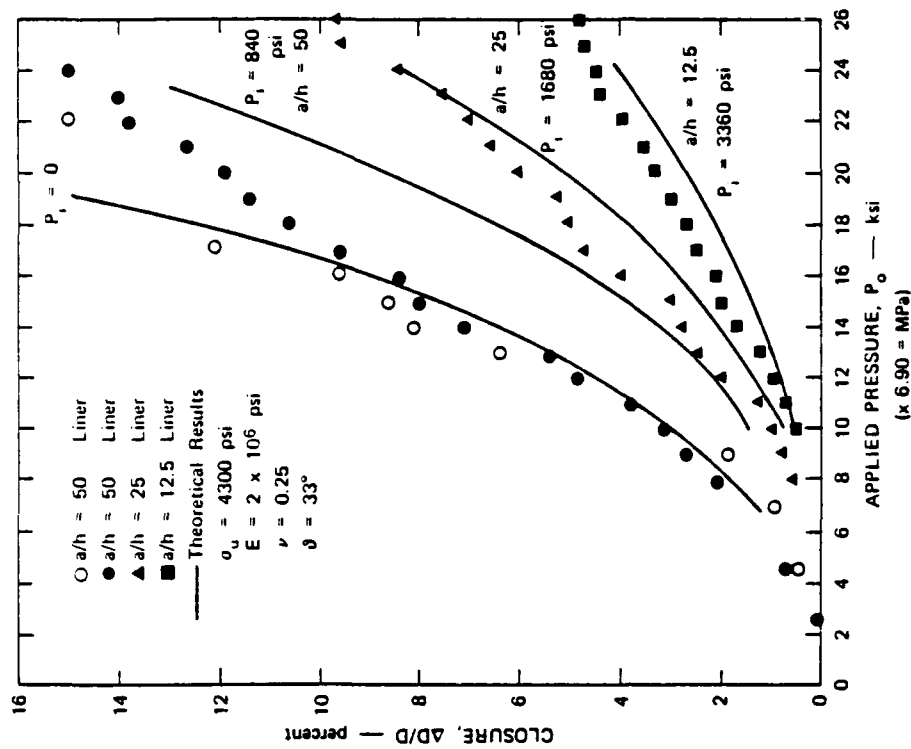


Figure 92. Experimental and theoretical closure versus applied pressure for static isotropic loading of 6B rock in the laboratory.

(Rock diameter = 4 in = 102 mm, rock opening diameter = 5/8 in = 16 mm, mild steel liners.)

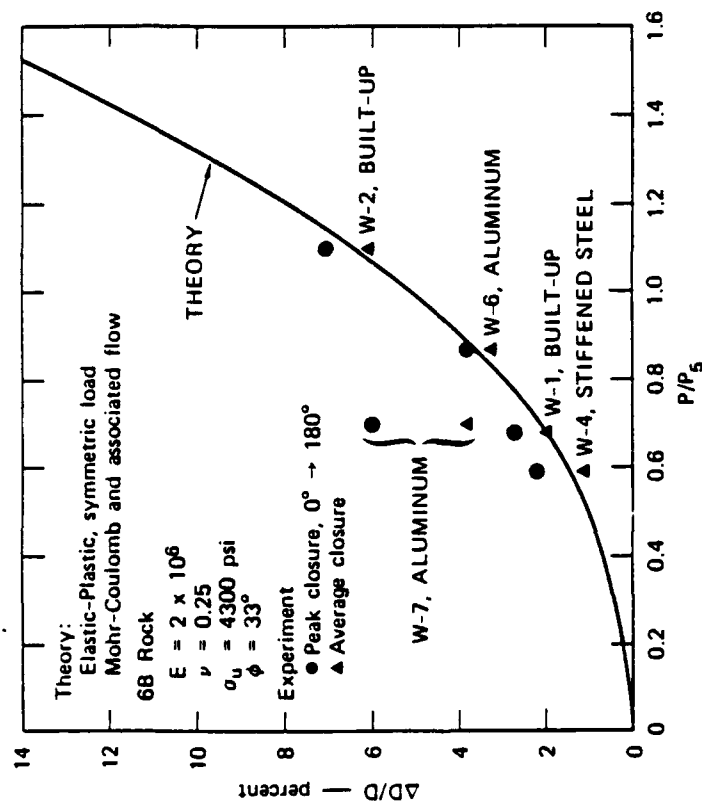


Figure 91. Rock opening diameter changes versus load-to-strength ratio  $p/p_5$  for ministructures in 6B rock.

prediction with lab data. The conclusion is obscured by the fact that laboratory data under isotropic loading is used for comparison rather than uniaxial strain loading.

#### 3.2.4 Assessment Of Replica-Scaling In MIGHTY EPIC.

Direct contact mini-structures compare favorably both qualitatively and quantitatively with analysis. The analytic curve in Fig.91, in particular, is basically the average curve for the data points. Since the same analytic model predicts the response of lab specimens, replica scaling is supported for 5/8" size (lab) and 6" size (field) specimens.

However, the rationale for selecting the Tuff 2 model is not stated, and this detracts from the rigor of the argument in favor of replica scaling based on correlation with analysis. The reviewers do not understand why lab data cannot be directly used in the comparison, or the effect of scaling the pressure by P5, the theoretical pressure to cause 5% closure for the structural configuration. A direct comparison would have been more informative.

An important opportunity to assess replica-scaling was lost because the backpacking in built-up structures did not meet design specification.

A significant contribution of the test is to show the scatter in the response for nominally identical structures in the same drift location (presumably the same loading environment) such as shown in Fig.88. At higher pressures in particular, the closures can be different by a factor of 2. Such is the uncertainty on which the present assessment is based.

### 3.3 DIABLO HAWK - JOINTED SPECIMENS ([POR 6998], 1981).

#### 3.3.1 Jointed Rock.

There are two parts to the jointed rock experiments in DIABLO HAWK. The first consists of 20 jointed, rock-simulant specimens (and mini-structures) designed to study the influence of joint orientation, double vs. single joint sets, joint spacing, strength of the infilled foam, and peak loading. Tunnel closure is the response measure. The second part consists of scaled models of tunnel structures (steel and reinforced composite liners) for comparison with similar structures previously tested in highly jointed granite (PILE DRIVER). The response measured is the damage mode and closure.

DIABLO HAWK is a tuff site, with three drifts located at three different pressure levels of interest. Most of the mini-structures models were fielded in cylindrical jointed-simulant (16A) with 22" diameter and surrounded by a grout collar. The grout is ME8-11R tuff-matching grout also used in MIGHTY EPIC (modulus of about  $10^6$  psi, strength of 2300 psi, and an average friction angle of 11 degrees). The basic tunnel diameter is 3", yielding a rock-mass-to-tunnel diameter ratio of 7.3. With reference to the PILE DRIVER structures, the scale factor for the mini-structures is 28:1. Documents available to us do not describe the liner system for the mini-structures in the parametric study. We assume they were unlined but filled with crushable foam of various strengths and the foam strength is one of the parameters investigated.

DIABLO HAWK is the single most extensive source of data for response of (mini) tunnels in jointed rock (simulant). The only tests of large size tunnels in jointed rock are PILE DRIVER and HARD HAT.

### 3.3.2 Parametric Specimens ([POR 6998], 1981).

The test matrix is shown in Table 18, and the joint configurations studied are illustrated in Fig.93. Hoop plus ovaling deformations (closures) measured after the test are summarized in Table 19. From comparisons of results of the relevant cases in the matrix as indicated in Table 19, the following conclusions are obtained:

#### Effect of Joint Orientation

Tunnel closure increases with an increase in the angle between the single joint plane normal and the loading direction. This increase is measured for two D/S (6 and 10). As the joint orientation increases from 0 to 45° the vertical closure increases from 1.6 to 3.5, and from 1.2 to 2.4, a consistent factor of 2. Lab data on the same issue gives a factor of about 2 also (based on two tests, see Section 2.1.3). The increase from 45 to 90° is very small.

Closure in a specimen with joints oriented at 0° is 3 to 4 times greater than in intact specimens. This result should be contrasted to laboratory test results described in Section 2.5.2, which show that 0° joints have no effects on tunnel closure. However, as pointed out in Section 2.5.2, lab data are difficult to interpret because of the initial closing of gaps between joints. On the other hand, the field data just described have limited value because the magnitude of the closures is so small. The present reviewers are reluctant to make much of the trends.

#### Effect of Double Joint Sets

A double set of orthogonal joints resulted in slightly more tunnel deformation than a single set, namely, 5.1% to 4%. This increase is obtained by double joints at ±45°.

#### Effect of Infilled Foam Strength

Tunnel closure is markedly smaller in tunnels with foam strength 1500 psi than in tunnels with 500 psi (about 1% to 4%). The reduction is achieved for joint orientations of 0, 45, and ±45°.

#### Effect of Loading Stress

The tunnel closure in double-joint-set models increases rapidly from 1.3% to 5.1% as the peak loading at the drift increases.

#### Effect of Joint Spacing

Tunnel closure decreased with an increase in number of joints per tunnel diameter. In particular:

joint angle = 0°, D/S = 6, closure = 2.3%  
D/S = 10, closure = 1.8%

joint angle = 45°, D/S = 6, closure = 4%  
D/S = 10, closure = 2.4%

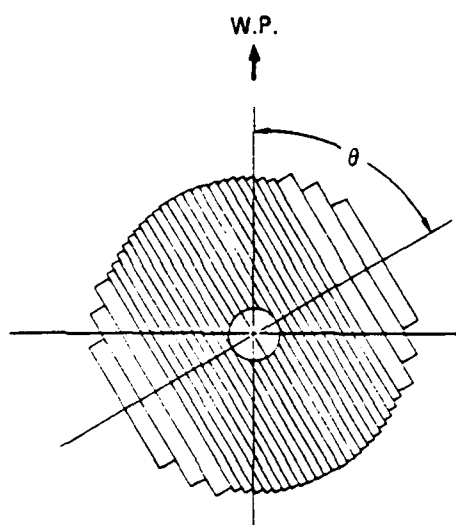
Table 18. Planned test matrix.

MODEL NUMBER		1	2	3	4	5	6	7	8	9	20*	10	11	12	13	14	15	16	17	18	19																			
NOMINAL INCIDENCE STRESS																																								
STRUCTURE	FOAM CRUSH STRENGTH, $P_f$																																							
	ANGLE, DEGREE																																							
JOINTS	SPACING D/S																																							
	RESPONSE, $\Delta D/D$ , PERCENT		<div>11 to 85</div>																																					
UPPER LIMIT $\sigma = 0, E/5$																																								
LOWER LIMIT $\sigma/2, E/2$																																								
PARAMETERS VARIED																																								
JOINT ANGLE																																								
JOINT SPACING																																								
JOINT SETS																																								
MODEL DESIGN (MODULUS VARIATION, STRUCTURE $P_f$ )																																								
LOADING																																								
LOADING DIRECTION																																								
BASELINE INTACT																																								

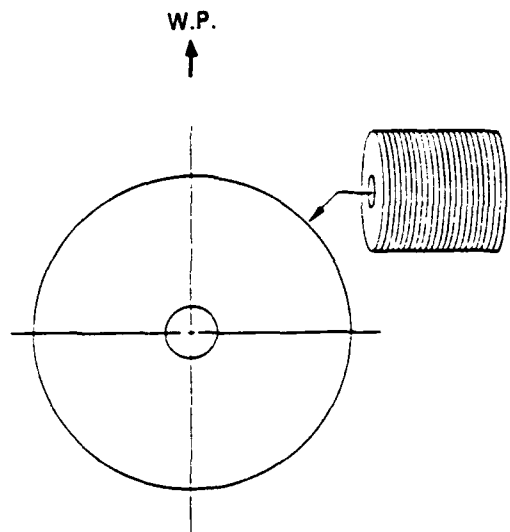
\*Model axis pointed toward working point (axisymmetric loading)

†Joint planes perpendicular to tunnel axis

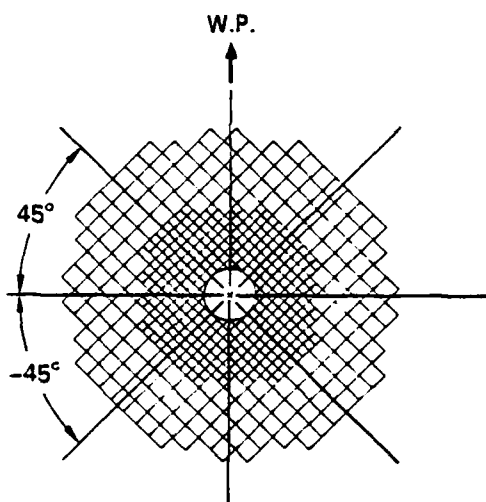
‡All 12.7 mm x 12.7 mm (1/2" x 1/2") bars



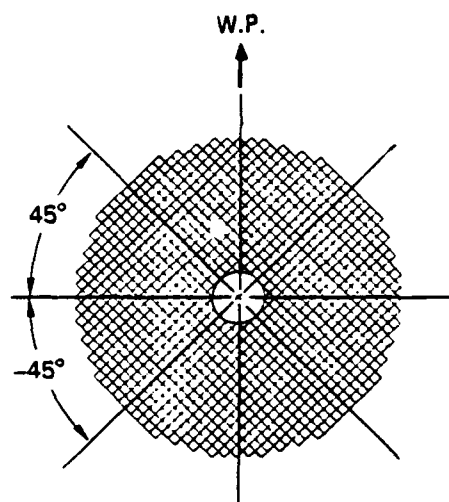
(a) Single Joint Set,  $\theta = 0^\circ, 45^\circ$  or  $90^\circ$



(b) Single Joint Set Perpendicular to Tunnel Axis



(c) Double Orthogonal Joint Sets with Coarse Joint Spacing in Outer Annulus. Also Fielded with Joints Oriented at  $0^\circ$  and  $90^\circ$  to W. P.



(d) Double Orthogonal Joint Sets with Uniform Joint Spacing

**Figure 93. Jointing arrangement for models assembled from 16A rock simulant.**

The models shown have a nominal diameter of 457.2 mm (18 in) with a 76.2 mm (3 in) diameter tunnel. Some models are 762.0 mm (30 in) in diameter with a 127.0 mm (5 in) diameter tunnel.

Table 19. Hoop and oval mode tunnel deformations in jointed rock.

MODEL No.	HOOP MODE		HOOP PLUS OVAL MODE		
	$R_{post}$ - mm	w - percent	CROWN - percent	SPRING - percent	$\theta^*$ - degree
S-DI-2-1	37.9	- 0.3	- 0.4	- 0.2	79
S-DI-2-2	38.0	- 0.1	- 0.7	0.5	-36
S-DI-2-3	37.6	- 1.4	- 3.6	0.8	-45
S-DI-2-4	37.4	- 1.8	- 3.5	0.1	-75
S-DI-2-5	37.6	- 1.0	- 1.6	- 0.4	75
S-DI-2-6	31.2	-18.2	-23.3	-13.0	-52
S-DI-2-7	36.7	- 3.3	- 4.4	- 2.3	89
S-DI-2-8	62.4	- 1.2	- 2.4	- 0.1	-82
S-DI-2-9	63.0	- 0.4	- 1.2	0.4	88
S-DI-2-10	38.1	0	- 0.1	0.2	-84
S-DI-2-11	38.0	- 0.2	- 0.8	0.5	78
S-DI-2-12	37.9	- 0.5	- 1.3	0.4	81
S-E-2-13	37.8	- 0.6	- 0.7	- 0.5	46
S-E-2-14			NOT SECTIONED		
S-E-2-15					
S-E-2-16	37.5	- 1.5	- 2.0	- 1.1	61
S-E-2-17	37.7	- 0.7	- 0.9	- 0.6	78
S-E-2-18			NOT SECTIONED		
S-E-2-19					
S-DI-2-20	37.8	- 0.7	- 1.3	- 0.1	-14

\*  $\theta$  is measured from the working point in the overall section photographs and is positive in the clockwise direction.

joint angle =  $\pm 45^\circ$ , D/S = 3, closure = 2.3%  
D/S = 6, closure = 1.3%

This has been referred to as the inverse joint spacing effect since the effect is counter-intuitive and conflicts with lessons drawn from PILE DRIVER. It is a significant finding, if confirmed, because the results conflict with those obtained from the mini-structure experiments. We recall previous lab tests which show that (1) strength of jointed rock and modulus decrease with increasing number of joints (WES material tests), (2) tunnel closure increases with number of joints at  $0^\circ$  (from earliest SRI dynamic tests), (3) tunnel closure is not affected by presence of joints when the orientation is  $0^\circ$  (from later SRI static tests). (1) is consistent with (2) but not with the DIABLO HAWK data, and (2) is not consistent with (3), and neither is consistent with DIABLO HAWK data.

However, note that all of the displacements involved are small\*, are measured after recovery and shipping of the specimens, and in most cases are nearly equal for the two values of D/S. Thus, any conclusions are at best tenuous.

### 3.3.3 Comparison Between Lab And Field Jointed-Rock Results ([POR 6998], September 1981, and DNA 4380F, February 1978).

A few jointed-rock experiments were performed in the lab using 16A simulant, 2" diameter tunnel in 12" specimen, and steel liner with  $a/h=12.5$ . Joint orientation angles of 0 and  $45^\circ$  were considered and the D/s ratio was 6. The pertinent results are reproduced in Fig.94. Direct comparison with the mini-structures in DIABLO HAWK is difficult because the latter do not have metal liners, but crushable foam core instead. Nevertheless, if comparison is attempted, assuming the internal pressure provided by the foam core is the same as that provided by the steel liner in the lab, the relevant cases are S-DI-2-5 and S-DI-2-4 for 0 and  $45^\circ$ , respectively, with percentage vertical closures of 1.6% and 3.5%. Their lab counterparts are 2.8% and 6.5%, respectively, and the difference is approximately a factor of 2.

### 3.3.4 PILE DRIVER Scaled Specimens ([POR 6998], 1981).

Three composite integral structures which were fielded at three stress levels in PILE DRIVER (AR11, BL10, CR7) and suffered damage ranging from complete closure through heavy to light damage, were modeled by three mini-structures in DIABLO HAWK. Efforts were made to simulate the joint profiles around the three structures (Figs. 95a, 95b, and 95c); joint planes are predominantly horizontal, vertical and at 30 and  $60^\circ$  to the horizontal; the joint spacing is about 0.3 m or 1/9 the excavation diameter. Figures 95 and 96 show the joint arrangement used in the mini-models; the joint spacing in the model is 1/8 the excavation diameter.

---

\* For a nominal tunnel diameter of 3 in, a 4% closure translates into  $3 \times 0.04 = 0.12$  in or 3 mm. The decrease in closure as D/S increases from 6 to 10, or from 3 to 6, is about 1%, or less than 1mm.

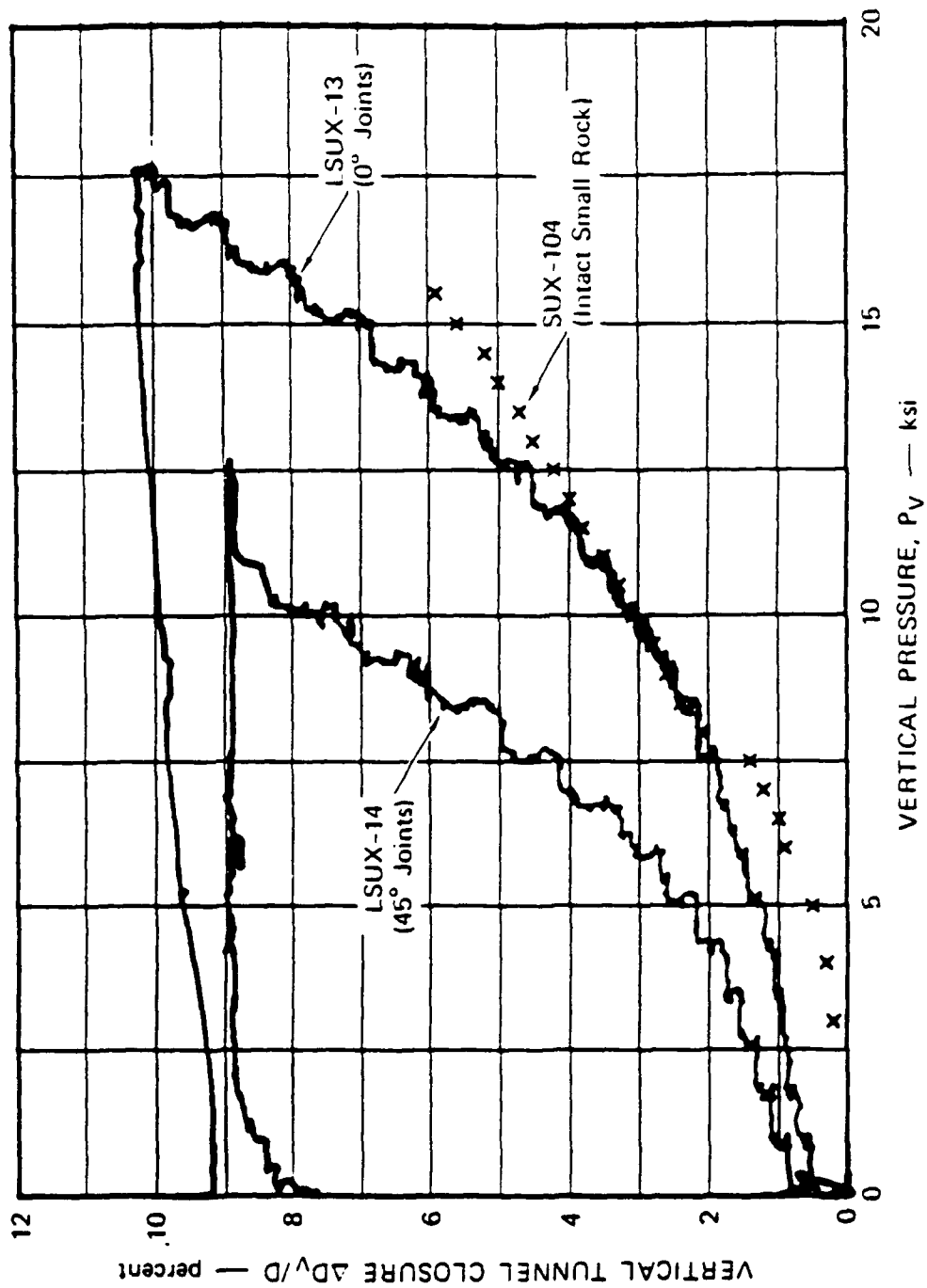


Figure 94. Vertical tunnel closure versus vertical pressure for uniaxial strain loading of jointed 16A rock specimens.

Data from a test on an intact 4-inch diameter specimen, SUX-104, is plotted for comparison.

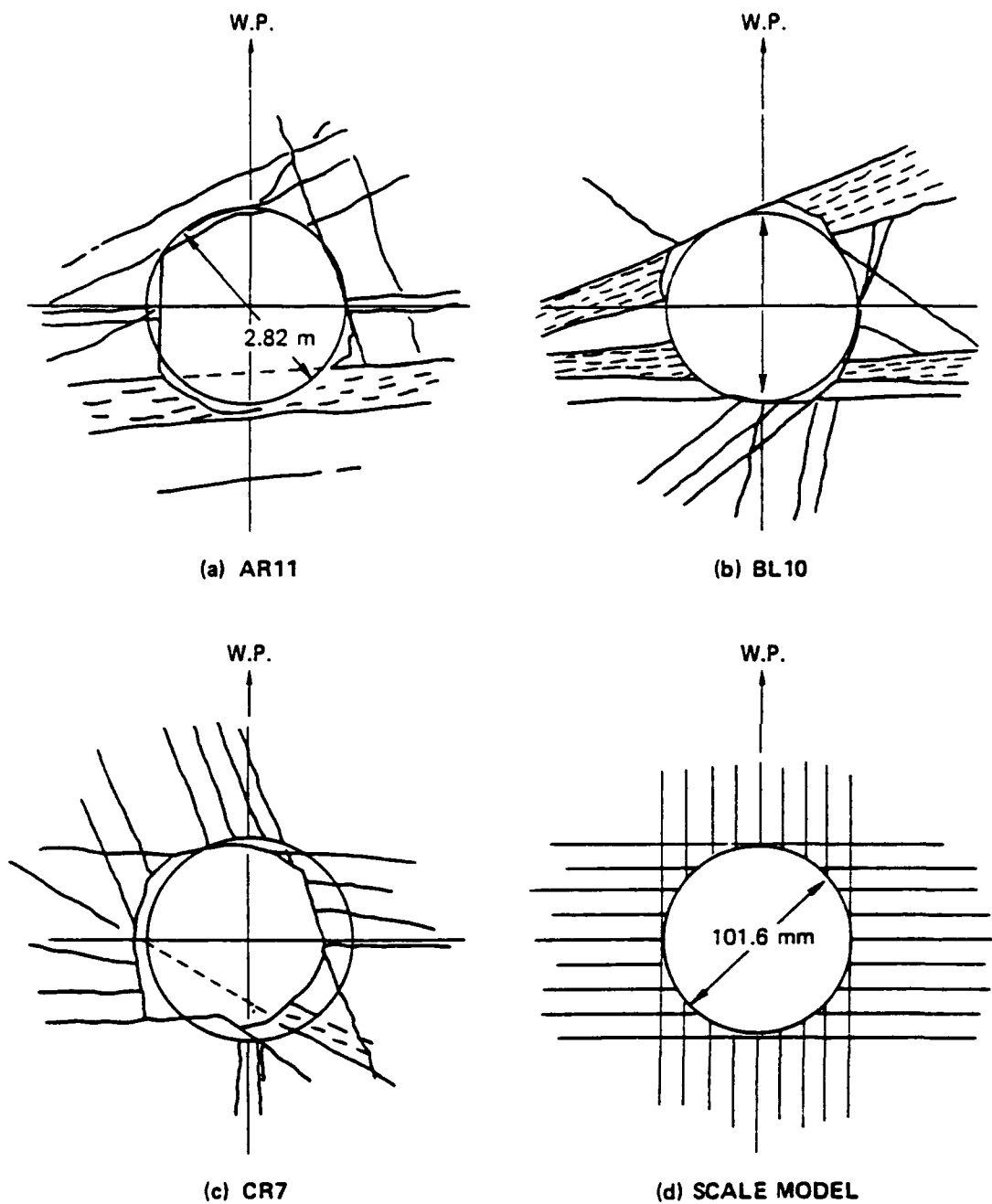
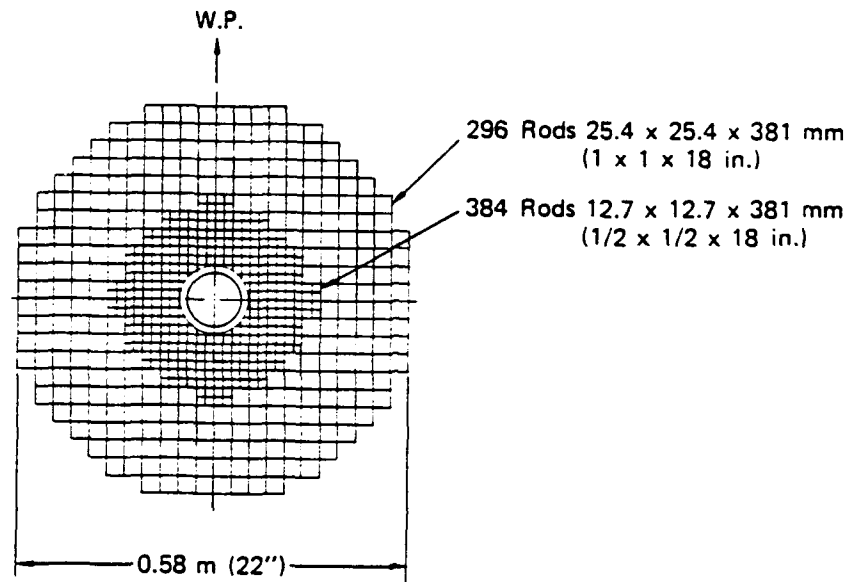
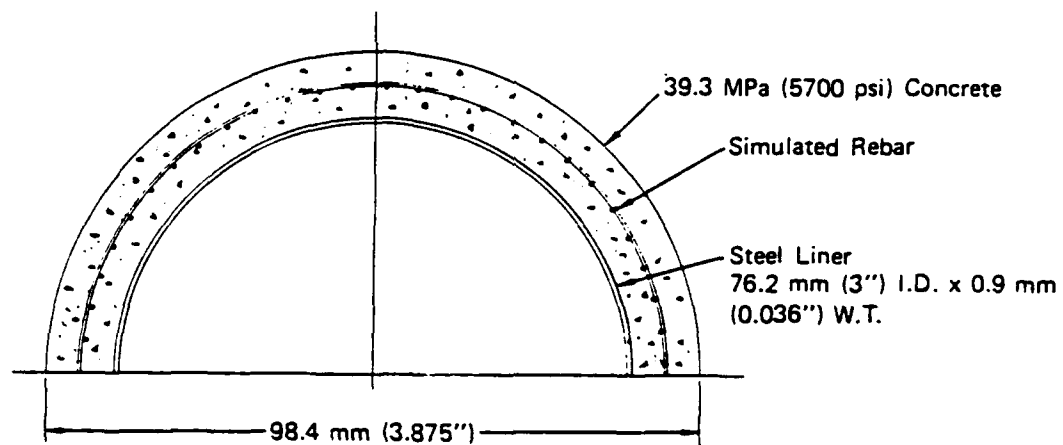


Figure 95. Joint profiled around pile driver structures (a), (b) and (c) and for laboratory scale model (d). (DNA POR 6998)



JOINT ARRANGEMENT IN ROCK SIMULANT



TUNNEL LINER

Figure 96. Scale model of pile driver structures. (DNA POR 6998)

The granite simulant is provided by WES and its properties are compared with PILE DRIVER granite as follows:

	PILE DRIVER granite	WES simulant	16A
modulus	6.9E6 psi	4E6 psi	3E6 psi
strength	30 ksi	18 ksi	3.74 ksi
ang friction	55 deg	33 deg	29 deg

This table shows that the WES simulant for the double-jointed model differs greatly from 16A simulant used in the parametric models discussed in the previous section. Though much stronger than 16A, the double-jointed material is much weaker than PILE DRIVER granite. According to the authors, it was not possible to cast a true granite simulant in the small dimensions needed. The authors justify using the much weaker simulant on the basis of calculations which indicate that the differences in closure between laboratory specimens made of WES Simulant and full size PILE DRIVER tunnels would be small.

Efforts to achieve replica scaling resulted in the following relation between the model and prototype:

	PILE DRIVER structure	small scale
tunnel dia.	7'	3"
steel liner	3/4"	1/28 x
r/c layer	12"	1/28x
reinforcement	double rebar cage	wire mesh
anchors	rockbolts	none

The effect on tunnel response of using wire mesh in place of double rebar cage and the absence of rockbolts was not evaluated.

As an aid to overcoming uncertainties in the environment, in properties of the jointed simulant and in properties of PILE DRIVER granite, upper and lower bound axisymmetric continuum analyses were performed to support design of the three mini-structures. The authors conclude that at least one of the mini-structures will correspond to one of the PILE DRIVER, structures, most likely BL10.

One scaled model (e.g., S-C1-3A at the drift with the highest working stress in DIABLO HAWK) of the PILE DRIVER structures (e.g., BL10, mid-level in peak stress in PILE DRIVER) is reported to respond similarly to the original structures (Fig.97). Tunnel responses consisted of failure of the reinforced concrete shell and severe buckling and tearing of the steel liner, just as in the original counterpart. The failure mechanisms of the tunnel and the motion along the rock joints are also more clearly demonstrated by the scaled models.

In the model S-C1-3A failure occurs when a vertical column of jointed simulant is pushed-in from both the top and bottom (see Fig.98). This result appears to be related to the fact that joint planes in the model are highly regular. Although joint orientations in the models are supposedly inspired by joint geometry measured near PILE DRIVER tunnels they are obviously highly simplified. Furthermore, the loading stress-time histories were not measured and can only be guessed at. The reviewers consider that the relationship between model and prototype has not been demonstrated.

Using wider joint spacing away from the tunnel affects tunnel response. Calculations show that effect can be significant (a factor of 2). We can check this estimate by comparing models S-DI-2-6 and S-DI-2-7, and S-DI-2-16 and S-DI-2-17 in the mini-structures series. The

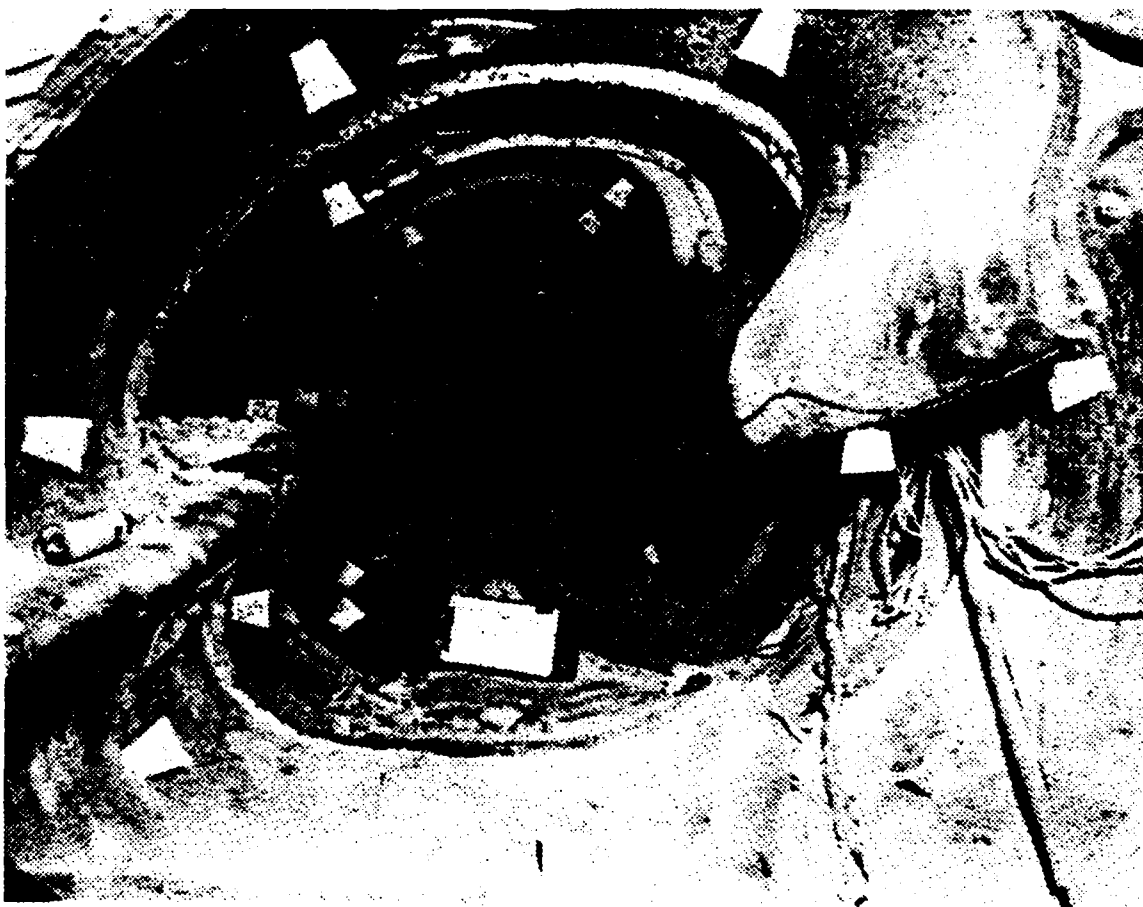
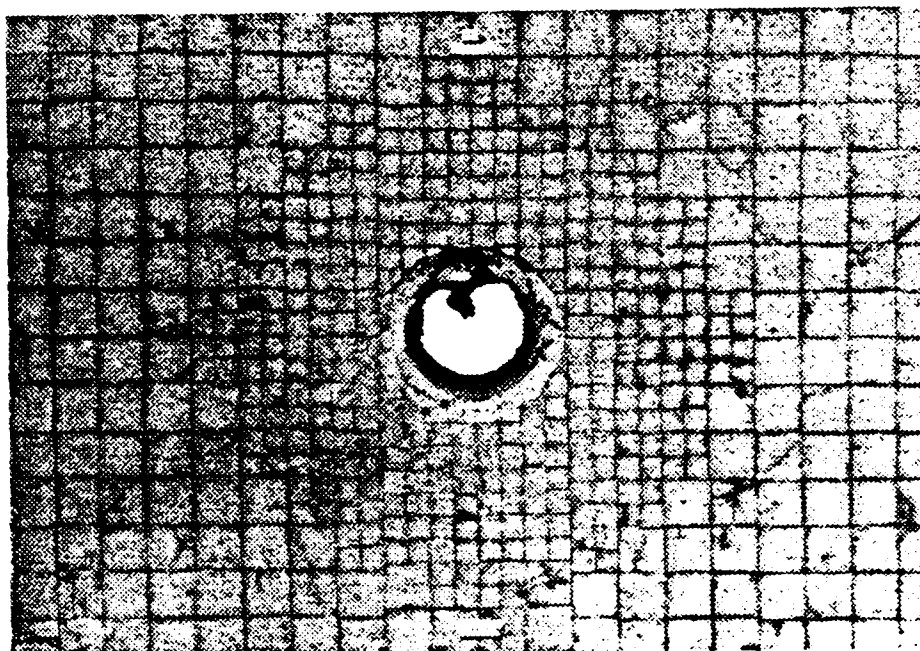
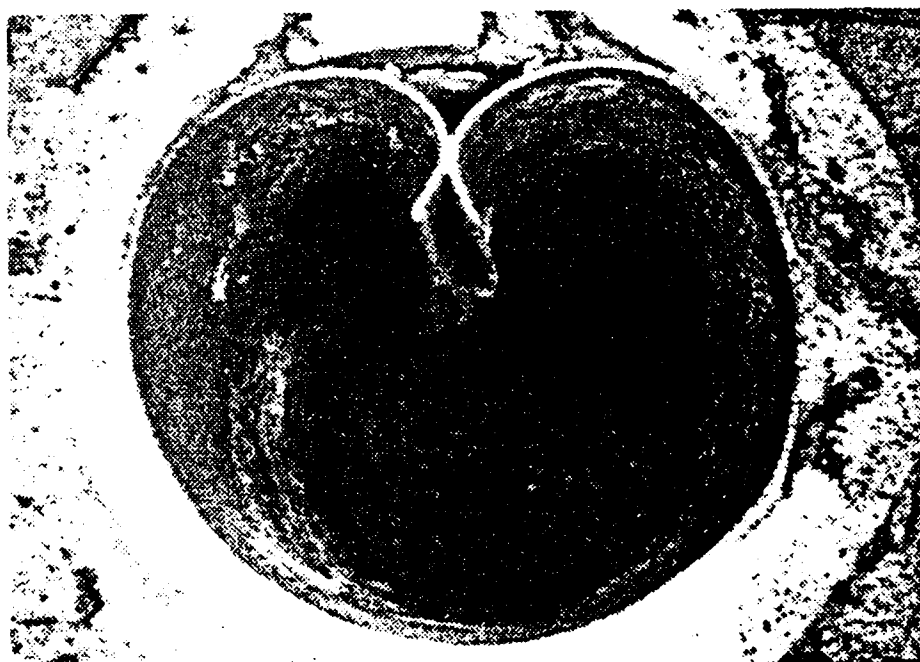


Figure 97. Liner buckling and fractures in pile driver structure BL10 (DNA POR 6998). Working point is toward right.



(a) Joint Overview



(b) Internal Tunnel Deformation

Figure 98. Response of pile driver ministructure model (DNA POR 6998).

first pair gives a factor of 6, and the second pair a factor of 2. Although the configurations are not exactly as that of interest, the experimental results corroborated at least the order of the effect; that is, the use of coarse spacing (double spacing) leads to factor of 2 or higher in closure. Hence, the use of the coarser joint spacing in the outer annulus in S-C1-3A will affect the response of the structure also. This is apparently an example of inverse size effect whereby coarser spacing leads to weaker or more compliant tunnels. The present reviewers note that this is counter-intuitive and counter to the prevailing ideas based on Hendron's interpretation of PILE DRIVER and HARD HAT.

### 3.3.5 Assessment Of Replica-Scaling.

Data are too limited to provide much confidence in scaling effectiveness. The only pair for comparison is S-C1-3A and BL10 (in PILE DRIVER). However, a one-to-one comparison of (a) simulatant and granite properties, (b) regularity of joint patterns vs. prototype pattern, (c) mini-structure vs. composite liner with rockbolts, and (d) loading environments, indicates that the best statement one can make is that the damage modes are similar. Both steel liners buckled and there was evidence of rock intrusion into the composite liner.

Regarding the comparison of S-C1-3A and BL10, many differences in the two test materials and joint patterns make a more definite conclusion impossible. Moreover, photographs show that the displacement of the rectangular prisms, the "jointed rock", viz., is confined to a vertical column with a width of about 4 large squares or 8 small squares is pushed towards the center of the tunnel from top and bottom. This column width coincides with the width (diameter) of the tunnel. We consider this deformation pattern highly unlikely in native rock where the joints (see Fig.95) are not perfectly aligned and regular. Hence, what relationship a model such as S-C1-3A has to prototype jointed rock remains unclear.

Perhaps, therefore, it is not surprising that a startling result such as the inverse joint spacing effect is observed, in which tunnel hardness is reported to increase with the number of joints. The reviewers do not accept this result as valid beyond the experiment in which it was obtained.

Apparently, the kinematic response of the rock block is different in S-C1-3A from the prototype due to differences in joint patterns with the result that the liner buckling is also different. Until the connection between the block kinematics in the laboratory and in the field are established, the laboratory results will be of little use, except as a worst case.

Replica testing of jointed rocks in the lab apparently must resemble the native rock more closely than it does. Furthermore, the intact materials must have properties of intact prototype rock.

## 3.4 DIABLO HAWK - CONTINUOUS ROCK ([POR 6998], 1981).

### 3.4.1 Mini-Structures.

Two mini-structure models, designated S-E-3B and S-D-3B, respectively, and representing the CX9 and CY12 tunnel structures in the MIGHTY EPIC event were included in DIABLO HAWK. The models consist of of 3" diameter steel liner surrounded by reinforced concrete built on double rebar cage. The composite liner is cast in homogeneous ME8-11 tuff-matching grout.

The MIGHTY EPIC structures have 3/4" steel liners surrounded by 15" of reinforced concrete. The structures have an inside diameter of 4' and were directly fielded in the tuff test bed. Hence, the mini-structures are 1:16 scale of the MIGHTY EPIC structures.

### 3.4.2 MIGHTY EPIC Results.

Both CX9 and CY12 suffered moderate damage in MIGHTY EPIC. CX9 was moderately damaged; the concrete failed and the liner buckled and split. Closure was reported about 10%. Damage to CY12 was caused by fault slip, since the structure was located at 1/2 of the pressure range of CX9.

### 3.4.3 Mini-Structure Response.

The stress level in  $D_H$  is about 70% of that in MIGHTY EPIC. S-D-3B has a maximum closure of 4.8%. S-E-3B was not sectioned because it has insignificant liner deformation. Pretest analysis indicated for the two structures are 1.3% and 9.5%, respectively.

### 3.4.4 Assessment Of Replica-Scaling.

This attempt at evaluating replica scaling is inconclusive because of differences in loading. Mini-structure responses are similar in some respects with the responses of their larger counterparts.

## SECTION 4

### REVIEW OF TERRA TEK MATERIAL SCALING EXPERIMENTS

#### 4.1 DESIGN OF TESTING APPARATUS.

The motivation and design of the basic testing facilities at Terra Tek are described in [DNA-TR-85-387]. As shown in Fig.99, the loading system consists of a frame which accommodates a specimen of approximately one meter on a side and which is capable of applying lateral loads to the specimen by means of independently controlled flat jacks. Vertical loads are applied by a 1.7 million pound hydraulic cylinder and loading frame modified for gas operation. Minimum times to peak load that can be achieved with the vertical loading machine are in the range 1/4 to 3/4 second.

One argument in favor of testing specimens at this scale is that it is easier and less expensive to prepare larger specimens. There may also be less variability from specimen to specimen if the failure mode is ductile because flaws tend to be the same size regardless of the dimension of the specimen. Hence, in a scaled sense, the flaws in the Terra Tek specimens are relatively smaller than flaws occurring in small specimens. Against testing at this scale is the fact that even a 1.7 million pound loading machine is capable of applying stresses of approximately 1600 psi maximum, which is much less than the strength of most naturally occurring rocks of interest. Therefore, the tests must be conducted using strength scaled material. As is pointed out in several Terra Tek reports, the material scaling is limited to properties governing onset of inelastic deformation; in the regime involving shear and tensile failure, the strength-scaled material does not necessarily correspond to any naturally occurring rock. It is part of the present review to decide how data developed from tests on such a material can be used in the DNA deep underground program.

As is described in DNA-TR-85-387, the lateral (confining) stresses are transferred to the specimen by distributing the forces from the flat jacks through steel shims which bear on teflon sheets. It is assumed that Poisson effects in the specimen are unresisted due to low friction between the teflon and the vertical surfaces of the block. A similar arrangement was used on the upper surface of the block where vertical load was transmitted to the teflon through a rubber sheet in the earlier tests; in the most recent tests, flat jacks were also used to transfer loads at this surface.

In the process of conducting several experimental series, Terra Tek developed insight into the effects of boundary conditions on the response of openings. The most current series of Terra Tek tests ([DNA TR-88-74]) use 2 inch diameter openings in about 36 inch blocks. Previous test series, in which the openings were 4.5 inch and 6.6 inch are considered by Terra Tek to have been influenced by the boundaries of the specimens ([Jones],1988). In contrast, a recent experimental program at SRI was conducted with 12 inch specimens and 2 inch openings, which was deemed to be adequate. (We note that a larger specimen to tunnel opening ratio is needed for the TT tests because they use weaker grout. In general, boundary effects become more important as weaker material is used for the specimen. However, as the analysis of Appendix C shows, even  $D/d=6$  may not be adequate; hence, it seems likely that boundary effects influence the TT results).

A typical procedure at Terra Tek involves quasistatically applying hydrostatic stress to the specimen in the range 20-150 psi. If the remainder of the test is to be performed quasistatically, the vertical load is then applied monotonically. If the remainder of the test is to be performed dynamically, the gas chambers of the actuator were charged first and then pressurized gas was rapidly admitted to the actuator chambers. During dynamic loading, the pressure in the flatjack

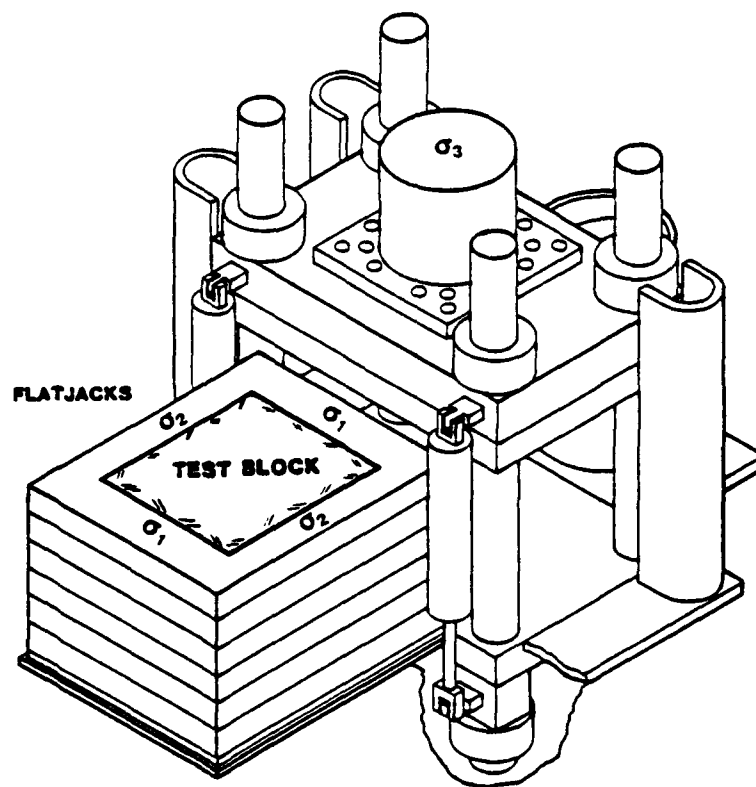


Figure 99. Terra Tek's polyaxial cube test facility for loading 1 m<sup>3</sup> blocks of intact or jointed rock.

chambers was also increased so as to maintain approximately proportional dynamic loading. (Do we have any measure of how successful this was?).

## 4.2 MECHANICAL PROPERTIES OF SIMULANT.

The earliest Terra Tek work reviewed was [DNA TR-85-387], which dealt with tests of unlined straight tunnels in a tuff simulant. The properties of natural tuff and the tuff simulant are compared in Table 20, the data for which came from pages 17 and 19 of [DNA TR-85-387]. There is a considerable variation in the strength of natural tuff. A scale factor of 27 is suggested in said reference. The scaled up properties [all stress quantities scaled according to Eq. B-22 of this report, Appendix B] are included in Table 20 for convenience. No attempt was made to scale stress strain curves; in fact, no such curves for tuff are given in said reference. Rather, the limited set of relations Eqs. B-28 to B-31 were addressed.

The scaled simulant unconfined compressive strength essentially matches that of Rainier Mesa tuff more or less by definition; i.e. the choice of scale factor,  $s$  is  $1/27$ . There is some scatter in the value of Young's modulus in natural tuff, and considerably more in the scaled values for the simulant. While the scaled values bracket those of tuff, the computed upper limit is more than ten times the upper limit of Young's modulus found in tuff. Thus, it is questionable whether Eq. B-28 is satisfied. Both Poisson's ratio [see Eq. B-29] and the angle of internal friction [Eq. B-31] appear to be modeled adequately. Also included in the table are the respective densities, cohesion and tensile strength. Except for tensile strength, these quantities match fairly well.

The derivation of the data for the simulant is described in Appendix B of said reference. In particular, four unconfined compression tests were run from grout batch #2. The results are summarized in Table 21 (Table 5 in said reference). The actual stress strain curves are shown in Fig. 100 (taken from Figures 66-69 of reference). There is considerable scatter in the values listed for Young's modulus and Poisson's ratio. Much less scatter exists in the values of the unconfined compressive strength. Average values of the three quantities as given in the text, as well as those computed directly, are included in the table. The discrepancy in the average values of Poisson's ratio is unexplained, as are the inconsistencies between the values of  $f'_c$  and  $E$  in Tables 20 and 21.

A second Terra Tek report, [DNA TR-86--275], describes tests of tunnels and tunnel intersections in two different rock simulants, a grout mix designed by Terra Tek, Inc. and one designed by SRI International. Both sets of tests were run at Terra Tek. The material properties of the two grouts are compared in Table 22. Except for the last column and the bottom line, which have been added for convenience, the table is identical to Table 3 of said reference. For one grout to be a model of the other grout,  $\sigma_c$  and  $E$  must scale by the same factor, or the ratio  $\sigma_c/E$  must be the same in both materials. The scatter in  $\sigma_c$  is much greater for the TT grout. Consequently, the ratio  $\sigma_c/E$  for TT grout contains a good deal of scatter. Nevertheless, the upper range of the data includes that for the SRI grout. Thus, selection of the stress scale of  $s = 1/17$  satisfies (approximately) both Eqs. B-28 and B-30. In addition, the two Poisson's ratios and the two friction angles must be equal. The first condition, Eq. B-29, is approximately true; the second, Eq. B-31, is somewhat off.

The stress difference at failure may be related linearly to the confining stress

$$\sigma_1 - \sigma_3 = (N_\phi - 1)\sigma_3 + \sigma_c$$

Table 20. Comparison of properties of natural tuff, tuff simulant and scaled simulant.

	Natural Tuff Rock	Tuff Simulant	Scaled Simulant ( $S = 1/27$ )
Unconfined Compressive Strength, psi (Yucca Mountain Tuff)	1200-4200 (4200)	152.5	4118
Young's Modulus, $10^6$ psi	1.17-2.90	0.04-1.17	1.08-31.6
Poisson's Ratio	0.16	0.15	0.15
Angle of Internal Friction, Degrees	15.9	15.5	15.5
Bulk Density, gm/cc	1.60-2.20	1.885	1.885
Cohesion, psi	1580	50	1350
Tensile Strength, psi	14.5-360	35	945

**Table 2:** Young's modulus, Poisson's ratio and unconfined compressive strengths of batch #2 tuff simulant grout.

Sample Designation	Young's Modulus (psi x 10 <sup>6</sup> )	Poisson's Ratio	Unconfined Compressive Strength (psi)
2-A	0.22	0.22	160
2-B	0.04	0.03	175
2-C	0.03	0.04	179
2-E	0.10	0.12	185
Average Given in Ref. [2]	0.10	0.15	174
Computer Average	0.098	0.102	174.8

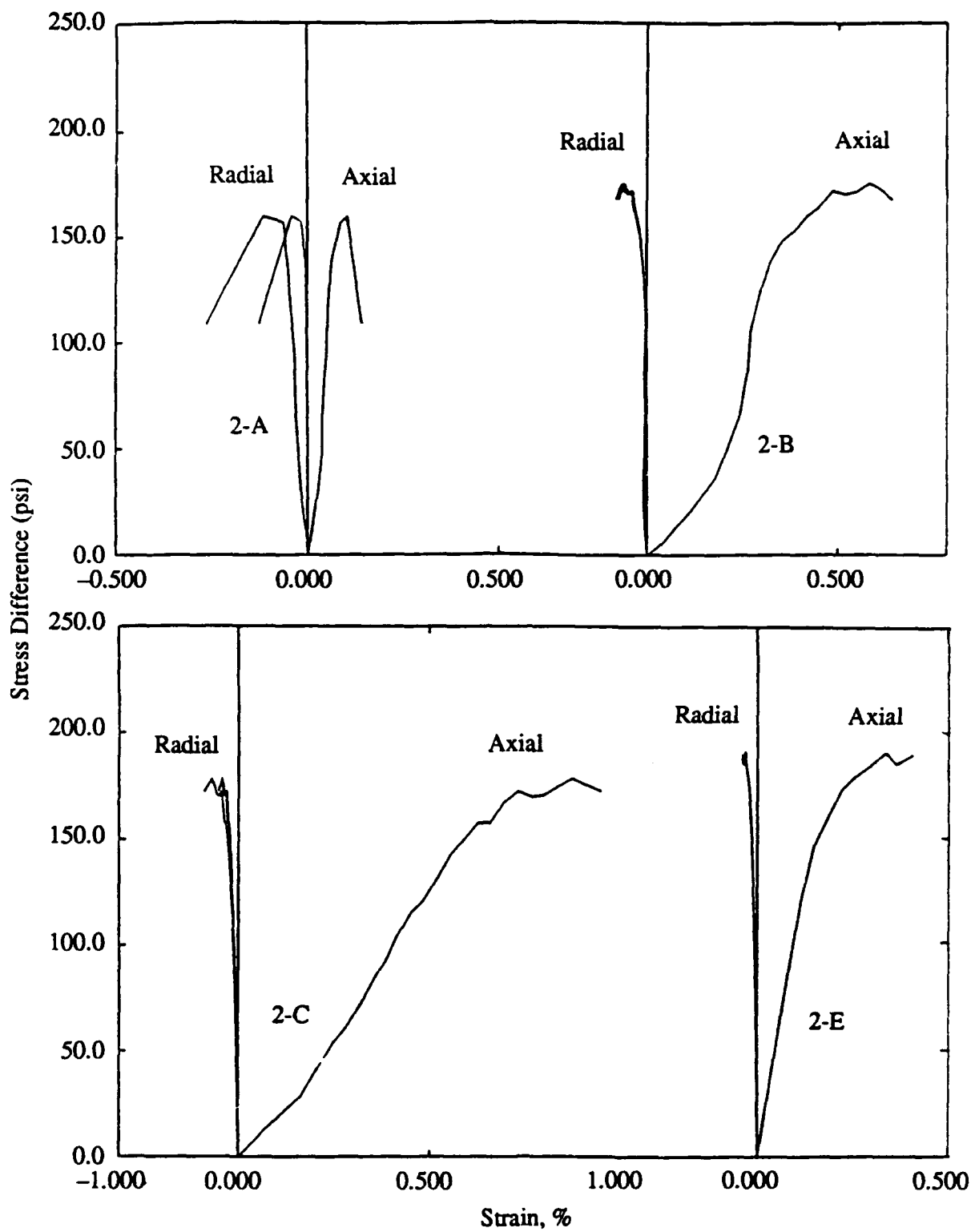


Figure 100. Unconfined compression tests of batch #2 of scaled tuff simulant grout.

Table 22. Comparison of material properties of Terra Tek and SRI grouts.

Property	Terra Tek Grout	SRI Grout	Scaled ( $S = 1/17$ ) Terra Tek Grout
$\sigma_c$	152-212 psi	3530-3650 psi	2584-3604 psi
E	$0.13 \times 10^6$ psi	$2.36 \times 10^6$ psi	$2.21 \times 10^6$ psi
$\nu$	0.22	0.20	0.22
$\phi$	32°	36°	32°
$\rho$	1.85 gm/cc	--	1.85 gm/cc
$\sigma_c/E$	.00117-.00163	.00153-.00158	.00117-.00163

where

$$N_{\phi} = \frac{1 + \sin \phi}{1 - \sin \phi}$$

The failure surfaces of the two grouts based on the values of  $\phi$  and  $\sigma_c$  in Table 22 are compared in Fig.101. Note, two sets of horizontal and vertical scales are given in Figure 3, so that the TT grout values may be compared directly with those for SRI grout ( $s = 1/17$ ). The TT grout failure surface generally falls below that for the SRI grout. In fact, for confining stresses greater than about 0.2 ksi (12 psi for TT grout) there is no overlap. Thus, at greater confining stresses, Fig.101 suggests that the TT grout would not be a good model of the SRI grout.

The stress strain curves in unconfined compression for the two grouts are compared in Fig.102, where the stress scale for the TT grout has been multiplied by 17. The curves for both grouts are given separately in [DNA TR-86-275]. The scaled axial stress-axial strain curve for the Terra Tek grout is considerably stiffer than that of the SRI grout, despite the nominal close agreement in the (scaled) value of  $E$  in Table 22. Note that radial strains were not measured for the Terra Tek grout.

The stress difference versus strain curves in triaxial compression of the two grouts are presented in Fig.103. Again, the stress scale for the TT grout has been multiplied by 17. The two tests are not at equivalent confining pressures. The  $\sigma_3 = 50$  psi for the TT grout scales up to 850 psi, less than the  $\sigma_3 = 1,016$  psi for the SRI grout. An idea of the difference in failure may be estimated from Fig.101. The distinct failure surfaces account for at least as much of the difference as the change in chamber pressure. Nevertheless, for the lower two thirds of the TT axial strain curve, where the behavior of both materials is essentially elastic, the two curves agree fairly well. Again, no data were presented in said reference for the TT grout radial strains.

#### 4.3 DATA FOR TUNNELS IN CONTINUOUS (UNJOINTED) SPECIMENS.

##### 4.3.1 Straight Tunnel Section.

An example of the basic experiment, a straight circular opening in simulant without joints, is discussed briefly in [DNA TR-86-275]. When these tunnels were subjected to proportional loading they exhibited a type of ovaling response whereby the crown-invert shortening is greater than the springline shortening. Since the report does not attempt to relate the loading path to any field test, it cannot be concluded whether the observation of direct ovaling (as opposed to reverse ovaling) in the laboratory experiment agrees or disagrees with field data. This is an unfortunate omission.

##### 4.3.2 Test of Tunnel Intersections in Two Grouts.

An effort was made by TT to demonstrate that the responses of geometrically similar, right angle intersections having different geometric scales and different material properties can be correlated using principles of material scaling. Terra Tek cast intersections in its own grout, which has reduced stiffness and strength, and in an SRI grout, which has prototype (tuff) stiffness and strength. By applying the rules of material scaling to the results from the two series, the validity of the material scaling approach was investigated. Comparison was made for specimens in which the tunnel diameter was 2.0 inches (Tests 2 and 3) and 4.5 inches (Tests 4 and 5).

Five static tests of unlined 90 degree tunnel intersections were reported in [DNA TR-86-275]. Uniaxial strain conditions were maintained in the far field. The first test was interrupted at

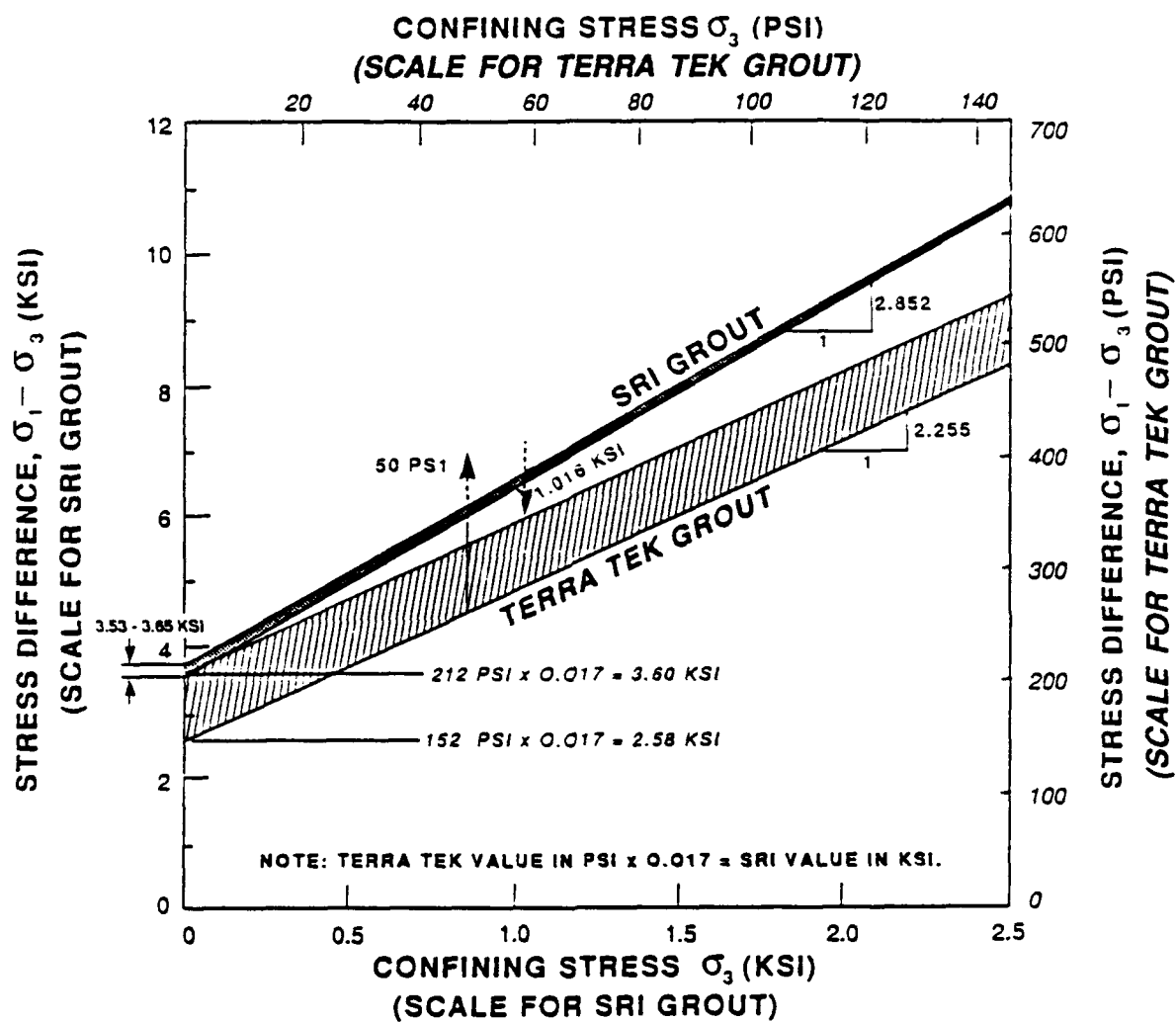


Figure 101. Comparison of failure surfaces for SRI and Terra Tek grouts.

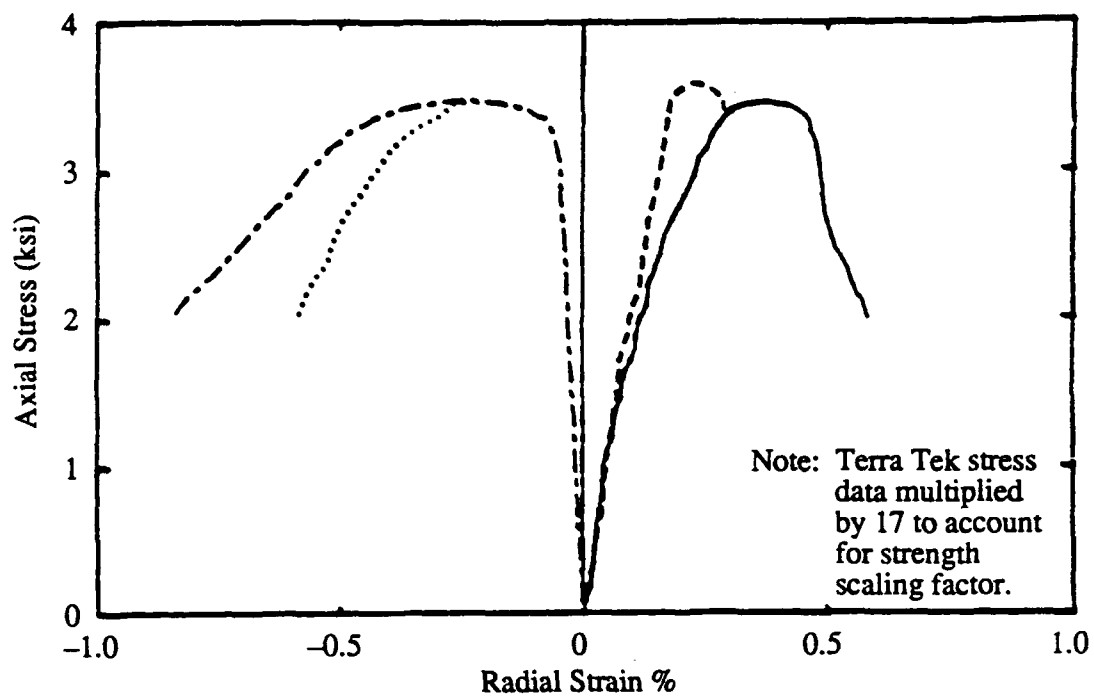


Figure 102. Stress strain for unconfined compression, SRI and Terra Tek grouts.

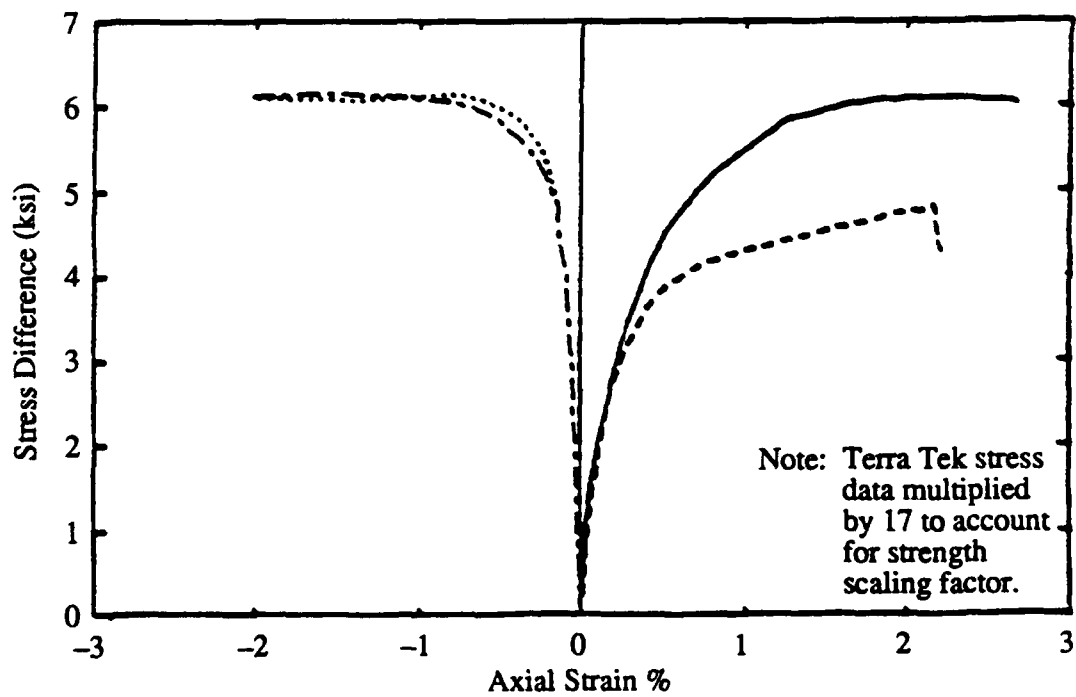


Figure 103. Stress difference versus axial and radial strain for triaxial compression, SRI and Terra Tek grouts.

2% vertical closure at the center of the intersection, before significant permanent deformations occurred. The other tests were loaded to at least 8% vertical closure at the intersection. The results of the other four tests, two with SRI grout, and two with TT grout, are summarized in Table 23. Closure measurements were taken at the center, one and two diameters from the center, and 4 -5 diameters from the center. The results more than 2 diameters from the center are not included in Table 23. The "N", "E", "S" and "W" in Table 23 refer to north, east, south and west designations of the particular measurement location. Note, the computed averages in Table 23 in some cases differ from those in Tables 5 and 6 of [DNA TR-86-275].

#### Vertical Closures, Tunnel Intersections

The individual closure versus (far field) vertical stress curves in said reference were digitized and are replotted in Figs.104 to 108. (In fact, the values appearing in Table 23 were obtained in this manner.) The results for the 2" tunnel intersections in both SRI and TT grouts are shown in Fig.104, all plotted to the same scale, after the stresses in the Terra Tek case have been multiplied by 17. The vertical closures one diameter from the center in the SRI grout tunnel agree well with each other and with that at the center. Somewhat more scatter appears at two diameters. The center closure in the TT grout is somewhat larger than those at the other locations. Except for a peak stress shift of about 20%, the results from the two tests are roughly similar.

The vertical closures for the two 4.5" tunnel intersections are shown in Fig.105. Except for the SRI result one diameter west of the intersection, which has an unusual shape above 3.5 ksi, there is little scatter in the various measurements. The vertical closures at the center of the intersections in all four tests are compared directly in Fig.106. The curves for both TT grout tests fall to the right of both SRI tests. The closest agreement happens to be between the 2 in SRI and 4.5 in TT results (Reviewers note: it is probably coincidental that a specimen diameter to tunnel diameter ratio of  $36/4.5=8$  for Terra Tek approaches that of  $12/2=6$  for SRI, given the cubical versus cylindrical geometries). Changing the stress scale factor to say 1/15 would make the closure curves agree better, but would make the disagreement in Figs.103 and 105 worse. The fact that the closure for any particular vertical stress is larger in the 4.5 in models than in the corresponding 2 in models in both grouts is noted, but its significance is not understood. Nevertheless, the agreement with respect to vertical closure is adequate to support the assertion that material and geometric scaling, as applied in this experiment, are valid.

#### Horizontal Closures, Tunnel Intersections

For both types of specimens, the springline closures at one and two diameters from the center of the tunnel intersections are shown in Figs.107 and 108. The results for the 2 in tunnels are summarized in Figure 107. The SRI horizontal closures are very small for vertical stresses less than about 3 ksi. They then increase rapidly reaching as high as 10%. While the scatter is more than that in the vertical closures, it is tolerable. The springline closure appears to decrease with increasing distance from the intersection. However, the springline closures in the TT grout are substantially smaller than those in the SRI grout. The largest Terra Tek value, 2.3%, is less than the smallest SRI one, 4.2%. Moreover, in two of the three Terra Tek models, the springline diameter increases; this contrasts to behavior of the SRI samples in which the springline diameters always decrease.

The agreement between the springline closures in the two grouts in the case of the 4.5 in tunnels, Fig.108, is somewhat better. Here, only a single curve shows any significant initial negative closure. Nevertheless, the magnitude of the springline closures for the SRI grout is still twice that in the TT grout.

In summary, in one of few examples undertaken in the DNA program where the material scaling approach can be validated by direct comparison with another controlled experiment the

**Table 23.** Summary of maximum closures in tunnel intersections in SRI and Terra Tek grouts.

Test	Grout	Tunnel Diameter (in)	Peak Vertical Stress (ksi) [x 17]	Center	Vertical Closure (%)		Springline Closure	
					1Diam	2Diam	1 Diam	2 Diam
2	SRI	2	5.20	7.9	N 6.8	8.0	9.2	5.2
					E 6.5	—	6.5	—
					S 6.8	6.3	10.0	4.2
					W 7.1	5.9	8.7	7.7
					Av 6.8	6.7	8.6	5.7
3	TTI	2	0.35 [5.95]	8.1	S 7.4	—	1.5	—
					W 7.8	7.4	1.7	2.3
					Av 7.6		1.6	
4	SRI	4 1/2	4.80	9.7	N 8.7*	8.1**	9.6*	8.8**
					E 5.6	4.9	9.4	7.8
					S 7.6	—	9.4	9.1
					W 9.5	5.8	9.8	9.2
					Av 7.8	6.3	9.6	8.7
5	TTI	4 1/2	0.32 [5.44]	9.2	N 8.5	7.3	2.2	4.5
					E 7.9	7.1	4.2	4.4
					S 8.2	8.2	5.6	3.9
					W 8.9	8.1	4.2	5.2
					Av 8.4	7.7	4.0	4.5

\* 1/2 Diameter from Center of Intersection.

\*\* 1 1/2 Diameters from Center of Intersection.

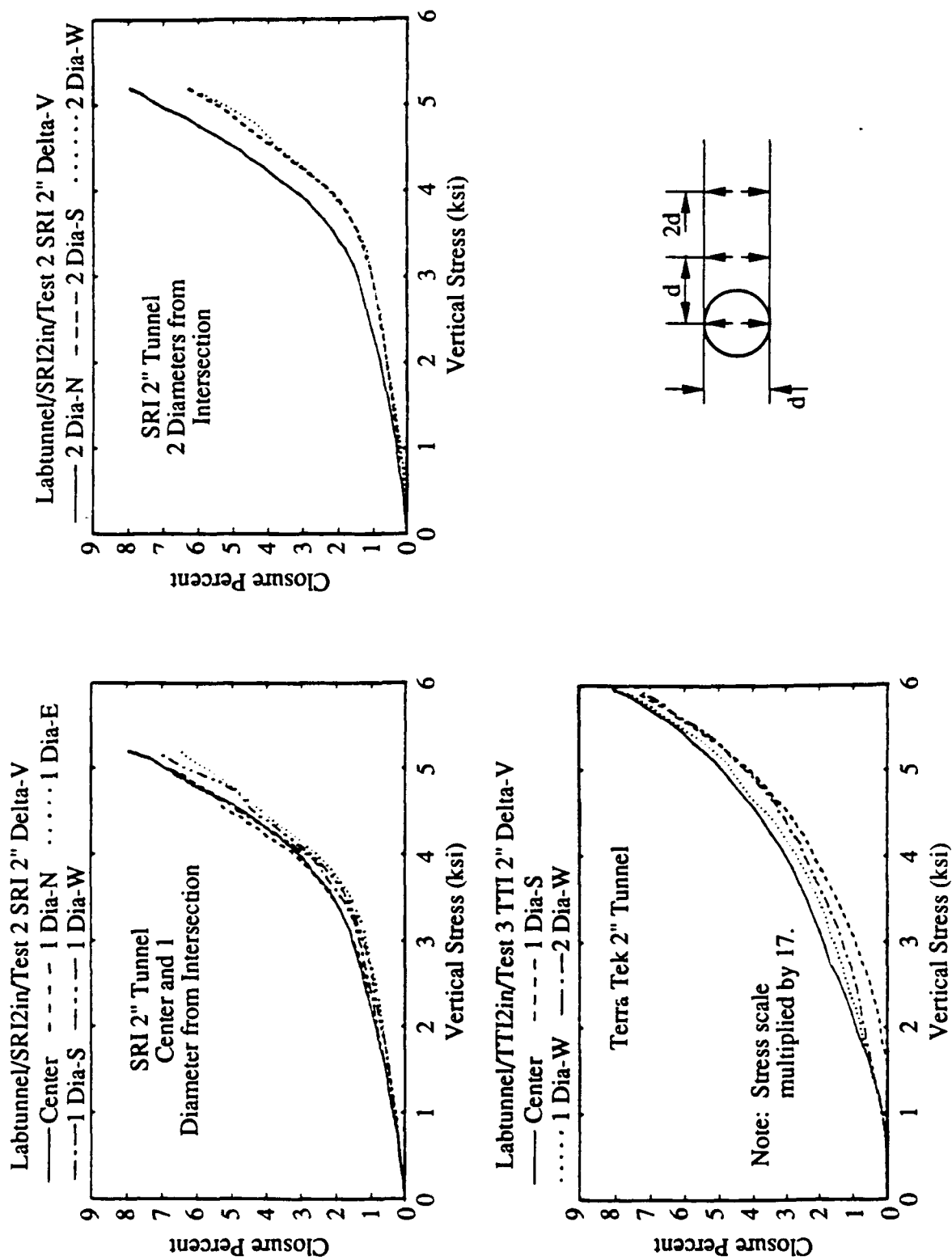


Figure 104. Vertical closure in 2 in. tunnel intersections in SRI and Terra Tek grouts.

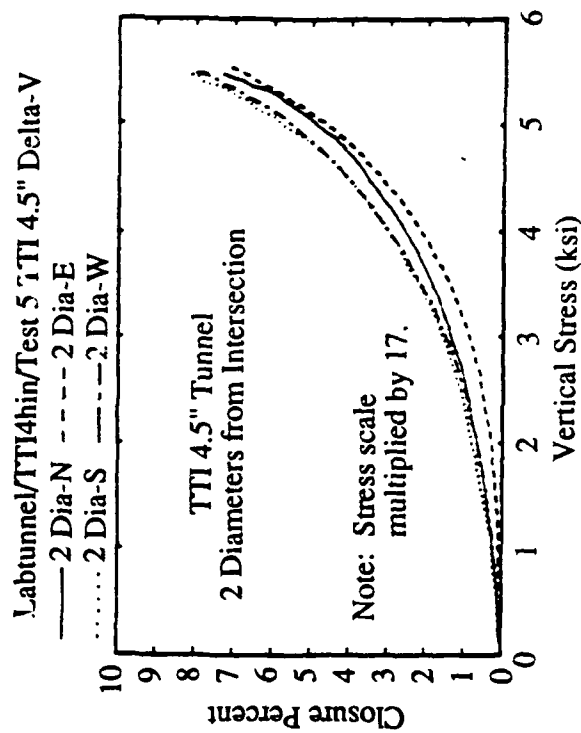
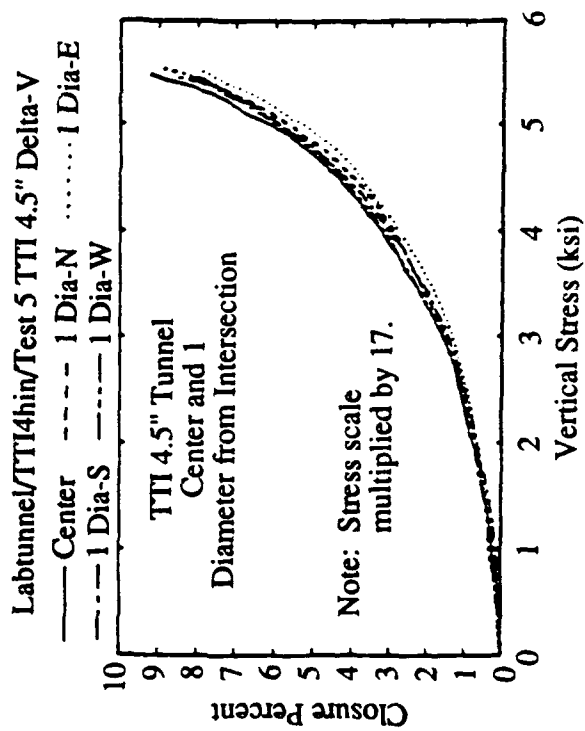
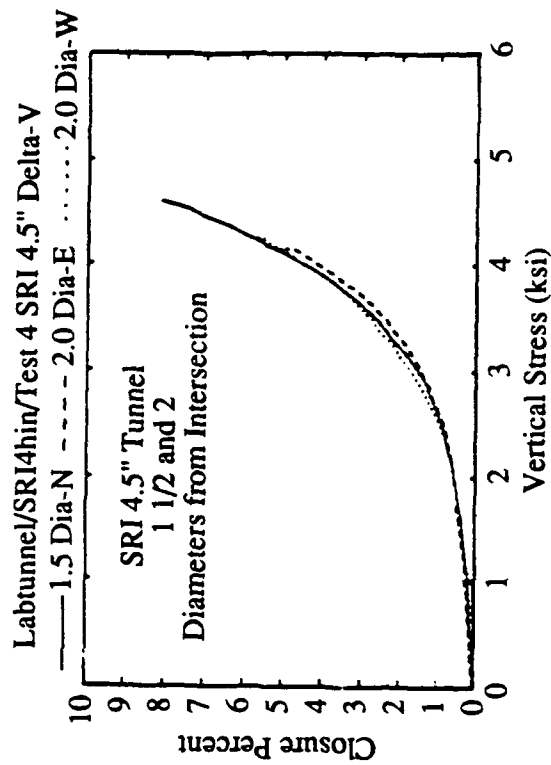
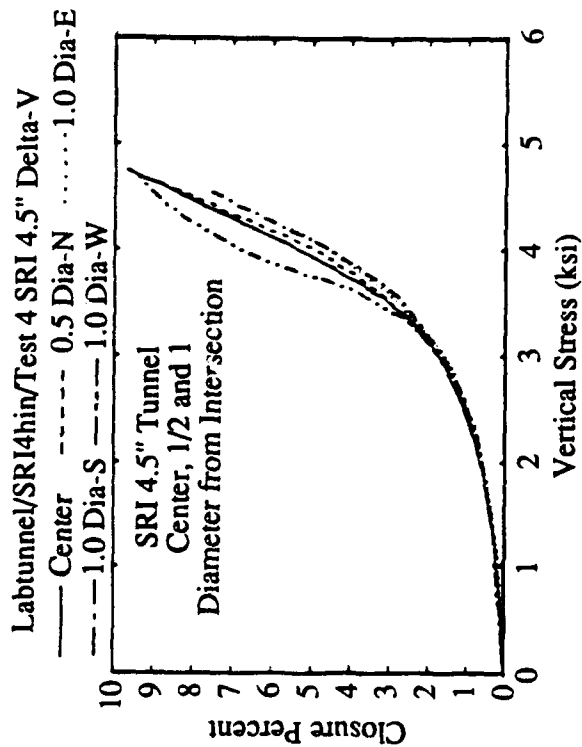


Figure 105. Vertical closure in 4.5 in. tunnel intersections in SRI and Terra Tek grouts.

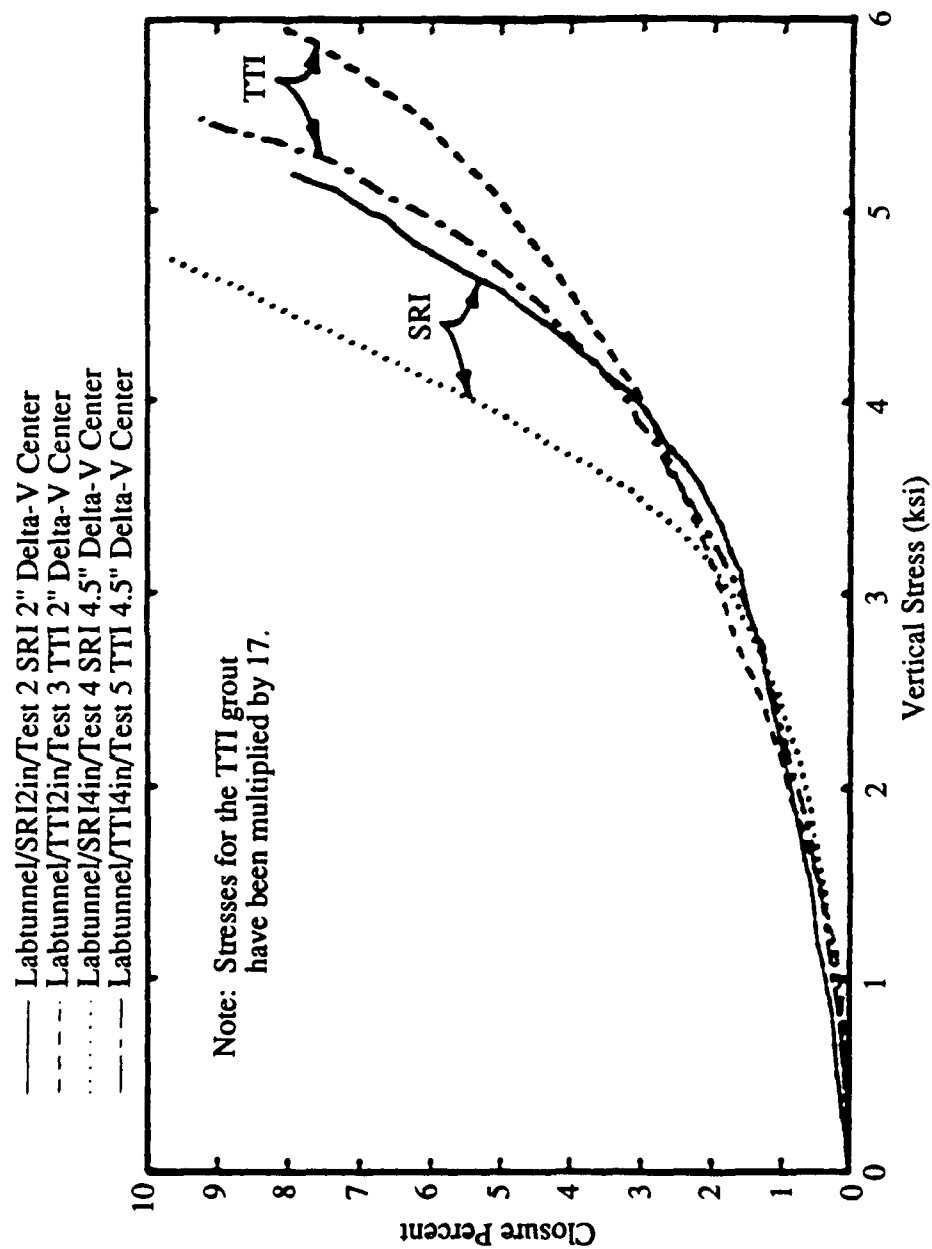


Figure 106. Comparison of vertical closure at center of tunnel intersections in SRI and Terra Tek grouts.

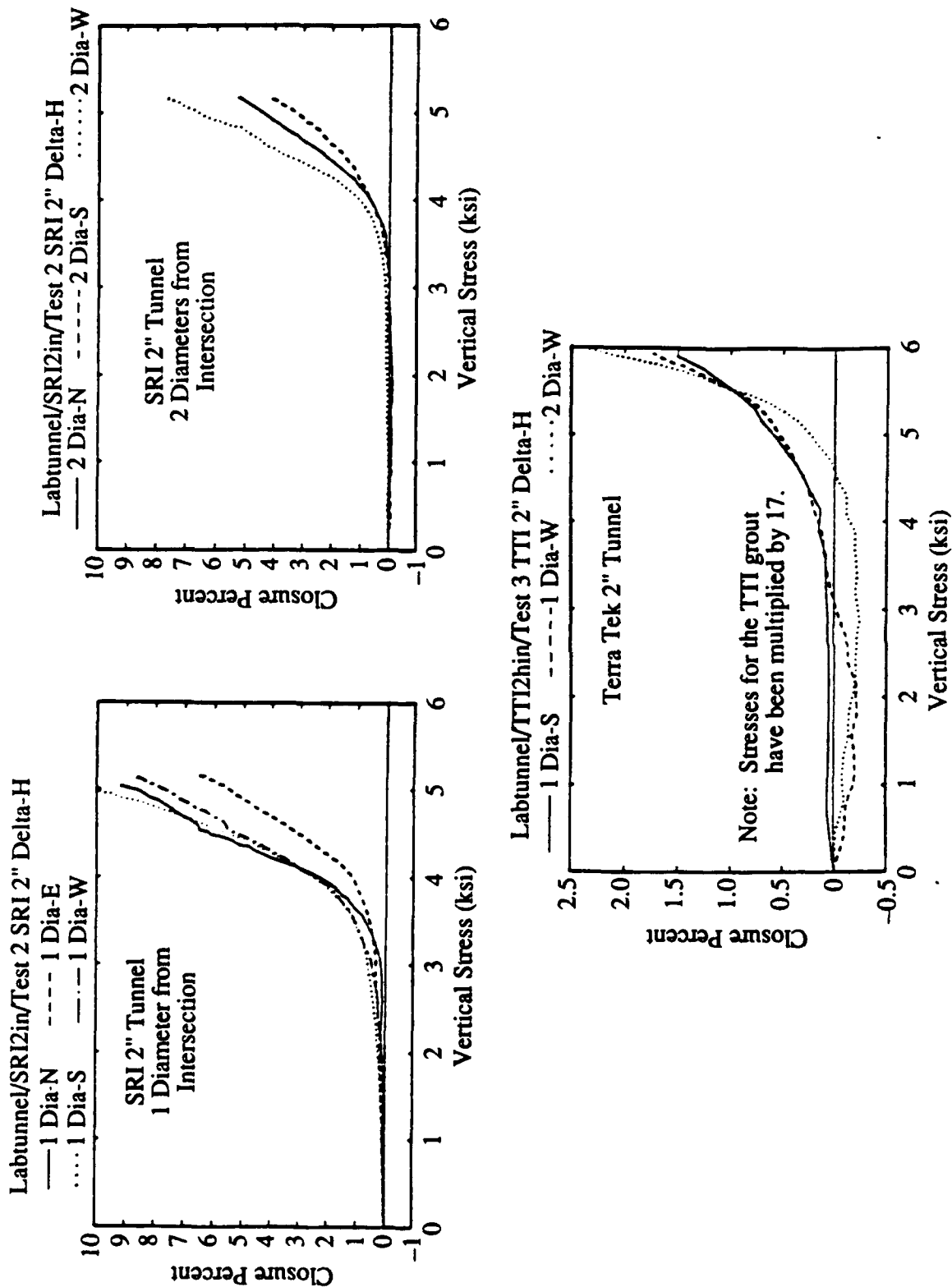


Figure 107. Springline closure in 2 in. tunnel intersections in SRI and Terra Tek grouts.

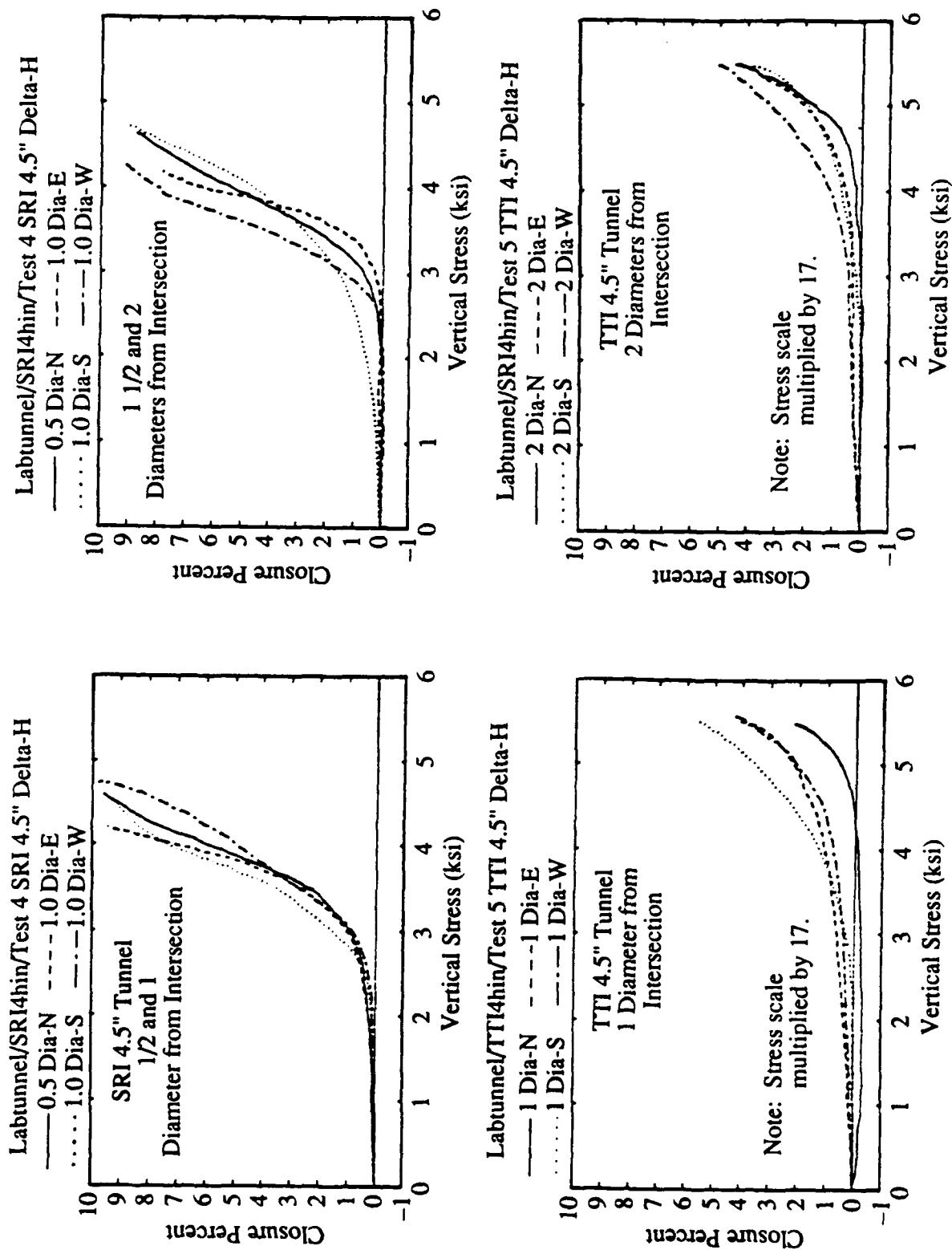


Figure 108. Springline closure in 4.5 in. tunnel intersections in SRI and Terra Tek grouts.

results are mixed. While agreement with respect to vertical closure is encouraging, the horizontal closures differed by enough to undermine confidence.

The issue discussed above considers the validity of material scaling. Another issue is whether any useful insight about deformation modes or hardness of tunnel intersections is gained by performing this experiment.

#### 4.3.3 Reliability of Experimental Results, Continuous Specimens.

Earlier in this section references were made to discrepancies, inconsistencies and scatter while discussing the Terra Tek experimental results. It is in order to remark on one's impression of the overall quality of the Terra Tek laboratory program, at least as indicated by [DNA TR-85-387] and [DNA TR-86-275].

One must conclude that the laboratory studies reported in these references were less than exemplary. The high scatter in the values of  $E$  and  $\nu$  given in Table 21; for example, makes the present reviewers cautious about using the results, if in fact  $E$  and  $\nu$  are key parameters in developing a rock simulant. The actual stress-strain curves, Fig.100, suggest that the basic measurements themselves were unreliable.

Another apparent problem was lack of control of the loading path. Tunnel test 1 of [DNA TR-86-275] was a static proportional loading test. The intended loading path was  $\sigma_2 = \sigma_3 = \sigma_1/2$ . The actual stress path is shown in Fig.109 (Fig.18 of [DNA TR-86-275]). Note, the loading took place over almost 2 minutes. If the load can deviate so much from the intended path in simple static case, how much confidence should be placed in the measured response? Can a trend be determined by comparing several tests when the load deviates from the nominal path as indicated in Fig.109 for a single test? Since dynamic tests are more difficult to control, how should the dynamic results be interpreted?

There are also a number of cases of incomplete documentation. Figure 24 of [DNA TR-86-275] shows the stress path,  $\sqrt{J_2}$  versus  $p$ , for "proportional loading test #3." The time history of the axial load is given in the following figure, but the individual lateral stresses  $\sigma_2$  and  $\sigma_3$  are nowhere to be found. A similar situation is found in [DNA TR-85-387]. For example, in Figs.110 (Fig.22 of Ref. [2])  $\sqrt{J_2}$  versus  $p$  is shown. Note, the corresponding axial load increases monotonically for the 55 sec test duration. The individual lateral stresses are not given. The description in the text refers to loading simultaneously up to the prescribed hydrostatic stress, followed by increasing the axial load until the maximum stroke was reached. The cause for the strange path shown in Fig.110 is unknown.

Dynamic tests are more difficult to control than static ones. The stress path for dynamic test #2, 100 psi initial hydrostatic loading, is shown in Fig.111 (Fig.44 of [DNA TR-85-387]). The path deviates from the intended triaxial compression state. The applied axial load for the test is shown in Fig.112 (Fig.48 of same reference). Loading takes place during 300 msec. Individual histories of  $\sigma_2$  and  $\sigma_3$  are again not given.

The deformations in static and dynamic tests #2, vertical and horizontal closure versus axial stress are given in Figures 30 and 56, respectively, in [DNA TR-85-387]. For any given closure, the stress level in the dynamic case is much larger, by roughly a factor of two. However, before concluding that the tunnels in rock simulants are stiffer under dynamic loading, one must consider the differences in stress paths. While the two paths, Figs.110 and 111, start at the same point,

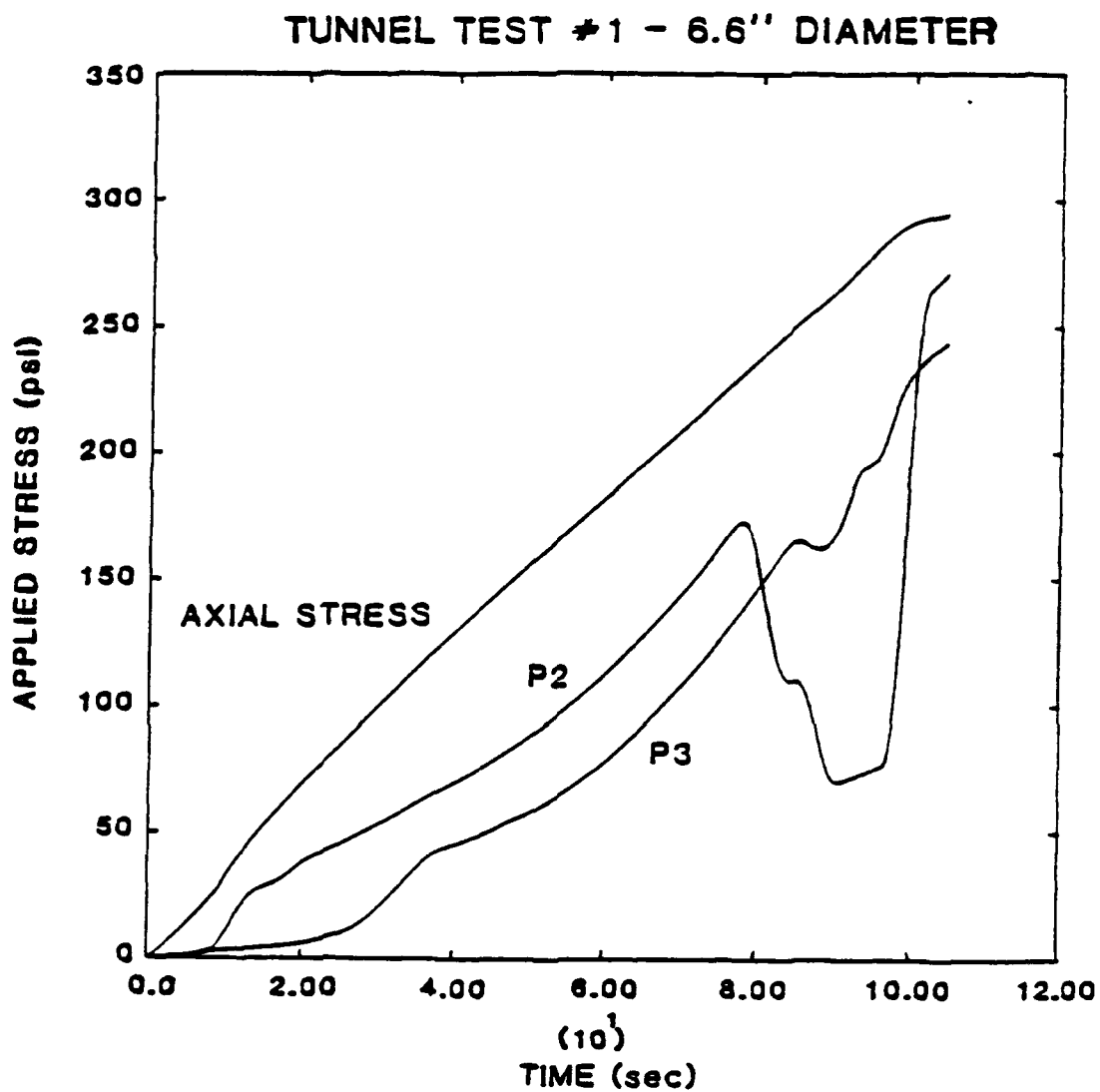


Figure 109. Variations of applied stress with time during proportional loading test #1. (DNA-TR 86-275)

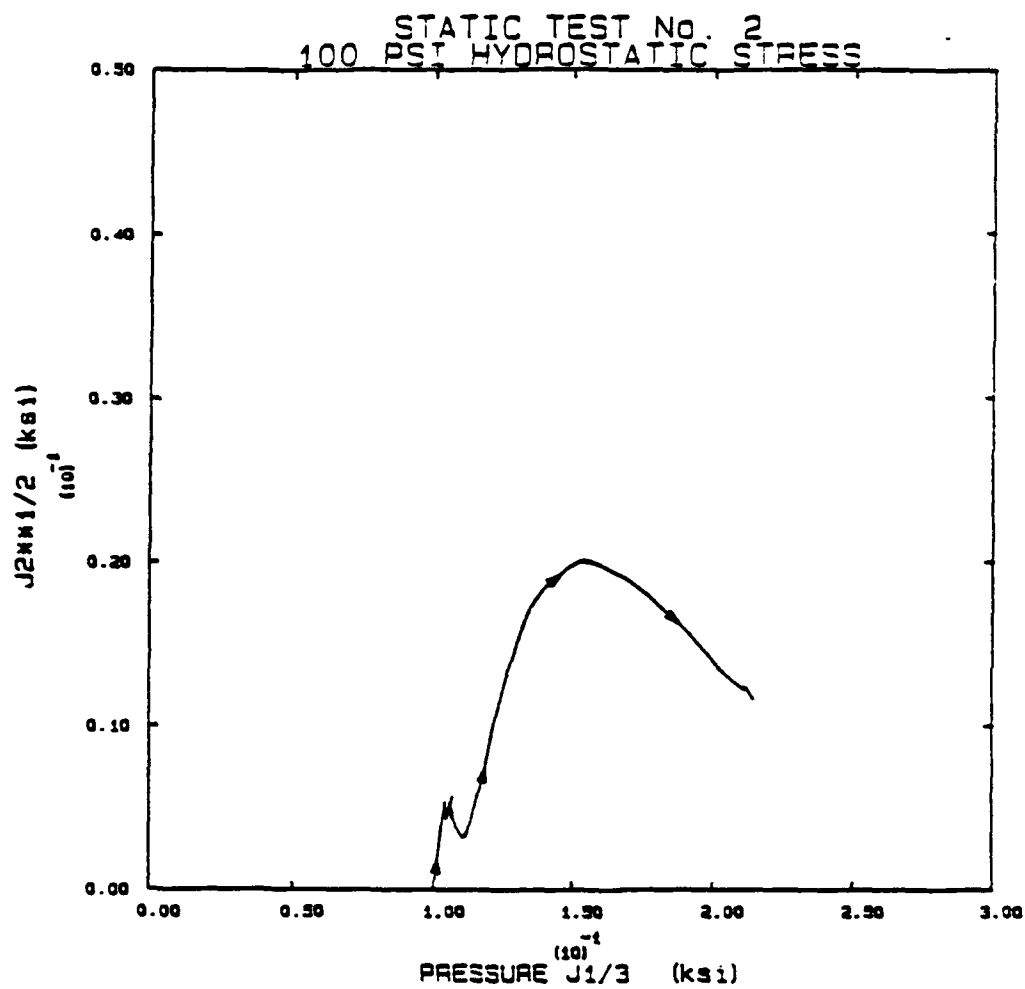


Figure 110. Stress Path for quasi-static test #2.

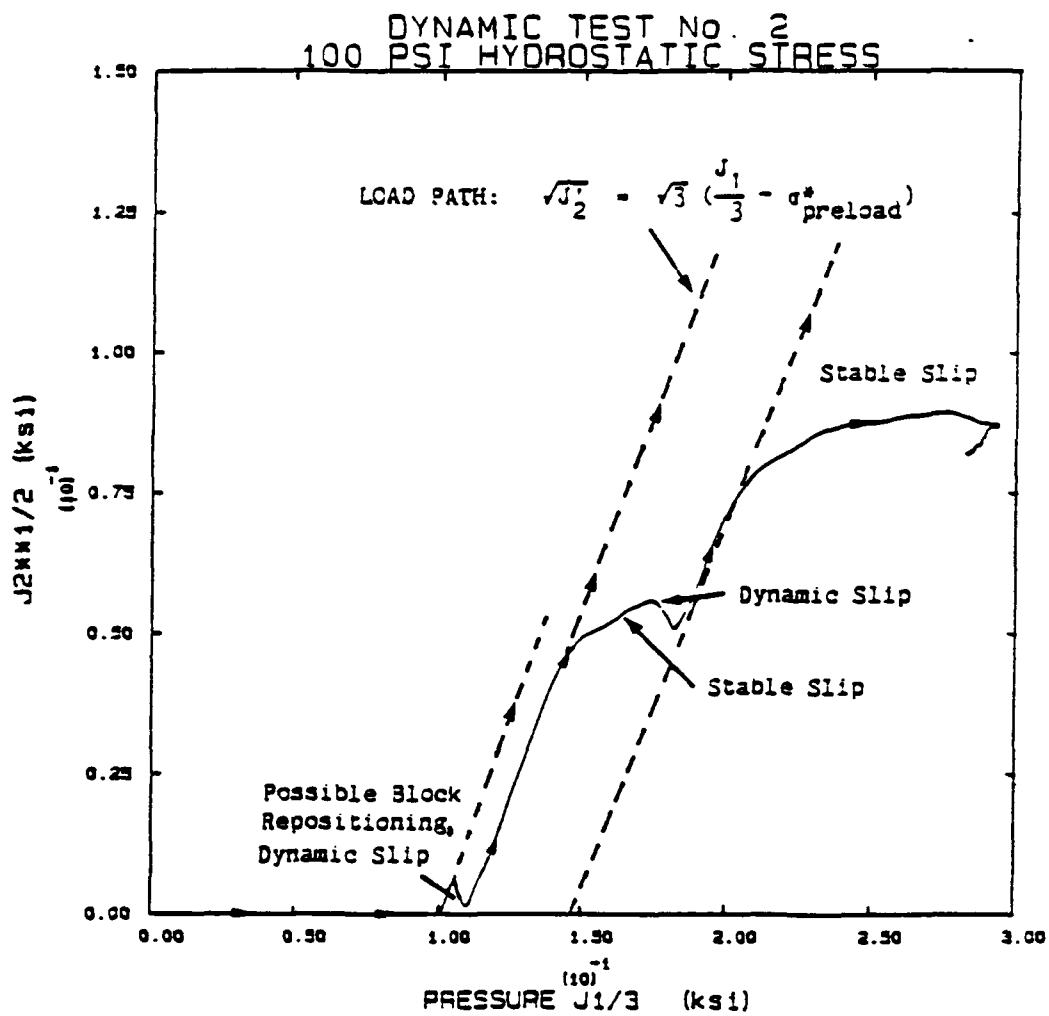


Figure 111. Stress path for dynamic test #2.

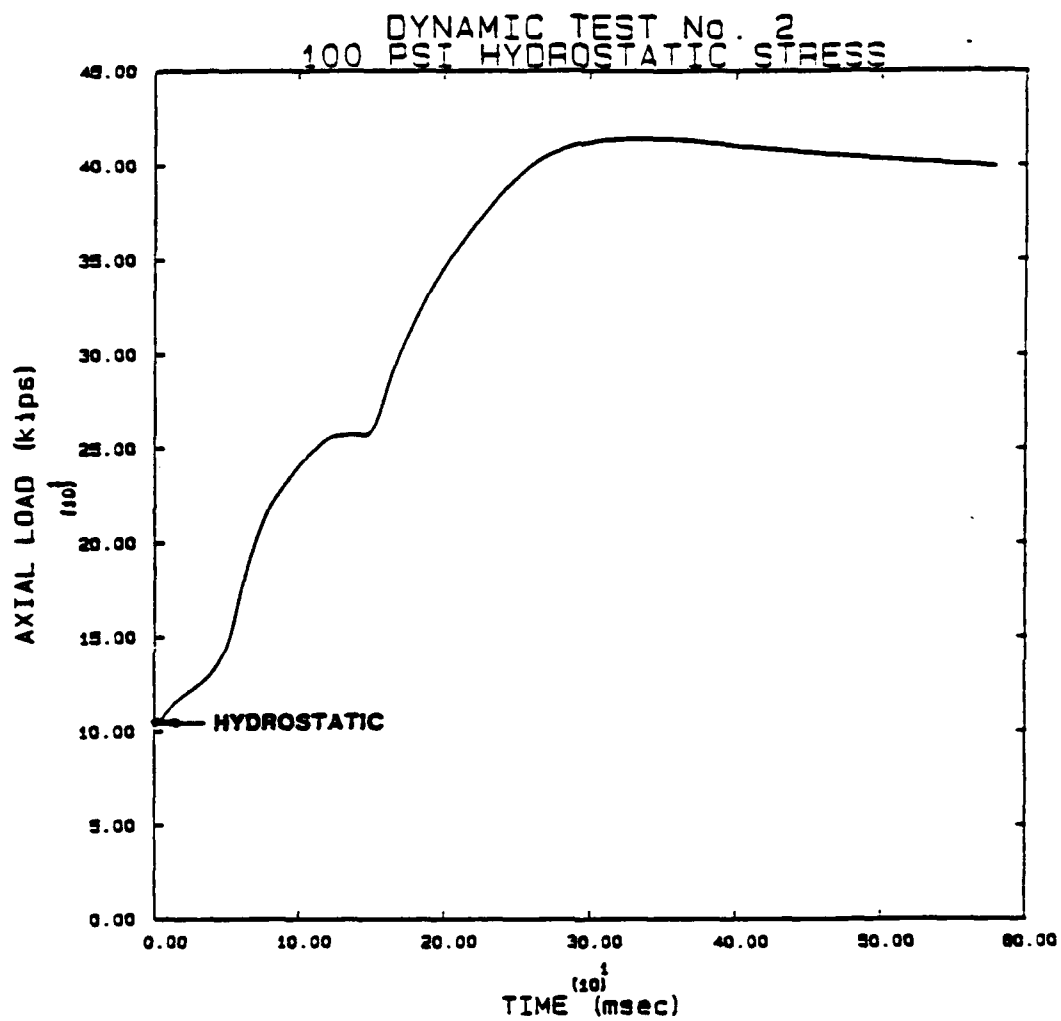


Figure 112. Variation of applied axial load with time for dynamic test #2.

they differ thereafter. The pressure at the peak value of  $\sqrt{J_2}$  is 150 psi in the static case, and close to 300 psi in the dynamic case. The particular simulant may be rate sensitive, but there is insufficient data to draw that conclusion from the Terra Tek tests.

One additional example of incomplete documentation is the lack of lateral strain data in the nominally far field uniaxial strain tunnel intersection tests reported in [DNA TR-86-275]. (The stress histories were given.) However, showing the measured exterior lateral strains would permit the reader to assess how well the uniaxial strain condition was maintained during the test.

Finally, one must comment on the apparent direction of the current Terra Tek program. While as of this writing structural tests have not yet been reported, the preliminary work on mix selection and material characterization is discussed in [DNA TR-89-203]. The entire approach appears much more systematic and more carefully executed than that indicated by the earlier works. For example, the unconfined compression test stress strain data for the final selected grout, utelite mix JN10B, is shown in Fig.113 (Figure 42 of said reference). The quality of the data is obviously much improved over that shown earlier in Fig.100. Also encouraging is that the plans outlined in the reference include a number of repeat tests, something sorely lacking in the previous program.

While examining Fig.113 it is worth noting that the stress strain curves start deviating from a linear relation at stress levels substantially below failure. (The tangent lines in Fig.113 are not in the original.) As discussed in Appendix B, once the material response deviates from an ideal linearly elastic, ideally plastic model, scaling a few key parameters (e.g.  $f_c$ ,  $E$ ,  $\nu$  and  $\phi$ ) as Terra Tek has done is insufficient. Entire stress strain curves for a few key paths (see section 4.2) must be modeled.

#### 4.4 DATA FOR TUNNELS IN JOINTED SPECIMENS.

Experiments were also conducted on specimens in which planes of weakness were introduced during the manufacturing process. During static and dynamic testing on a wide range of artificial joints, as reported in [DNA TR-86-275], Terra Tek developed experimental procedures that yielded insight into the influences of roughness, loading rate and properties of the adjacent, intact rock. The method for fracturing an originally intact block consisted of applying a principal stress in the direction of the desired fracture plane and then slowly driving a wedge into a slot in the top of the specimen. It was found that the behavior of the assemblage depended closely on a parameter called the large scale joint roughness coefficient JRCn (see Eq.13 of [TT TR-84-01]).

It is unfortunate that this interesting and apparently realistic approach was not adapted to testing of tunnels. Instead, a procedure was adopted in which the specimen was manufactured from rock simulant by pouring layers with a cold joint between pours. As is mentioned in [DNA TR-85-387], all the (potential) fractures were smooth and plane parallel, so no attempt was made to characterize their surface. Their JRC, based on the work of Bakhtar and Barton, is virtually 1. Thus there is little or no relationship between the realistic joints created in real rock and rock-like materials and the joints which were introduced into specimens with an opening.

Quasistatic and dynamic tests were performed in which a hydrostatic preload was followed by proportional loading in the manner described for monolithic specimens in Section 4.3. The simulant is designed to represent some properties of tuff according to the principles of material scaling and a scale factor of 27. The angle of friction for the matrix material is about 16 degrees, whereas that for the joints in the natural tuff (it was not reported for the model material) is 55 degrees; even though the stress states used to define these quantities differ, it appears that matrix failure is much more likely than joint failure in the natural tuff.

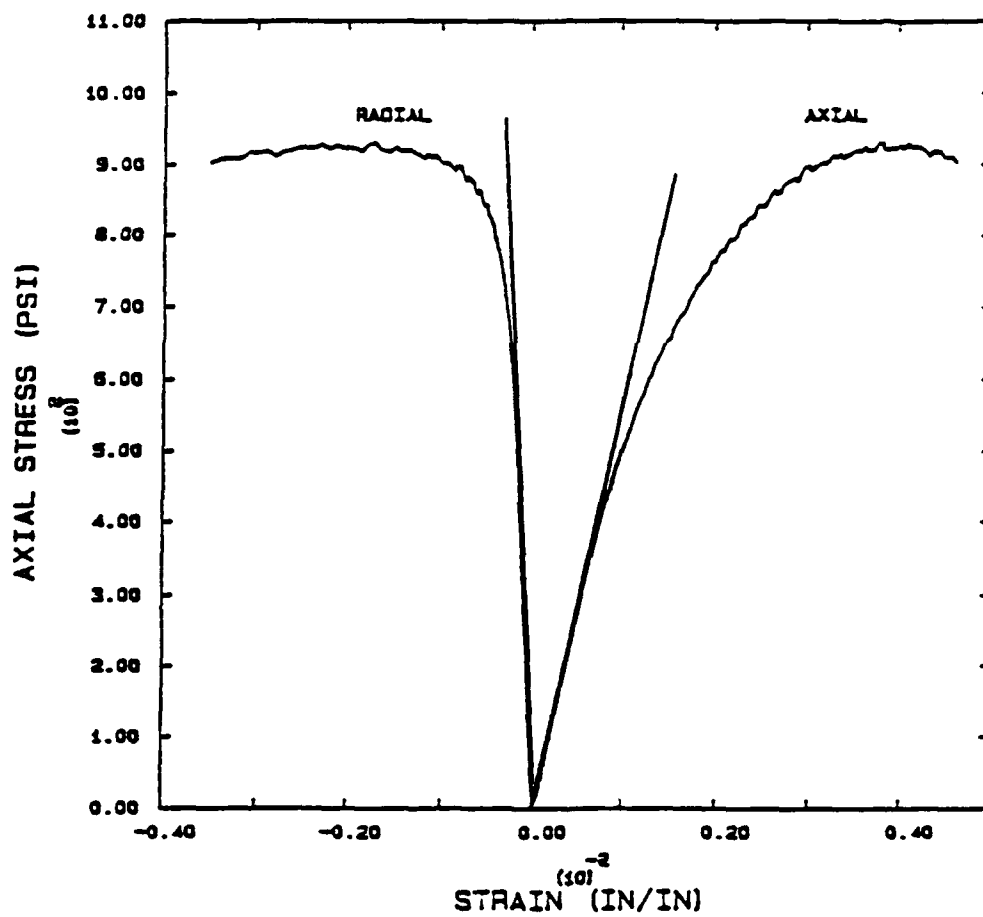


Figure 113. Unconfined compression test for final, selected grout, utelite mix JN10B.

At this point, a basic flaw in the test planning is apparent. A great deal of effort is made to create specimens with planes of weakness, yet only a reference is given [TT TR-84-01] to describe the frictional properties which govern slip on those planes. It is not clear to the present reviewer which, if any, of the nine materials reported in [TT TR-84-01] corresponds to the material whose tests are reported in [DNA TR-85-387]. Furthermore, if the model material behaves as the native tuff does, matrix failure is much more likely than slip along joints. If matrix failure is going to dominate anyway, introducing joints only confuses the results; if the investigators never tested the model material for its joint properties, they may not know whether joint displacement is going to occur in the model. Finally, this confusion is made moot by the fact that, due to the high normal stresses acting on joint planes following the hydrostatic phase of loading, slip on planes of weakness was prevented ([DNA TR-85-387], p.21). The present reviewer cannot understand in what sense these tests are studies of jointed rock.

#### 4.4.1 Quasistatic Tests.

Two quasistatic tests were performed using the configuration shown in Fig.99. Initial hydrostatic preloads of 20 psi and 100 psi were applied to specimens of Tests Nos. 1 and 2. This was followed by increasing axial load, or deviator stress in the terminology of triaxial compression tests which these tests resemble, up to maximum deviatoric stress. After maximum deviatoric stress, there is a significant phase of increasing confining stress at constant or decreasing deviator stress. The authors do not comment on this phase or its effect on deformations of the openings.

The dominant mode of deformation is uniform decrease in the opening accompanied by a small amount of direct ovaling, whereby the reduction of the vertical diameter is slightly greater than that of a horizontal diameter. There is no measured deformation of the opening under hydrostatic preload of 20 psi and only a negligible amount under preload of 100 psi. As shown in Fig.114, the total amount of vertical closure is much greater (0.6 inches) in Test 2 for 150 psi of deviator stress than it is in Test 1 (about 0.1 inch) for the same amount of deviator stress. This is consistent with observations in 3 of the 4 dynamic tests summarized below that total closure is greater if the preload is greater. These observations suggest that hydrostatic preload conditions the specimens by inducing a hydrostatic stress concentration (theoretically, in an elastic material, this would be 3 times the applied far field stress). It would follow that the preconditioned specimen is more readily damaged further by deviatoric stress. This interpretation is also consistent with the hypothesis that matrix failure occurs in preference to frictional slip along joint planes; if the latter mode were to dominate deformation, higher initial confining pressure would lead to a less compliant specimen. However, the opposite effect is observed.

Physical damage occurs by slabbing and spalling near the springlines of the specimens. It is not known how much of the horizontal closure is due to such effects.

#### 4.4.2 Dynamic Tests.

Four dynamic tests were performed. Initial hydrostatic preloads of 70 psi, 100 psi, 150 psi, and 20 psi were applied to specimens of Tests 1-4, respectively. This was followed by proportional loading in which the ratio of  $\sqrt{J_2}$  to  $J_1/3$  was intended to be 1.73. This load path was actually achieved for all but test No. 3, where the ratio was about 0.6; no comment is made regarding the deficiency in Test No. 3. The time to peak stress ranged from 0.187 sec in Test No 4 (initial prestress 20 psi) to 0.830 sec in Test No. 3 (initial prestress 150 psi); longer rise times were required for higher prestress, apparently due to some feature of the loading apparatus.

The dominant mode of deformation described in the text and confirmed by photographs of the damaged tunnels is spalling and slabbing of the walls, mainly at the springlines. This is similar to observations of the corresponding static tests mentioned above. A quantitative measure of

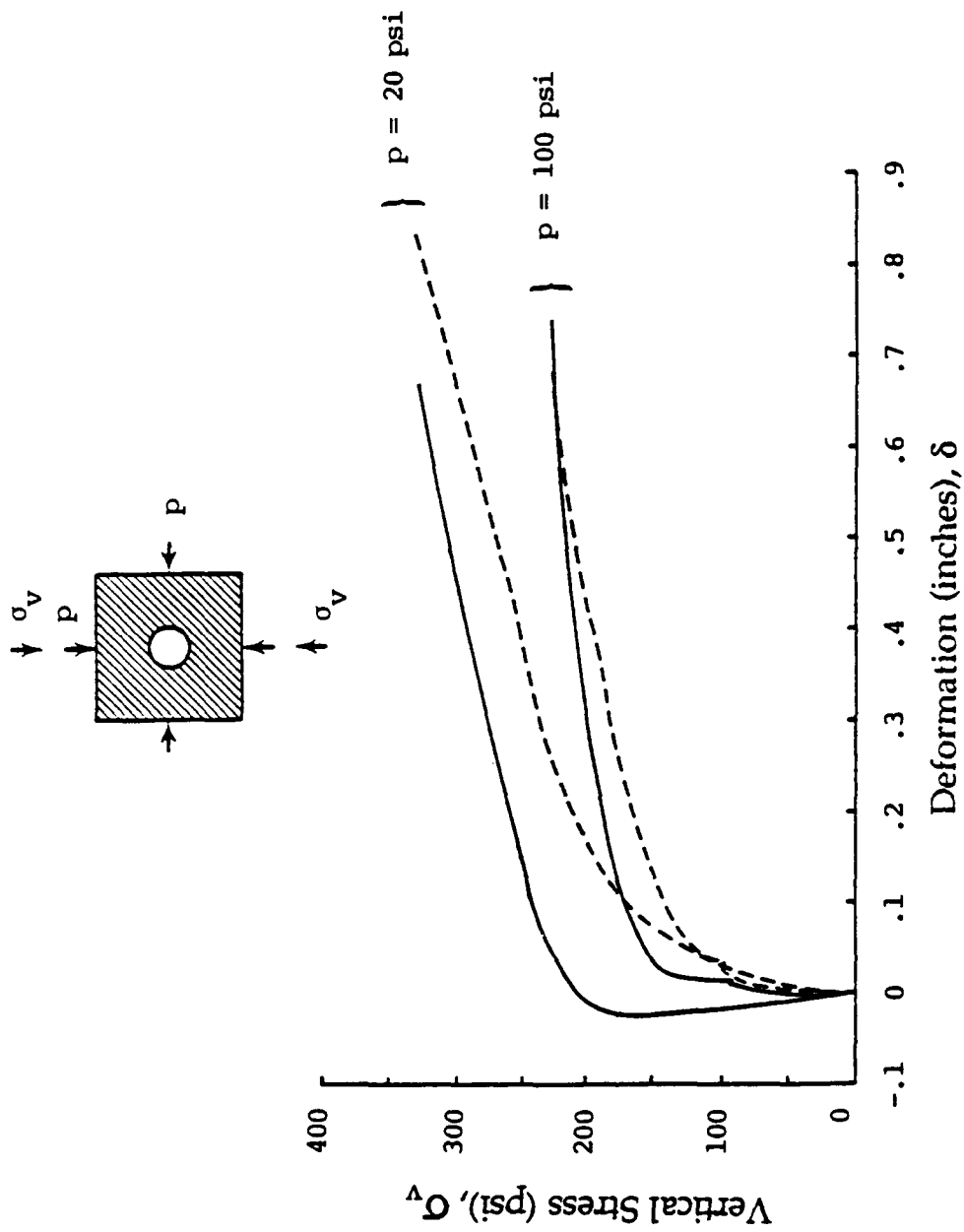


Figure 114. Quasi-static tests on jointed specimens.

damage is the closure, or decrease in length of the diameters parallel and perpendicular to the maximum principal stress (see Figs.115 and 116). Tests Nos.1-3 show an apparent trend, contradicted by Test No 4, in which vertical closure is greater for higher initial hydrostatic compression. The authors do not comment on this striking trend, which is interpreted above as originating in damage caused by the initial hydrostatic compression. As is shown in the figures, direct rather than reverse ovaling is observed; that is, vertical diameter shortening is greater than horizontal diameter shortening. The significance of this point was not, perhaps, appreciated in April, 1985 when the work was completed. Subsequent observations in Event MIGHTY OAK indicate that reverse ovaling can and frequently does occur in field scale tests. Since this is the kind of phenomenon that one would like to investigate at laboratory scale, if possible, its absence in the Terra Tek series is noteworthy.

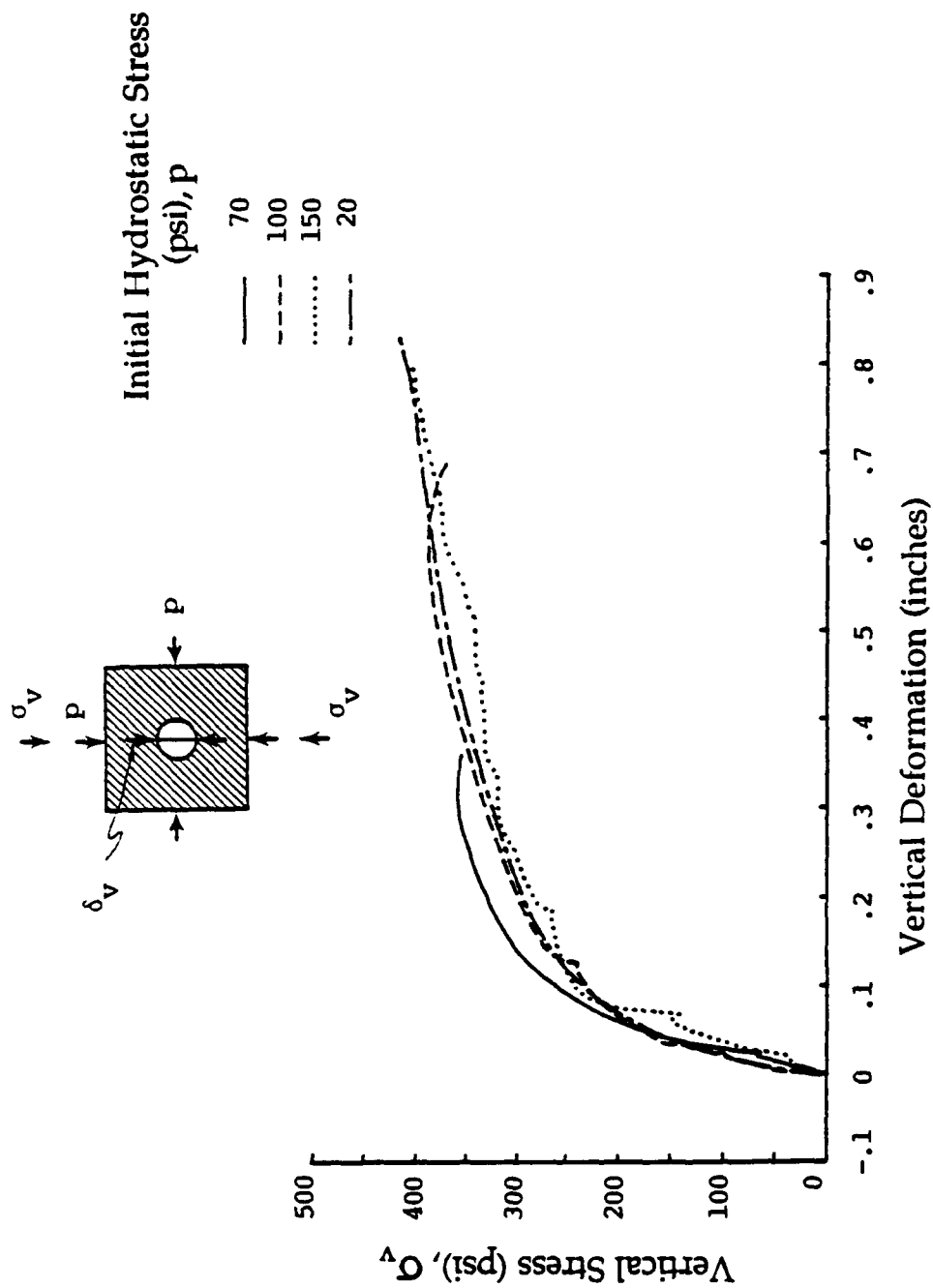


Figure 115. Dynamic tests on jointed specimens, vertical deformation.

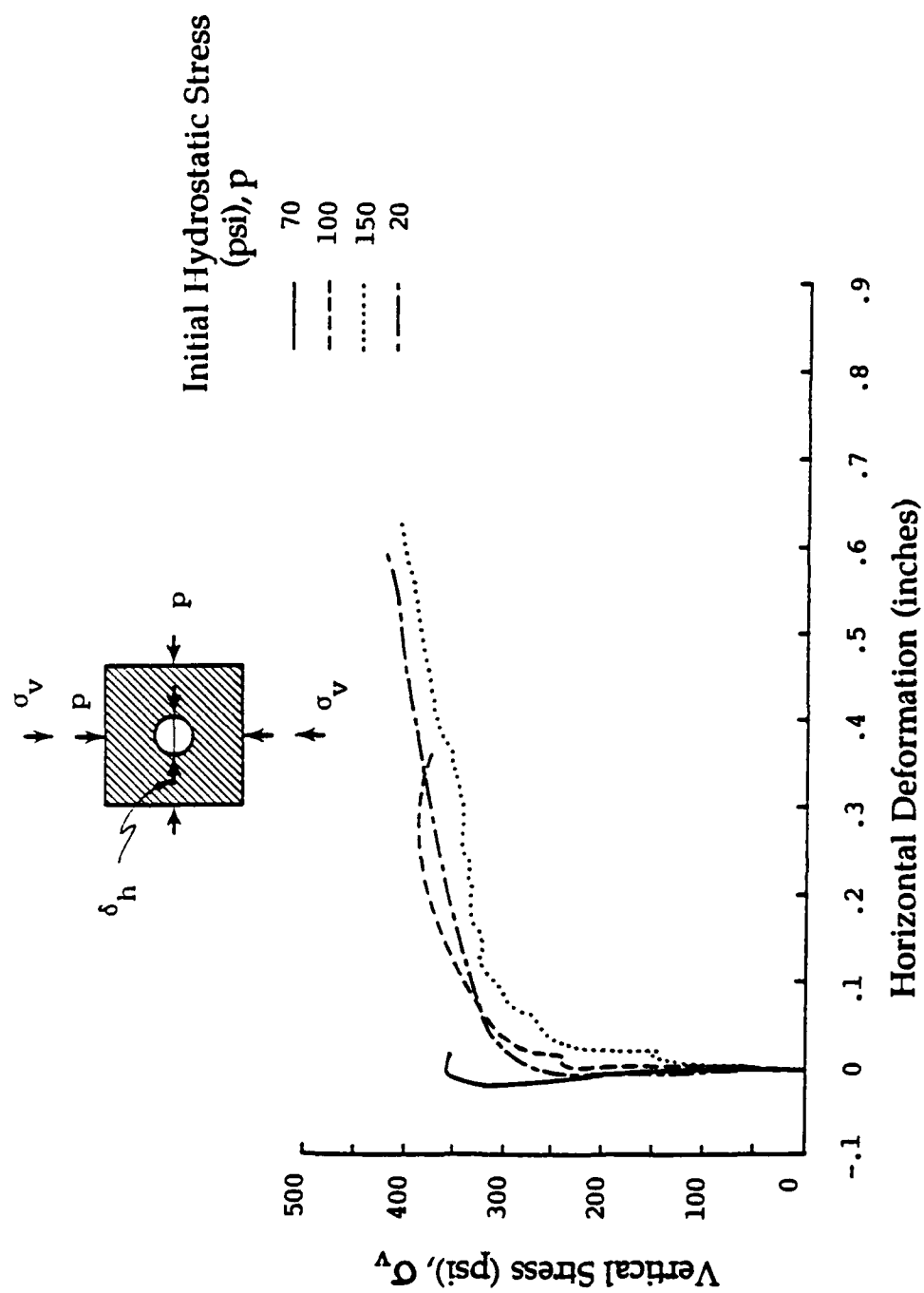


Figure 116. Dynamic tests on jointed specimens, horizontal deformation.

## SECTION 5

### THE UI PROGRAM INVOLVING STRENGTH-SCALED MATERIALS AND SYSTEMATICALLY JOINTED SPECIMENS

The University of Illinois at Urbana-Champaign (UI) pioneered the concept of strength scaling for model tests of tunnels [Heuer & Hendron]. They have continued to use this concept, and the results of the eight tests summarized in this section are obtained using this technique. Due to funding limitations, no direct analyses of the special conditions included in their tests, notably discrete jointing, were conducted by the UI as part of their program. This Section provides only a summary of the highlights of the program conducted at the UI. The tables and figures presented here are copied directly from [DNA TR-86-167]; only figure numbers have been changed.

#### 5.1 THE TEST PROGRAM.

The general configuration of the eight tests is shown in Fig.117. The specimens were approximately 6 feet in plan view and each specimen was 20 inches deep. (The loading plane of the testing frame was horizontal). In the first two tests, the loads across the top surface (see Fig.117) were applied by individual bearing plates under each of the eight sets of three jacks represented by the individual arrows at the top of the specimen. In the succeeding six tests, the individual bearing plates were replaced by a single, 6 in. thick steel plate. The purpose of this plate was to simulate the conditions which would occur if the tunnel were at a greater depth below the surface than the two tunnel diameters implied in the figure.

The specimen was "encapsulated" in a specially designed test frame and grout was installed between the two sides and the bottom of the specimen to provide continuous support to those surfaces. The specific configuration of the eight specimens is shown in Fig.118. Each of the specimens was manually constructed from specially designed and fabricated Portland cement based materials with each square block having dimensions of 4-1/2 inches on a side and 20 inches deep. Each block also had a steel rod cast through its center and steel plates were installed over the ends of each rod and a measured amount of tension was induced in the rod by measuring torque imposed on nuts in order to maintain an approximately constant force in the 20 in. direction. The UI staff was concerned about the possibility of premature failure in this direction, and consequently, these rods and plates were installed in order to provide an approximation of plane strain conditions. Neither the rods nor the blocks were instrumented to determine how much expansion of the individual blocks occurred in the lateral direction during any test.

All of the model tunnels were reinforced with rockbolts at five separate locations, along the length of the tunnel. The details of the rockbolts are shown in Fig.119. In the last three tests vellum between two plexiglass sheets was installed in two areas shown as bolder lines in Fig.119, one actually intersecting the tunnel and the other located a half a block dimension (2 1/4 in.) away from the edge of the tunnel to represent the situation that might develop if parallel "faults" intersected or passed in proximity to the tunnel. In the other cases, only uniform jointing was created in constructing the specimens from the square blocks.

The individual blocks were installed in the test frame manually. In the later tests, an expansive grout cast around the periphery of the completed specimen was used to provide some tightening of the joints internally. In the first three tests, no special effort was made to tighten the joints, prior to applying the loads. It turned out that the stiffness of the specimens of like character, was the same after the application of about 400 psi surface pressure; consequently it was possible to "subtract out" the effects of the deformations created by the tightening of the joints. The general results of all tests are summarized in Table 24.

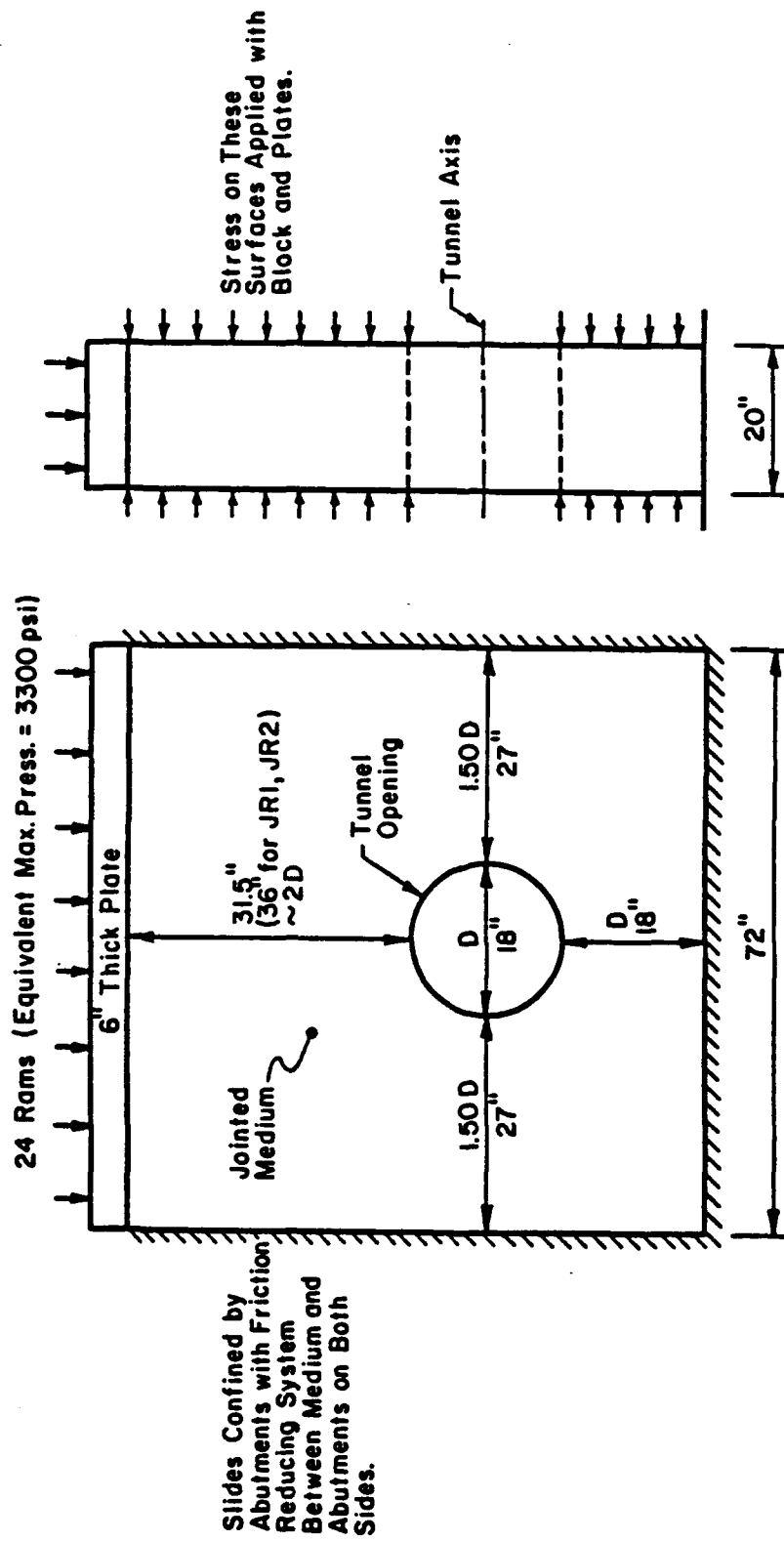


Figure 117. Dimensions of the specimen and test arrangement.

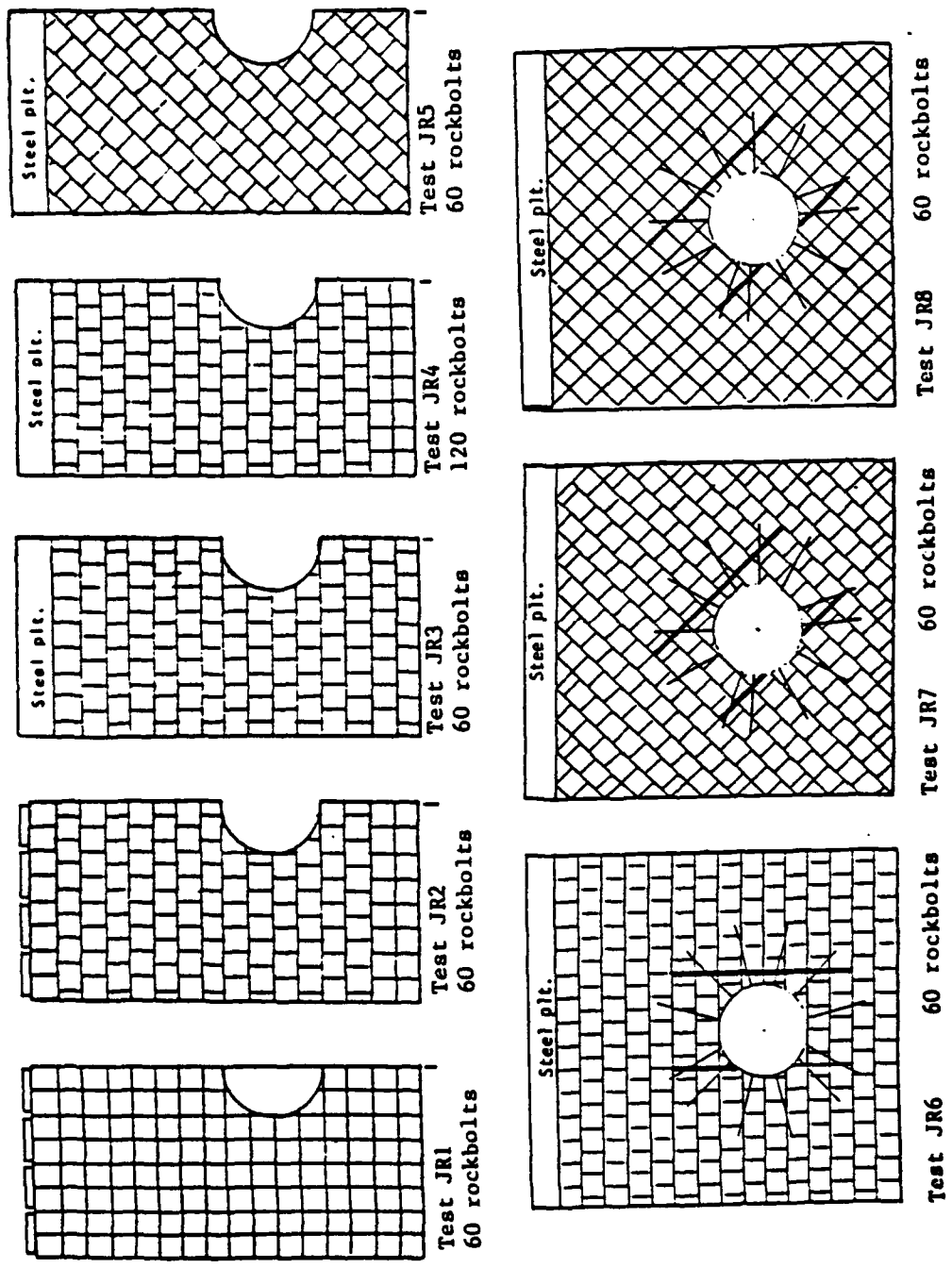
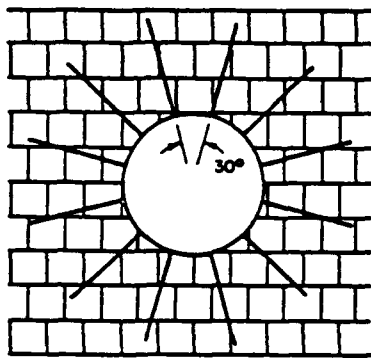
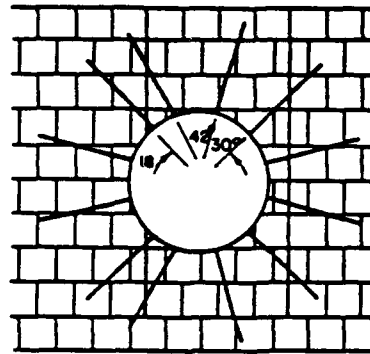


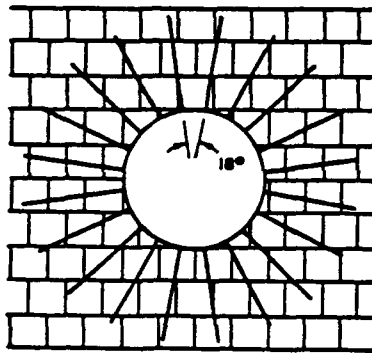
Figure 118. Summary of specimen geometry.



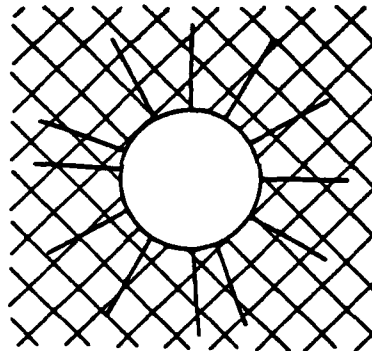
Tests JR2, JR3, JR5, and JR1  
Except Vertical Joints Aligned



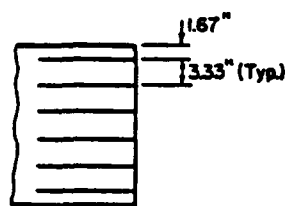
Tests JR6 and JR7 Except  
Rotated 45°



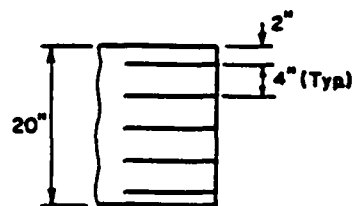
Test JR4



Test JR8



Vertical Spacing of Rock Bolts  
In Test JR4



Vertical Spacing of Rock Bolts  
In All Other Tests

Figure 119. Rock bolt configuration relative to the joint pattern.

Table 24. Summary of test results.

Test	Number of Rock Bolts	$\alpha$	q, psi		Initial Medium Crushing		Initial Rock Bolt Breaking		Vertical $\Delta D/D = 5\%$		Notes
			East	West	p, psi	p/q	p, psi	p/q	p, psi	p/q	
JR1	60	0°	2150		--	--	148	0.069	190	0.088	Vertical Joints Aligned, Uniform Pressure
JR2	60	0°	2020 2020		1115	0.55	1250	0.62	2200	1.09	Uniform Pressure
JR3	60	0°	2250 2150		930	0.41 0.43	1250	0.56 0.58	2560	1.14 to 1.19	SP
JP4	120	0°	2290 2300		825	0.36	1410	0.61	2800	1.22	SP
JR5	60	45°	1950 2000		615 1245	0.32 0.62	1245 1010	0.51 0.64	2510	1.26 to 1.29	SP
JR6	60	0°	2290 2310		530 720	0.23 0.31	1630 1405	0.61 0.71	2540	1.10	SP, Low Friction Planes
JR7	60	45°	2040 2090		860 1030	0.42 0.49	860 1030	0.42 0.49	2210	1.07	SP, Low Friction Planes
JR8	60	45°	2470 2350		940 940	0.39 0.39	550 1380	0.23 0.57	2820	1.16	SP, Low Friction Planes

$\alpha$  = Angle of bedding planes from horizontal  
q = Compressive strength of medium

p = Surface pressure, psi  
SP = Six-in.-thick steel plate on loaded surface

The general properties of the material are shown in typical form in Fig.120. Individual tests of the sanded surfaces of the blocks indicated a joint friction of 37.2 degrees. All surfaces of the blocks are sanded prior to testing of the blocks and prior to assembly in the frame for the main tests. This value turned out to be highly reproducible among the various separate tests made as described briefly below. The angle of internal friction for the solid material was approximately 32 degrees and the cohesion was approximately 500 psi.

Figure 121 shows the special device designed and built to define the properties of the joints. Fifty-five tests were conducted of the type shown, and it was from these tests that the mean value of 37.2 degrees for the angle of internal friction on the sanded joints was defined. The standard deviation in the various tests varied among the top, bottom and the lateral surfaces of the blocks with definition of surface based on the position as cast. The minimum standard deviation was 1.5 degrees for the bottom surfaces,  $2.7^{\circ}$  for the top surfaces and  $1.6^{\circ}$  for the lateral surfaces.

Staff at UI also made individual tests of the teflon sheets which were installed along the lateral surfaces between the test frame and the specimens. The results of those tests are shown in Fig.122. The coefficient of friction was small, especially for the tests with lubricating grease as was used in the main tests, at the typical values of confining pressure. Therefore, even though there were difficulties in measuring the normal force at the lateral boundaries, the magnitude of "friction stress" was likely to have been rather small, typically in the range of 1.5 to 2 psi.

A special photogrammetric technique was used for measuring the key deformations on the exposed major surface of the specimen. This technique allowed an unambiguous definition of the deformations over the entire surface of the specimen at a single time. This is important, not only from a standpoint of saving labor in making such measurements, but also in defining displacements at a precise time to avoid uncertainties in the magnitude and direction of displacement as the specimen approaches failure. A typical result of applying the photogrammetric technique for a "horizontally bedded" specimen is shown in Fig.123 and for a "45 degree bedded specimen" in Fig.124. The radially inward deformations of the interior of the tunnel were measured by dial gages typically placed at 45 degrees around the opening, and the details of mounting are shown in Fig.125.

The UI staff had to solve a number of other challenging problems. The most important was probably the means of installing the rockbolts. These were installed manually after the specimen was completed by drilling a 3/16 inch hole into the specimen, installing the rockbolt and then grouting it in place. Bearing plates 1/8 inch thick were installed to distribute the force more uniformly over the surface of the tunnel.

In the early tests, where individual bearing plates were used to distribute the applied load over the surface, there appears to have been an inadequate amount of constraint over the top of the tunnel to allow significant arching to develop. Consequently, the individual plates were replaced by a thick steel plate in all tests beginning with JR3. An indication of the difficulties of having groups of blocks with aligned joints parallel to the direction of primary loading and with individual bearing plates is shown in Fig.126 for specimen JR1. The invert and both springlines showed very little deformation, while the "tunnel crown" and the "surface above crown" show displacements which parallel one another with the surface above the crown being delayed by approximately a 1/10 inch in following nearly exactly the deformation of the tunnel crown. Also, as shown in Fig.126 and Table 24, the surface load achieved in this test was much smaller than that for any of the subsequent tests. (The stiffness or effective modulus of elasticity of the continuous material as implied in Fig.120, is approximately 800,000 psi. The stiffness of the jointed specimen, determined by testing the "pillars" next to the opening in specimen JR1 after the main test, is shown in Fig.127. The jointed pillars had a stiffness approximately half as great as that for the unjointed material).

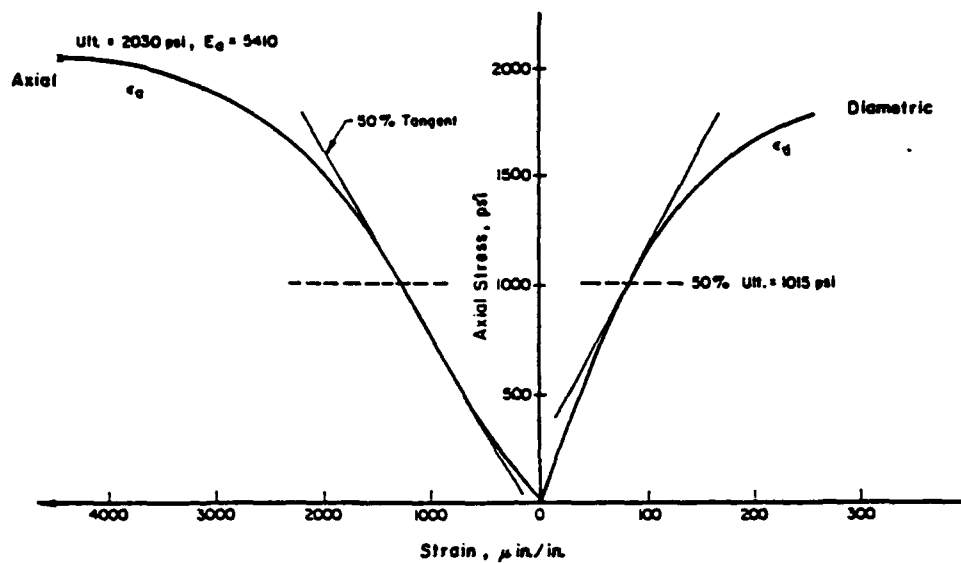


Figure 120. Typical unconfined stress-strain curves for a cylinder to determine modulus and Poisson's ratio.

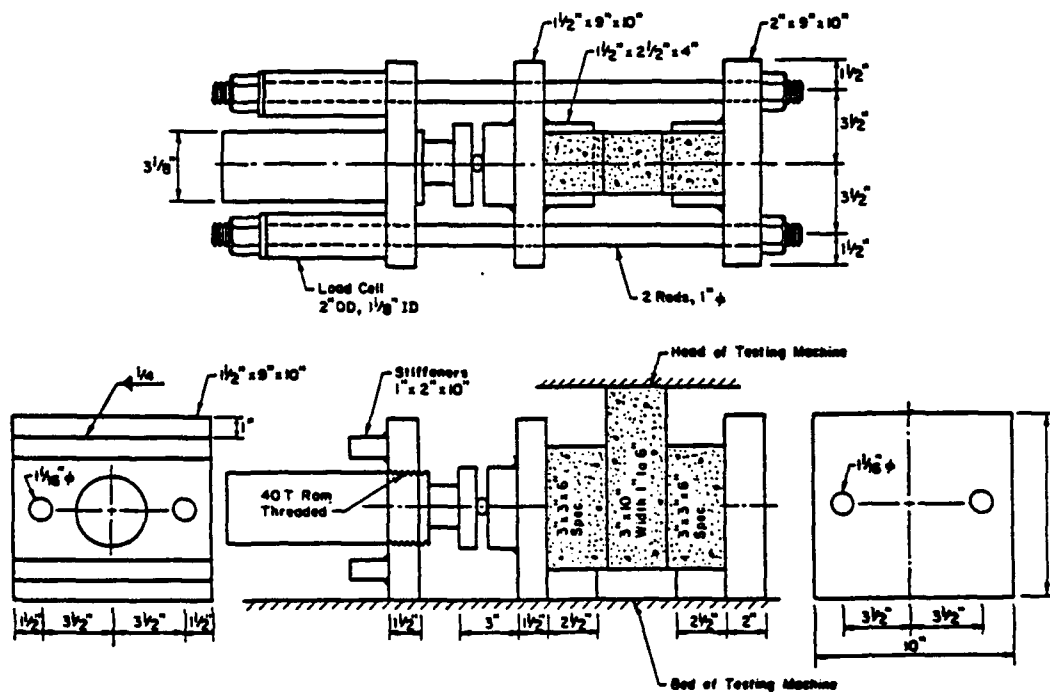
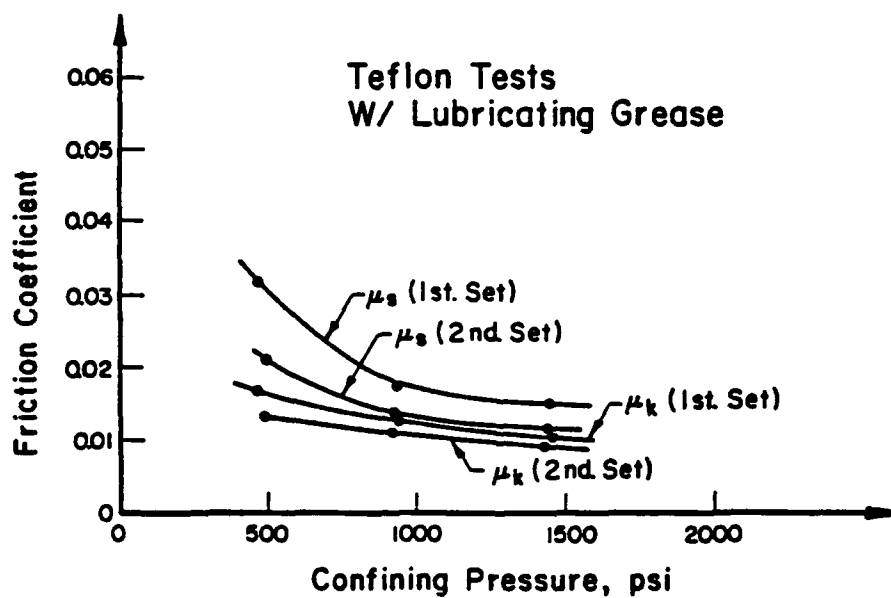
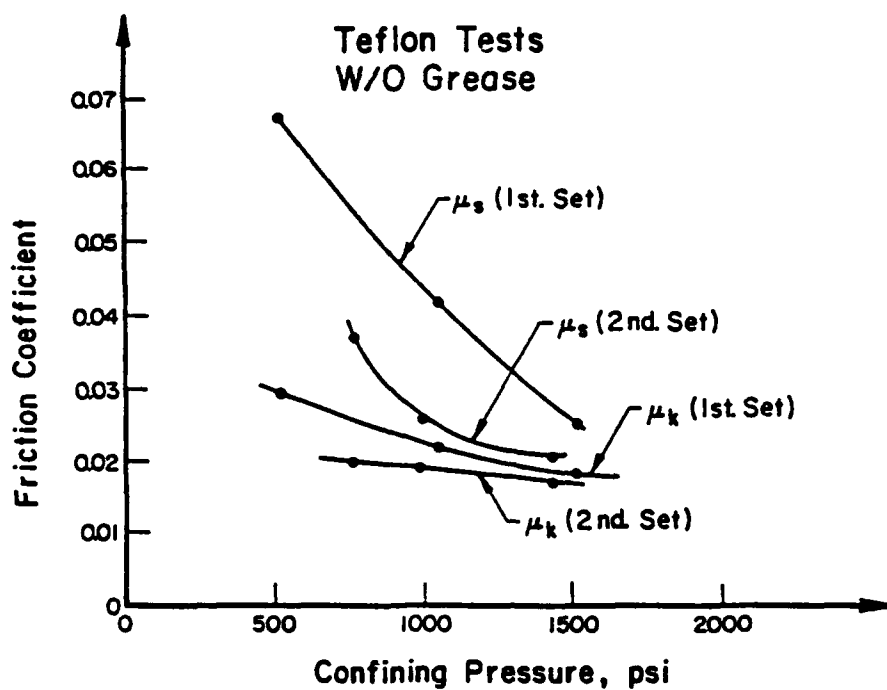


Figure 121. Joint shear test device.

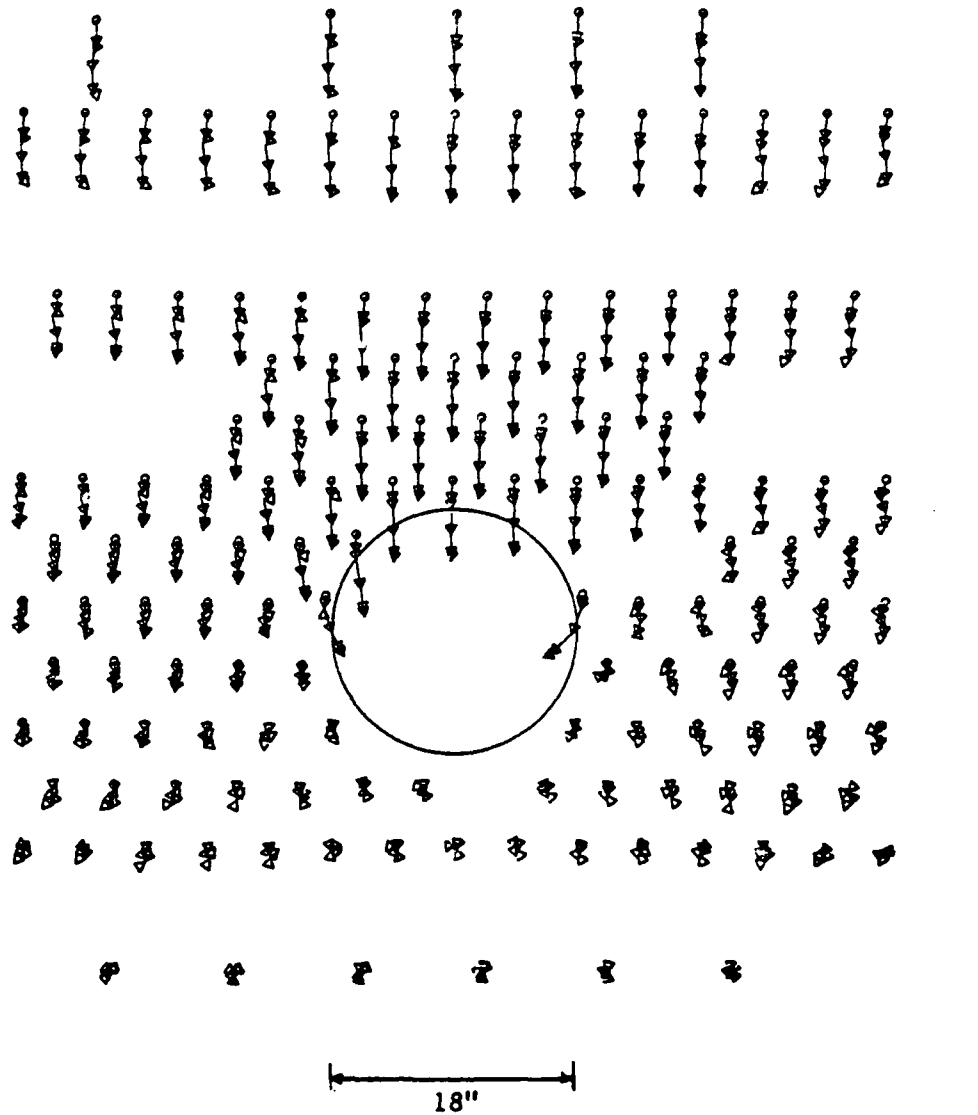


**Notes:**

$\mu_s$  = Initial Coefficient of Friction  
 $\mu_k$  = Residual Coefficient of Friction  
 1st. Set is For Teflon Previously Untested  
 2nd. Set is For the First Tests Retested

**Figure 122.** Friction coefficient of Teflon to Teflon friction reducing system with and without lubrication.

Test JR3



Surface pressures:  
 930 psi      2,670 psi  
 1,440 psi    2,760 psi  
 2,150 psi

Vector scale/position  
 scale = 1/5

Figure 123. Deformation in Test JR3 from the photographic analysis.

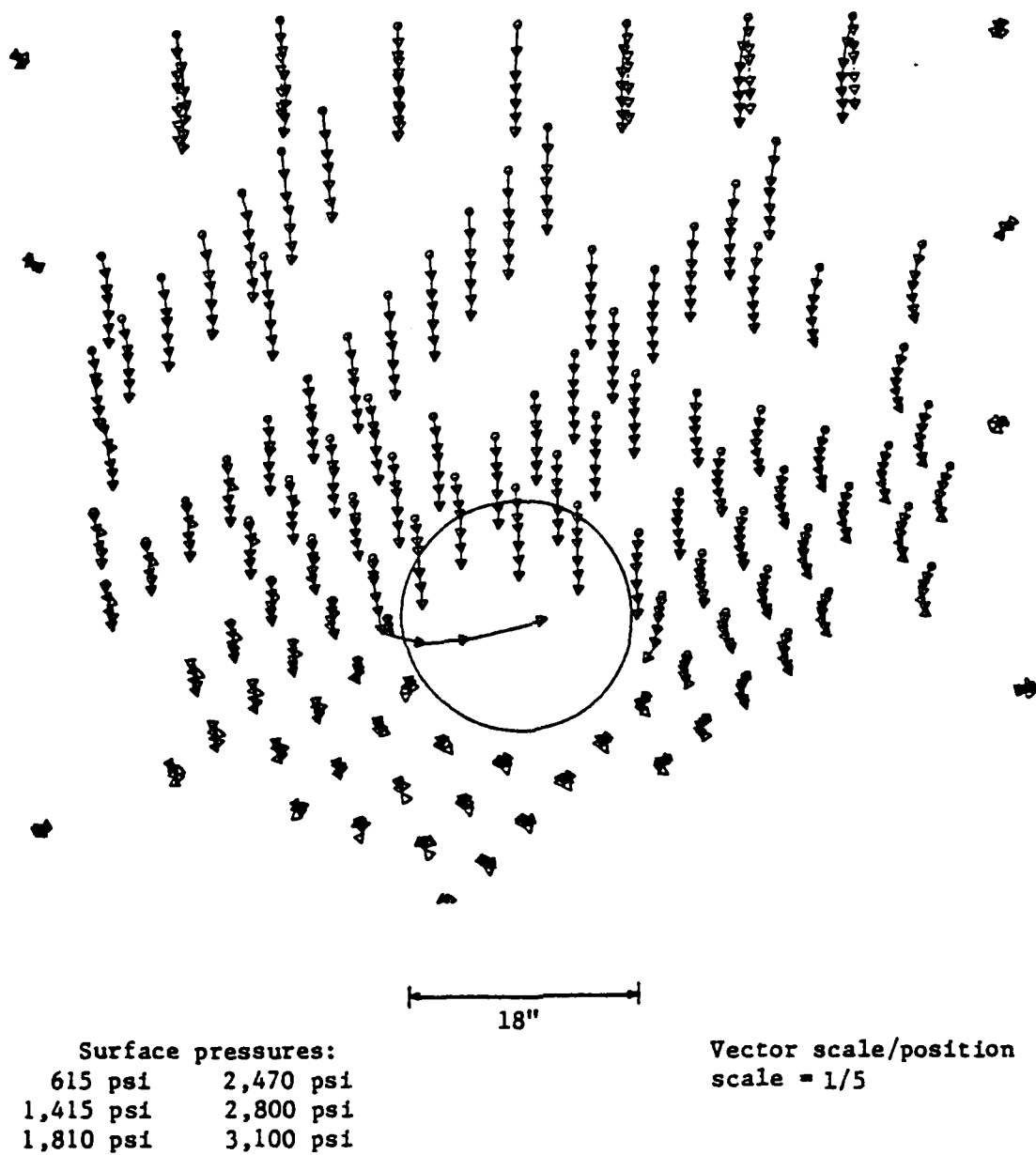
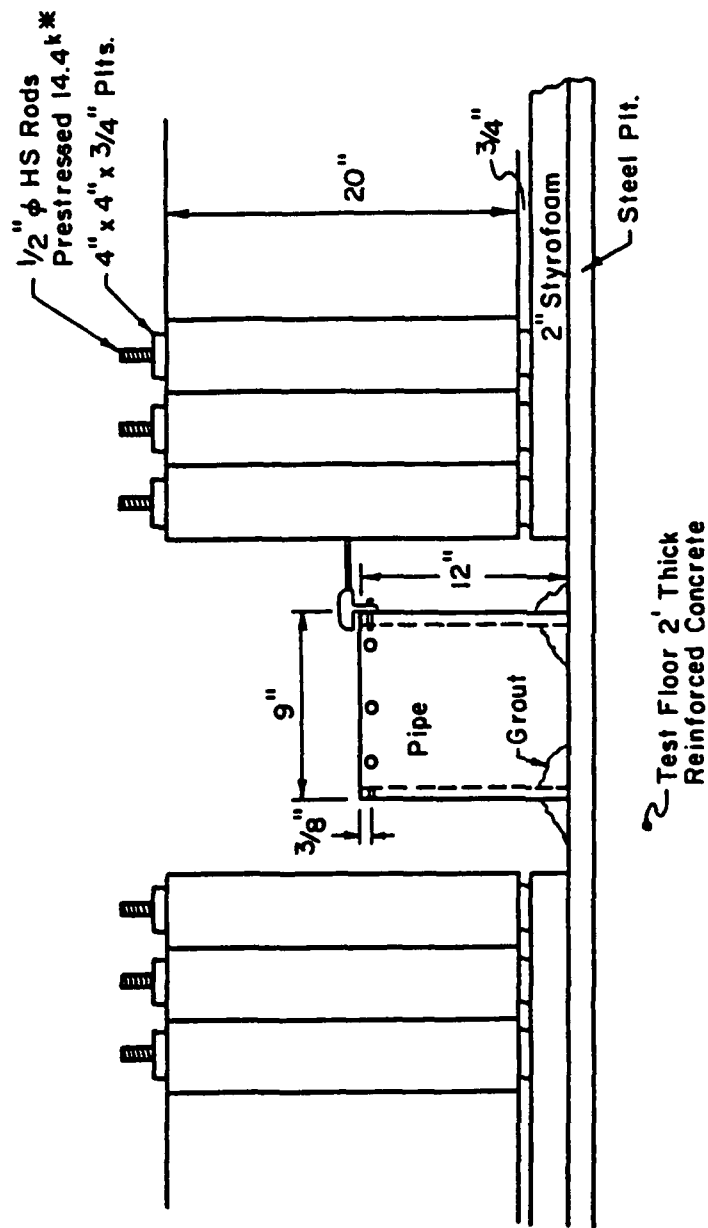


Figure 124. Deformation in Test JR5 from the photographic analysis.



Note: In Test JR3-JR8 an Angle Was Attached to the Pipe and the Dial Gage Was Attached by a Bolt Through a Slot in the Upstanding Leg so the Gages Could be Adjusted and Reset More Easily.

Figure 125. Dial gage setup for measuring tunnel deformations.

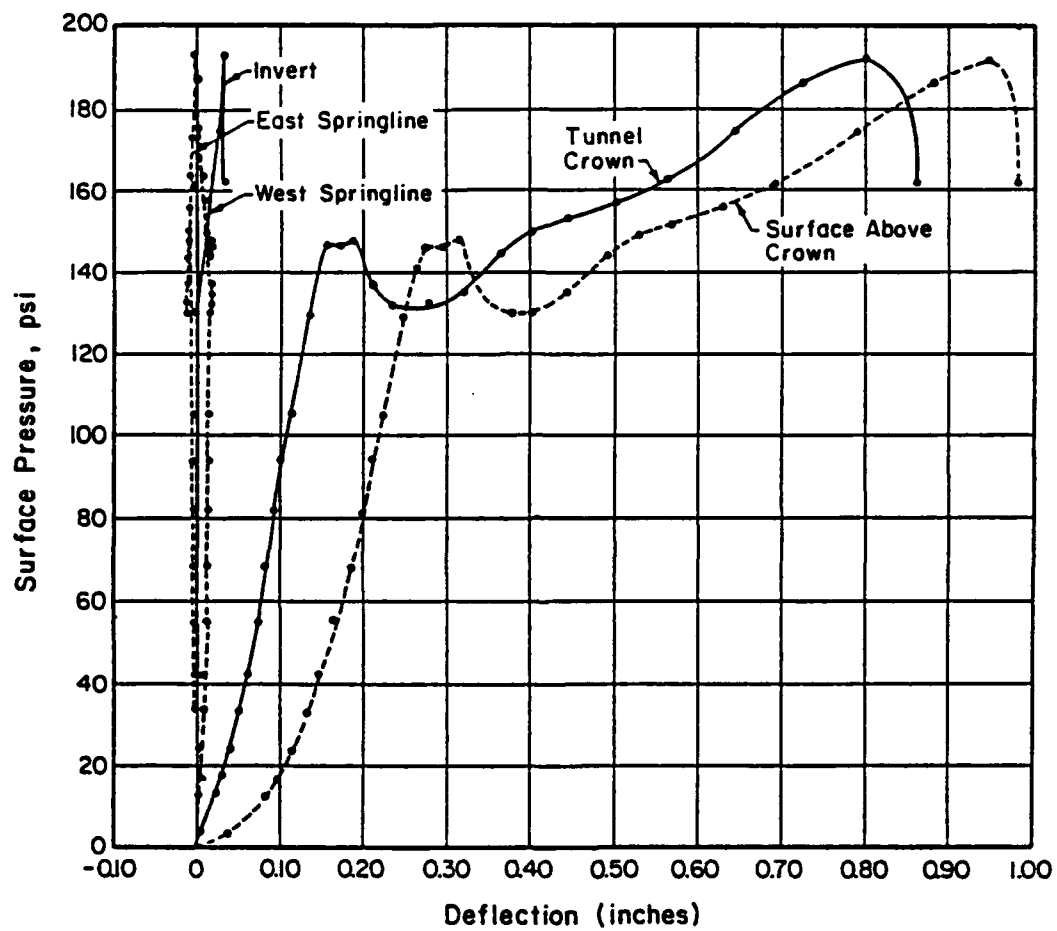


Figure 126. Deformation of the tunnel opening and surface above the crown for specimen JR1.

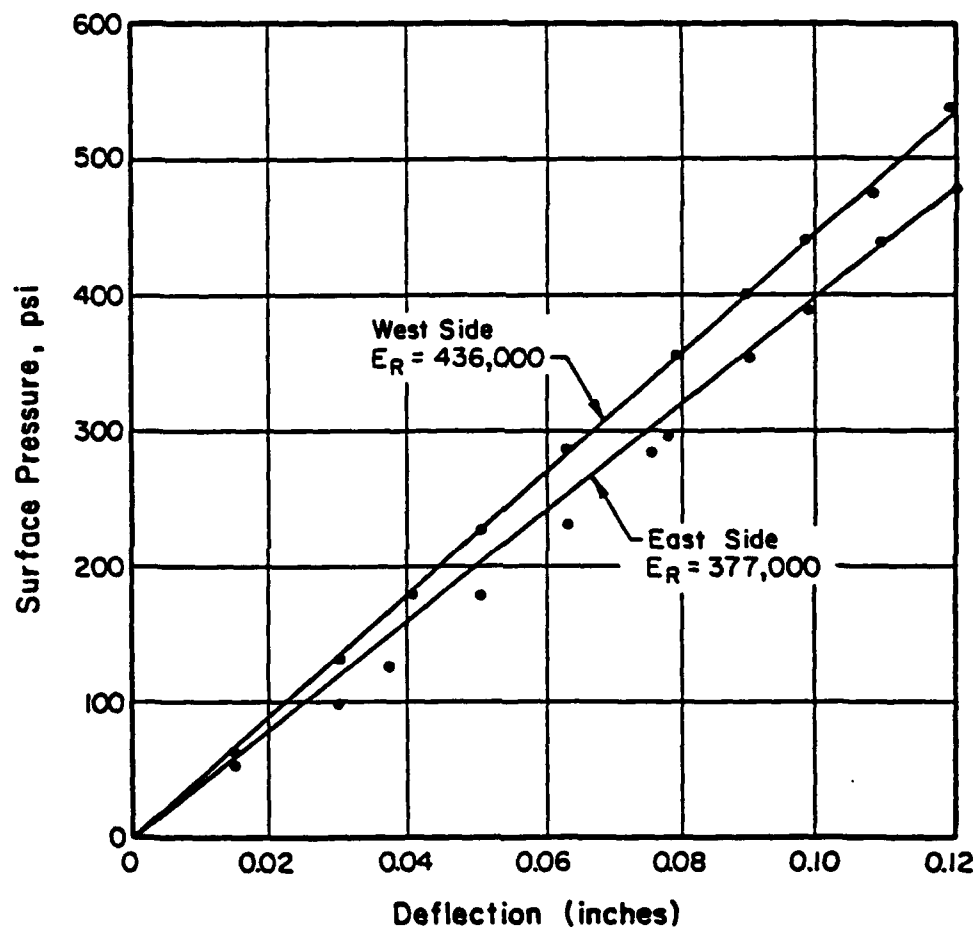


Figure 127. Deformation of the loaded surface with surface pressure for specimen JR1 after the original test of the specimen.

In all cases, the conditions of the rockbolts were documented as the specimen was taken apart following a test. In the later tests, a "break-wire" was also installed with the rockbolt to indicate when the bolt failed. Typical results of the last system are shown in Fig.128.

Mapping of crushing of the individual blocks was done as the tests proceeded. Also as the specimens were disassembled following the test, the crushing was further documented. The typical result of these data for a horizontally bedded specimen is shown in Fig.129, and for a 45 degree bedded specimen in Fig.130.

A typical result of the surface pressure versus displacements recorded in a test is shown in Fig.131.

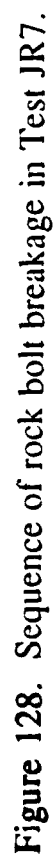
## **5.2 BRIEF COMPARISON OF RESULTS.**

The results of comparable tests are shown in Fig.132 through 140. Figure 132 compares results of tests JR2 and JR3. The principal difference in these tests is the fact that JR2 had the individual bearing plates on the loaded surface while JR3 had the thick single plate across the entire surface. The results of the two tests overlay one another or remain essentially parallel up to a surface load corresponding to approximately 1200 to 1400 psi. Beyond that point, specimen JR2 shows significantly greater displacement than that for JR3. This was attributed by the original staff to the inability of specimen JR2 to develop the arching mechanism fully above the tunnel. Specimen JR3 probably did not fully develop the arch either, but clearly there was a significantly stiffer system represented by JR3 than JR2 after a surface pressure of about 1400 psi.

In Figs.133 and 134, the results from tests JR2 and 4, and 3 and 4 are compared respectively. The "JR3 corrected" in Fig.134 results from "subtracting out" (as interpreted by the original staff) the portion of the curve believed to be represented by the closing of the looser joints in JR3. The doubling of the number of rockbolts does not have any clear effect in these comparisons. As pointed out by the original staff, this should not be surprising since the amount of average interior pressure applied by the first case is approximately 20 psi, and the second 40 psi. This small increase in interior pressure would have only a modest, perhaps indistinguishable among the inevitable variation in parameters, effect on the response of the tunnels.

Probably the most surprising result is shown in Fig.135 where the results of JR3 and 5 are compared. The results are very comparable despite the rotation of the joints by 45°. In this regard, the original authors stated, "It appears that if the joint friction is large enough to prevent slip with a normal stress on the joint, the crush zone around the opening remains similar to that of a horizontally bedded medium".

The remaining figures illustrate the comparison of the tests without and with the superimposed "faults" in the vicinity of the tunnel, one of the faults intersecting the opening and the other being one half a block width (2 1/4 in.) away from the edge of the tunnel. It is surprising that these faults had relatively little impact on the measured displacements of the tunnels. In fact specimen JR8 had both surprising stiffness and strength compared to all other cases (See Figs.139 and 140). Certainly the normal force on this 45 degree fault is much higher in JR8 than in JR6, but a similar condition for normal force prevails for specimen JR7; and JR8 is significantly stronger and stiffer than JR7. The fact that the joints between the blocks were aligned in both directions in JR8 as compared to staggered in one direction in JR7, does not immediately suggest that JR8 should be stronger nor stiffer than JR7.



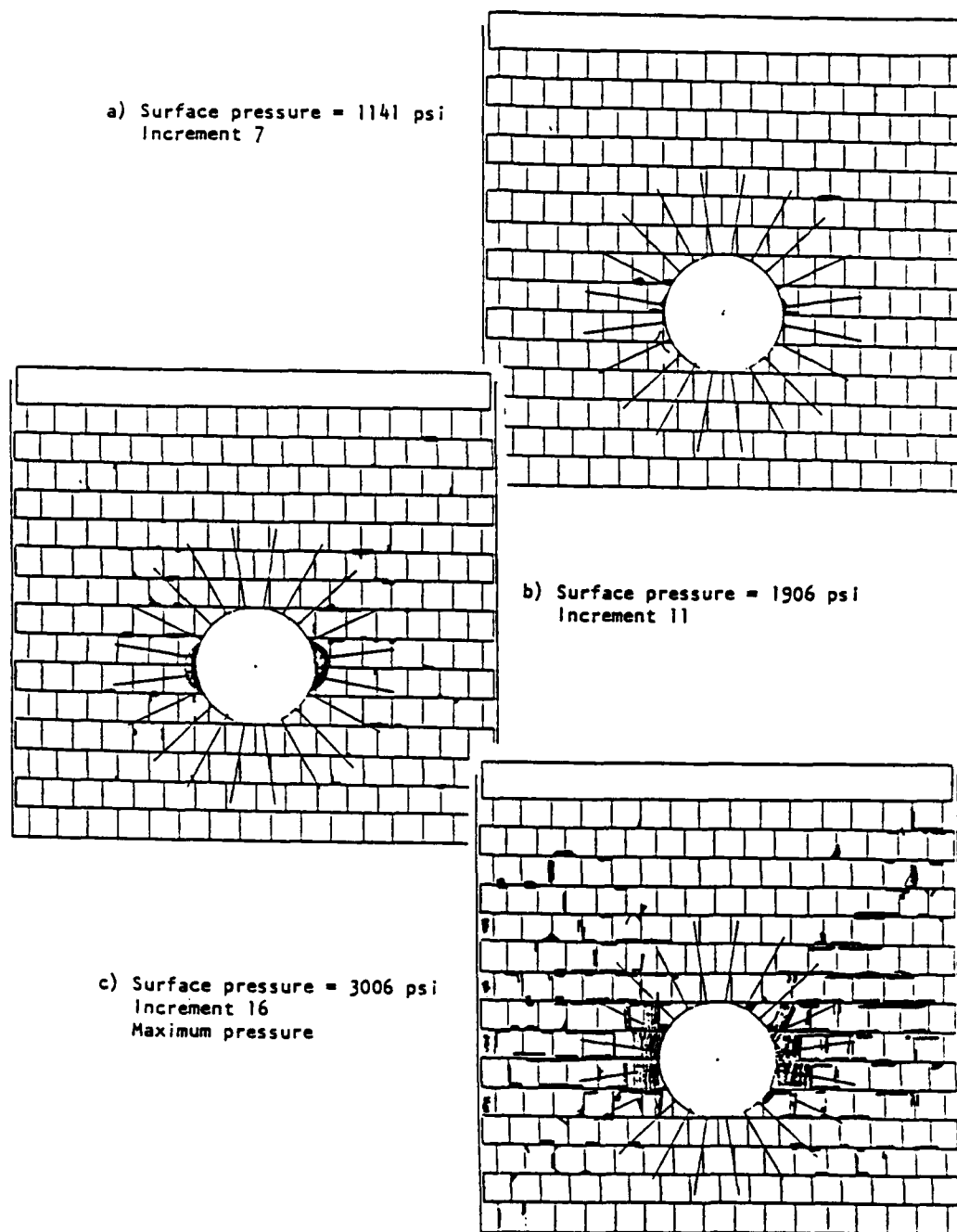
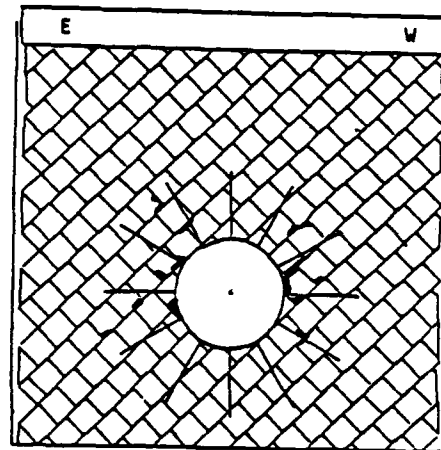
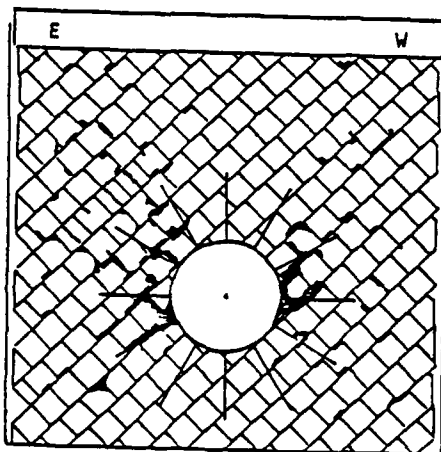


Figure 129. Damage to specimen JR4.

a) Surface pressure = 1809 psi  
Increment 10



b) Surface pressure = 2800 psi  
Increment 13



c) Surface pressure = 3111 psi  
Increment 14  
Maximum pressure

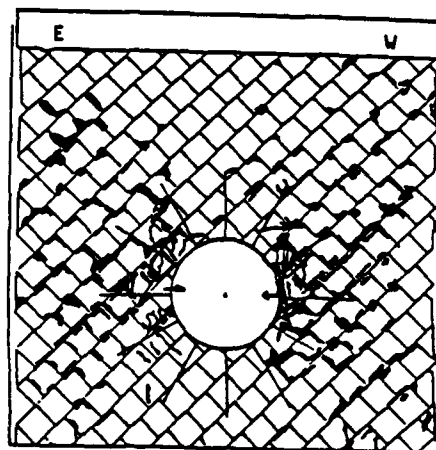


Figure 130. Damage for specimen JR5.

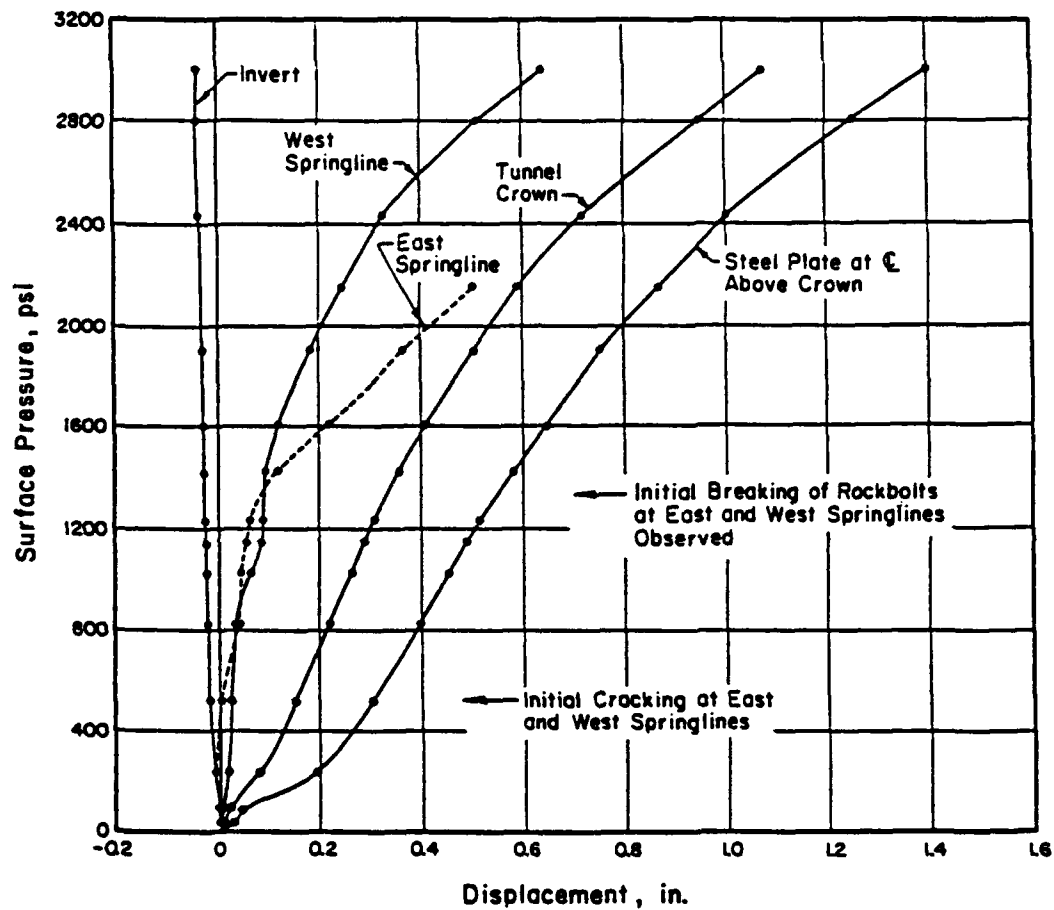


Figure 131. Deformation of the tunnel opening and surface above the crown in Test JR4.

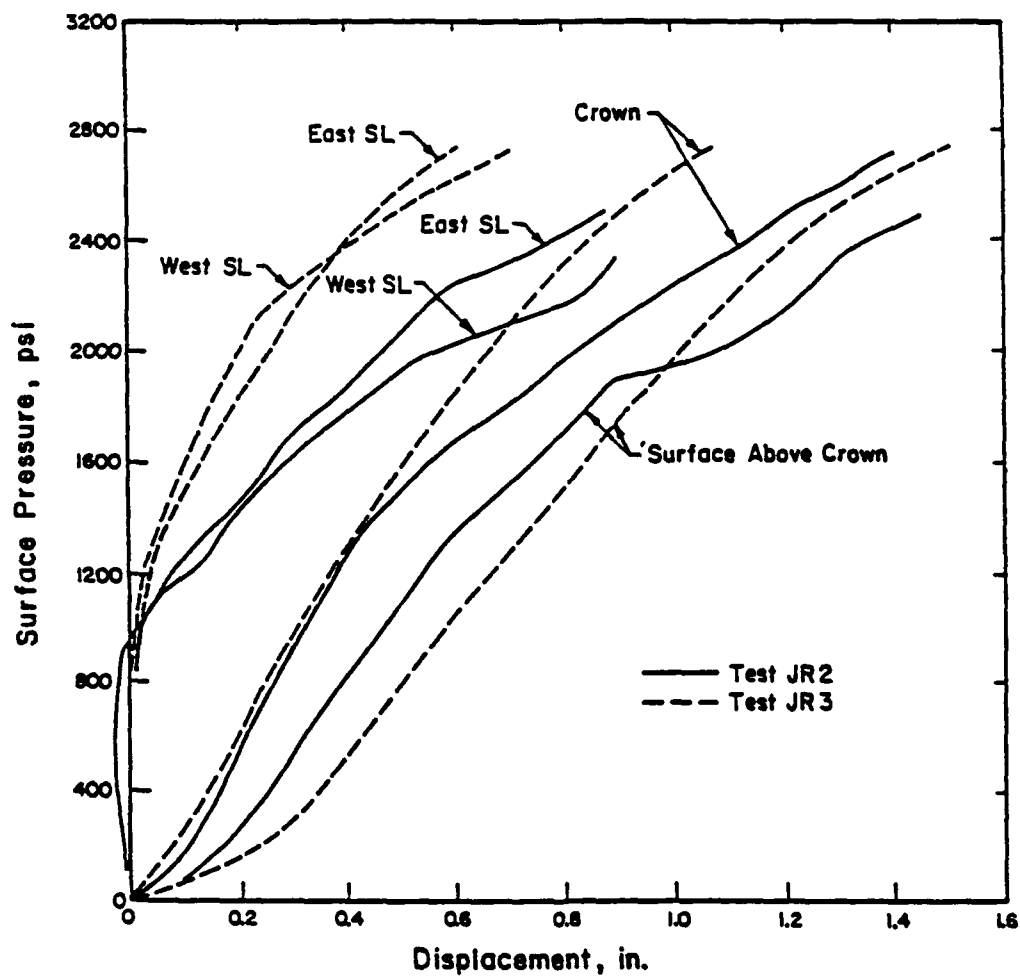


Figure 132. Comparison of Tests JR2 and JR3.

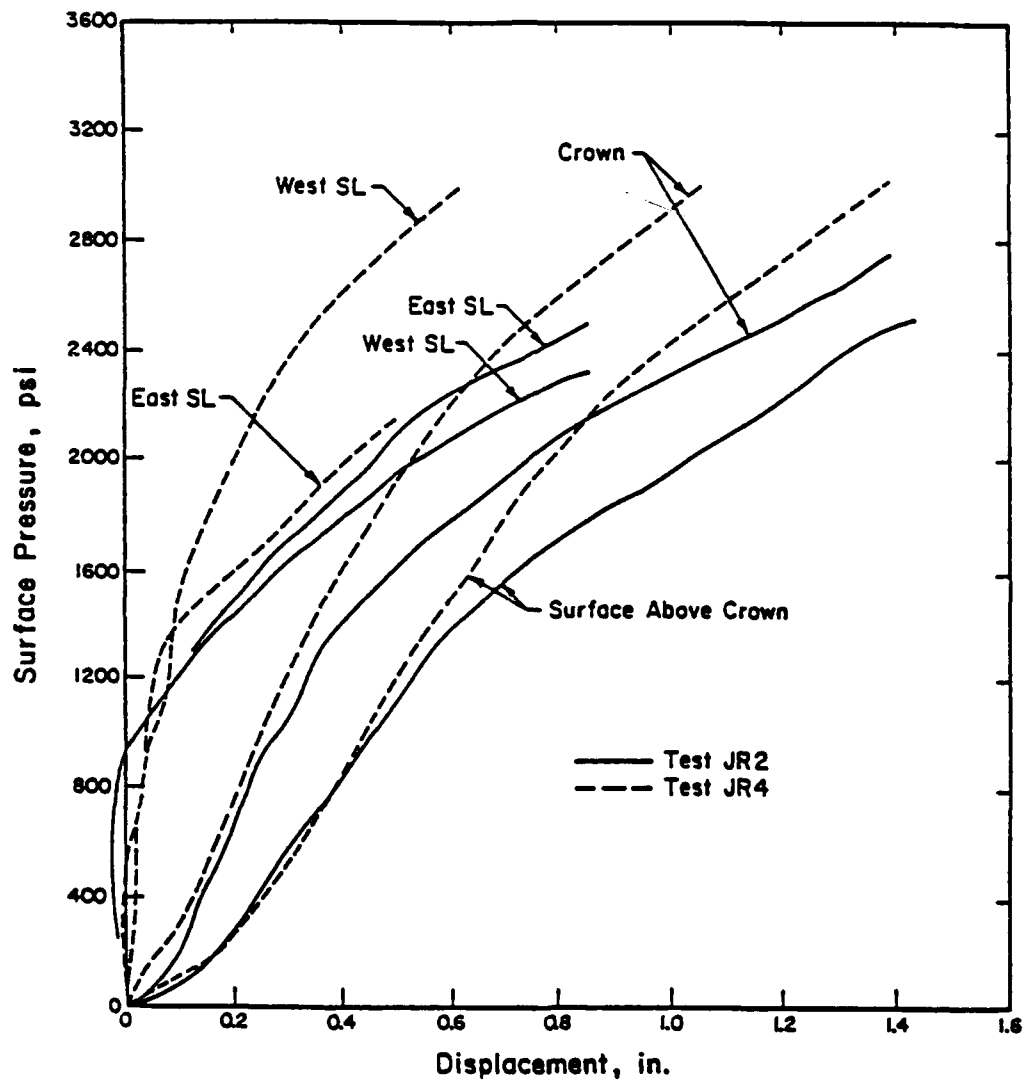


Figure 133. Comparison of Tests JR2 and JR4.

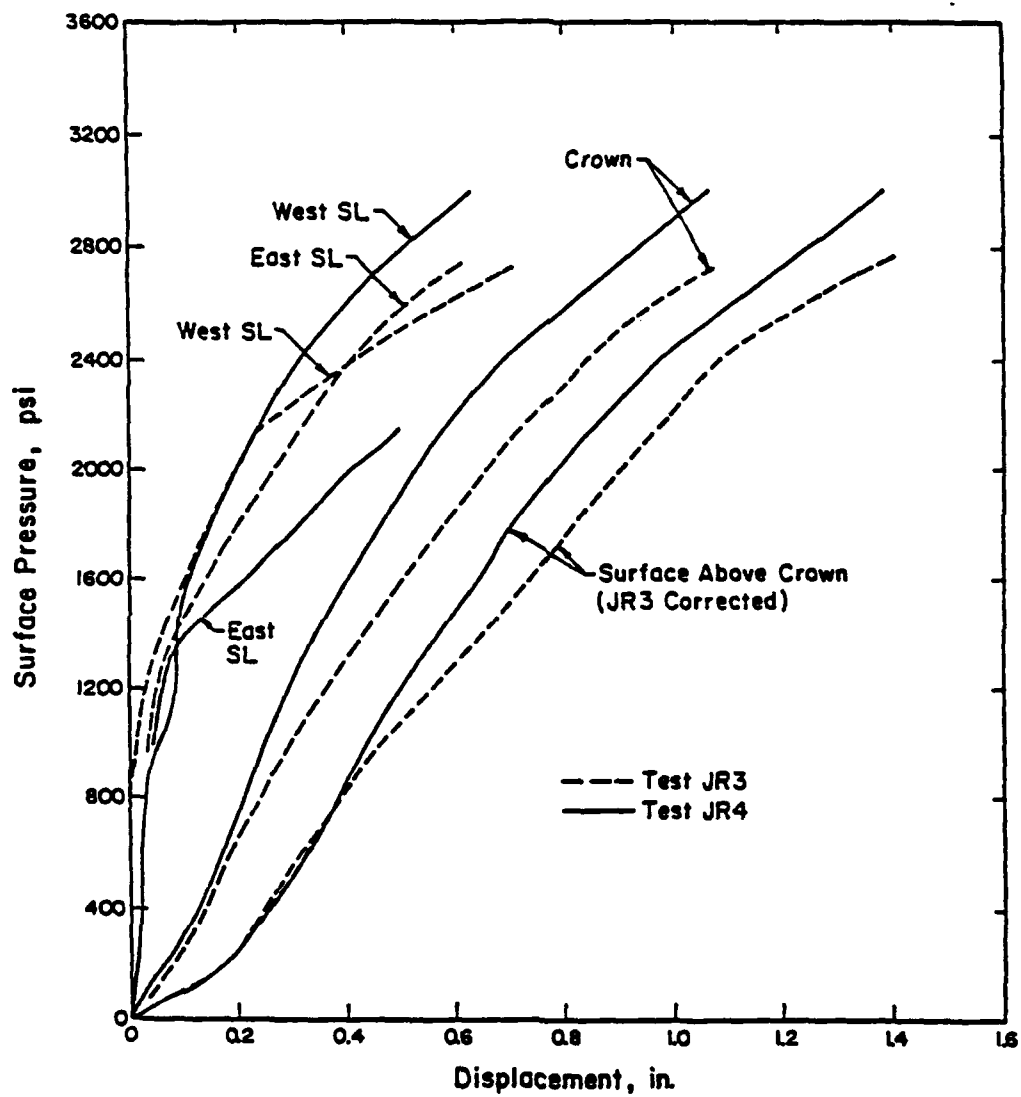


Figure 134. Comparison of Tests JR3 and JR4.

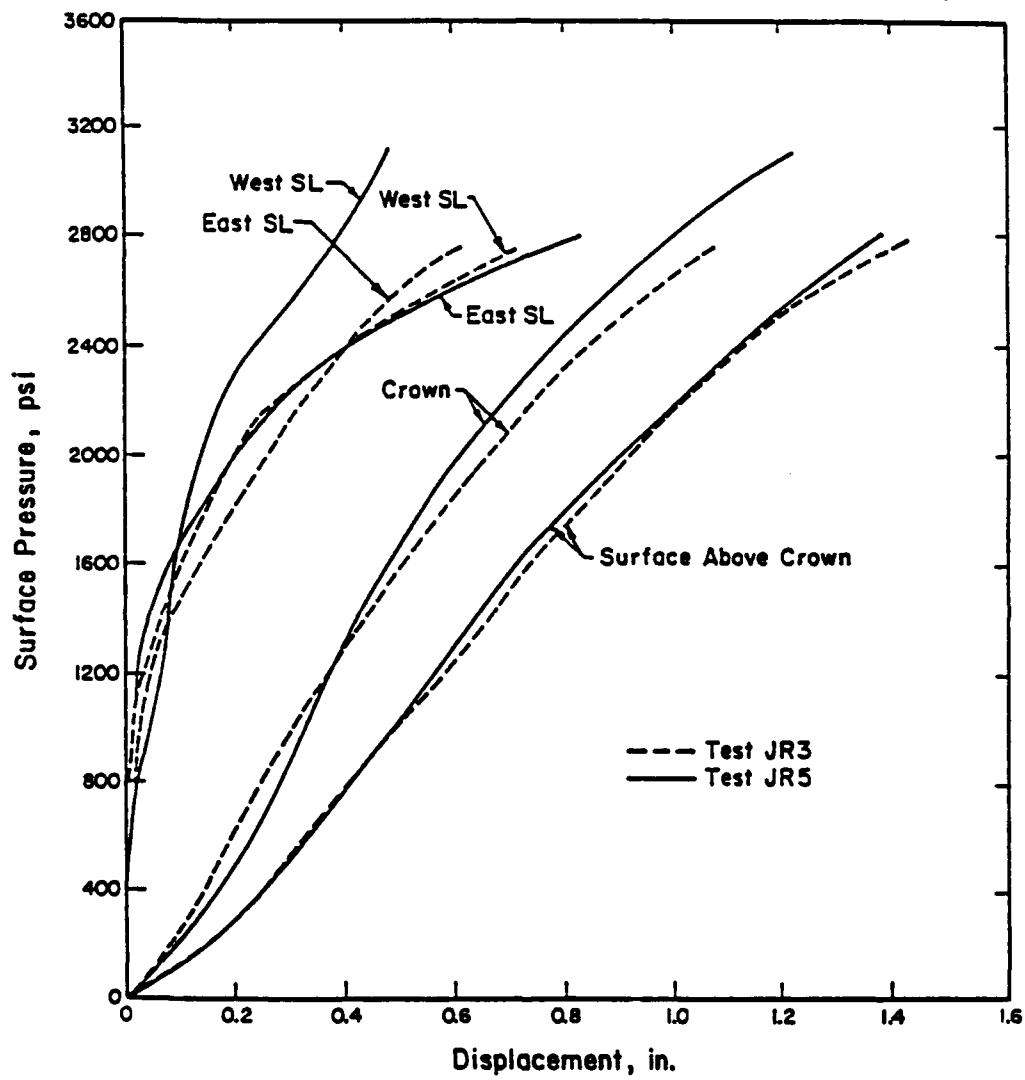


Figure 135. Comparison of Tests JR3 and JR5.

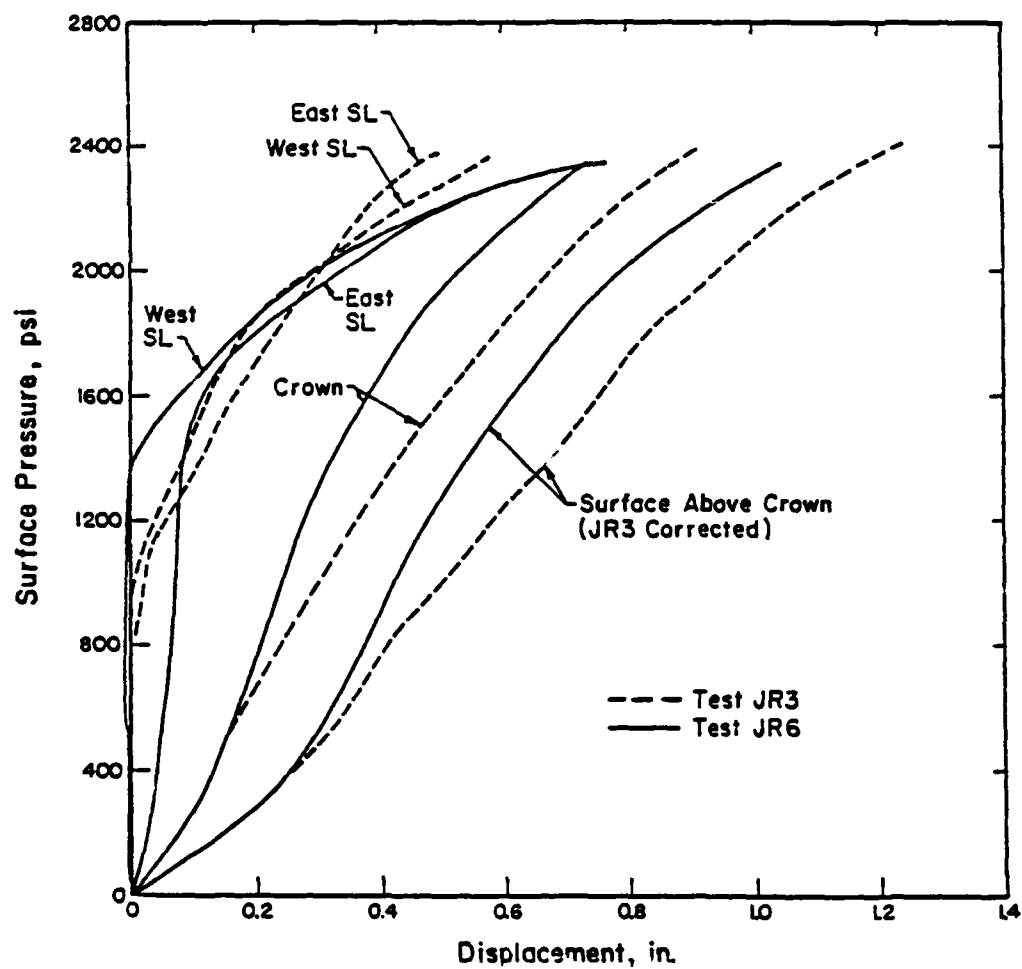


Figure 136. Comparison of Tests JR3 and JR6.

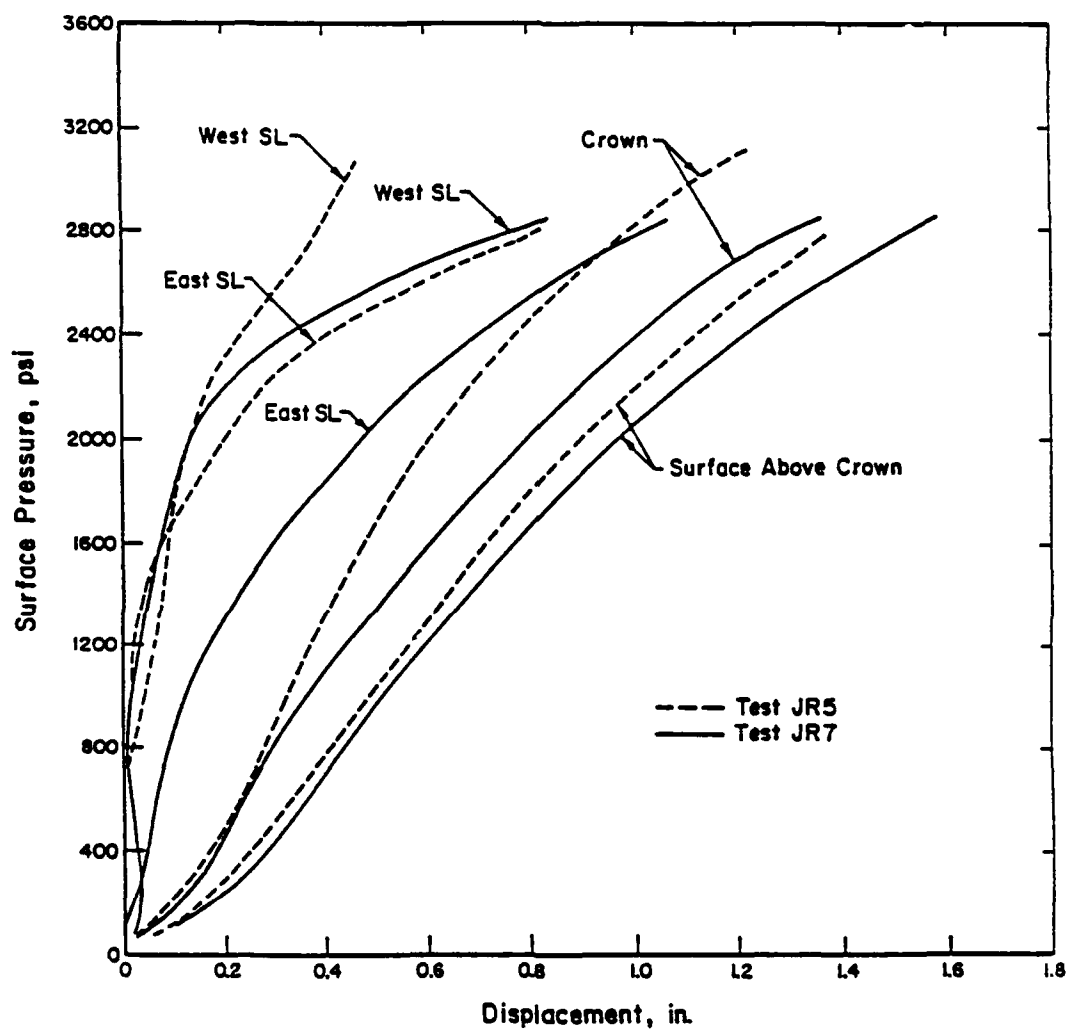


Figure 137. Comparison of Tests JR5 and JR7.

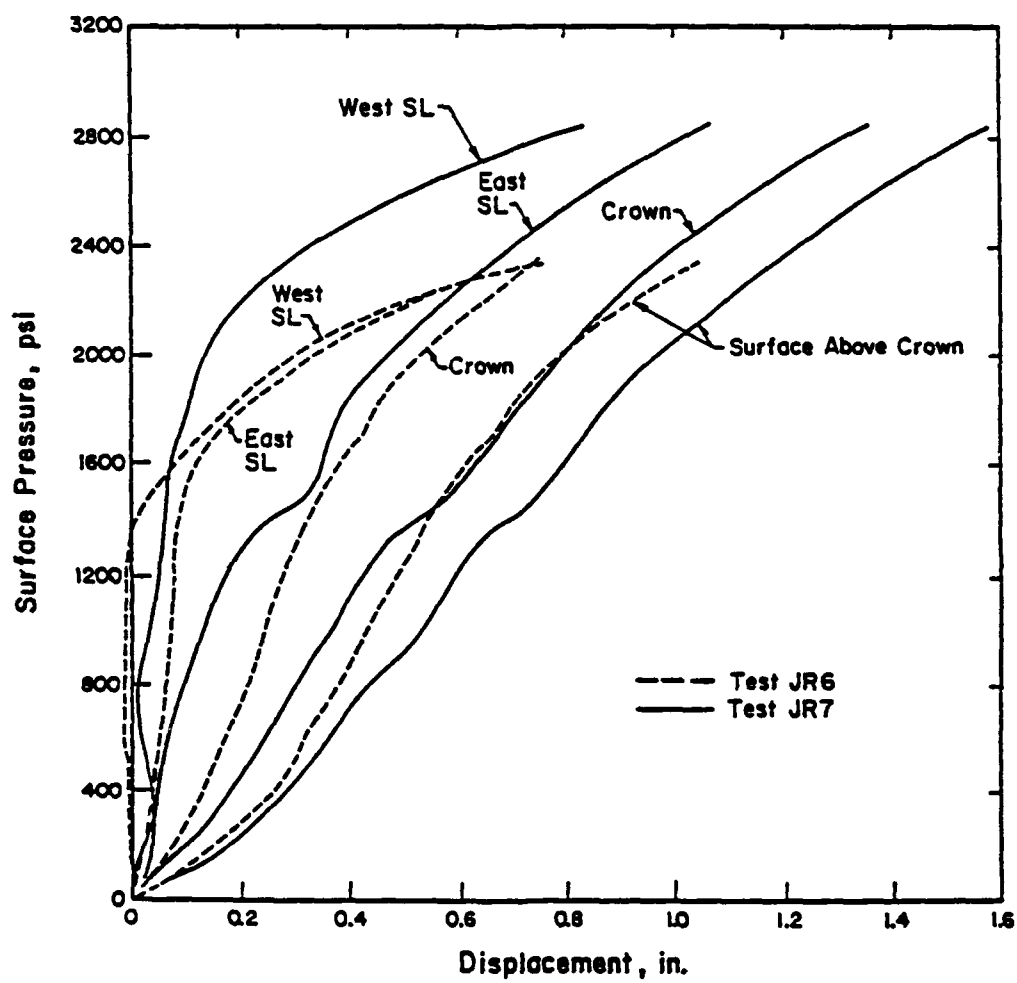


Figure 138. Comparison of Tests JR6 and JR7.

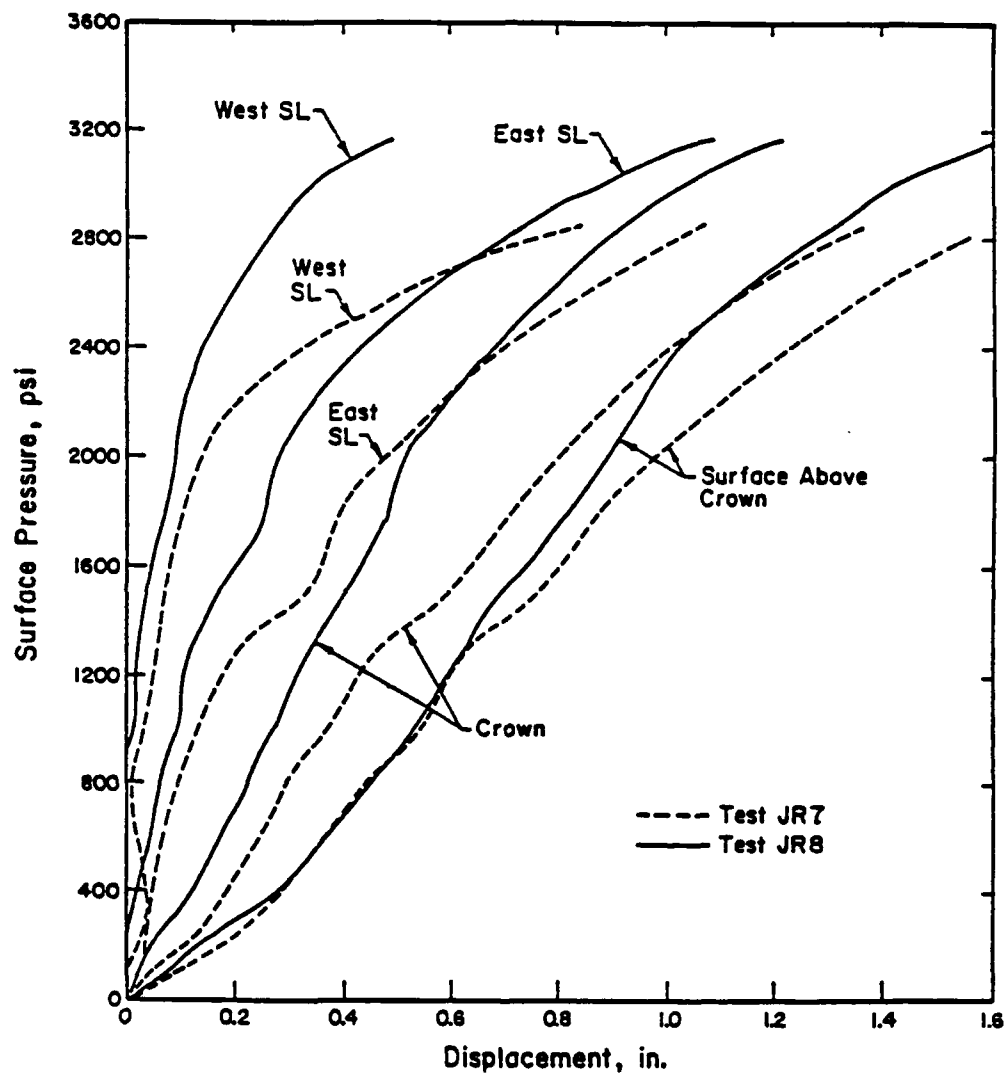


Figure 139. Comparison of Tests JR7 and JR8.

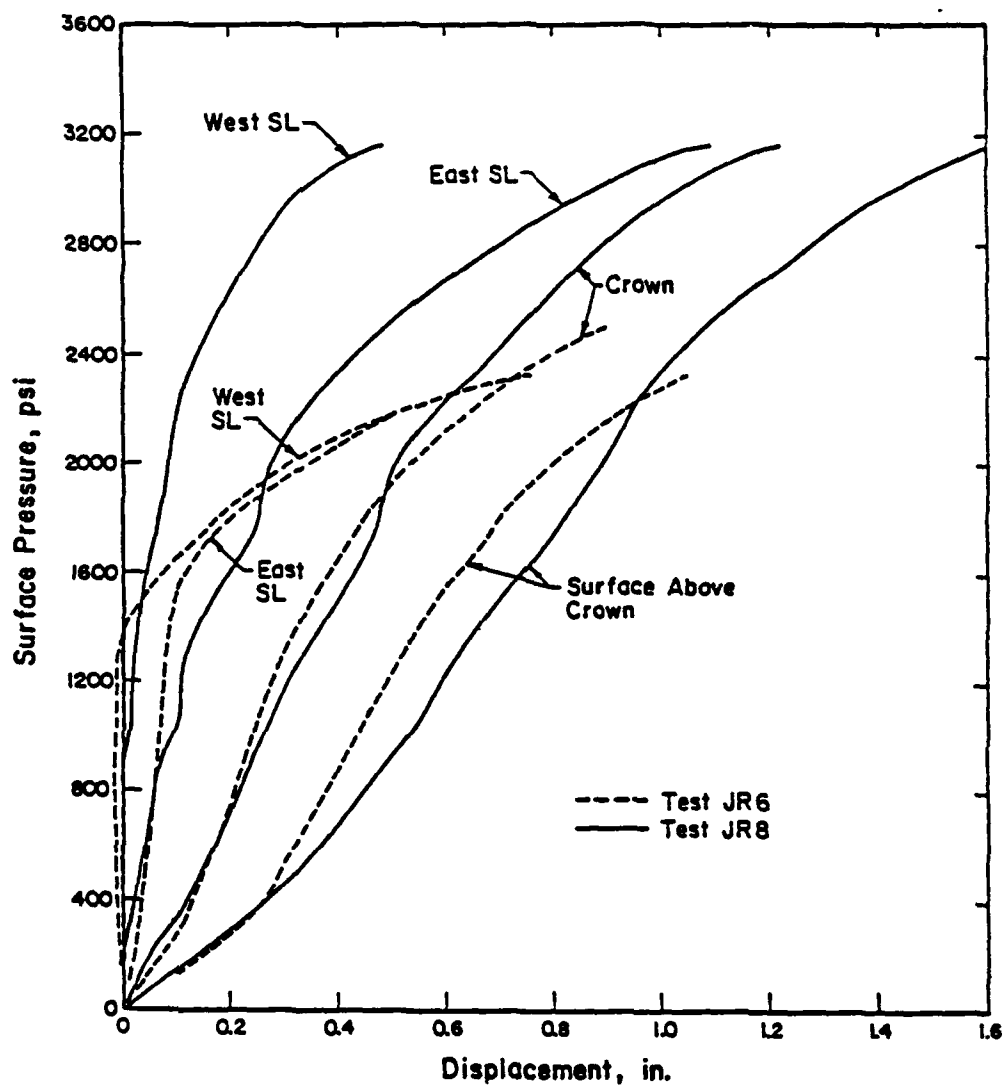


Figure 140. Comparison of Tests JR6 and JR8.

### 5.3 OBSERVATIONS ON RESPONSE OF JOINTED-SPECIMENS.

The UI results shed light on the response of jointed rock in two areas. When the joint friction is higher than that of the intact material, the jointed-medium responds as a continuum. This is confirmed by the classic plastic zones at the springlines exhibited in all the tests despite differences in joint angle, joint pattern, and the introduction of "fault" lines. Even in JR1 and JR2 where the joint columns are vertical, the friction is sufficient to retard the downward slide of the column above the opening when pressure was applied by individual plattens.

The second observation is that kinematic boundary constraints significantly affect the response of opening in jointed rock. Witness the fundamental differences between the case where the load is applied directly to the blocks (JR1 and JR2) and the case where the load is applied indirectly through a single platten (all other JR tests). The lack of kinematic boundary constraints on the joint columns in JR1 and JR2 leads to large rigid body displacement of individual columns into the opening, as expected, despite the high joint friction present. The condition in the field is closer to the latter case than the former.

In retrospect, two additions to the program might have enhanced the value of the test data. The out-of-plane condition needs to be quantified. The configuration used in the test leaves the out-of-plane surfaces open so as to allow for photogrammatic measurements, but the prestress bars should have been monitored. As it stands, we only know that the condition is neither plane stress nor plane strain. We do not even know how non-uniform the out-of-plane distribution of confining stress is.

The program should have included joint friction which is lower than the friction angle of the intact material. While test results obtained for high frictional joints are very useful, the value of the data set would have been significantly enhanced if a companion set with low frictional joints had been obtained. We expect the lower frictional joints will amplify the effect of jointed rock, just as higher frictional joints are shown to retard such effects.

Because rock bolts were not included in any tests involving joints at SRI, it is dangerous to compare results from UI and SRI. Similarly, the lateral boundary conditions used in the UI and SRI tests probably are not at all comparable. Thus any comparisons would probably lead to dubious conclusions.

## **SECTION 6**

### **SUMMARY AND RECOMMENDATIONS**

#### **6.1 SUMMARY OBSERVATIONS ON SRI PROGRAM.**

##### **6.1.1 Significant Strengths.**

This has been a continuing program for about fifteen years with no major interruptions. Although there has been a series of personnel assigned to the program, management has remained involved and has provided continuity. Also there frequently was an overlapping of operational staff and technician support.

There has been reasonable synergy between the laboratory studies of containment physics and this program at least insofar as definition of properties of the 2c series of tuff simulants.

There has been a reasonable evolution of instrumentation and control systems. Data from the test program have demonstrated certain important trends in tunnel response, viz., the effects of boundary proximity, lateral confinement, liner thickness, strain path, pore water, dynamic loading and strain rates.

Although generally brief, there were some efforts made to simulate analytically the experimental results.

With some concerns, as stated below, the methods used and documentation of the program are excellent.

##### **6.1.2 Some Concerns.**

The general philosophy of the program as espoused by the original investigators (and related programs such as the model shallow buried structures program) has been that the laboratory results can emulate all of the significant aspects of behavior of larger scale or even prototype structures. Because of effects of important implementation details such as the finite specimen size and the absence of field scale imperfections introduced in lab scale fabrication, a potentially more interesting philosophy would involve the use of the very small scale tests to screen the more viable concepts from among various lining types. For example, is a composite integral lining substantially harder (more resistant) than a simple lining surrounded by backpacking emplaced in a given material. The concern of the reviewers, therefore, is the underlying philosophy used in planning test sequences.

Characterization of the various simulants (e.g., 2C-, 6A, 6B, 16A and High Friction) has, in general, not been carried to the point where analytical simulation of the tests can be carried forward with confidence.

Instrumentation of lateral deformation (strain) was quite limited in many of the uniaxial loadings. There is no question that the tests were different than those specified as isotropic, but the lateral boundaries could and should have been more completely instrumented to allow analytical modeling without nagging questions of what the real boundary conditions were.

Although they are difficult to simulate realistically at the small scale, efforts are needed to model rock bolts, Nelson studs and other potentially important details in the real structures.

"Exact" replication of tests was needed but largely absent; the variations of as much as 50 per cent in a stress to produce a given diameter change in a given monocoque lining and in a given simulant casts serious doubt on some results, especially those on effect of tunnel to specimen size on results.

There was no effort expended in defining the effects of carrying joints all the way to the specimen boundaries in tests involving jointed media in the laboratory and field.

Cross-correlation among the laboratory programs and between laboratory and field programs was not as complete as it could have been; in fact most efforts were reported separately.

The implementation and the philosophy used in the laboratory size tests in the field needed further analytical and then possibly experimental evaluation. Until this is done, decisions on future roles of these tests cannot be made in final form.

The analytical efforts done under the current contract reported in Appendix C to define effects of tunnel to specimen size need to be completed. Until these are done, decisions on specimen geometry cannot be made in final form.

## **6.2 SUMMARY OBSERVATIONS ON TERRA TEK PROGRAM.**

### **6.2.1 Significant Strengths**

Although there has been a series of personnel assigned to the program, management has remained involved and has provided continuity. Also there frequently has been an overlapping of operational staff and technician support.

The program has made an efficient use of hardware developed largely for other tasks.

There has been a reasonable evolution in developing and measuring material properties in the more recent tests and of methods for avoiding some of the major problems of applying and controlling uniform loads on the specimens.

Although very limited in nature and applicability, some effort was expended to define analytically the geometry of the test specimens and the possibility of including other openings in the same block.

With some concerns, as stated below, the methods used and documentation on the program are excellent.

### **6.2.2 Some Concerns.**

Several difficulties were encountered in the dynamic tests; as a consequence, the results are difficult, if not impossible, to interpret and draw conclusions from.

As documented in Section 4, there were inconsistencies among parameters, difficulties in reproducing similar strength properties among samples and uncertainties in load distribution over the top of the specimen in the first series of static tests. As a result, it is difficult also to interpret these results and draw conclusions. In the effort made in preparing for the 1988-89 series of tests, the materials were more carefully developed and characterization was improved; thus, these results should be much better (This new work is discussed in Appendix E).

In the early series of static tests it was argued by Terra Tek that the results had to be interpreted on the basis of elastic behavior and the results were so presented. So long as the stress-strain curve for the strength-modeled material is geometrically similar to that of the real material, there is no need to restrict the interpretation to elastic behavior; however, the variability of properties from sample to sample precluded our making a realistic separate evaluation of the results.

To be valuable to the DNA program, Terra Tek must extend material modeling into the nonlinear regime, including post peak stress behavior. At best, the results obtained to date are relevant to design of defensive (i.e. US) structures; this is not compatible with goals of the current DNA programs which emphasize targeting. The more recent results, discussed in Appendix E, are much more internally consistent and the tests and general observations by TTI pertain to large deformations.

### **6.3 SUMMARY OBSERVATIONS ON U OF I PROGRAM.**

#### **6.3.1 Significant Strengths.**

This and the related Department of Transportation (DOT) and Washington Metro programs have proceeded for about twenty years with no major interruptions.

The professorial staff assigned to this and the predecessor or parallel programs have remained constant.

An extraordinary effort was made to develop methods to install model rock bolts in a realistic manner.

An excellent effort was used independently to define key parameters such as joint friction properties.

The materials for strength modeling were based on similar materials developed and documented earlier and a reasonable fraction of the limited funding was expended in characterizing the material used.

With some concerns, as stated below, the methods used and documentation of the program are excellent.

The photogrammetrically based system of measuring displacements was unique and greatly benefited the interpretation of results.

#### **6.3.2 Some Concerns.**

Only very limited effort was expended in performing parallel analytical interpretation of the test configuration and results.

The labor intensive nature of constructing the specimens, installing rock bolts and loading the specimens made the tests difficult and time consuming; some effort must be expended to automate some of the more tedious procedures.

No effort was expended in defining the effects of carrying the joints to the specimen boundaries; this could have had some significant effects on the results.

The lack of ability to control or measure some of the stresses at the lateral boundary were recognized by the U of I staff in their interpretation of the results.

Also the project staff had recognized that simpler devices might be used in the future to study the effects of rock bolts on strengthening jointed rock at selected regions around a circular opening as compared to testing the entire opening and significant regions of surrounding material.

#### **6.4 SOME GENERAL, RETROSPECTIVE CONCERNS ABOUT LABORATORY TESTING OF TUNNELS IN ROCK.**

All agree that a few tests cannot answer significant, all-inclusive questions; as an example, "exact" replication of tests must be done and a sufficient number of tests must be repeated to define the reproducibility of failure modes, measured quantities and overall behavior.

Both DNA and their contractors need to provide more continuity in the testing programs. In the programs reviewed, it is obvious that there was interest sequentially in behavior of tunnels in tuff, in sandstone, in granite and in limestone. Before the behavior of simple tunnels in any one material was understood even cursorily, interest shifted to behavior of intersections in sandstone. As a result, each report addresses only one configuration or material, and, often as not, the next report addresses a new material or configuration. The current status is that there has not been a program in laboratory evaluation of tunnels in rock; there have been sub-programs of tests of tunnels in various simulated media and of intersections in a medium. The pressures which caused this are obvious: new programs required early answers; budgets generally had to be tied to operational systems and the litany of former policy statements or varying interpretations of policy.

Too often testing in general has not carried an appropriate parallel analytical effort. Testing is expensive, but testing without appropriate analytical support runs the risk of being uninterpretable. Only the parallel analytical effort can assure that the right measurements are made at the right time and place to provide a coherent picture of behavior. As failure develops, even in a static test, changes to deformation with load can be steep that simultaneous recording of several channels may be necessary; having a time delay of only a few milliseconds can mean that one value of strain was measured as a buckle was imminent while the next value of strain on an adjacent gage after the buckle had formed. Such a result would certainly give a confusing picture. The real concern, therefore, is whether sufficient funding will be provided for parallel analytical efforts and adequate instrumentation systems to record the data with the required temporal simultaneity. Fortunately the evolution of micro-computers has dramatically reduced the cost of nearly or truly simultaneous recording of multiple channels of data. But DNA must be prepared to provide adequate funding to support the analysis and recording equipment required.

Having summarized our perceptions of the principal strengths and concerns we are now prepared to present our recommendations for the next phases and issues to be addressed in laboratory testing. These are given in the following subsections. The reader should keep in mind the last set of concerns above as he proceeds through the following material: adequate funding must be forthcoming to allow parallel analytical effort and adequate instrumentation for each test program. There must also be adequate funding to provide proper replication in the tests. Finally the programs must be relatively long term at a given laboratory and with a generally focused objective.

#### **6.5 RECOMMENDATION FOR FUTURE LABORATORY TESTING.**

After careful review of the dynamic tests conducted at SRI International (SRI) [DNA 4425F] and Terra Tek [DNA TR-85-387] the project team has decided not to recommend the

continuation of dynamic testing in the laboratory at this time. The principal reasons for this recommendation are:

(1) Despite the fact that testing has proceeded on the behavior of lined and unlined tunnels in U.S. laboratories for more than 30 years [Heuer & Hendron], we do not yet understand the fundamental behavior of lined tunnels including what many consider simple linings such as rock bolts in laboratory tests. It, therefore, seems an unnecessary complication, and possibly even a deterrent to gaining an understanding of behavior, to proceed with dynamic tests prior to gathering data on the fundamental behavior of lined tunnels regardless of the complexity of the lining.

(2) Laboratory scale tests which emulate existing field data require the use of rise times of the loading in the range of several hundreds of microseconds. Such rapid loadings imply very high strain rates in the material. In turn, these high strain rates expose rate effects in the cement-based simulants.

(3) The necessary finite boundaries of the specimens introduce peculiar artifacts in the loading which frequently are atypical of the conditions that would be encountered in a prototype situation. These depend principally on the rate of loading relative to the transit time across the specimen. If this value is short, the boundary reflections will typically destroy the phenomena sought; if long, the result is quasi-static.

(4) Although it has not yet been demonstrated whether the in situ stress is an important adjunct defining the behavior of lined and unlined tunnels, there is no simple way to introduce the gravity stresses into the test schemes. There is a great deal of sophisticated centrifuge work being done. The reason it appear not to be useful here is that gravity loads are negligible relative to live loads and dead loads, which do not need to be simulated in a centrifuge. In view of this, a centrifuge unnecessarily constrains the size of the specimen and the loads that can be applied.

The remainder of this section discusses the methods used to develop the recommended matrix of static tests. It also presents the recommendations and the reasons for proceeding with the testing included in that matrix. The material as presented here has been reviewed, discussed in considerable detail and placed in the final format as given here by the entire project team. This work represents the principal final output and recommendations of the total project.

#### 6.5.1 Fundamental Issues.

The persons listed in Table 25 were contacted either individually or one of the persons of the group was contacted and he, in turn, coordinated development of the material for the entire group. The purpose was to develop a list of outstanding issues on deep basing for planning of potential future test programs to be conducted primarily in the field. These issues, of course, are equally applicable to the laboratory program, and, consequently, the same issues were carried over to this program.

Because some of the thoughts overlapped one another, we have paraphrased the entire list of issues in Fig.141. We, in turn, studied this general listing of issues to determine which of them could be addressed at least partially in laboratory or laboratory scale programs. The general concept of the laboratory scale programs is illustrated in Fig.142 which is copied directly from [DNA POR 6887]. The result of the initial study is illustrated in Fig.143 by enclosing in boxes those issues which are amenable to laboratory or laboratory scale testing.

Table 25. Persons, other than members of project team,  
contacted individually or by groups.

**RDA**

Ms. B. Killian  
Dr. C. P. Knowles  
Mr. J. G. Lewis

**UNIVERSITY OF ILLINOIS AT URBANA-CHAMPAIGN**

Dr. E. J. Cording  
Dr. W. J. Hall  
Dr. A. J. Hendron, Jr.  
Dr. S. L. Paul

**ARA**

Mr. S. Blouin  
Mr. J. L. Drake  
Dr. J. C. Galloway

**PSR**

Dr. H. L. Brode  
Dr. A. Laupa

**SRI**

Dr. J. Colton  
Dr. J. Simons

**PRIVATE CONSULTANT**

Dr. R. P. Kennedy

**IMPELL CORP.**

Mr. S. A. Short

**CRT**

Mr. K. Kreyenhagen  
Mr. J. Thomsen  
Mr. S. Schuster

**LLNL**

Dr. D. Oakley

**PRIVATE CONSULTANT**

Mr. E. B. Waggoner

**DNA**

Mr. J. W. LaComb

Effects of rock mass properties on structural response

New Medium -- "Bridge" to existing data

Size effects and scaling

Cheap, improved protection especially rock bolting

Top-loading and effects of in situ stress

Range to effect in jointed limestone

Aging of materials

Water inflow and control

Asymmetries in stress wave

Coupling

Modern data for range to effect in granite/tuff, etc.

Layering

Carbon dioxide contamination

Achievable hardness

Failure criteria for targeting

Shock isolation

Support to DUGHEST and data for design and validation of simulator

Validity of model testing

Figure 141. Key technical issues for deep basing.

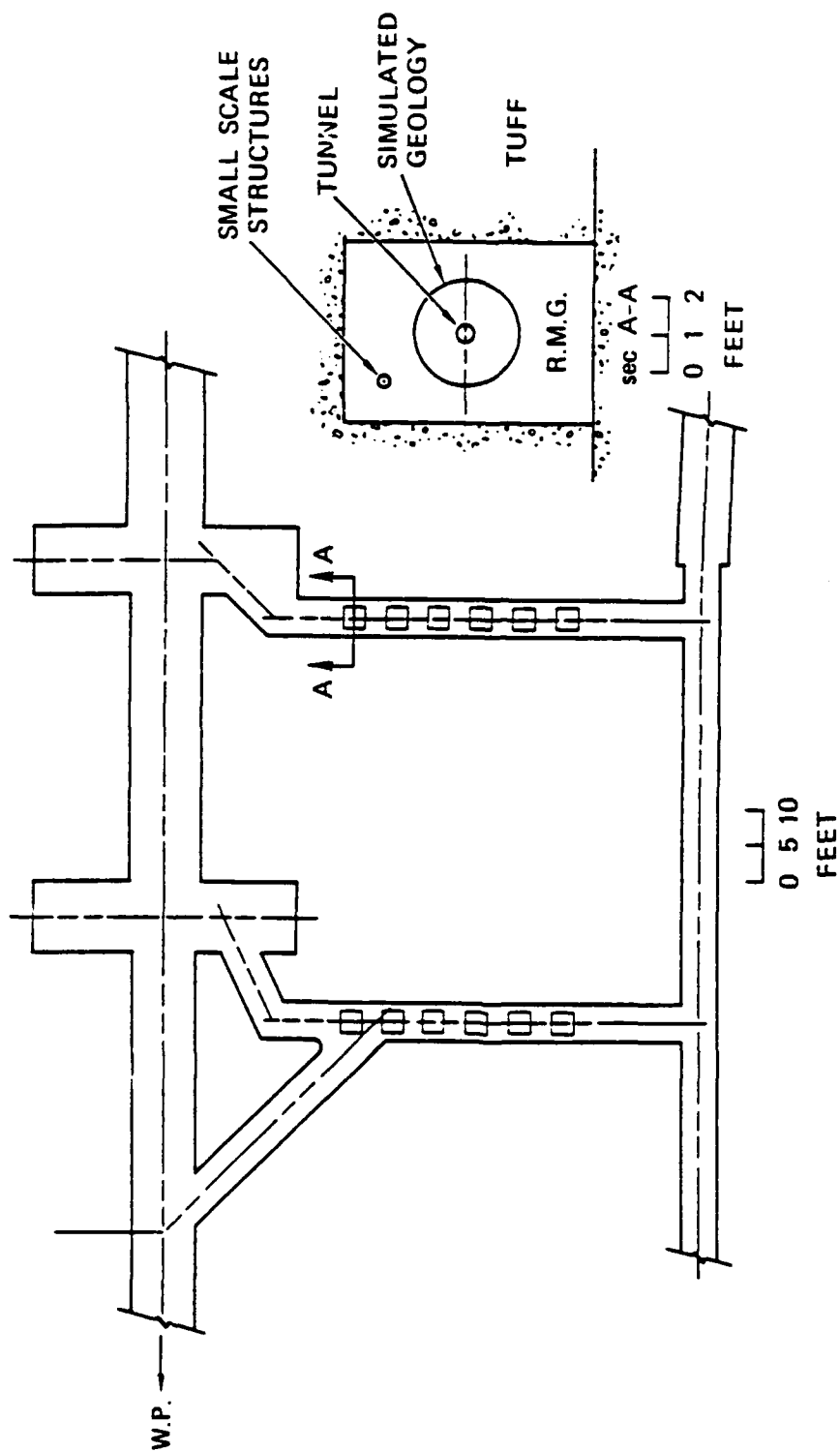


Figure 142. Experiment layout in DINING CAR crosscuts. (DNA4023F)

Effects of rock mass properties on structural response

New medium -- "Bridge" to existing data

Size effects and scaling

Cheap, improved protection especially rock bolting

Top-down loading and effect of in situ stress

Aging of materials

Water inflow and control

Asymmetries in stress wave

Coupling

Modern data or range to effect in granite/tuff, etc.

Layering

Carbon dioxide contamination

Achievable hardness

Failure criteria for targeting

Shock isolation

Support to DUGHEST and data for design and validation of simulator

Validity of model testing

Figure 143. Boxes enclosing issues from Figure 141 where laboratory testing applies.

### 6.5.2 Outstanding Fundamental Questions In Laboratory Testing.

Active consideration was given to the fundamental questions which have not been adequately answered in the earlier programs. The listing of those questions is given in Table 26 which is discussed in detail in the following section.

Table 26 is subdivided into three parts. The first provides a listing of questions pertinent to laboratory testing in general; the second addresses model testing with simulated joints in the medium; and the third is devoted to laboratory scale tests using "the mountain as a testing machine". Following, is a discussion of the fundamental questions as listed in Table 26.

#### Degree of Reproducibility in Identical Tests.

In the review of the earlier tests, it was disappointing to learn that there was relatively little direct repetition of tests in any single laboratory program. As a result, it was difficult to determine directly the degree of reproducibility of the results of one test in a subsequent identical test. In the one laboratory program [DNA 5208F] to evaluate the effects of the size of the opening relative to the size of the overall specimen, there were duplicate tests. Unfortunately, the data expressed in terms of the load required to produce a change in diameter of the opening divided by the size of the original opening at a given scaled displacement varied by as much as 50%. As a result, the minor amount of data available indicates the potential for wide variations in results. This variation may have been exacerbated by the fact that the test involved only unlined openings. Because the behavior of such openings can be influenced by minor variations in material properties, measured displacements can be magnified if a local area of weakness exists in the vicinity of the measurement. If this speculation is valid, use of nominal, thin linings may reduce the variations in the data among identical tests. Regardless of the causes of the variations in the tests which have already been conducted, it is important in any future laboratory program to include identical tests to give specific data on the degree of reproducibility on that test program. In turn, as each new major set of variables is introduced into a test program, additional needs for identical tests are indicated.

#### Effects of Proximity of Model Tunnel to Specimen Boundary.

Because relatively little data existed on the influence of structural as compared to specimen size on behavior, the analytical program presented in Appendix C was embarked upon by this team. Unfortunately, the limits of funding within the contract did not allow a complete analytical definition of the effects of the proximity of the specimen boundary. It is, therefore, recommended that additional funding be made available to carry the analytical studies to a reasonable conclusion. The continued analytical study should include at least the five elements listed in Table 2 for the effects of relative tunnel to specimen size. The interrelationship of strengths and compactability may have a significant impact on the required relative size of opening to specimen dimensions. Additionally, whether the loading state is uniaxial, hydrostatic, or follows some other prescribed strain path may have a significant impact on the required ratio.

The relative sizes also influence the means of measuring and controlling the deformations and stresses applied to the external boundaries. If the tunnel is too close to the boundary, strains measured on that boundary will be influenced by the tunnel. In this rather extreme case, strain measurements would not be an appropriate means of controlling a test intended to represent plane strain.

Some lining types require inducing large strains up to, perhaps, 15% at the surface of the opening. To achieve such strains requires inducing large amounts of plastic flow and, in turn, creates relatively large regions of "yielding" material. When these zones intersect the boundaries it is likely to influence the response.

Table 26. Fundamental questions outstanding in laboratory testing.

**MODEL TESTING IN GENERAL**

What is the degree of reproducibility of results in identical tests?

What are the effects of proximity of the model tunnel to the specimen boundary given:

Different strengths and compactibilities of rock simulants (or natural rock) used in model tests.

The stress or strain path desired.

Requirements and methods to control lateral and vertical deformations especially on the loaded surfaces above and/or adjacent to the model tunnel.

Amount of plastic flow required to induce significant failure in lined and unlined tunnels.

Means of applying stress or deformation to the exterior of the specimen?

What is the required fidelity of the lining (or what procedures are needed to emulate in the model the conditions imposed by fabrication of the prototype) including possible simulated in situ stresses for:

Rock bolts; for example, can effects of in situ stress be ignored?

If so, rock bolts can be assembled, held in place and cast into the simulant or drilled into the walls of the model tunnel with the specimen stress free.

If not, the specimen must be cast and the in situ stress imposed and maintained while the tunnel is "mined" (probably drilled) and the rock bolt system installed.

Composite integral linings consisting of steel plate, Nelson studs and reinforced concrete.

Composite integral linings consisting of steel plate, reinforced concrete and rock bolts to impede buckling of the steel plate.

Corrugated steel and reinforced concrete linings surrounded with packing of various strengths and ability to compact under nearly constant stress.

Articulated linings

Other lining types?

Table 26. Fundamental questions outstanding in laboratory testing (continued).

What are desirable constitutive properties of simulants for use in model tests if natural rock or conventional concrete is not used?

What is the minimum instrumentation needed to:

Properly control the test conditions such as the lateral stress in a case involving uniaxial strain conditions.

Properly interpret the results?

#### **FOR MODEL TESTING WITH JOINTS IN MEDIUM**

What are the effects of:

Extending joints to the boundaries of the specimen

Over all specimen size

Details of joint geometry such as:

Continuity  
Curvature  
Asperities

How should specimens be assembled, linings installed and loaded?

#### **FOR MODEL TESTS USING "THE MOUNTAIN AS A TESTING MACHINE"**

What are the required properties of:

The simulant (or rock) forming the specimen

The grout used to surround the specimen within the emplacement tunnel in natural rock.

What sizes, shapes and types of tunnel lining are susceptible to testing in this manner?

Especially for targeting, what are the ultimate modes of failure which can be induced in this method of testing?

Tests to date have used steel plates to distribute the load over the surface of the specimen, flat jacks to apply the stress to the surface of the specimen, or fluid pressure acting directly against the specimen. Because the steel plates or the material in the flat jack induce shears at the specimen boundary, important artifacts can be introduced in the test if the specimen boundaries are too close to the openings.

In addition to the analytical program suggested here, it is, of course, important to also run laboratory evaluations early in any program to demonstrate that the specimen boundaries for the specific configuration adopted will not have an untoward influence on the behavior of the subsequent tests.

#### Required Fidelity of Model Tunnel Linings Including Laboratory Simulation of In Situ Stress.

Field tests of lined tunnels to date have emphasized either the composite integral system or relatively simple linings surrounded by crushable packing. The composite integral lining has been constructed in two ways. In the PILE DRIVER Event achieving composite action and impeding the buckling of the interior steel plate was accomplished by installation of rock bolts. In the MIGHTY EPIC Event, welded studs were used to fasten the steel plate "integrally" to the concrete and impede the development of buckling. Ideally, these structural features should be included in laboratory specimens. The tests at Illinois used rock bolts installed in a method similar to the one that would be used for installing rock bolts in the field. Feasibility of simulating other construction details in laboratory specimens should be investigated.

Construction imperfections caused by rolling of the steel plate, welding of the seam, the installation of reinforced concrete around the steel plate, and possible out-of-roundness of the steel plate, which may be very important in that field tests indicate severe buckling as a principal mode of failure, have not yet been considered by laboratory testing; such effects could be considered, however. Similar difficulties exist in terms of fabricating simple corrugated steel and reinforced concrete linings which, in turn, are to be surrounded by crushable packing. Tests with laboratory specimens with artificially created imperfections, should be conducted in parallel with analysis. The analytic model can be used to evaluate the effects of imperfections which cannot be emulated in small specimens.

In situ stresses can be considered in the laboratory. Tunnels at significant depth in weak rock can be affected by in situ stress, which should be considered in simulating such cases. The 4-inch and 12-inch testing machines normally used in the tests at SRI can impose idealized stresses consisting of a uniform circumferential stress laterally and a different uniform axial stress. Full simulation of at least the lithostatic stress field would require independent control of the three principal stresses which is not easily accomplished by modification of the testing machines in existence at SRI. The testing devices available at Terra Tek do allow independent control of the three principal stresses. However, providing access to create the simulated mined opening and subsequent installation of any lining system would be difficult and potentially expensive in the existing Terra Tek devices.

The large testing facility recently built for Ballistic Systems Division (BSD) of the Air Force at Waterways Experiment Station (WES) [Miller, 1988] may be modified to allow the simulation of in situ stress and allow for the mining of the simulated opening under controlled simulated natural stress fields. However, the physical size of the machine at WES implies relatively large cost in both modifying the machine as well as creating the simulated opening. The facility at BDM discussed in [Davis et al, 1979] can also be readily and cheaply modified for independent control of the three principal stresses and drilling simulated tunnels.

Without modification, the facilities at SRI, Terra Tek, WES and BDM should in the future be used to determine the effect of a varying biaxial lateral stress field on the behavior of a simulated tunnel.

#### Effects of Constitutive Properties of Medium on Model Test Results.

As noted in Section 2.2 it is probably impossible to create a simulant which will emulate all of the important properties of a natural medium through the range of stress from, let's say, five kilobars down to an eighth kilobar, the range of hardness of potential interest. In tuff, for example, the 2C4 series is probably applicable in the range from several kilobars down to, perhaps, one or two kilobars while the ME8-11 series is applicable in the range from one to a quarter kilobar. One is therefore faced with either forming specimens from the natural rock or developing a simulant for the range of stress expected to create significant deformations in the tunnel support systems being tested. Because conventional concrete has many interesting attributes similar to natural rock and because of the wealth of data developed on the constitutive properties of such materials, it seems that normal concrete is an important material for consideration in the early stages of any test program. For test programs using materials other than concrete, it is essential to conduct an extensive laboratory program to define all of the relevant strength, stiffness and compaction characteristics.

#### Tests With Jointed Media.

In regard to models involving simulated joints in laboratory specimens, the following comments are made. The team is not yet prepared to say whether testing of this nature has been properly configured in the past or not. Carrying the calculations reported in Appendix C to a reasonable conclusion will help make this decision.

In the conduct of tests involving jointed specimens, at least a few of the early tests must be devoted to a direct demonstration of the capability of the adopted configuration to represent realistic conditions. As an example, it would be desirable to have one set of tests with the joints extending to the actual boundaries of the specimen to compare with results of another series of otherwise identical tests where the joints are truncated by an encapsulating continuum made of the same material as used in fabricating the jointed specimen. In this way, the potential difficulties associated with having the "slabs of simulant" intersect the fluid, steel, flatjack or other boundary of the testing machine can be evaluated.

Overall specimen size is of particular concern in the jointed specimens because to date there is no analytical or experimental evidence of the effect of the specimen size on the behavior of the tunnel included in the specimen. There is no question that simple planar joints should be the point of departure in any jointed specimen tests in the future. Since nothing is known about the detailed response of specimens with joints, the simple planes have some hope of being analyzed. On the other hand, natural joints are seldom continuous; they are never planar; geometrically, they are just very complicated. If testing of jointed specimens turns out to be a viable laboratory approach, procedures will have to be worked out to cast, construct and instrument more realistic joints at some point in the future after behavior of specimens with simple joints is understood.

#### Laboratory Scale Experiments in Field Tests.

Finally, with regard to laboratory size specimens included in UGT test beds, the following comments are appropriate. The analyses reported in Appendix C need to be carried to a reasonable conclusion to provide data from which important decisions can be made. In the context of the preceding comments, all of the questions at the end of Table 26 need to be answered before the full viability of this testing technique can really be determined.

### 6.5.3 Recommended Test Matrix.

An important consideration in the development of the recommended test matrix was the size of the tunnels to be included in the tests. We have constrained our thoughts here to openings of several inches in size but significantly less than that required to allow a person actually to work inside the opening. All access is restrained to that provided by the openings at the ends of the specimens. As demonstrated by the work at the University of Illinois [DNA TR-86-167] even model rock bolts can be installed in specimens of the size envisioned here, that is, openings up to 18 inches in diameter. The types of tests are envisioned to be literally experiments in the laboratory or laboratory scale specimens tested in the field.

It is certainly possible to construct laboratory specimens from natural rock, as was done in a limited way at Terra Tek [DNA TR-85-387]. Obtaining natural rock of the appropriate size and quality is, of course, expensive and difficult. Furthermore, if the natural rock is not well characterized in terms of its physical and mechanical properties, an extensive laboratory program to define such properties is required. As a result, it is infrequent that specimens are constructed from natural rock. Instead, rock simulants have been developed to represent the important features of the natural rock under consideration. We have found, however, that many of the simulants have not been well characterized. As a result, the analytical interpretations of the results of the laboratory programs using simulants has been hampered.

Because the fundamental behavior of lined tunnels is not yet well understood and because their behavior is apt to be qualitatively similar in any rock simulant, it seems appropriate to consider the use of conventional concrete as a simulant. The advantages of this material include the facts that it is cheap; it is well characterized under various loading conditions; and, most of all, it has many of the characteristics of natural rock such as low tensile strength and the ability to be modeled analytically using Prager-Drucker or related material models.

The full recommended test matrix is given in Fig.144. For emphasis it is noted that all recommended tests are static.

Under the subheading "Items From Table 26", the team has listed all of the main headings from Table 26, and under the "recommended program/action", the steps developed by the team for addressing the question specified. In view of the discussion in the preceding section, no additional comments are made here. The recommended action or program follows directly from the thoughts presented in the preceding section.

Under the subheading in Fig.144 entitled "Items From Fig.143", we first list the technical question posed by the issue in Fig.143 in the left column. In the right column, we indicate the team's recommendation for the action to be taken or the program to be embarked upon.

Following is a discussion of the recommended action for each of the items.

#### Effects of Rock Mass Properties On Structural Response.

There are pertinent data available on structural response in granite from Events HARD HAT and PILE DRIVER and in tuff from Events MIGHTY EPIC, DIABLO HAWK and MIGHTY OAK. In limestone there will be data developed from the Underground Technology Program (UTP). Because of the difficulty of building into small-scale models the details of the structures tested in earlier events, there really are no quantitative data from laboratory tests on the response of the various structures that have been tested in the earlier events. We firmly believe that a laboratory program must continue because laboratory programs are a less expensive means of doing parametric evaluations; they must be carefully developed to make sure that a viable alternative is available when a comprehensive test ban or other impediment to field testing comes to pass. This

## TECHNICAL ISSUE

Items from Table 26 :

Reproducibility of identical tests

Effects of proximity of model tunnel to specimen boundary

Required fidelity of model tunnel linings and laboratory simulation of in situ stress (behavior of simple, idealized linings in continuous media is already reasonably understood analytically; the fidelity addressed here is for more complex lining types.)

Effects of constitutive properties of medium on model test results

Required instrumentation

## RECOMMENDED PROGRAM ACTION

When a new major variable is introduced in any test program, perform an adequate number of tests to define degree of reproducibility.

Continue to a reasonable conclusion the analytical program initiated in this effort and described in Appendix C.

For any new program with significant departures from those considered here, perform analyses of the general type presented here to define proper dimensions of test articles.

Perform a brief series of repetitive tests to confirm the analytical results. Typically the tests will involve varying the size of the tunnel within the specimen to define the largest tunnel for which the proximity of the boundary has no obvious effect.

Use fabrication techniques identical to those used in the prototype and incorporate them into sufficient sizes of specimen to avoid effect of proximity of the boundary.

Or define typical tolerances for out-of-roundness, for example, and generate processes for emulating the typical distortions to be expected.

Carefully document the full set of relevant properties, using standard tests. If a simulant is used, carefully document the properties of the natural rock being simulated as well as those for the simulant.

Carefully select appropriate instruments and recording/feedback systems to assure adequate control and interpretation.

Figure 144. Recommended text matrix and related actions/programs

NOTE: All recommended tests are static.

## TECHNICAL ISSUE

### Items from Table 26 (continued)

#### Testing with jointed media

Continue to a reasonable conclusion the analytical program of the type discussed in Appendix C to assure that the geometry and means of imposing the stresses appropriately emulate the real conditions.

Perform single and/or double shear tests separately to define properties of joints.

#### Field tests of laboratory scale specimens

Continue to a reasonable conclusion the analytical program initiated in this effort and described in Appendix C. This effort when completed is expected to produce a listing of those dimensions and material properties required for this type of test to be conducted in tuff.

For any new natural medium, an analytical effort similar to that presented in Appendix C will probably be required to define the constraints to be imposed on the techniques.

### Items from Figure 143:

#### Effect of rock mass properties on structural response

Once the items in Table 26 are more fully understood by the actions summarized above:

- (1) Emulate in model tests selected structural behavior from Events **HARD HAT** and **PILE DRIVER**.
- (2) Emulate in model tests selected structural behavior from Events **MIGHTY EPIC**, **DIABLO HAWK** and **MIGHTY OAK**.
- (3) Begin emulation of structural behavior in **MIDDLE KEY**.

Figure 144. Recommended text matrix and related actions/programs  
NOTE: All recommended tests are static. (continued)

## TECHNICAL ISSUE

Items from Figure 143 (continued)

Experiments in fundamental behavior of rock bolts and improved rock bolt systems

Effect of in situ stress on structural behavior

## RECOMMENDED PROGRAM ACTION

Pursue a series of tests of type suggested in Figure 5 or other tests to address the key parametric effects.

This is a complicated problem; thus, a three step approach to define feasibility seems indicated:

- (1) Use conventional concrete as a simulant and perform a test where everything remains "elastic" and, thus more straightforwardly predictable and:
  - (a) Apply a simple stress state to a cylindrical specimen with embedded strain gages in the medium surrounding the hole to be drilled later along the axis of the cylinder
  - (b) Maintain the stress state and drill the hole while monitoring the changes in strain created by the drilling. It is also possible to emulate the observational, or NATM, techniques by periodically measuring convergence in the hole by removing the drill, installing a measuring system and documenting hole displacement.
  - (c) Increase the stress until failure of the unlined opening occurs and compare results analytically and experimentally to behavior of an otherwise identical specimen with a hole cast in it or, better, one drilled in it without applying in situ stress and tested to failure under an identical stress distribution but without the earlier emulated in situ stress state.

Figure 144. Recommended text matrix and related actions/programs

NOTE: All recommended tests are static. (continued)

## TECHNICAL ISSUE

Items from Figure 143 (continued)

## RECOMMENDED PROGRAM ACTION

- (2) Repeat step (1), but induce an emulated in situ stress state where the solid cylinder is in the elastic range, but the stresses around the opening, when drilled through it, will be inelastic.
- (3) Repeat step (1) but induce an emulated in situ stress state where the initial stress in the cylinder in general is in low non-linear range.

If feasibility is demonstrated, proceed with a test program where the simulated tunnel is lined with the lining installed while the emulated in situ stress state is maintained.

### Aging of materials

Recover samples of materials from Events HARD HAT (28-30 years old), PILE DRIVER (23-26 years old) and MIGHTY EPIC (13-14 years old) and make physical tests of properties to compare with those measured when the materials were installed.

### Water inflow and control

Tests of this type have never been attempted; thus a feasibility study of the following type is required:

- (1) Cast a solid cylinder of conventional concrete similar to the one suggested above for evaluating effects of in situ stress.
- (2) Cure the cylinder by complete submergence in water to maintain nearly saturated conditions.

Figure 144. Recommended text matrix and related actions/programs  
NOTE: All recommended tests are static. (continued)

## TECHNICAL ISSUE

Items from Figure 143 (continued)

## RECOMMENDED PROGRAM ACTION

- (3) Place the cylinder in a test frame similar to the one for evaluating effect of in situ stress and enclose the top of the specimen in a jacket which maintains a constant head of water and also provides a port for drilling simulated tunnel.
- (4) Maintain the constant pressure in the water in contact with the specimen while the simulated tunnel is drilled.
- (5) Allow specimen to sit, stress free and observe the quantity of water, if any, which flows into the simulated tunnel.
- (6) Increase stresses around the outside of the specimen to created failure and attendant cracking around the tunnel while constantly monitoring the quantity of water which flows into the tunnel.

*If this concept works, install various types of lining and/or means of intercepting the flow of water trying to enter the tunnel.*

### Achievable hardness

A program to define achievable hardness would be a next logical step following completion of studies to define effects of rock mass properties on structural behavior. The concept involves conceptualizing the most likely structural configurations to create "extreme hardness", building models of such structures in the simulants and testing them to failure to define the level of hardness achieved. Also modes of failure must be defined to aid a parallel analytical effort and to suggest concepts for later tests which may preclude or impede development of that mode of failure thereby achieving still greater hardness.

Figure 144. Recommended text matrix and related actions/programs  
NOTE: All recommended tests are static. (continued)

### TECHNICAL ISSUE

Items from Figure 143 (continued)

Failure criteria for targeting

### RECOMMENDED PROGRAM ACTION

In most laboratory programs to date, the tests have been discontinued as soon as the mode of failure was sufficiently defined to provide reasonable assurance that useful maximum capacity had been reached from the designer's perspective. For targeting, the deformations and associated damage must be carried to the point that at least unreasonable cost would be required to rehabilitate the structure. To define failure criteria for targeting will require carrying tests of models to much larger deformations. Because of the severe distortions, much larger specimens would be required for those test concepts involving models of structures surrounded by natural rock or simulants. For those test concepts involving tests of the bare lining under loads which simulate the boundary conditions in the field, achieving the large displacements will require adopting additional safety measures and/or means of constraining the outward deformations as occurs in a real tunnel due to the natural rock's tendency to preclude significant outward deformations.

Figure 144. Recommended text matrix and related actions/programs  
NOTE: All recommended tests are static. (concluded)

laboratory program should start with emulations of the conditions observed in the field of various earlier events and expected to be coming from the field in UTP. There is no question that the recommended laboratory program is going to be expensive but it is equally likely that the laboratory program will be much less expensive than a fully configured UTP event and/or probably a UGT involving an add-on structures experiment. This is not to say that major field tests involving structures should not be performed. They are essential to provide data in natural media for structures approaching operational size and fabricated/and installed by normal methods. Without these data, model tests in the laboratory could be totally misdirected. On the other hand we must carry laboratory development along with the field events so that they achieve sufficient maturity to replace UGT's when they become banned and augment UGT and UTP events so that all permutations of variables do not have to be accomplished in the field tests.

#### Experiments In Fundamental Behavior Of Rock Bolts And Improved Rock Bolt Systems.

Figure 145 summarizes a concept for a suggested series of tests to address the key parameters which potentially affect the behavior of rock bolts. Despite the seemingly simple nature of rock bolt reinforcement, the interaction of the bolt with the surrounding rock and its means of developing strength and ductility in rock openings is really not understood. To proceed with laboratory programs emulating full rock bolt systems still seems a bit premature. It seems better to proceed with simple, directly interpretable tests and then build on those to more complex emulations of what happens in a rock bolted tunnel. The scheme shown in Fig.145, including suggested means of measuring the response as well as several potential variables, is a concept developed by the team for addressing the fundamental questions of behavior of a rock bolt in rock. Our approach is a simplification of the proposal developed earlier by staff at the University of Illinois.

#### Effects Of In Situ Stress On Structural Behavior.

A number of pertinent questions regarding the effects of in situ stress have been posed. Among these are: what is the magnitude of in situ stress; how does it vary along the length of a tunnel; what is its effect on the response of the tunnel; how can it be simulated in the laboratory or the field; and how do we measure the ultimate response of the tunnel as it is affected by the in situ stress field? Because of these questions there are literally no data on the effect of in situ stress on the response of tunnel support systems subjected to ground shock. Efforts were made to measure the natural stress field in at least the HARD HAT, PILE DRIVER, MIGHTY EPIC and DIABLO HAWK test beds. At the moment, there is no direct correlation of the response of the structures in these test beds to these measured stresses. Many analyses totally ignore the natural stress field, and yet the analytical results directly correlate with the experimental results. This may be a result of the fact that the tunnel lining is emplaced long after the redistribution of stress around the opening has occurred. It could also mean that the uncertainty in the strength parameters in place are as great as the effects of the in situ stress. It is also possible, particularly in the media where the in situ stress is a small fraction of the strength of material, that no important effect has developed. As a result, there is no direct means of interpreting the effect of the in situ stress in the available data. Certainly at great depths, in situ stress must be a consideration in the design and in assessing the response of lined tunnels; therefore, it is important to embark upon a feasibility study to determine whether natural stress conditions can be emulated in the laboratory. The development of a feasibility study is outlined in Fig.144. The steps outlined in Fig.144 appear to be self explanatory so no additional discussion is presented here.

#### Aging Of Materials.

Aging may be important because strength or other major factors may degrade with time. Because of the age of materials emplaced on the earlier events, it is not necessary to use the somewhat uncertain methods of artificially aging materials to gather appropriate data. It seems

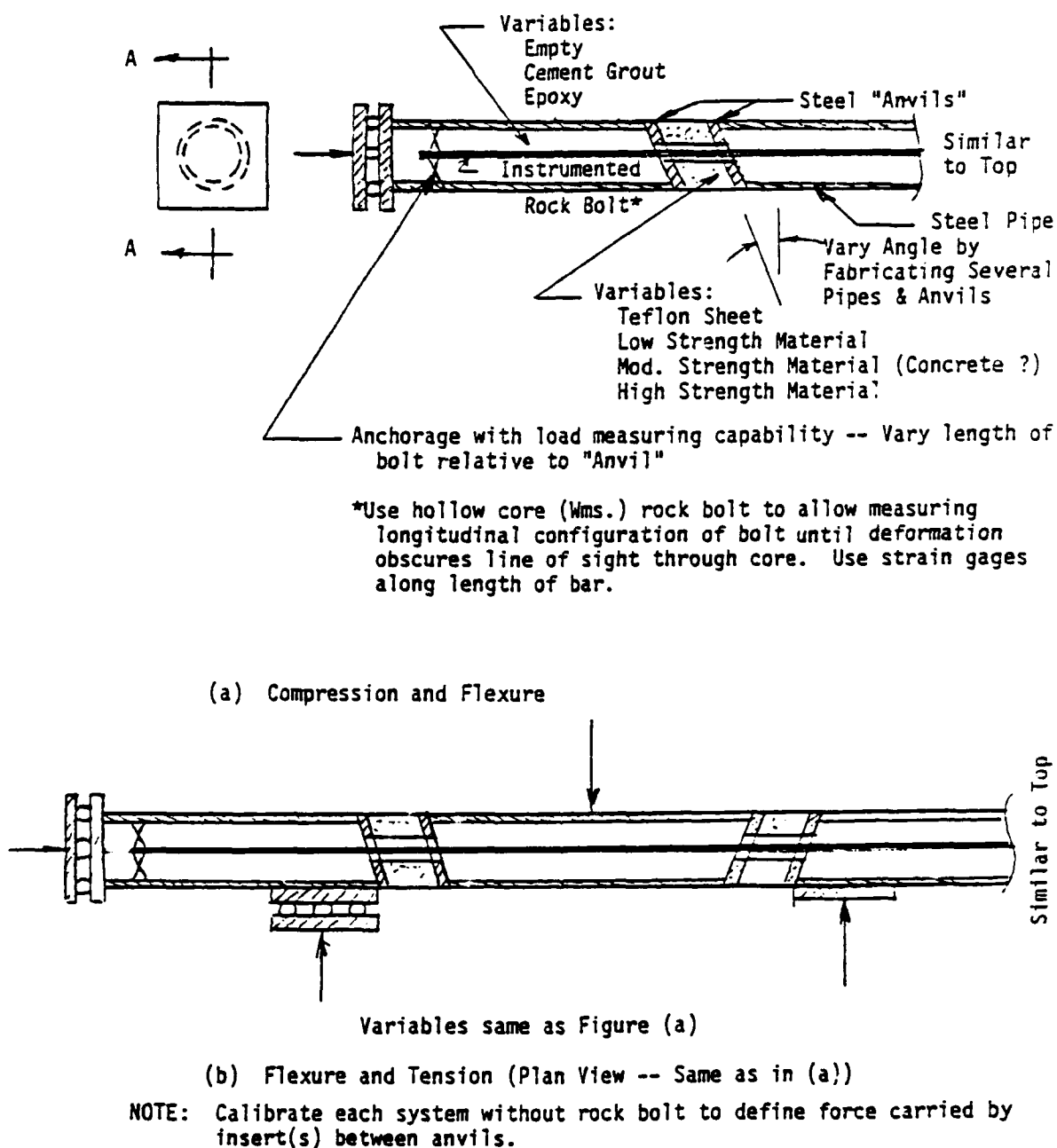


Figure 145. Schematic configurations for tests of rock bolts.

more appropriate to lay out a plan for recovering some of the materials used in the earlier events, and to design a plan for testing those materials in the laboratory. The team has not gone beyond the considerations outlined here. To a large degree the area of study is dependent upon policy decisions, such as what types of media should be considered from the standpoint of targeting and potential future designs; what hardness levels seem appropriate for those media and what structural configurations seem most appropriate to achieve those hardness levels; and, finally, what materials are required to achieve those hardnesses? If policy decisions of this sort are made, a program to define what tests and what materials should be recovered could be developed quickly. It is beyond the scope of the current study to embark upon such policy studies.

#### Water Inflow And Control.

Water was present in the various workings where structures experiments have been constructed and executed. In all cases, the original mining effort modified the water content near the opening where structures were emplaced. Only feasibility studies such as those in [Sweet & Merritt, 1986] have been pursued to define the viability of using analytical techniques for addressing major questions. There have been no experimental efforts pursued to address the question of water inflow. A feasibility study for a laboratory program to address this potential problem is outlined in Fig.144. The laboratory program uses some of the same concepts as suggested above to address the question of in situ stress. Therefore it may be prudent and cost effective to embark upon a combined program of addressing the feasibility of studying in situ stress and water inflow and control.

#### Achievable Hardness.

As a result of original design or evaluation of response of earlier tests of lined openings, there are concepts for linings which raise the question of what is the practical achievable hardness that might be obtained. A laboratory program to address the question of practical achievable hardness is a logical follow-on to the suggested tests of tunnels with linings discussed earlier. Thus no additional discussion appears needed here except to re-emphasize that it is important to emulate in any model the imperfections created in the prototype as a result of the means of fabrication.

#### Failure Criteria For Targeting.

Addressing this question in a laboratory program also is a direct extension of work which previously has been done. However, as noted in Fig.144, there are no data to date to indicate the modifications of test frames that would be necessary to assure either the safety of the system when the large deformations attending the actual failure occur or to assure that these large deformations can truly be imposed. These are straightforward problems of test fixture design, but they are also unique to the configurations available. Therefore, only the issues which must be addressed in such modification are implied in Fig.144.

## SECTION 7

### LIST OF REFERENCES

\_\_\_\_\_, "Automatic Dynamic Incremental Nonlinear Analysis (ADINA) - Theory and Modeling Guide", No. ARD 87-8, ADINA R&D Inc, Watertown, December 1987.

Abrahamson, G. R., Florence, A. L. and Colton, J. D., "Scale Modeling in Structural Dynamics Involving Plastic Deformation and Fracture," SRI Poulter Laboratory Technical Report 002-76, April 1976; Presented at 3rd International Conference on Structural Mechanics in Reactor Technology, London, 1-5 September 1975.

Bakhtar, K and N. Barton, "Large Scale Dynamic Joint Friction Testing for Improved Prediction of Block Motion and Tunnel Hardening", TR 84-01, prepared by Terra Tek, Inc, for DNA Contract No. DNA 001-82-C-0253.

Bakhtar, K. and DiBona, B. G., Dynamic Loading Experiments on Model Underground Structures," DNA-TR-85-387, prepared by Terra Tek, Inc. for Defense Nuclear Agency, Contract No. DNA 001-84-C-0144, 15 October 1985.

Bakhtar, K. and Jones, A. H., "Scaled Model Testing of Tunnel Intersections," DNA-TR-86-275, prepared by Terra Tek, Inc. for Defense Nuclear Agency, Contract No. DNA 001-84-C-0435, 30 June 1986.

Baron, M. L., Bleich, H. H. and Weidlinger, F., "Theoretical Studies on Ground Shock Phenomena," Report SR-19, prepared by Paul Weidlinger, Consulting Engineer for the MITRE Corporation, October, 1960.

Baron, M. L. and Matthews, A. T., "Diffraction of a Pressure Wave by a Cylindrical Cavity in an Elastic Medium", Journal of Applied Mechanics, Vol. 28, Series E, No. 3, September 1961, pp. 347-354.

Baron, M. L. and Parnes, R., "Displacements and Velocities Produced by the Diffraction of a Pressure Wave by a Cylindrical Cavity in an Elastic Medium", Journal of Applied Mechanics, Vol. 29, Series E, No. 2, June 1962, pp. 385-395.

Baron, M. L. and Parnes, R., "Diffraction of a Pressure Wave by Cylindrical Shell in An Elastic Medium", Proceedings of the Fourth U.S. National Congress of Applied Mechanics, ASME, June 1962, pp. 63-75.

Brace, W. F. and Jones, A. H., "Comparison of Uniaxial Deformation in Shock and Static Loading of Three Rocks," J. Geophyscial Res., v76, 1971.

Butters, S. W., Jones, A.H. and Green, S.J., "Properties of Rock Matching Grout Prepared by Stanford Research Institute," TR-75-8, Terra Tek, Inc., Salt Lake City, UT, 1975.

Butters, S. W., et al, "Characterization of Tuff and Development of Grouts for MIGHTY EPIC Structures Program", Concrete Laboratory, US Army Engineer Waterways Experiment Station, Vicksburg, MS, June 1976; also published as TR-76-21, Terra Tek Inc., Salt Lake City, UT.

Cizek, J.C. and Florence, A.L., "Laboratory Studies of Containment in Underground Nuclear Tests", DNA 5601F, January 1980.

Cizek, J. C. and Florence, A. L., "Laboratory Investigation of Containment in Underground Nuclear Tests," DNA 6121F, prepared by SRI International for Defense Nuclear Agency, Contract No. DNA 001-80-C-0040, 15 February 1982.

Cooley, C.H. et al., "Material Properties of 2C-4 Grout in Support of the Nevada Test Site Nuclear Test Program", TT-TR-81-56, Terra Tek Incl, May 1981.

Davis, H. C., Morrill, K. B., and Merritt, J. L. "Static Tests of Segments of Tunnel Linings", Volume II Data, DNA 4976F-2, Merritt CASES, Inc., Redlands, CA, 30 June 1979.

Davis, H. C., Morrill, K. B., and Merritt, J. L. "Continuation of Static Tests of Segments of Tunnel Linings", Volume II - Data, DNA 5000F-2, Merritt CASES, Inc., Redlands, CA, 30 June 1979.

Doll, E.B. and Salmon, V., "Scaled HE Tests, Operation JANGLE Project 1 (9)-1", Final Report, Stanford Research Institute, December 1952.

Florence, A. L., "Laboratory Investigation of Stemming of Underground Nuclear Tests", DNA 3935F, February 1976.

Florence, A. L., "Laboratory Investigation of Stemming and Containment in Underground Nuclear Tests," DNA 4149F, prepared by SRI for Defense Nuclear Agency, Contract No. DNA 001-75-C-0083, October 1976.

Florence, A. L., private communication, Stanford Research Institute, 1978.

Heuer, R. E. and Hendron, A. J., Jr., "Geomechanical Model Study of the Behavior of Underground Openings in Rock Subjected to Static Loads", Report 1, Development of Modeling Techniques, Contract Report N-69-1, U.S. Army Engineer Waterways Experiment Station, Corps of Engineers, Vicksburg, MS, October 1969.

Heuer, R. E. and Hendron, A. J., Jr., "Geomechanical Model Study of the Behavior of Underground Openings in Rock Subjected to Static Loads", Report 2, "Tests on Unlined Openings in Intact Rock", Department of Civil Engineering, University of Illinois, Urbana, IL, February 1971.

Isenberg, J. et al., "Analysis of Deep Underground Tunnels and Intersections Including Key Block Theory with Equilibrium Analysis", DNA-TR-88-102, December 1987.

Jones, A. H., Sinha, K. and Khodaverdian, M., Private Communication, I. Nelson's visit to Terra Tek, October 10, 1988.

Kennedy, T.C., Zaccor, J.V. and Lindberg, H.E., "Laboratory Investigation of Response of Deep-Based Structures", DNA 3610F, October 1975.

Kennedy, T.C. and Lindberg, H.E., "Laboratory Investigation of Rock Cavity Reinforcement", DNA 4023F, April 1976.

Kennedy, T. C. and Lindberg, H. E., "HUSSAR SWORD Series. DINING CAR Event. Model Structures Experiment on monocoque Direct Contact and Backpacked Liners", (CONFIDENTIAL - FORMERLY RESTRICTED DATA), POR 6887, SRI International, May 1976.

Khodaverdian, M. and Jones, A. H., "Material Characterization for Scaled Model Testing of Tunnel Intersections," Draft Report TR 88-74, prepared by Terra Tek, Inc. for Defense Nuclear Agency, Contract No. DNA 001-87-C-0003, July 1988.

Khodaverdian, M. and Jones, A.H., "Testing of Scaled Underground Tunnels", DNA-TR-89-203, March 1990.

Lev, O.E., et al., "High Explosive Model Structure Simulation (HEMSS) - Phase I, DNA 4560F, CONFIDENTIAL, January 1979.

Lindberg, H.E., "Large- and Small- Scale Deep Buried Structures Experiments", DNA POR 6950, MIGHTY EPIC, CONFIDENTIAL, February 1977.

Lindberg, H.E., Holmes, B.S. and Sanai, M., "Deep Buried Structures Experiments in Tuff and Simulated Jointed Rock", DNA POR 6998, DIABLO HAWK, CONFIDENTIAL, September 1981.

Malvern, L., "Unconfined Dynamic Compression Tests with Split-Hopkinson Bar", DNA Concrete Material Properties Meeting, Terra Tek Research, April 3, 1985.

Miller, W. O. and St. John, C. M., "Large-Scale Model Studies of a Rockbolted Tunnel", Paper presented at Key Questions in Rock Mechanics: Proceedings of the 29th U.S. Symposium at University of Minnesota/Minneapolis 13-15 June 1988.

Nelson, I., "Constitutive Models for Use in Numerical Computations," Dynamic Methods in Soil and Rock Mechanics, Proceedings, Karlsruhe, 1977, Vol. 2: Plastic and Long-Term Effects in Soils, Balkema, Rotterdam, 1978, pp. 45-97.

Paul, S. L., Cording, E. J. and Jenkins, J. R., "Model Test Simulation of Deeply Buried Openings in Jointed Rock", DNA-TR-86-167, University of Illinois at Urbana-Champaign, Urbana, IL, 1 May 1986.

Persen, L. N., Rock Dynamics and Geophysical Exploration - Introduction to Stress Waves in Rocks, Elsevier, Amsterdam, 1975.

Polatty, J.M. and Bendinelli, R.A., "Project Dribble, SALMON Event. Laboratory Design, Analysis and Field Control of Grouting Mixtures Employed at a Nuclear Test in Salt", US Army Engineer Waterways Experiment Station, Vicksburg, MS, May 1965.

Rinehart, J.S., "Model Experiments Pertaining to the Design of Underground Openings Subjected to Intense Ground Shocks", Colorado School of Mines, January 1960.

Rosenblad, J.L., "Geomechanical Model Study of the Failure Modes of Jointed Rock Masses", Technical Report MRD 1-61, Department of the Army, Missouri River Division, Corps of Engineers, Omaha, NE, January 1971.

Sachs, D.C. and Swift, L.M., "Small Explosion Tests, Project MOLE", Volume I, Final Report AFSWP-201, SRI, December 1955.

Sauer, F. M., Schoutens, J. E., Perret, W. R. and Bass, R. C., "Ground Motion from Underground Explosions," Schoutens, J. E. ed., Nuclear Geoplosics Sourcebook, Vol. IV, Part I - Empirical Analysis of Ground Motion from Above and Underground Explosions, DNA 6501H-4-1, prepared by General Electric Co. - TEMPO for Defense Nuclear Agency, Contract No. DNA 001-79-C-0081, 1 March 1979.

Selberg, H. L., "Transient Compression Waves from Spherical and Cylindrical Cavities, Arkiv For Fysik (Sweden), Bands nr7, 1952, pp 97-108.

Senseny, P. E. and Lindberg, H. E., "Laboratory Study of Deep-Based Structures in Support of Diablo Hawk", DNA4380F, prepared by SRI International for Defense Nuclear Agency, Contract No. DNA001-76-C-0385, 1 February 1978.

Senseny, P.E. and Lindberg, H. E., "Theoretical and Laboratory Study of Deep-Based Structures, Volume I - Triaxial Machine for Static and Dynamic Testing of 12-Inch Diameter Rocks", Final Report DNA 4425F-1, SRI International, Menlo Park, December 1977.

Senseny, P.E. and Lindberg, H.E., "Theoretical and Laboratory Study of Deep-Based Structures, Volume II - Model Tests and Analysis of MIGHTY EPIC Structures", DNA4425F-2, January 1979.

Senseny, P. E. and Lindberg, H. E., "Theoretical and Experimental Study of Deep-Based Structures in Intact and Jointed Rocks," DNA 5208F, prepared by SRI International for Defense Nuclear Agency, Contract No. DNA 001-76-C-0385, 1 September 1979.

Simons, J. W. and Florence, A. L., "Role of Laboratory Tests for Deep-Basing Using Replica Scaling," Draft Report prepared by SRI International for DNA Deep-Basing Meeting at SRI on November 4, 1987.

Simons, J. W., "Model Testing of Tunnel Sections and Intersections," Monthly Progress Reports 9 through 11, prepared by SRI International for Defense Nuclear Agency, Contract No. DNA001-87-C-0006, PYU-3771, September 87, November 87, June 1988.

Simons, J. W., Florence, A. L. and Colton, J. D., "Simple Models Based on Laboratory Data for Predicting the Strength of Unlined Tunnels Loaded in Uniaxial Strain," Letter to Capt. Mike Reed, Defense Nuclear Agency from SRI International, 29 September 1988.

Simons, J. W., Private Communication, I. Nelson's visit to SRI International, October 11, 1988.

Simons, J.W., Colton, J.D. and A.L. Florence, "Model Testing of Tunnel Sections and Intersections", DNA TR-89-155, March 1990.

Suaris, W1 and Shah, S.P., "Mechanical Properties of Materials Subjected to Impact", Proceedings RILEM-CEB-IABSE Symposium, Berlin, West Germany, June 1982.

Sweet, J. and Merritt, J. L., "Subterranean Water Management Study, Prediction of Dynamically Induced Water Flow in NTS Tunnels in Tuff", BMO TR-86-17, Merritt CASES, Inc., Redlands, CA, 11 March 1986.



## **APPENDIX A**

### **BIBLIOGRAPHY**

#### **SRI Tests and Simulants**

##### **DNA 3610F**

Kennedy, T.C., Zaccor, J.V. and Lindberg, H.E., "Laboratory Investigation of Response of Deep-Based Structures", DNA 3610F, October 1975.

##### **DNA 3935F**

Florence, A. L., "Laboratory Investigation of Stemming of Underground Nuclear Tests", DNA 3935F, February 1976.

##### **DNA 4023F**

Kennedy, T.C. and Lindberg, H.E., "Laboratory Investigation of Rock Cavity Reinforcement", DNA 4023F, April 1976.

##### **DNA 4149F**

Florence, A. L., "Laboratory Investigation of Stemming and Containment in Underground Nuclear Tests," DNA 4149F, prepared by SRI for Defense Nuclear Agency, Contract No. DNA 001-75-C-0083, October 1976.

##### **DNA 4380F**

Senseny, P. E. and Lindberg, H. E., "Laboratory Study of Deep-Based Structures in Support of Diablo Hawk", DNA4380F, prepared by SRI International for Defense Nuclear Agency, Contract No. DNA001-76-C-0385, 1 February 1978.

##### **DNA 4425F**

Senseny, P.E. and Lindberg, H. E., "Theoretical and Laboratory Study of Deep-Based Structures, Volume I - Triaxial Machine for Static and Dynamic Testing of 12-Inch Diameter Rocks", Final Report DNA 4425F-1, SRI International, Menlo Park, December 1977.

Senseny, P.E. and Lindberg, H.E., "Theoretical and Laboratory Study of Deep-Based Structures, Volume II - Model Tests and Analysis of MIGHTY EPIC Structures", DNA 4425F-2, January 1979.

##### **DNA 5208F**

Senseny, P. E. and Lindberg, H. E., "Theoretical and Experimental Study of Deep-Based Structures in Intact and Jointed Rocks," DNA 5208F, prepared by SRI International for Defense Nuclear Agency, Contract No. DNA 001-76-C-0385, 1 September 1979.

##### **DNA 5601F**

Cizek, J.C. and Florence, A.L., "Laboratory Studies of Containment in Underground Nuclear Tests", DNA 5601F, January 1980.

##### **DNA 6121F**

Cizek, J. C. and Florence, A. L., "Laboratory Investigation of Containment in Underground Nuclear Tests," DNA 6121F, prepared by SRI International for Defense Nuclear Agency, Contract No. DNA 001-80-C-0040, 15 February 1982.

DNA POR 6887

Kennedy, T. C. and Lindberg, H. E., "HUSSAR SWORD Series. DINING CAR Event. Model Structures Experiment on monocoque Direct Contact and Backpack Liners", (CONFIDENTIAL - FORMERLY RESTRICTED DATA), POR 6887, SRI International, May 1976.

DNA POR 6950

Lindberg, H.E., "Large- and Small- Scale Deep Buried Structures Experiments", DNA POR 6950, MIGHTY EPIC, CONFIDENTIAL, February 1977.

DNA POR 6998

Lindberg, H.E., Holmes, B.S. and Sanai, M., "Deep Buried Structures Experiments in Tuff and Simulated Jointed Rock", DNA POR 6998, DIABLO HAWK, CONFIDENTIAL, September 1981.

DNA TR-89-155

Simons, J.W., Colton, J.D. and A.L. Florence, "Model Testing of Tunnel Sections and Intersections", DNA TR-89-155, March 1990.

SRI Progress Reports

Simons, J. W., "Model Testing of Tunnel Sections and Intersections," Monthly Progress Reports 9 through 11, prepared by SRI International for Defense Nuclear Agency, Contract No. DNA001-87-C-0006, PYU-3771, September 87, November 87, June 1988.

Terra Tek Tests and Simulants

DNA-TR-84-01

Bakhtar, K and N. Barton, "Large Scale Dynamic Joint Friction Testing for Improved Prediction of Block Motion and Tunnel Hardening", TR 84-01, prepared by Terra Tek, Inc, for DNA Contract No. DNA 001-82-C-0253.

DNA TR-85-387

Bakhtar, K. and DiBona, B. G., Dynamic Loading Experiments on Model Underground Structures," DNA-TR-85-387, prepared by Terra Tek, Inc. for Defense Nuclear Agency, Contract No. DNA 001-84-C-0144, 15 October 1985.

DNA TR-86-275

Bakhtar, K. and Jones, A. H., "Scaled Model Testing of Tunnel Intersections," DNA-TR-86-275, prepared by Terra Tek, Inc. for Defense Nuclear Agency, Contract No. DNA 001-84-C-0435, 30 June 1986.

DNA TR-88-74

Khodaverdian, M. and Jones, A. H., "Material Characterization for Scaled Model Testing of Tunnel Intersections," Draft Report TR 88-74, prepared by Terra Tek, Inc. for Defense Nuclear Agency, Contract No. DNA 001-87-C-0003, July 1988.

DNA TR-89-203

Khodaverdian, M. and Jones, A.H., "Testing of Scaled Underground Tunnels", DNA-TR-89-203, March 1990.

**U Tests**

**DNA TR-86-167**

**Paul, S. L., Cording, E. J. and Jenkins, J. R., "Model Test Simulation of Deeply Buried Openings in Jointed Rock", DNA-TR-86-167, University of Illinois at Urbana-Champaign, Urbana, IL, 1 May 1986.**

## **DISTRIBUTION LIST**

**DNA-TR-90-216-V1**

### **DEPARTMENT OF DEFENSE**

ASSISTANT TO THE SECRETARY OF DEFENSE  
ATTN: EXECUTIVE ASSISTANT

DEFENSE ADVANCED RSCH PROJ AGENCY  
ATTN: DEFENSE SCIENCES OFFICE

DEFENSE INTELLIGENCE AGENCY  
ATTN: DB-6  
ATTN: DB-6E2 J DOPERALSKI

DEFENSE NUCLEAR AGENCY  
ATTN: OPNA  
ATTN: OPNS  
ATTN: SPSD  
ATTN: SPSD P SENSENY  
2 CYS ATTN: TITL

DEFENSE TECHNICAL INFORMATION CENTER  
2 CYS ATTN: DTIC/FDAB

DNA PACOM LIAISON OFFICE  
ATTN: DNALO

FIELD COMMAND DEFENSE NUCLEAR AGENCY  
ATTN: FCNM  
ATTN: FCTT  
2 CYS ATTN: FCTT W SUMMA  
ATTN: NMHE

THE JOINT STAFF  
ATTN: JKC ATTN DNA REP  
ATTN: JLWD  
ATTN: JPEM

### **DEPARTMENT OF THE ARMY**

U S ARMY CORPS OF ENGINEERS  
ATTN: CERD-L

U S ARMY ENGINEER DIST OMAHA  
ATTN: MROED-S H

U S ARMY ENGR WATERWAYS EXPER STATION  
ATTN: C D NORMAN  
ATTN: CEWES J K INGRAM  
ATTN: CEWES-SD DR J G JACKSON JR  
ATTN: DR D BANKS CEWES-GS  
ATTN: G ALBRITTON  
ATTN: J BALSARA CEWES-SS-R  
ATTN: J WARRINE WESGR-M  
ATTN: RESEARCH LIBRARY  
ATTN: W MILLER

### **DEPARTMENT OF THE AIR FORCE**

AIR FORCE CTR FOR STUDIES & ANALYSIS  
ATTN: AFCSA/SAMI R GRIFFIN

AIR FORCE OFFICE OF SCIENTIFIC RSCH  
ATTN: AFOSR/NA

AIR UNIVERSITY LIBRARY  
ATTN: AUL-LSE

DEPUTY CHIEF OF STAFF/AFRD-M  
ATTN: AFRD-M A RAVGIALA

PHILLIPS LABORATORY  
ATTN: NTCA  
ATTN: NTE

STRATEGIC AIR COMMAND/XRFS  
ATTN: XRFS

### **DEPARTMENT OF ENERGY**

LOS ALAMOS NATIONAL LABORATORY  
ATTN: REPORT LIBRARY

SANDIA NATIONAL LABORATORIES  
ATTN: DIV 9311 L R HILL  
ATTN: DR CARL W SMITH DIVISION 9311  
ATTN: TECH LIB 3141

### **OTHER GOVERNMENT**

CENTRAL INTELLIGENCE AGENCY  
ATTN: OSWR/NED

DEPARTMENT OF THE INTERIOR  
ATTN: P SANDS

### **DEPARTMENT OF DEFENSE CONTRACTORS**

AEROSPACE CORP  
ATTN: LIBRARY ACQUISITION

ANALYTIC SERVICES, INC (ANSER)  
ATTN: K BAKER

APPLIED RESEARCH ASSOCIATES, INC  
ATTN: C J HIGGINS

APPLIED RESEARCH ASSOCIATES, INC  
ATTN: S BLOUIN

APPLIED RESEARCH ASSOCIATES, INC  
ATTN: R FRANK

BDM ENGINEERING SERVICES CO  
ATTN: D BURGESS

CALIFORNIA RESEARCH & TECHNOLOGY, INC  
ATTN: J THOMSEN

IIT RESEARCH INSTITUTE  
ATTN: DOCUMENTS LIBRARY  
ATTN: M JOHNSON

INSTITUTE FOR DEFENSE ANALYSES  
ATTN: CLASSIFIED LIBRARY

**DNA-TR-90-216-V1 (DL CONTINUED)**

KAMAN SCIENCES CORP  
ATTN: LIBRARY B KINSLOW  
ATTN: RICHARD KEEFFE

KAMAN SCIENCES CORP  
ATTN: DASAC

KAMAN SCIENCES CORPORATION  
ATTN: DASAC

NTS ENGINEERING  
ATTN: R KENNEDY  
ATTN: S SHORT

PACIFIC-SIERRA RESEARCH CORP  
ATTN: D WILSON  
ATTN: H BRODE

PACIFIC-SIERRA RESEARCH CORP  
ATTN: D GORMLEY

R & D ASSOCIATES  
ATTN: LIBRARY

R & D ASSOCIATES  
ATTN: T EDWARDS

R & D ASSOCIATES  
ATTN: D PIEPENBURG

RAND CORP  
ATTN: B BENNETT

S-CUBED  
ATTN: K D PYATT JR

SCIENCE APPLICATIONS INTL CORP  
ATTN: DR M MCKAY  
ATTN: H PRATT  
ATTN: TECHNICAL REPORT SYSTEM

SCIENCE APPLICATIONS INTL CORP  
ATTN: W LAYSON

SOUTHWEST RESEARCH INSTITUTE  
ATTN: B THACKER

SRI INTERNATIONAL  
ATTN: B HOLMES  
ATTN: J GRAN  
ATTN: J SIMONS

THE TITAN CORPORATION  
ATTN: K KREYENHAGEN  
ATTN: LIBRARY  
ATTN: S SCHUSTER

TRW INC  
ATTN: B BALACHANDRA

TRW SPACE & DEFENSE SECTOR  
ATTN: P N MATHUR

UTD, INC  
ATTN: E FOSTER

WEIDLINGER ASSOC, INC  
ATTN: F WONG  
ATTN: H LEVINE  
ATTN: I NELSON  
ATTN: J ISENBERG  
ATTN: J MERRITT  
ATTN: R GOODMAN  
ATTN: P J PERIE

WEIDLINGER ASSOCIATES, INC  
ATTN: I SANDLER  
ATTN: M BARON